5-2017

Synthesis and Characterization of Novel Single-Site Titanosilicates with Targeted Connectivites and Geometries as Selective Oxidation Catalysts

Lena Elenchin
University of Tennessee, Knoxville, lelenchi@vols.utk.edu

To the Graduate Council:

I am submitting herewith a dissertation written by Lena Elenchin entitled "Synthesis and Characterization of Novel Single-Site Titanosilicates with Targeted Connectivites and Geometries as Selective Oxidation Catalysts." I have examined the final electronic copy of this dissertation for form and content and recommend that it be accepted in partial fulfillment of the requirements for the degree of Doctor of Philosophy, with a major in Chemistry.

Craig E. Barnes, Major Professor

We have read this dissertation and recommend its acceptance:

David Jenkins, Janice Musfeldt, David Keffer

Accepted for the Council:

Dixie L. Thompson

Vice Provost and Dean of the Graduate School

(Original signatures are on file with official student records.)

Synthesis and Characterization of Novel Single-Site Titanosilicates with Targeted Connectivities and Geometries as Selective Oxidation Catalysts

A Dissertation Presented for the

Doctor of Philosophy

Degree

The University of Tennessee, Knoxville

Lena Elenchin

May 2017

Dedication

To Pap and in loving memory of Pop,

Without your support, guidance, and love I would not be the woman I am today. You blessed me with wisdom, perseverance, and most of all what it means to excel. This journey would not have been possible with you.

Acknowledgements

Over the past six years I have had the pleasure of meeting and working alongside a great number of individuals who have helped me through this incredible journey. They have not only impacted the work presented in this dissertation, but they have changed the way I see and interact in both the chemistry community and society.

First and foremost, I would like to express my sincere gratitude to my advisor Dr. Craig Barnes. Without his constant support, drive, intuition, and vast chemical knowledge, I would not be where I am today. He has taught me, through example, that if you have patience and perseverance you can make great strides toward achieving your ultimate goals,

I must thank my committee members, Dr. David Jenkins, Dr. Janice Musfeldt, and Dr. David Keffer for agreeing to commit their time and energy to be a part of my journey here at the University of Tennessee. Your insightful comments, encouragement and hard (but intriguing) questions incented me to expand my chemical intuition from various perspectives.

I would also like to thank Dr. Carlos Steren for his willingness to be a collaborator on this project. Without his deep understanding of NMR spectroscopy and genuine affection for teaching, the determination of reaction intermediates would not have been possible.

In addition, I am forever grateful to past and present members of the Barnes groups: Dr. Nan Chen, Dr. Joshua Abbott, Dr. Michael Peretich, Dr. Jiri Pinkas, Dr. Austin Albert, Dr. Ales Styskalik, James Humble, Matt Dembo, Desta Bume, Michael Kandziolka, Paul Kravchencko and Michael Orick for their knowledge, laughs, and support. They have truly been a joy to work and learn with.

A special thanks to the entire chemistry department staff. Without your hard work, dedication and most of all patients these past six years would have been a nightmare. From filing the right paperwork, to dealing with incorrect chemical orders, and from custom glassware to always having a spare computer charge you were there for me. Without you, I would have been lost.

Finally, I must thank my parents for always putting my education and well-being above all else. You were my strength when I felt weak. Your constant love and support has pushed me to continually strive for success.

Abstract

The primary focus of this research was to synthesize and characterize two families of titanosilicate catalysts, first generation and second generation, that were single site, atomically dispersed with targeted connectivities to the silicate matrices but had different geometries about the active sites. First generation catalysts have tetrahedral active sites, while second generation catalysts have altered geometries for a more accessible active site, but maintain the same targeted connectivities.

A building block methodology is employed to prepare single site, isolated, atomically dispersed titanium active sites within a silicate matrix. The synthetic approach uses a molecular precursor, i.e., building block and the method of sequential additions to construct the support matrix around the active site. This methodology can be used to target titanium connectivities (2, 3, or 4 linkages) to the matrix, namely 2-connected (2C-), 3-connected (3C-Ti) and 4-connected (4C-Ti).

Several characterization techniques are used to compare and contrast first and second generation catalysts; NMR, gravimetric analysis (determine connectivity), FTIR, XAS (XANES/EXAFS), DRUV, and catalytic activity are used to characterize the final catalysts. Based on spectroscopic characterization, two families of catalysts with different geometries were successfully synthesized.

Catalytic studies showed two distinct relationships could be made: 1) The activities of these catalysts correlate with the connectivity of the titanium site as long as leaching does not occur. 4C-Ti catalysts were less active than 3C-Ti catalysts. The 2C-Ti catalysts leached from the support matrix and therefore cannot be considered true heterogeneous catalysts. 2) Second generation catalysts were more active than first generation catalysts due to the more open geometry of the active site.

Table of Contents

Chapter I: A Brief Overview of Heterogeneous Catalysts 1

Introduction to catalysis 1

Heterogeneous Catalysts 3

Catalytic Activity 30

Selectivity 32

Leaching 33

Overview of Dissertation 34

Chapter II: General Synthesis and Characterization with Experimental Procedures 40

Building Block Methodology 40

Characterization 55

Secondary Characterization 93

Conclusion 105

Chapter III: Synthesis and Characterization of First Generation Passivated Atomically Dispersed Ti Catalysts with $SiCl_4$ 106

Introduction 106

Titanium Precursors 106

Synthesis of first Generation Single-Site Titanosilicate Catalysts 107

Methanol Passivation 112

Characterization of First Generation Methanol Passivated Catalysts 112

Catalytic Activity of First Generation Catalysts 117

Confocal Microscopy 121

General Conclusion of Methanol Passivation 121

Chapter IV: Problems and Solutions to Methanol Passivation 125

Methanol Passivation in the Presence of Base 125

Non-Passivated Catalysts 127

Addition of Base to Non-Passivated Catalysts 127

Methyl-*tert*-butyl ether (MTBE) Passivation 132

Changing Inert Linker 136

Chapter V: Synthesis and Characterization of Non-Passivated First and Second Generation Single-Site Titanosilicate Catalysts 137

Introduction 137

Experimental 137

Characterization of “New” First Generation Catalysts 138

Second Generation Single-Site Catalysts 155

Synthesis of Second Generation Single-Site Titanosilicate Catalysts 175

Blocking Ligands and the First Dose 178

FTIR and XAS Investigation into the First Dose 179

Blocking Ligand Added After the First Dose – Third Generation 181

Blocking Ligand and the Second Dose 183

XAS Data First and Second Generation 186

Characterization of Second Generation 3C-Ti and 2C-Ti Catalysts 192

Characterization of the Reaction Volatiles After the Second Cross-linking 192

Second Generation Catalysts with Blocking Ligands Removed 196

General Conclusion 211

Stability and Recyclability 211

Reproducibility 218

Investigation of Intermediates and Byproducts of TMP Oxidation 218

Chapter V Conclusion 237

Chapter VI: First and Second Generation as Epoxidation Catalysts 240

Introduction 240

Catalytic Protocol 240

Characterization of Epoxidation Aliquots 241

Results and Discussion of First Generation Titanosilicate Catalysts 243

Results and Discussion of Second Generation Titanosilicate Catalysts 245

Stability of 2-Connected Catalysts 248

Summary 249

Chapter VII: Research Conclusions and Future Work 250

General Conclusion 250

First Generation Catalysts with Targeted Connectivities 250
Second Generation Catalysts with Targeted Connectivities and Altered Geometries . 251
Future Work 252
References 258
Vita 266

List of Tables

Table 1 TS-1 synthetic methodologies and parameters vs. final Si/Ti and morphology. Reprinted from ref [42]. 26

Table 2 Summary of reaction conditions necessary for reaching high selectivity for the oxidation of TMP to TMBQ. 29

Table 3 List of inert and catalytically active linkers. 45

Table 4 Summary of ICP-OES parameters. 67

Table 5 Summary of the nomenclature for specific X-ray absorption transitions (X-ray absorption edges). 80

Table 6 List of collection parameters for XAS measurements. 89

Table 7 Summary of porosity based on isotherm type. 92

Table 8 Summary of the integrations without $MgSO_4$, with $MgSO_4$, and with double the amount of $MgSO_4$. 99

Table 9 List of integration regions used for NMR workup. 102

Table 10 Precursors, Ti : cube ratios, connectivity and titanium weight percent used for synthesizing first generation single site titanosilicates. 110

Table 11 Summary of the elemental composition of Ti and Sn before and after methanol passivation for a 2C-Ti catalyst. Table obtained from ref [42]. 115

Table 12 Results of catalytic properties of first generation methanol passivated titano-silicates in the oxidation of TMP to TMBQ obtained by Dr. Chen. 119

Table 13 Results of catalytic activity for first generation catalysts synthesized in this work compared to two titanium free catalysts for the oxidation of TMP to TMBQ. 120

Table 14 Catalytic results of the oxidation of TMP to TMBQ by first generation methanol passivated in the presence of base. 126

Table 15 Catalytic results of first generation non-passivated titanosilicates in the oxidation of TMP to TMBQ. 129

Table 16 Catalytic results of first generation non-passivated titanosilicates with added base in the oxidation of TMP to TMBQ. 131

Table 17 Catalytic results of first generation MTBE passivated catalysts with added base in the oxidation of TMP to TMBQ. 134

Table 18 Comparison of gravimetric and ICP-OES weight percent. 141

Table 19 DRUV absorption wavelength maxima for first generation catalysts. 147

Table 20 Results of catalytic activity for first generation titanosilicates, two control reactions, and two literature catalyst for the oxidation of TMP to TMBQ. 151

Table 21 Results of catalytic activity for first generation, two control reactions, and two literature catalyst for the oxidation of DMOP to DMOBQ. 151

Table 22 List of structural parameters obtained from FEFF calculations for trans $TiCl_4(THF)_2$. 166

Table 23 List of structural fit parameters obtained from FEFF calculations for trans for $TiCl_4py_2$. 174

Table 24 Summary of the amount of blocking ligand lost after the first cross-linking reaction at both room temperature and 80 ^{0} C. 179

Table 25 Summary of the precursor, connectivity, percent blocking ligand lost, remaining ratio of pyridine to titanium after the drying the catalysts following the second cross-linking reaction. 196

Table 26 Summary of the amount of blocking ligand lost after the first dose and after the second dose. 197

Table 27 Temperature needed to remove 100% of the pyridine blocking ligands after the second cross-linking reaction. 199

Table 28 Summary of DRUV wavelength absorption maxima. 204

Table 29 Summary of catalytic properties for 2nd generation Ti catalysts with pyridine

blocking ligands for the oxidation of TMP to TMBQ. 206

Table 30 Summary of catalytic properties for 2nd generation Ti catalysts with pyridine blocking ligands for the oxidation of DMOP to DMOBQ. 206

Table 31 Summary of catalytic properties for 2nd generation Ti catalysts pyridine removed for the oxidation of TMP to TMBQ. 207

Table 32 Summary of catalytic properties for 2nd generation Ti catalysts pyridine removed for the oxidation of DMOP to DMOBQ. 207

Table 33 Comparison of catalytic activities between catalyst with the same connectivities but different geometries for the oxidation of TMP to TMBQ. 209

Table 34 Comparison of catalytic activities between catalyst with the same connectivities but different geometries for the oxidation of DMOP to DMOBQ. 210

Table 35 Summary of leaching studies for first and second generation titanium catalysts for oxidation of phenols to benzoquinones with aqueous hydrogen peroxide. 215

Table 36 Results of Sn leaching detected by ICP-OES. 216

Table 37 Carbon and proton assignments for side product A. 233

Table 38 Carbon and proton assignments for side product B. 234

Table 39 Carbon and proton assignments for the dimer byproduct. 239

Table 40 Proton integrations of the epoxidation of cyclohexene to cyclohexene oxide. ... 243

Table 41 Summary of catalytic properties for cyclohexene epoxidation of first generation titanosilicates, TS-1, grafted Ti-MCM-41, and a Ti free platform. 244

Table 42 Summary of catalytic activity for all catalysts synthesized in this work for the epoxidation of cyclohexene. 246

Table 43 Summary of the leaching studies for the family of 2C-Ti. 249

List of Figures

Figure 1 Illustration of the energy diagram for an uncatalyzed reaction (red) and a catalyzed reaction (purple) showing the catalyzed reaction exhibits a lower energy barrier (activation energy) than its analogous uncatalyzed reaction. Figure modifed from ref [4]..... 2

Figure 2 Overview of the sol gel process illustrating the difference between xerogels and aerogels. 6

Figure 3 Ilustration of soft templating process. Figure obtained from ref [28]. 9

Figure 4 Illustration of the different pore structures of three MCM materials (layered MCM-41, hexagonal MCM-41, and cubic MCM-48). Figure obtained from ref [28]. 10

Figure 5 Illustration of the zeolite mineral mordenite (MOR): SiO_4 polyhedra are represented as yellow tetrahedron; AlO_4 polyhedra are aqua tetrahedron. Figure obtained from ref [37]. 13

Figure 6 Different types of surface silanols. 14

Figure 7 Illustration of larger pores will take up a larger volume and result in larger crystallites. Figure was reproduced from ref [18]. 16

Figure 8 Illustration of grafted verse tethering active sites to a solid support. Figure modified from ref [38]. 17

Figure 9 Connectivity of grafted complexes and secondary M-O(X)Si interaction. Figure reproduced from ref [38]. 18

Figure 10 Mononuclear zwitterionic rhodium complex tethered to silica support via sulfonate linkage. Figure obtained from ref [53]. 22

Figure 11 Pictogram of Co(Salen) inside the super cage of zeolite Y. Figure obtained from

ref [40]. 23

Figure 12 Illustration of the different types of reactions catalyzed by TS-1. Figure reprinted from ref [56]. 25

Figure 13 The structure of orthorhombic form of silicalite-1 (MFI type) showing the 12 crystallography distinct T sites. The oxygen atoms have been omitted for clarity. Figure reprinted from ref [57]. 28

Figure 14 Illustration of the possible mixtures of active sites in grafted titanosilicates. 28

Figure 15 a) mononuclear Ti center, b) dinuclear Ti centers as a result from grafting. 30

Figure 16 Tetrahedral Titanium centers with different connectivities to the matrix. 35

Figure 17 Second generation titanosilicate catalysts with tailored connectivities and geometries other than tetrahedral. 36

Figure 18 Oxidation of phenols to benzoquinones with aqueous hydrogen peroxide. 37

Figure 19 Epoxidation of cyclohexene to cyclohexene oxide with cumene hydroperoxide. 37

Figure 20 Illustration of catalytic ensemble showing the metal to surface binding, the metal terminating ligands (L) and the support (SiO_2). 41

Figure 21 Illustration of the core structure of the tin functionalized building block $Si_8O_{12}(OSnMe_3)_8$ where silicon atoms are blue, oxygen atoms red, and trimethyltin groups green. 42

Figure 22 Illustration of the separation distances for the terminal oxygen linking points on the building block $Si_8O_{12}(OSnMe_3)_8$. Figure was obtained from ref [71]. 44

Figure 23 Generic cross-linking reaction between building block and linking agent with complimentary functional groups. 47

Figure 24 Illustration of the method of sequential additions. Figure was obtained from ref [75]. 49

Figure 25 Illustration of the formation of 4-connected embedded titanium center. 51

Figure 26 Illustration of the 2nd dose of the method of sequential additions the formation of the matrix by cross-linking the oligomers of the 1st dose. 52

Figure 27 Illustration of the two-dose strategy employed in the method of sequential additions for fully embedded 4-connected titanium centers. 53

Figure 28 Mononuclear titanium precursors used to target specific connectivities to the matrix; 2-connected (left), 3-connected (middle), 4-connected (right). 54

Figure 29 Illustration of three different titanium connectivities to the silicate. 56

Figure 30 Illustration of a 2-connected matrix after second cross-linking illustration silyl chloride groups remain and pose the risk of disrupting the targeted connectivities. 56

Figure 31 FTIR spectra following the dehydration of TS-1, low H_2O absorption dotted lines, high concentration solid lines. Figure modified from ref [56]. 60

Figure 32 FTIR spectrum of the tin-cube building block illustrating the fingerprint regions used for characterization. 61

Figure 33 FTIR spectra of pure SiO_2 (bottom) and TiO_2 showing the absence of the 960 cm^{-1} shoulder when Ti is not present in the matrix. Figure was obtained from ref [82]. 63

Figure 34 Modes and frequencies of pyridine binding on aluminosilicates (left) silanols, (middle) Brønsted, (right) Lewis. 64

Figure 35 Photograph of the IR spectrometer located inside a nitrogen atmosphere glovebox. 65

Figure 36 Illustration of the calibration curves obtained for each titanium wavelength. ... 68

Figure 37 Illustration of specular reflection showing the incident angle is equal to the reflectance angle. 70

Figure 38 Illustration of diffuse reflections where the incident angle does not equal the

reflected angles. 72

Figure 39 DRUV spectra for dehydrated (-) and hydrated (- -) TiO_2 (a, offset by 0.4) and TS-1 (b). Figure was reprinted from ref [87]. 74

Figure 40 Illustration of the two different types of tetrahedral titanium sites found in titanosilicates, closed (left) and open (right). 76

Figure 41 Photograph of the DRUV sample cell prepared inside a nitrogen atmosphere glovebox, left-without cover, right-with black cover to mask the tape. 76

Figure 42 A core electron is excited by an X-ray photon of the proper energy. 78

Figure 43 Fluorescence decay of the excited state. 78

Figure 44 Plot of X-ray absorption energies as a function of atomic number. 80

Figure 45 XAS spectrum of Ti K-edge illustrating the two distinct regions, XANES (red) and EXAFS (Blue). 81

Figure 46 Illustration of the pre-edge feature of a 6-coordinate titanium species (left) and a 4-coordinate complex (right) in the XANES region of XAS. Figure modified from ref [93]. 82

Figure 47 Illustration of how coordination geometry influences the Ti pre-edge intensity and peak position. Figure was reprinted from [107]. 84

Figure 48 Illustration of deconstructive (left) and constructive (right) interface, absorbing atom is blue and the backscattering atoms are red and green. 84

Figure 49 Illustration of the scattering spheres. 85

Figure 50 Illustration of the different types of scattering paths. Figure obtained from ref [94]. 85

Figure 51 UHMW polyethylene plate loaded with samples and sealed with polypropylene windows. 87

Figure 52 IUPAC description of adsorption/desorption isotherms. Figure was obtained

from ref [100]. 92

Figure 53 Nitrogen adsorption/desorption isotherm for 2-connected first generation catalysts (blue is adsorption branch and orange is desorption branch). 94

Figure 54 Picture of catalysis set up. 96

Figure 55 NMR spectra of an aliquot without $MgSO_4$ (blue) showing the presence of a broad feature at ~6.5 ppm and an aliquot with $MgSO_4$ (red) illustrating the absence of the broad feature in the presence of $MgSO_4$. 98

Figure 56 Typical NMR spectrum for the oxidation TMP to TMBQ. 101

Figure 57 Generic plot of the reaction kinetics, conversion of substrate (blue), formation of products (red), selectivity (green). 104

Figure 58 Overlaid 1H NMR spectra of $Ti(Oipr)_4$ (red), $Ti(OiPr)_2Cl_2$ (blue), $Ti(OiPr)Cl_3$ (green). 108

Figure 59 Illustration of the three different targeted connectivities to the matrix, 4C-Ti (left, purple), 3C-Ti (middle, blue), and 2C-Ti (right, green). 110

Figure 60 4C-Ti first generation catalyst matrix after the first dose. All titanium centers (purple) have the same connectivity while the silicon centers (blue) have multiple connectivities to the matrix. 111

Figure 61 Illustration of methanol passivation reducing the number of silyl chloride groups in the final matrix along with remaining trimethyltin groups. 113

Figure 62 DRUV spectra overlays, 2C-Ti (black), 3C-Ti (red), and 4C-Ti (blue). Figure obtained from ref [42]. 115

Figure 63 XANES spectrum for 4C-Ti 1st generation catalysts showing a single peak pre-edge feature indicative of 4-coordinate tetrahedral Ti. 116

Figure 64 Infrared spectra of 2C-Ti (black), 3C-Ti (blue), 4C-Ti (orange), and Ti free platform (green.) Figure was reprinted from ref [42]. 118

Figure 65 Illustration of unwanted side relation with HCl during methanol passivation leading to mixtures of active sites. 122

Figure 66 Confocal microscopy images of three different 2-connected first generation titanium catalysts, 2-connected MTBE passivated (left), 2C-MeOH passivated (middle), and 2C-non-passivatd (right). 123

Figure 67 Illustration of the surface roughness for a 2C-Ti-non-passivated catalyst. 123

Figure 68 Optical 3D surface reconstruction of the 2C-Ti-MTBE passivated catalyst (left) and the 2C-Ti-MeOH passivated catalyst (right). 124

Figure 69 Kinetic plot of the conversion of TMP to TMBQ by 4C-Ti-1st gen MeOH passivated in the presence of base. Hydrogen peroxide has been completely consumed by 60 minutes. 128

Figure 70 IR Spectrum of dried sodium acetate illustrating water is not present. 130

Figure 71 NMR spectra t = 0 minutes (1, blue) and t = 60 minutes (2, pink) illustrating the consumption of H_2O_2. 133

Figure 72 NMR spectrum of the volatiles from MTBE passivation. ……135

Figure 73 Final matrix of first generation catalysts left cross-linked with $SiCl_4$ and right... cross-linked with Me_2SiCl_2. ……..139

Figure 74 Overlay of FTIR spectra of two non-passivated 4C-Ti catalysts, cross-linked with $SiCl_4$ (blue) and cross-linked with Me_2SiCl_2 (purple). 142

Figure 75 FTIR spectra overlay for first generation catalysts cross-linked with Me_2SiCl_2, 2C-Ti (green), 3C-Ti (Blue), 4C-Ti (purple), and Ti-free platform (yellow). The inlay is the full FTIR window. 143

Figure 76 DRUV spectrum of titanium free platform. 145

Figure 77 DRUV spectra of 2C-Ti-1st gen, 3C-Ti-1st gen, and 4C-Ti-1st gen after the tin .. correction. 146

Figure 78 Typical NMR spectrum used for the characterization of catalytic activity for the oxidation of TMP to TMBQ. 149

Figure 79 NMR Spectrum of a typical oxidation reaction for the conversion of DMOP to DMBQ. 150

Figure 80 Illustration of the three different active sites. 153

Figure 81 Illustration of how the surrounding matrix effects the accessibility of substrate to the active site. 153

Figure 82 Illustration of the proposed open the 4C-Ti active site. 154

Figure 83 Illustration of the accessibility of two fully embedded 4-connected catalysts, first generation tetrahedral (left) and second generation square planar after imprinting ligand removed (right). ……156

Figure 84 Flow chart illustration the modification of the Ti active site. Blue arrows indicate first dose, red arrows indicate second dose, and green arrows indicate heating. Boxes of the same color represent catalysts predicted to have the same active site but different synthetic pathways. 158

Figure 85 Illustration of the trans (left) and cis (right) metal chloride complexes. 159

Figure 86 FTIR Spectrum of cis $TiCl_4(MeCN)_2$. 161

Figure 87 FTIR spectrum of $TiCl_4(THF)_2$. 162

Figure 88 XANES spectrum for $TiCl_4(THF)_2$. 163

Figure 89 EXAFS spectra (blue) overlaid with fits obtained from FEFF modeling (red) for k space (top left), q space (top right), and R space (bottom center) for *trans* TiCl4(THF)2. 165

Figure 90 FTIR spectrum of $TiCl_4py_2$ after the first addition of pyridine (purification step). The inlay is a blow up of the pyridine finger print region illustration both BrØnsted and Lewis pyridine are in the material. 168

Figure 91 FTIR spectrum of purified $TiCl_4py_2$ showing only Lewis pyridine. 169

Figure 92 FTIR spectrum showing the pyridine fingerprint region of $TiCl_4py_2$ after being stored for six months. 170

Figure 93 FTIR spectrum of $TiCl_4py_2$ illustration the absorption bands are not split indicating this complex has D_{4h} symmetry. 171

Figure 94 XANES spectrum of trans $TiCl_4py_2$. 172

Figure 95 EXAFS spectra (blue) overlaid with fits obtained from FEFF modeling (red) for k space (top left), q space (top right), and R space (bottom center) for *trans* $TiCl_4py_2$. 173

Figure 96 FTIR comparison of the 2C-1st generation precursor ($Ti(OiPr)_2Cl_2$, blue) and the 2C-2nd generation precursor ($Ti(OiPr)_2Cl_2py_2$, green) with an inset of the pyridine fingerprint region. 176

Figure 97 FTIR comparison of the 3C-1st generation precursor ($Ti(OiPr)Cl_3$, blue) and the 3C-2nd generation precursor ($Ti(OiPr)Cl_3py_2$, green) with an inset of the pyridine fingerprint region. 177

Figure 98 FTIR spectrum of a 4C-2nd gen Ti catalyst heated to 80 ^{0} C after the first dose to remove the pyridine blocking ligand. 180

Figure 99 XANES spectrum for a 4C-Ti-2nd generation catalysts with blocking ligand removed after the first dose. 182

Figure 100 FTIR spectra showing only the pyridine finger print region for 3rd generation catalysts, 2C-Ti-3rd gen (green), 3C-Ti-3rd gen (blue), 4C-3rd gen (purple), and a titanium free platform (yellow). 184

Figure 101 XANES spectra comparing 4C-1st gen (green) to 4C-3rd gen (red) and 4C-2nd gen pyridine removed after the first cross-linking (blue). 185

Figure 102 FTIR spectra of 4C-1st gen (red) and 4C-2nd gen with THF_2 (blue). 187

Figure 103 FTIR spectra of 4C-1st gen (red) and 4C-2nd gen with $MeCN_2$ (blue). 188

Figure 104 FTIR spectra of 4C-1st gen (red) and 4C-2nd gen with THF_2 (blue) with THF as the reaction solvent. 189

Figure 105 FTIR spectrum of 4C-2nd gen with py_2 dried at room temperature after the second cross-linking. The inset is a blowup of the pyridine fingerprint region illustrating only Lewis absorption bands. 190

Figure 106 XANES spectra of 4C-1st Gen (red) and 4C-2nd Gen with py_2 (blue). 191

Figure 107 R plot for 4C-2nd gen with py_2 after the second cross-linking reaction illustration two different coordination ligands. 193

Figure 108 FTIR spectra of 2C-2nd gen with py_2 (green) and 3C-2nd gen with py_2 after the second cross-linking reaction. 194

Figure 109 NMR spectrum of the volatiles after drying 2C-2nd gen with py_2 at room temperature after the second dose. 195

Figure 110 Illustration of heating 2nd gen with py_2 catalysts to create 2nd gen py removed catalysts and thus opening the active sites. 198

Figure 111 Pyridine finger region of the IR spectrum of the 3C-2nd gen py removed catalyst. 201

Figure 112 XANES spectrum for 4C-2nd gen py removed. 202

Figure 113 R plots for 4C-2nd gen with py2 (left) and after heating to remove blocking ligands, 4C-2nd gen py-removed (right). 202

Figure 114 DRUV overlays for 4C-Ti catalysts. 203

Figure 115 DRUV overlays for 3C-Ti catalysts. 203

Figure 116 DRUV spectra for 2C-Ti catalysts. 204

Figure 117 Illustration of a suspected geometry of 3C-2nd gen py-removed catalyst. 208

Figure 118 Recyclability of 3C-2nd gen py-removed (blue) and 3C-1st gen (green) in terms of conversion (solids) and selectivity (hashed). The additional bars (red and

orange) on cycles 2 and 3 illustrate the percent conversion at infinity. 219

Figure 119 NMR spectrum of a typical aliquot take ten minutes after the addition of hydrogen peroxide. 221

Figure 120 Typical NMR spectrum taken at 60 minutes after the addition of hydrogen peroxide illustration the two sets of doublets corresponding to the two major side products. 223

Figure 121 Proposed structures of three side products formed during the oxidation of TMP..... 224

Figure 122 1H NMR spectrum of the isolated side product A. 225

Figure 123 HMBC spectrum of reaction mixture before separation identifying four different non-protonated carbons. 227

Figure 124 HMBC spectrum of side product A. 228

Figure 125 Structural pattern confirmed through HMBC experiments. 229

Figure 126 HSQC of side product A. 230

Figure 127 COSY spectrum of side product A. 231

Figure 128 NOESY spectrum of side product A. 232

Figure 129 Side product A with number carbon atoms. 233

Figure 130 Structure of side product B with numbered carbon atoms. 234

Figure 131 NMR spectrum of column fraction containing both side product B and its corresponding dimer. 235

Figure 132 Proton spectrum illustration increase in dimer concentration and decrease in the concentration of side product B. 236

Figure 133 Proposed structure of the dimer with numbered carbon atoms. 238

Figure 134 Illustration of the epoxidation of cyclohexene to cyclohexene oxide with cumene hydroperoxide in the presence of a titanosilicate catalyst. ……...241

Figure 135 An example of a typical NMR spectrum form an aliquot of the epoxidation reaction. Figure obtained from ref [128]. ……..242

Figure 136 Illustration of a 4C-Ti fully embedded site reacting with peroxide and ultimately breaking a Ti-O-Si linkage. 246

Figure 137 Illustration of imprinting the catalytic center of a 4C-Ti to a more open site. .. 251

Figure 138 Proposed structures of a 4C-2nd gen catalysts imprinted with a cis molecular precursor (left) and the proposed resulting active site after the active site is locked into the matrix and blocking ligand are removed (right). 255

Figure 139 Illustration of mononulear titanosilicates (a) and dinuclear titanosilicates (b). 256

Figure 140 Proposed mechanism for the oxidation of phenols with dinuclear titanium catalysts. Figure obtained from ref [59]. 256

Figure 141 Polynuclear titanium precursors, Trinuclear (top left), tetranuclear (top right), and dinuclear (bottom). The titanium atoms are illustrated in yellow, bridging oxygens in red, and reactive chloride ligands in green. 257

Chapter I: A Brief Overview of Heterogeneous Catalysts

Introduction to Catalysis

What is catalysis?

The first records of catalysis date back to the early signs of civilization when fermentation was used to produce alcohol. However, it was not until 1835 when the Swedish chemist, Jön Jacob Berzelius coined the term catalysis while trying to unify and understand what other scientists had been accomplishing over the last several decades.[1,2] Berzelius stated:

> *"It is, then, proved that several simple or compound bodies, soluble and insoluble, have the property of exercising on other bodies an action very different from chemical affinity. By means of this action they produce, in these bodies, decompositions of their elements and different recombinations of these same elements to which they remain indifferent."[3]*
> *"This unknown body acts by means of an internal force, whose nature is unknown to us. This new force, up till now unknown, is common to organic and inorganic nature. I do not believe that this force is independent of the electrochemical affinities of matter; I believe on the contrary, that it is a new manifestation of the same, but, since we cannot see their connection and independence, it will be more convenient to designate the force by a new name. I will therefore call it the "Catalytic Force" and I will call "Catalysis" the decomposition of bodies by this force, in the same way that we call by "Analysis" the decomposition of bodies by chemical affinity."[2]*

In other words, a catalyst is a substance that alters the rate of a reaction without experiencing permanent changes to itself, and without influencing the overall thermodynamic equilibrium for the reaction, Figure 1.[4] Catalysis is defined as the chemical process of increasing reaction rate. Essentially all biochemical processes use catalysts to achieve high efficiency and today, more than 90% of industrial chemicals and chemical processes utilize catalysts in one or more of their reaction steps.[5-7]

There are two types of catalysts, enzymatic and synthetic. Enzymes are naturally occurring catalysts that the human body and living organisms utilize to enhance virtually all reactions needed for survival, e.g., photosynthesis, breakdown of proteins, and oxidation of sugars to CO_2, water, and energy.[7] The active site of enzymes are often proteins surrounded by inorganic nanoclusters in solution or they are supported by membranes.[8] Enzymes can be considered the ideal model for synthetic catalysts. Enzymes are able to convert biological molecules at high

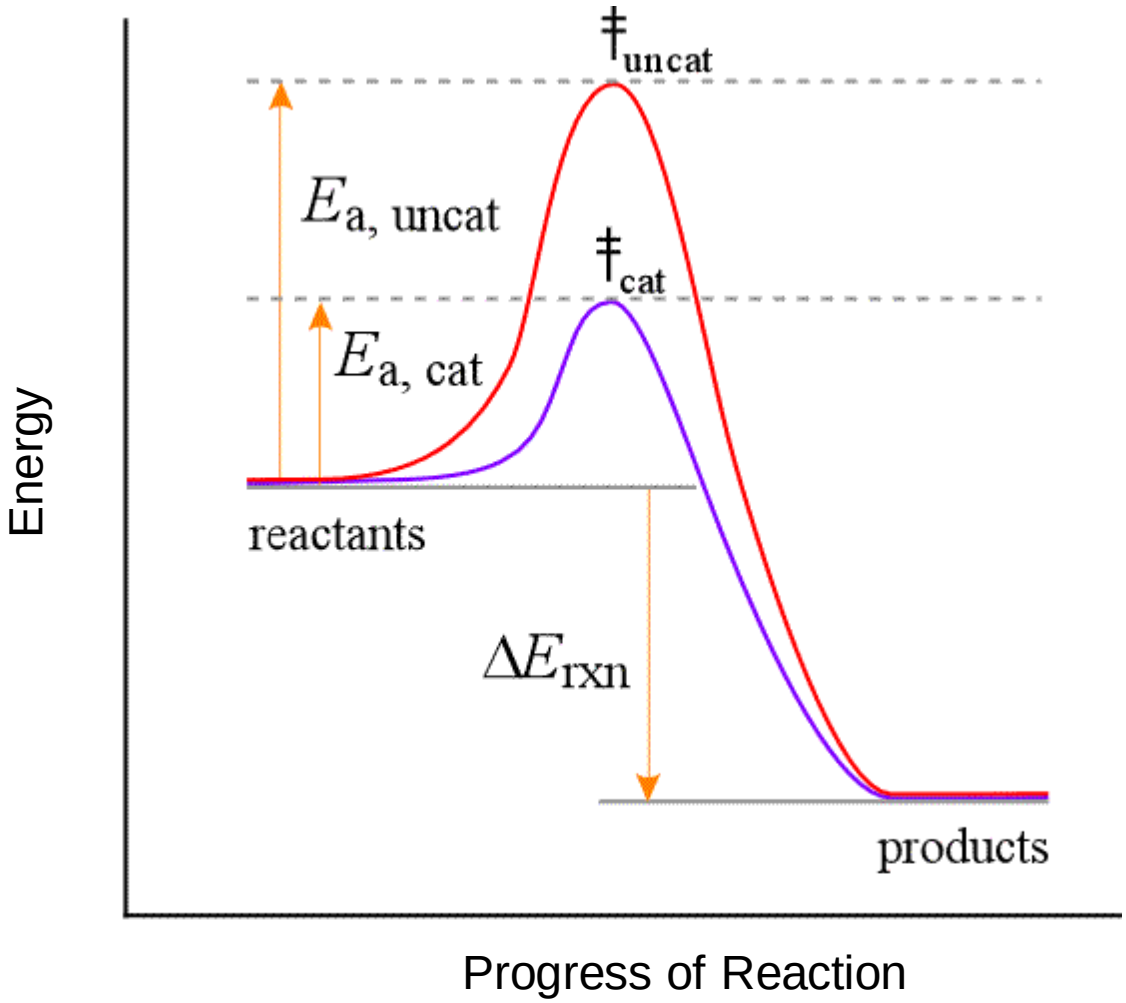

Figure 1 Illustration of the energy diagram for an uncatalyzed reaction (red) and a catalyzed reaction (purple) showing the catalyzed reaction exhibits a lower energy barrier (activation energy) than its analogous uncatalyzed reaction. Figure modifed from ref [4].

rates with extraordinary selectivities.[7]

The second type of catalyst is used in industrial chemical processes. Industrial catalysts are used as a cost effective method in a wide range of processes involving the production of fine chemicals as well as the large-scale production of fuels. These catalysts can be found in a wide range of industries; from food production to pharmaceuticals. The United States produces several trillion dollars of goods via catalysts annually while the cost of new catalysts and replacement/regeneration of catalysts is approximately 1% of the revenue.[9]

Synthetic catalysts are broken down into two different sub groups, homogenous and heterogeneous catalysts. Homogenous catalysts are in the same phase as the reactants and products, typically, but not limited to, the liquid phase.[10] Homogeneous catalysts are often soluble acids and bases or metal complexes that operate under mild reactions conditions; 0 – 150^0 C. High pressures are frequently needed to keep the reactants and catalysts in the same phase when functioning at higher temperatures. This leads to higher costs in such processes.

A major benefit of using homogenous catalysts is that typically all catalytic entities are identical and each acts as an identical active center. This property leads to high activity and selectivity.[10] The ability to tailor homogenous catalysts also gives rise to an increase in selectivity. In the case of metal based homogeneous catalysts, frequently, varying the metal center, ligands, and reaction conditions, leads to catalytic reactions having selectivities greater than 90%. The major disadvantage of homogeneous catalysts is the difficulty of separation due to the catalyst, reactant, and/or product(s) being in the same phase. While methods for separating and recycling these catalysts exist, they can be extremely costly and reduce their potential as industrial catalysts.[11]

Heterogeneous Catalysts

Heterogeneous catalysts are in a different phase than the reactants and products. They are commonly present in the following phase combinations: 1) solid catalysts – gas reactants; 2) solid catalyst – liquid phase reactants; and 3) catalysts and reactants dissolved in immiscible solvents.[12,13] Unlike homogenous catalysts, heterogeneous catalysts are often inorganic solids that are both chemically and thermally robust, capable of enduring temperatures up to many in which a substrate binds to an active surface site. The interaction between the active surface site and the reactants produces intermediates with lower energy barriers than the analogous uncatalyzed reaction.[14]

Heterogeneous catalysts are preferred over homogeneous catalysts in industry because they are more cost effective than homogenous catalysts with their ease of recovery, reusability, and separation from products.[15] However, the synthetic methods for synthesis are not as well developed as for homogenous catalysts, often leading to multiple active sites, low atom efficiency, and low selectivity. Additionally, the high energy (high temperature) reaction conditions potentially activate several reaction pathways which also leads to lower selectivity and raises environmental concerns.[16]

Preparation of Heterogeneous Catalysts

In general, heterogeneous catalysts are either supported metal catalysts or as single component materials.[17,18] The focus of heterogeneous catalysts in industry primarily relies on high surface area solid supports doped with an active component.[19] A variety of strategies have been developed for the synthesis of supported heterogeneous catalysts. These preparation methods can be broken down into two groups depending on the type of active site they produce namely embedded or surface catalytic sites. Embedded sites are typically prepared by incorporating the active site during synthesis and generally have multiple bonds to the supporting matrix. On the contrary, surface sites are deposited onto the solid support post synthesis and typically have fewer linkages to the matrix than embedded sites. In extreme cases, only one bond may link the active site to the matrix.

Embedded Sites

The most common methods for producing embedded heterogeneous catalysts are hydrothermal synthesis, sol-gel synthesis, and templating which is sometimes considered subcategories of the sol-gel method.[20] Each method of synthesis is described in the following sections.

Sol-gel Synthesis

Sol-gel synthesis has become the most common procedure for producing heterogeneous catalyst due to the relatively inexpensive nature of the reactants, simplicity of the reaction, and mild reaction conditions. The first discovery of this strategy was in the middle of the 19th century by Ebelman and Graham. They observed that in acidic medium, the hydrolysis of tetraethylorthosilicate (TEOS) resulted in a “glass like material” of SiO_2.[21] Since then, sol-gel synthesis has been extensively studied and there are two primary categories for sol-gel chemistry,

aqueous and non-hydrolytic. These synthetic approaches produce solids with high surface areas and high porosities, typically in the mesoporous or macroporous range at low temperatures.[22]

Aqueous sol-gel synthesis revolves around two reactions, hydrolysis and condensation, typically with metal alkoxides because they are relatively inexpensive and they readily react with water. The term *sol* refers to the dispersion of colloidal particles in a solution while the term *gel* denotes the unified, rigid network of discrete monomers or polymers.[21]

The first step in this process is to form the sol. This can be achieved by mixing colloidal particles in water at a specific pH that prevents precipitation followed by hydrolysis. Metal alkoxides, in the presence of water, hydrolyze to form metal hydroxides and alcohols, Equation 1.

$$M - OR + H_2O \rightarrow M - OH + R - OH \qquad \text{Equation 1}$$

After the formation of metal hydroxides, a condensation reaction occurs between the metal hydroxide and metal alkoxide (Equation 2) or between two molecules of metal hydroxide (Equation 3), producing either alcohol or water respectively.[23]

$$M - OH + M - OR \rightarrow M - O - M + R - OH \qquad \text{Equation 2}$$

$$M - OH + M - OH \rightarrow M - O - M + H_2O \qquad \text{Equation 3}$$

Following the condensation reaction, a process known as gelation occurs. During gelation, a repetitive series of hydrolysis and condensation reactions forms a 3D network resulting in a gel. A gel's physical characteristics depend on both the size of the particles and the number of cross-linking reactions that occur prior to gelation.[21] It is important to note that during the gelation process, the solid remains impregnated by the solution.[20]

Next, the gel is allowed to age. The aging process, also known as syneresis, involves forming more cross-links and can last for a few hours or several days. The aging process ultimately increases the thickness of the gel and decreases the porosity of the material.

After the aging process, the gel is dried to remove remaining solvent from the pores of the network. The drying process ultimately determines the type of material synthesized, xerogels or aerogel, Figure 2. A xerogel is characterized by solvent evaporation under normal conditions.

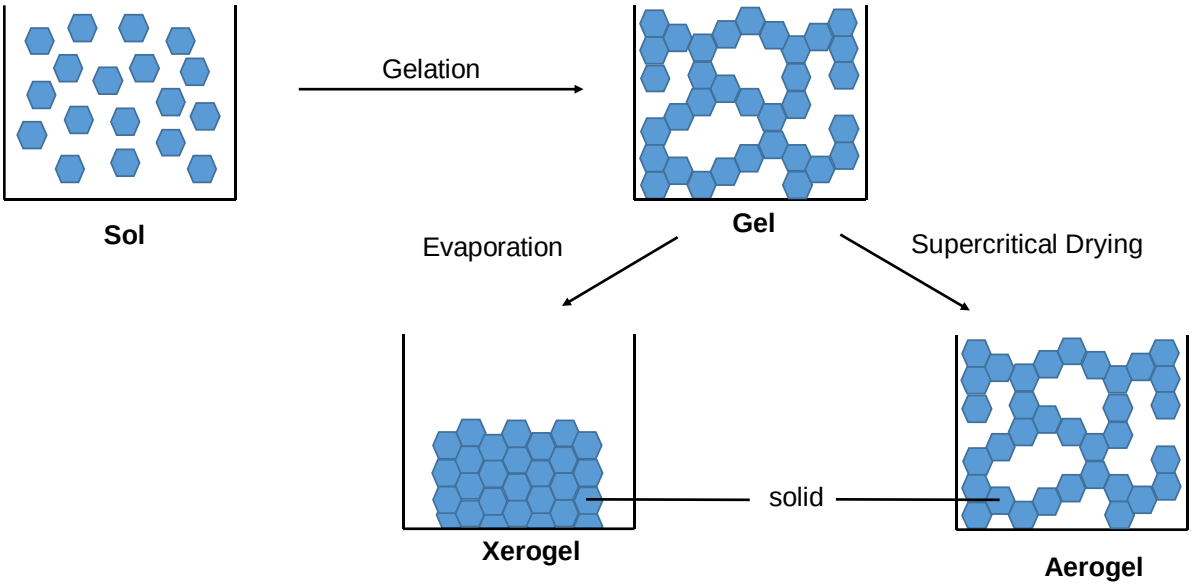

Figure 2 Overview of the sol gel process illustrating the difference between xerogels and aerogels.

Unfortunately, this drying process often leads to large capillary stresses which ultimately lead to the pores collapsing during the drying process. In contrast, aerogels are dried in autoclaves under super critical conditions which does not produce capillary stresses and therefore the pores are relatively stable.[21,24]

There are several key advantages to aqueous sol-gel chemistry; 1) the materials synthesized are often very pure and their compositions are precisely controlled. 2) At the molecular level, the structure and homogeneity can be controlled by tailoring various parameters such as concentrations of precursors, amount of water, temperature, etc. 3) The texture of the gel material can be controlled by the aging process.[25] These properties are often tailored by the adjusting the rates of the hydrolysis and condensation reactions.[26]

At the same time, it is very difficult to precisely and simultaneously control all three of these advantages when preparing mixed metal oxides. In addition, these materials frequently are microporous as a result of capillary forces at the liquid vapor interfaces which ultimately leads to pore collapse. One way to overcome capillary forces is through the use of templating agents.

Templating

Over the past two decades, significant effort has been devoted to developing synthetic methodologies for producing mesoporous materials for heterogeneous catalysis. Materials are classified as mesoporous by having pores with diameters ranging between 2 nm – 50 nm. The most practiced approach to achieving mesoporous materials is through templating. Templating synthesis is a subcategory of the sol-gel process producing amorphous materials with high surface area and well-ordered pore structures.

There are two types of templating methods: hard or soft templating. Hard templates contain well defined voids with rigid shapes capable of forming channels, pores, or linked hollow spaces. Soft templates are frequently organic surfactants, polymers, and occasionally biological viruses. In contrast to hard templates, soft templates are relatively flexible in shape.[27] Soft templates generally act as structural directing agents assisting the formation of the mesophase. Initially, the soft template is added to an aqueous solution where micelles form. In low concentration, the surfactant templates exist as monomers but as the concentration increases, the micelles spontaneously self-assemble to arrangements specific to the original template to decrease the entropy of the system.[28] The silica precursor is then added to form the silica matrix around the micelles. The templating agent is then removed from the matrix by either calcination at high temperature or repetitive washings.[24] The resulting materials exhibit high

surface areas with ordered porosity. Figure 3 illustrates the general soft templating process often used to synthesized templated mesoporous silica.

The most widely studied and used templated mesoporous materials are MCM-41 (Mobil Crystalline Material) and SBA-15 (Santa Barbra Amorphous).[24] Both materials are synthesized using soft templates, but MCM-41 is synthesized using cationic surfactants while SBA-15 is synthesized using nonionic surfactants. By varying the ratio of silicon precursor to surfactant template, the structures of the resulting material can be influenced. For example, Figure 4 illustrate three different MCM materials with different structures: MCM-50 (left) has a layered structure while MCM-41 (middle) exhibits a hexagonal structure, and MCM-48 (right) has a cubic structure. If the ratio of surfactant to silicon is less than one, MCM-41 is produced. When the ratio is greater than one, MCM-48 is produced and at even larger ratios the layered structure of MCM-50 is obtained.[29,30] Similarly, different structures of SBA materials have been synthesized.

Metal cations can be incorporated into the framework of these mesoporous materials during synthesis by first constructing a gel containing the metal cations and silicon followed by the addition of the surfactant templates.[31] The resulting heterogeneous catalysts have high surface areas, but there is little, if any, control of the dispersion on metal cations.

While templating agents eliminate the collapse of the pore structure and allow for the synthesis of mesoporous materials, there are several drawbacks to templating sol-gel synthesis. First, the cost of the templating materials is relatively high in comparison to traditional sol-gel syntheses. Second, the stability of the support and the active material is insufficient for many industrial properties. The active species in these templated materials often leaches from the surface therefore negating the title of a heterogeneous catalyst.[32]

Non-hydrolytic Sol-gel

Another limitation to traditional sol-gel syntheses is the dependence on the rate of hydrolysis. In the case of mixed metal oxides such as $ZrTiO_4$ the rates of hydrolysis are very different for the zirconium and titanium precursors. In order to overcome the difference in rates, complexing agents are used to decrease the hydrolysis rate of the more reactive precursor. Unfortunately, this typically leads to a significant increase in cost and decrease in the regulation of homogeneity. One way to eliminate the problem of different hydrolysis rates is to use a non-hydrolytic sol-gel approach.[26,33]

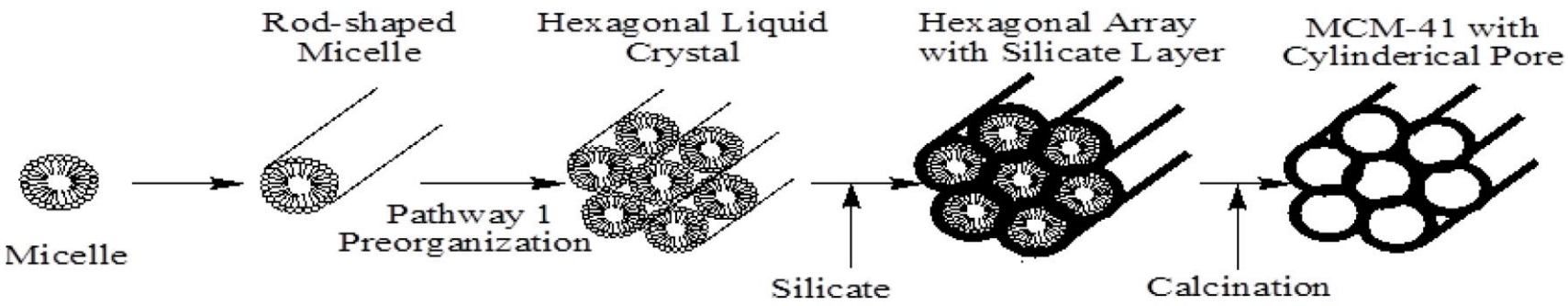

Figure 3 Illustration of soft templating process. Figure modified from ref [28].

Figure 4 Illustration of the different pore structures of three MCM materials (layered MCM-41, hexagonal MCM-41, and cubic MCM-48). Figure obtained from ref [28].

About 20 years ago, an alternate route to sol-gel chemistry was developed by Vioux and coworkers in which the condensation step occurs in a non-aqueous medium.[33,34] In contrast to aqueous sol-gel chemistry, when water is neither the oxygen donor nor produced *in situ* the reaction is considered non-hydrolytic.[25] Typically oxygen donors include, but are not limited to, ethers, alkoxides, ketones, alcohols, etc. Non-hydrolytic synthesis routes (NHS) can be classified depending on the precursors (chlorides, alkoxides, acetylacetonates, etc.), the oxygen donor, and the nature of the molecule eliminated (alkyl halide, ether, ester, etc.). For example, Equation 4 shows the generic reaction of a metal chloride with a metal alkoxide and thus eliminating an alkyl halide, namely *alkoxide route*.

$$M - Cl + M - OR \rightarrow M - O - M + R - Cl \qquad \text{Equation 4}$$

In the *ether route*, a metal alkoxide is produce *in situ* according to Equation 5 followed by the formation of the M-O-M bond in a second step according to Equation 4. While these are not the only two non-hydrolytic routes, they are the most common and the most investigated.

$$M - Cl + ROR \rightarrow M - OR + R - Cl \qquad \text{Equation 5}$$

Non-hydrolytic synthesis routes have been able to overcome several limitations of aqueous sol-gel synthesis. In contrast to traditional aqueous routes and hydrothermal synthesis (which will be described below), the syntheses of mixed metal oxide proceed at relatively mild temperatures 80-150^0 C under non-hydrolytic conditions. Additionally, it is fairly simple to tailor the structure and morphology of these materials due to the wide variety of precursors and oxygen donors available. Furthermore, capillary stress is rarely observed for materials prepared by NHS. This can be attributed to the lack of interaction between the surface (precursor) and the liquid phase (solvent) accompanied by the low surface tension of these solvent compared to water.[25] Non-hydrolytic syntheses have been shown to be very successful in the production of well-defined amorphous metal oxides with precise shapes and sizes, but lacks control of the number of linkages from the catalytically active metal to the support leading to mixtures of active sites within these matrices.

Hydrothermal Synthesis

Hydrothermal synthesis, or solvothermal synthesis, was first discovered by Sir Rodrick Murchison, a geologist, when he observed different formations of rock at elevated temperatures and pressures. Hydrothermal refers to a closed system of heterogeneous solutions dissolved at high temperatures and pressures followed by subsequent recrystallization.[35] While there is no

regulations on the conditions necessary to qualify as a hydrothermal synthesis, the process Iusually occurs above 100^0 C and above 1 atm.

Zeolites are a prime example of materials which are produced via hydrothermal synthesis. Zeolites are crystalline silicate materials with tunable frameworks and discrete micropores, Figure 5.[36] These materials have been widely used in ion exchange, adsorption and separation, and heterogeneous catalysis.[37] While zeolites have been shown to be effective catalysts in the conversion of small molecules, they suffer from mass transport issues as a result of their microporous structure, typically 4 – 12 Å.

Surface Sites

In contrast to the syntheses presented above, heterogeneous catalysts with surface active sites can also be fashioned. The most common synthetic routes to surface species are impregnation, grafting, and tethering catalytically active species (typically metal ions) to a solid support. These supports may include complex metal oxides, aluminosilicates, and polymers with amorphous or crystalline properties. However, the most common support is silica (SiO_2) due to its wide variety of surface morphologies and high surface area. The catalytic active sites are bound to the surface of silica via surface hydroxyl groups (Si-OH) which can exist as three different types pictured in Figure 6. Similar to approaches for producing embedded sites, these techniques rarely produce single-site catalysts, but rather a mixture of sites. Each of these approaches will be briefly discussed in the following paragraphs.

Impregnation

Impregnation, is one of the oldest techniques used for producing heterogeneous catalysts and is dependent on the interactions between a solid support and ions dissolved in solution followed by drying. There are two types of interaction. The first interaction is simply physisorption of ions to the pores of a solid support; there is no chemical interaction. The second interaction relies on ion exchange between the acidic protons of surface hydroxyl groups on the silicate matrix and the ions in solution. The total volume of ion solution dictates the classification of the impregnation process, either “wet” impregnation or “dry” impregnation.

Wet impregnation refers to the use of an excess of ion solution compared to the total pore volume. In contrast, the total volume of ion solution is equal to the total pore volume in dry impregnation. Consequently, dry impregnation typically relies on physisorption while wet

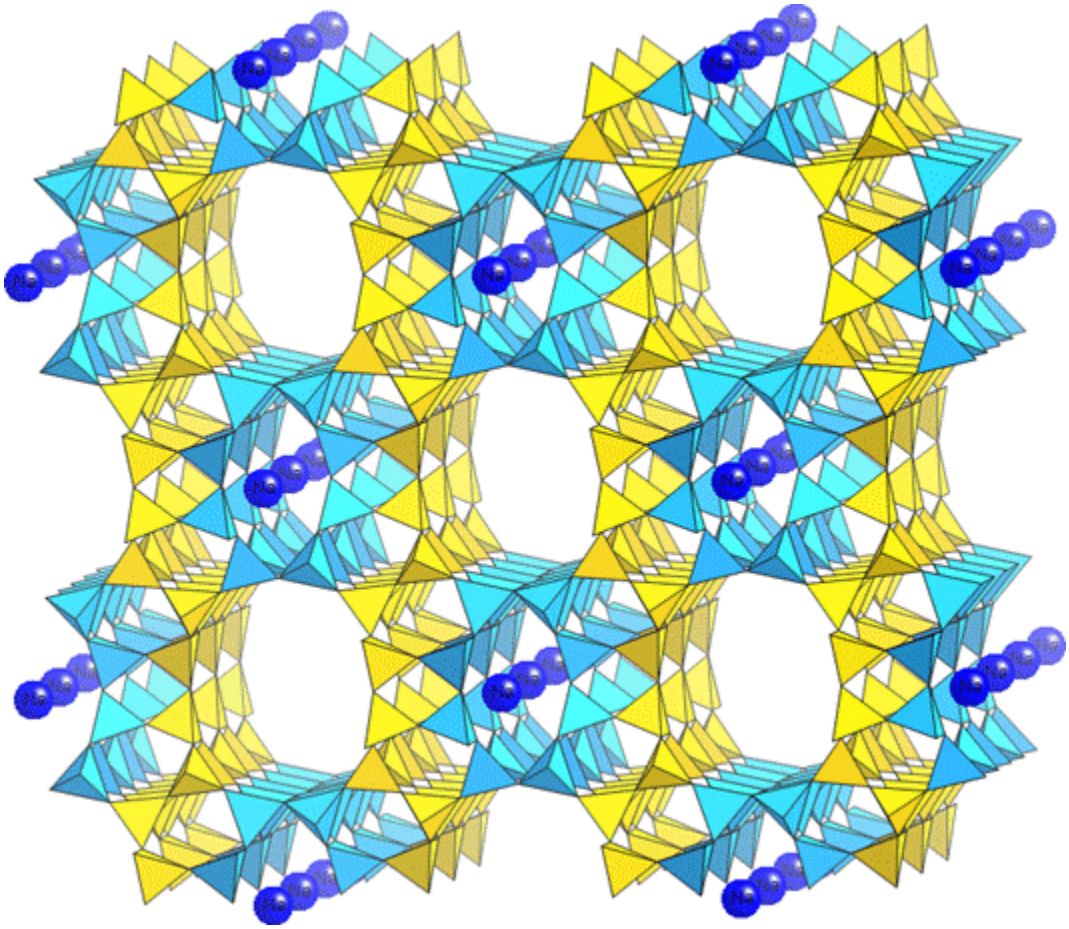

Figure 5 Illustration of the zeolite mineral mordenite (MOR): SiO_4 polyhedra are represented as yellow tetrahedron; AlO_4 polyhedra are aqua tetrahedron. Figure obtained from ref [37].

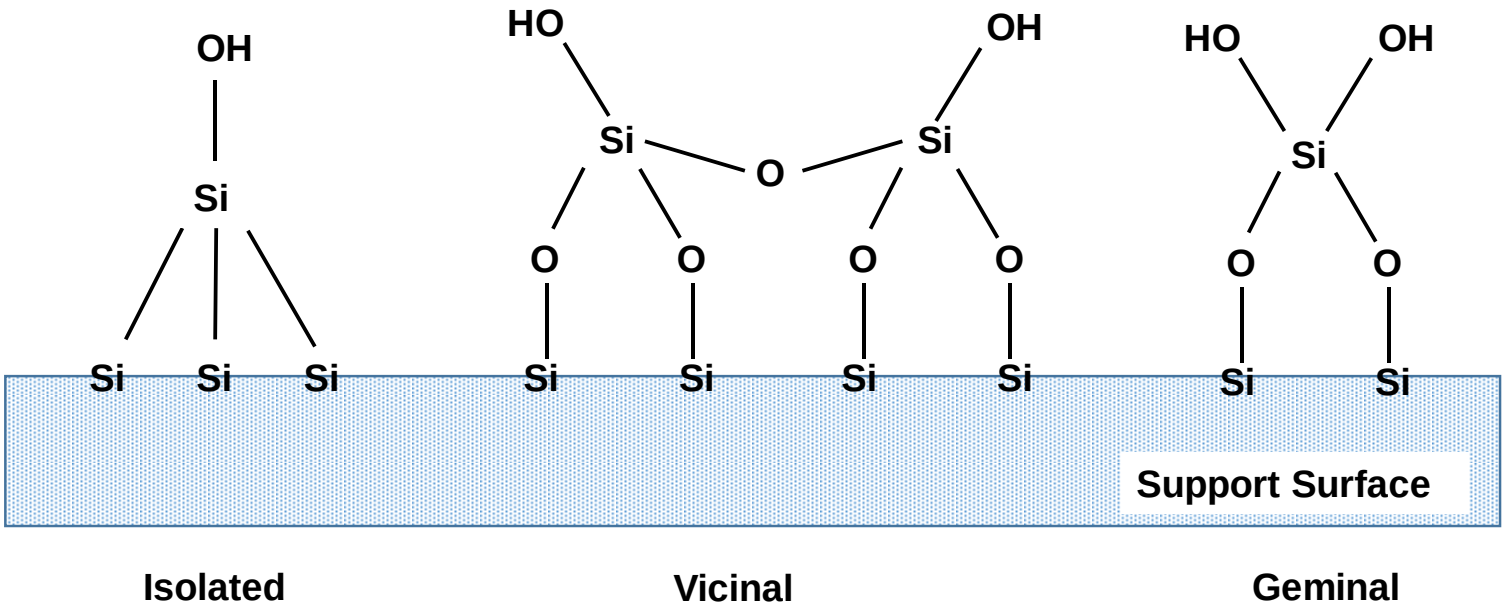

Figure 6 Different types of surface silanols.

impregnation generally utilizes ion exchange. The main advantage of dry impregnation is that the weight of the active catalyst added to the support can be easily controlled by regulating the concentration of ions in solution. However, this does not mean the active sites will be uniformly distributed throughout the matrices. This results in catalytic domains throughout the surface. Figure 7 shows that catalyst loading is dependent on pore volume, i.e., the larger the pore volume the more solution that fills the void, and the more catalyst remains after drying.

While dry impregnation is easier to control, wet impregnation can be tailored to yield a uniform distribution of active sites. By using multiple does, or going through the wet impregnation process more than once, the active sites can be distributed through the bulk of the material. This can be attributed to the ion change of acid hydrogens and the ions in solution.

In either case, control of the drying step is critical. If drying occurs too rapidly, vapors form in the deep pores pushing the catalysts to the outskirts of the pores or even onto the exterior surface of the support. This buildup may actually lead to pore blockage.[18]

Grafting and Tethering

Grafting and tethering, sometimes referred to as anchoring, are a slight variation of impregnation in that the organometallic or inorganic precursors are specifically chosen to interact with the surface functionalities of the support materials. The difference between grafting and tethering occurs in the type of linkage between the surface and the active metal, Figure 8. Grafting refers to the direct linkage of a metal to the surface through an oxygen bridge. In contrast, tethered sites are attached to the surface via a linker or spacer.[38]

Different synthetic strategies are employed for grafting and tethering approaches. Grafting involves the elimination of a labile ligand from the precursor. To tether an active site, one must first modify either the precursor, or the support to form this new linkage. Most frequently, tethering is used to anchor homogenous catalysts to a support while grafting is used as synthetic approach to produce more traditional heterogeneous catalysts.

Unfortunately, grafting can lead to multiple active sites. Previously, we saw that there are several types of silicate surface functionalities: isolated, vicinal, and germinal. Depending on the preparation protocol of the silica support, either a specific type of surface species or a mixture of species can be present. Therefore, the resulting material can have a variety of active sites. In addition, the concentration of surface silanols plays an important role on the type of grafted site, Figure 9.[38] This mixture of sites has the potential to decrease selectivity and significantly

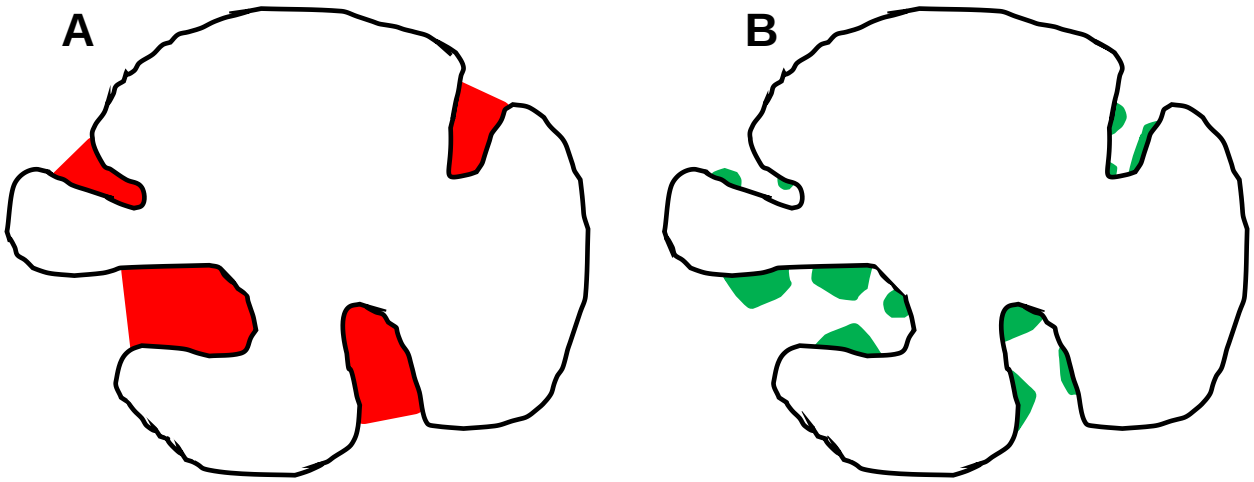

Figure 7 Illustration of larger pores will take up a larger volume and result in larger crystallites. Figure was reproduced from ref [18].

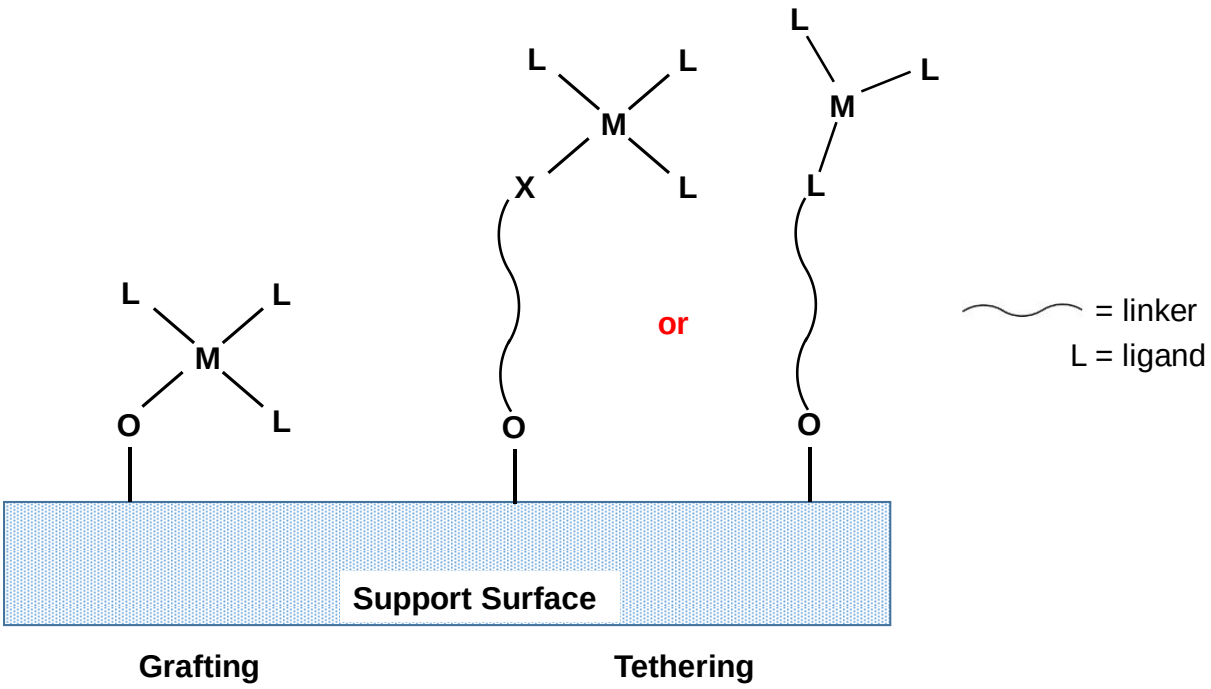

Figure 8 Illustration of grafted verse tethering active sites to a solid support. Figure modified from ref [38].

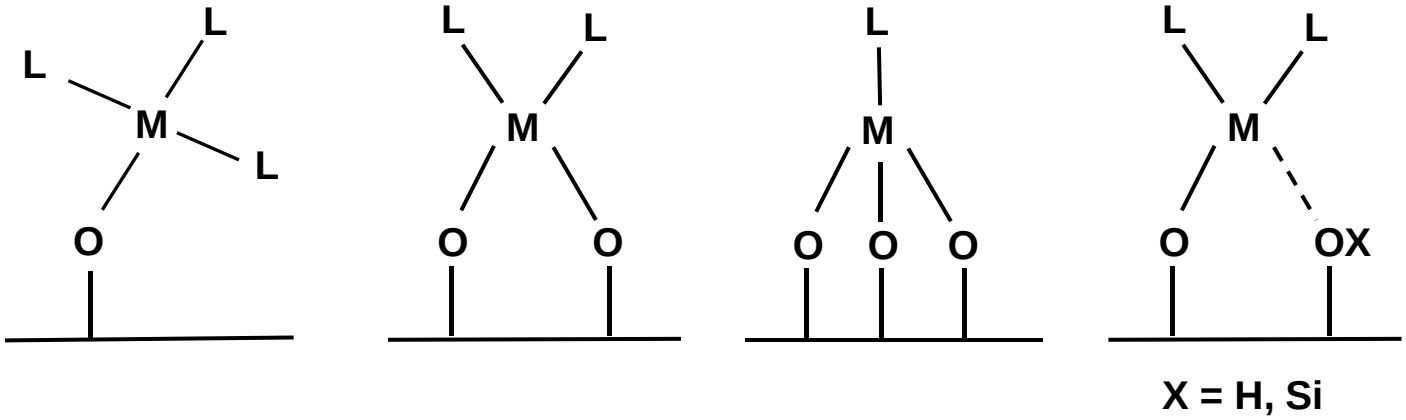

Figure 9 Connectivity of grafted complexes and secondary M-$O_{(X)}$Si interaction. Figure reproduced from ref [38].

increases the difficulty of characterization. Unique active sites can produce different interfering spectroscopic signals.

General Conclusion on Traditional Synthesis of Heterogeneous Catalysts

Heterogeneous catalysts are typically composed of an active metal either embedded within a solid support matrix, or on the surface of the supporting material. While there are other synthetic approaches to synthesizing, and designing heterogeneous catalysts, the strategies presented here are the most common. Unfortunately, the majority of these synthetic methodologies do no produce catalysts that are stable enough in application or lack the control to incorporate identical, single-site active centers within support matrices. While hydrothermal synthesis is capable of producing single-site catalysts, it lacks the mesoporosity ideal for catalytic applications. Therefore, a synthetic approach that allows for the synthesis of single-site mesoporous heterogeneous catalysts is still desired. This notion of single-site heterogeneous catalysts has been brought up over and over. The next sections discuss the components of the active site and the meaning of a single-site heterogeneous catalyst.

The Active Site

In order to understand how to tailor a heterogeneous catalyst, one must first understand the components that make up the active site. In heterogeneous catalysis, an active site is more complex than the catalytic metal center and the support matrix. A synthetic approach for designing specific active sites, should include everything in the immediate vicinity of the catalytic center the metal itself, the support, the number of linkages between the metal center and the support along with the organization of the bonds, i.e., the metal imprint and accessibility to the site by the substrate. Additionally, one must consider the surface area and site density of the material, i.e., porosity. Furthermore, the rate at which substrate travels through the pores to the active site must be considered. In heterogeneous catalysis, the mesopore range has proven to be ideal for reducing mass transport issues.

Single-Site heterogeneous catalysts

The primary advantage of homogeneous catalysts to heterogeneous catalysts is the notion that their active sites are both well-defined and spatially separated from one another leading to single site catalysts similar to enzymes in nature. Therefore, a primary focus in heterogeneous catalysis over the last two decades has been the synthesis of well-defined heterogeneous single-site catalysts. J. M. Thomas *et al.* describes the principle theory behind single-site heterogeneous catalysts as each and every active site being identical not only in their

atomic environment, but also in their energetics from interaction with substrates.[39,40] Each active site, consisting of one or more atoms, is spatially separated from other catalytic sites so that there is no interaction, spectroscopically or energetically, between one active site and another.[41] Additionally, all active sites are well-defined similar to homogenous catalysts.[39,40] Perhaps the *nonpareil* example of single-site catalysts are enzymes. There are several advantages to catalysts being both single-site and heterogeneous:

1. More selective towards products
2. Easily separated from products and reactants
3. Recyclability of the catalyst
4. Simplified characterization of the active site
5. Computational approaches become available
6. Broad spectrum of strategies of designing new catalysts
7. Tailoring of the active site both structurally and electronically

Synthesis of Single-Site Heterogeneous Catalysts

Single-site heterogeneous catalysts can be broken down into four principal categories based on the type of catalytic species produced: 1) distinct isolated ions, atoms, molecular complexes and clusters on high surface area supports, 2) anchored organometallic complexes, 3) “ship-in-bottle” structures, and 4) open-structure porous solid catalysts.[39] A brief description and example of each category will be presented below.

1. Individually isolated ions, atoms, and molecular complexes on supports. Each subcategory of isolated catalytic sites on supports will be described individually since they each possess their own distinct characteristics.

   Ions – The most common transition metal precursors used to graft metal ions to the surface silica supports are metallocene and metal alkoxy species.[42] After the discovery of MCM-41 by Mobil Oil Company, the preparation of ions on supports became of great interest.[43] Incorporation of a variety of metals, including (but not limited to) Ti(IV)[44], Mo(VI)[45,46], Co(III)[47], and VO(IV)[48] have been reported. By grafting these materials onto the surface of silica followed by calcination, covalent bonds are formed and the remaining organic groups are removed. Two different types of active sites can be formed, atomically dispersed, or polynuclear clusters. However, in order to obtain atomically

dispersed centers, the amount of precursor must be small enough to avoid the formation of M-O-M bridges leading to low concentrations of active sites.

Atoms – Single atoms are often localized to an oxygen anion vacancy in the solid support via electron charge transfer.[40] Abbet and coworkers have shown that a single palladium atom supported on magnesia (MgO) is responsible for the cyclotrimerization of acetylene.[49]

Molecular Complexes – Like atoms and ions, molecular complexes are either grafted or tethered to the support. However, molecular complexes are typically used when a non-symmetrical environment around the active site plays a key role in catalysis. For example, microcrystalline α-$TiCl_3$ Ziegler-Natta catalysts have three different chloride vacancies: 1) at a regular site, 2) a step site, or 3) a corner site and thus lead to polymers with broad molecular weight distributions. Ultimately, if the complex is anchored to a specific type of site, a more uniform distribution of molecular weights is produced similar to homogeneous metallocenes.[40,50]

2. Supported organometallic complexes – frequently, these single-site catalysts are used to improve enantioselectivity.[51] The idea behind supported organometallic complexes is to take homogeneous analogue and tether it to a silica support.[52] In order to link the active site to the support without unwanted interactions, the silica support is modified with spacers such as tri-alkoxysilane or sulfonate, Figure 10, and then passivated prior to incorporating the active site.[53,54] This ensures site isolation and reduces unwanted reactions with the silica surface.

3. Ship-in-bottle catalysts – refers to large guest molecules being encapsulated inside the cage of zeolitic material. The active sites are not on the external surface of the material but they are essentially trapped without the possibility of diffusing out of the system. In comparison to grafting and tethering which alter the catalytic active site by covalent bonding, the ship in a bottle approach does not alter the catalysts in any way and therefore, does not alter any of the properties of its homogeneous analog. This is of particular importance when catalysts are designed to optimize enantioselectivity.[55]

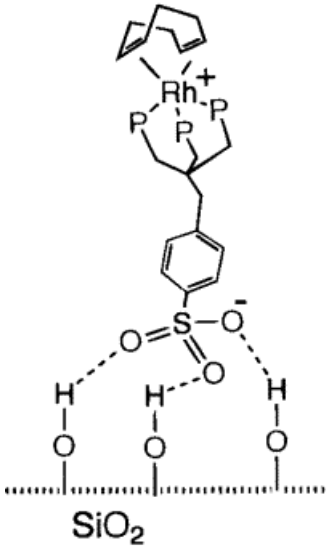

Figure 10 Mononuclear zwitterionic rhodium complex tethered to silica support via sulfonate linkage. Figure obtained from ref [53].

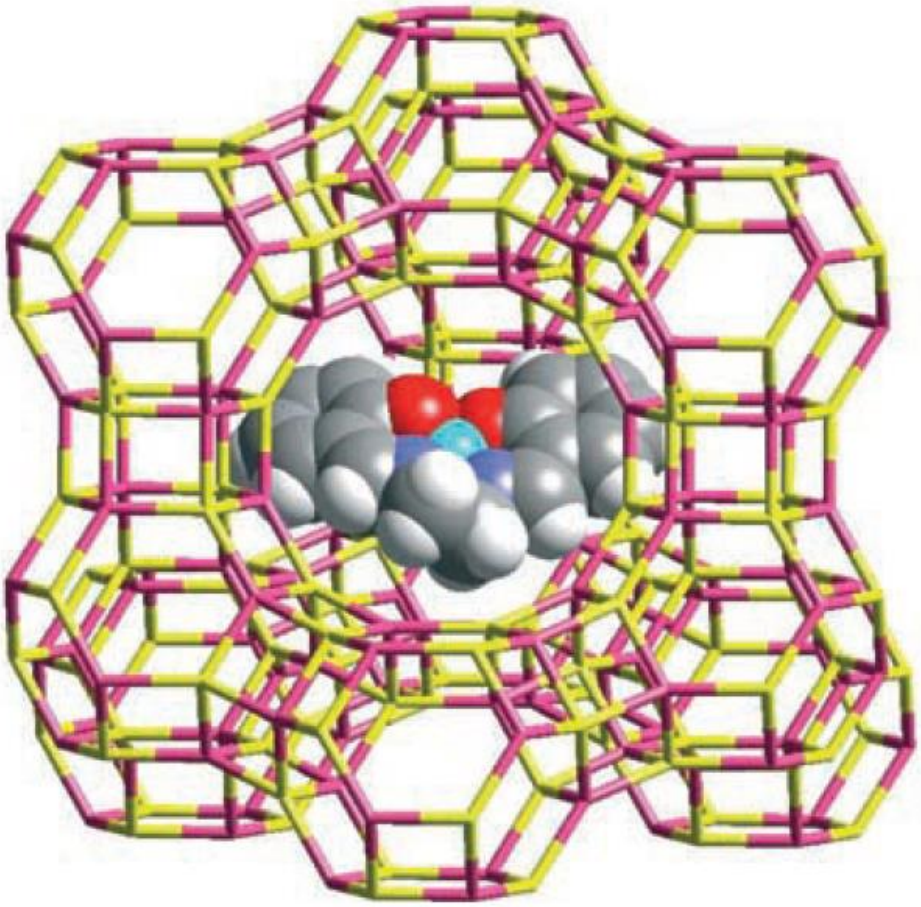

Figure 11 Pictogram of Co(Salen) inside the super cage of zeolite Y. Figure obtained from ref [40].

4. Open-structure solids – generally, zeolites and framework substituted alumino-phosphates. In these materials, the active sites are distributed uniformly with spatial isolation thereby satisfying the single site criterion. Perhaps the most widely used open-structure solid is TS-1 where Ti(IV) is substituted for some of the silicon atoms.

Titanosilicates

Since the discovery of Shell's catalyst in the late 20th century, titanosilicates have been extensively studied as pure heterogeneous catalysts. The success of these catalysts can be attributed to the vast number synthetic pathways that allows for the tailoring of their structural and electronic properties. Titanium containing silicates have gained considerable attention as catalysts for a broad range of reactions including hydroxylation and epoxidation, but perhaps the most studied titanosilicate catalyst has been TS-1.

Titanium Silicalite-1 (TS-1)

Titanium silicalite-1 (TS-1) is a zeolitic material with MFI structure and has a low percentage of Ti(IV) sites dispersed throughout the silicate matrix. It was discovered in 1983 by Taramasso *et.al.* and is most widely known for its stability in partial oxidation reactions with aqueous hydrogen peroxide, Figure 12.[56] It has been characterized by a number of spectroscopic and other techniques that have identified its active site as the isomporphous substituted Ti(IV) in the framework of silicalite.[56]

Synthesis of TS-1

Traditionally, TS-1 has been synthesized by either wet impregnation or hydrothermal synthesis, but there have been over a dozen methodologies reported. Table 1 summarizes several protocols and their effects on final structure and composition of TS-1.

Characterization

While TS-1 is often considered a model single-site catalyst, the lack of information about the active site due to the low titanium content has left questions about the true nature of the active site unanswered. To gain a better understanding of the titanium active sites, several independent characterization techniques have been employed such as X-ray and neutron diffraction, IR,

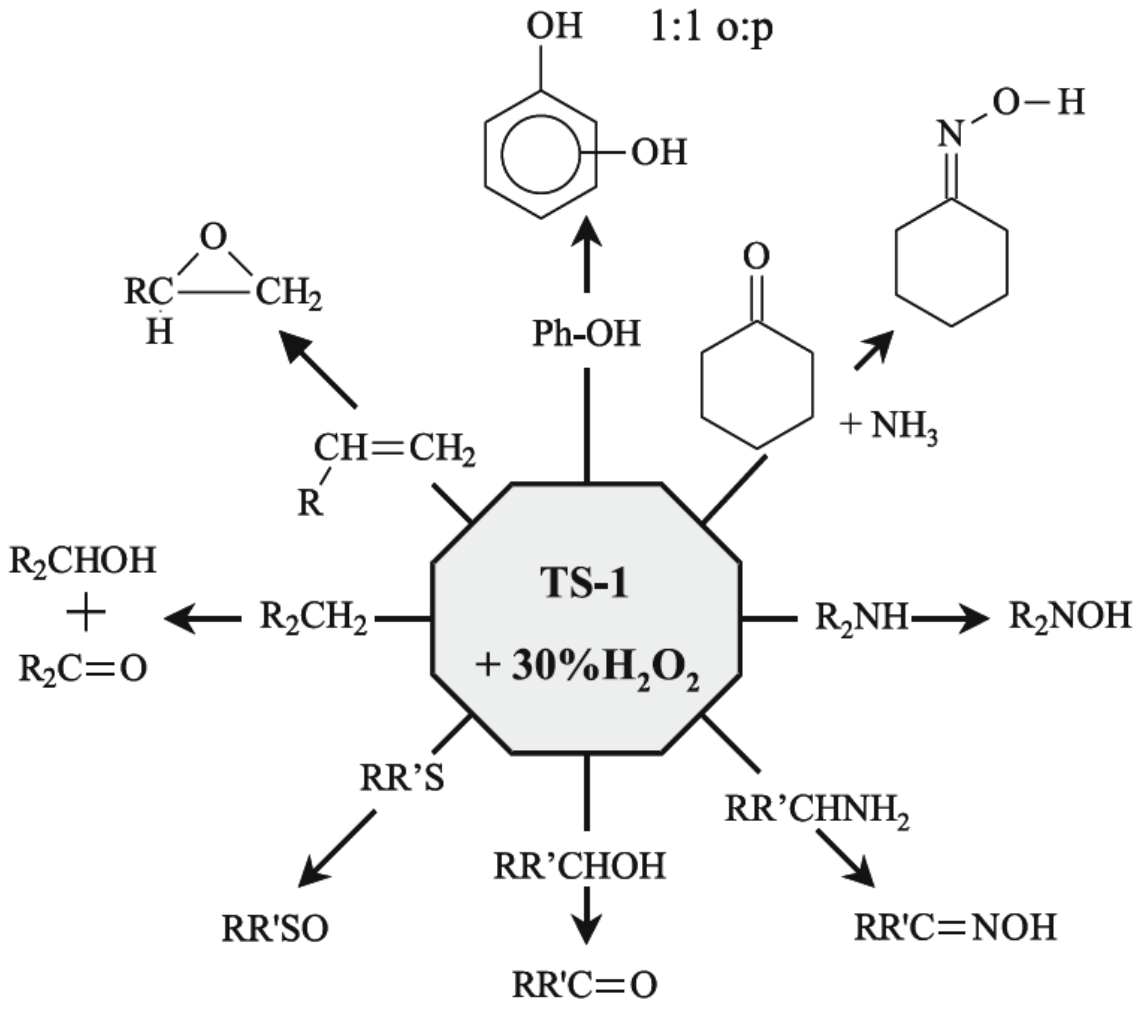

Figure 12 Illustration of the different types of reactions catalyzed by TS-1. Figure reprinted from ref [56].

Table 1 TS-1 synthetic methodologies and parameters vs. final Si/Ti and morphology.

Reprinted from ref [42].

Synthesis Methodology	Composition	Temp Time	Si/Ti	Crystalline Size and Morphology
Hydrothermal Synthesis (mixed alkoxide)	TEOS TEOT TPAOH Base, distilled water	448 K 6-30 d	90-30	Parallelepipeds with round edges
Hydrothermal Synthesis (dissolved Ti)	1) Tetrapropylammonium peroxytitanate; TEOT in distilled water, aqueous H_2O_2, and aqueous TPAOH 2) Add colloidal silica and TPAOH	278 K	90-30	Parallelepipeds with round edges
Wetness Impregnation (prehydrolysis)	1) TEOS in dry iPrOH is hydrolyzed in aqueous TPAOH 2) $Ti(OBu)_4$ as titanium source	433 K 1-5 d	≥ 10	Cuboid (<1 μm)
Growth from TS-1 Seeds	TS-1 seeds TPABr (structure directing agent) Ammonia, water, amines	nr	nr	100% Crystallinity
Sol-Gel (Template – Impregnation)	1) Obtained dried SiO_2-TiO_2 cogel 2) Dry impregnation by adding aqueous TPAOH and heated in microwave 3) Dry and then calcine the crystalline product	823 K 5 h (calcine)	50	Round shaped particles (`0.5 μm)

Raman, UV-Visible, and XAS spectroscopies. For example, the structure of TS-1 was determined by XRD measurements, but the location of Ti(IV) was left unanswered. Two different structures exist for silicalites with MFI structure, orthorhombic and monoclinic. Figure 13 depicts the structure of the orthorhombic structure of silicalite illustrating the 12 crystallographically different framework sites. Titanium has the possibility of substituting into any one of these sites, or a mixture of these sites. Extensive studies have shown that titanium preferential substitutes on sites T8, T10, and T3 and in addition, on two silicon vacancies, T1 and T5. Each of these sites has the potential to incorporate Ti(IV) into the silicon vacancy and each of these positions has the possibility to possess individual catalytic properties. Therefore, it is debatable as to whether TS-1 is truly a model for single-site catalysts.[57]

Mesoporous Titanosilicates

The primary limitation of TS-1 is the size of the pores, i.e., micropores. Therefore, TS-1 is only capable of catalyzing small molecule reactions. To overcome this limitation, there have been many attempts to synthesize titanosilicate molecular sieve with larger pore sizes so that a wider range of substrates can be investigated. Several mesoporous titanosilicates have been successfully synthesized. These molecular sieves are characterized by their large surface areas (up to 2500 m^3/g), uniform pore sizes (2 – 50 nm) and their tunable structures.[58] Amongst these molecular sieves, MCM-41, MCM-48, and SBA-15 have been extensively studied.

While these catalysts have a wider range of substrates, as previously mentioned these catalysts are frequently synthesized using post synthesis grafting which often leads to a mixture of active sites, Figure 14. Therefore, these catalysts frequently exhibit selectivities lower than the selectivity of their homogeneous analogs. Additionally, surface grafted titanium centers typically have fewer connections to the matrix than the framework Ti(IV) sites of TS-1. Therefore, these active centers are more likely to leach from the matrix.

Kholdeeva *et.al.* have extensively studied the use of mesoporous titanosilicate catalysts for the selective oxidation of phenols to benzoquinones with aqueous hydrogen peroxide.[59-61] Quinones are of great interest because they serve as intermediates in the production of high value fine chemicals and pharmaceuticals. Specifically, 2,3,6-trimethyl-1,4-benzoquinone (TMBQ) is a vital intermediate in the synthesis of Vitamin E.[62]

Kholdeeva and coworkers focused their research efforts on optimizing reaction conditions for reaching 100% selectivity in H_2O_2 based oxidation of 2,3,5-trimethylphenol (TMP) to TMBQ.[59] Table 2 presents a summary of the optimum conditions for this reaction.

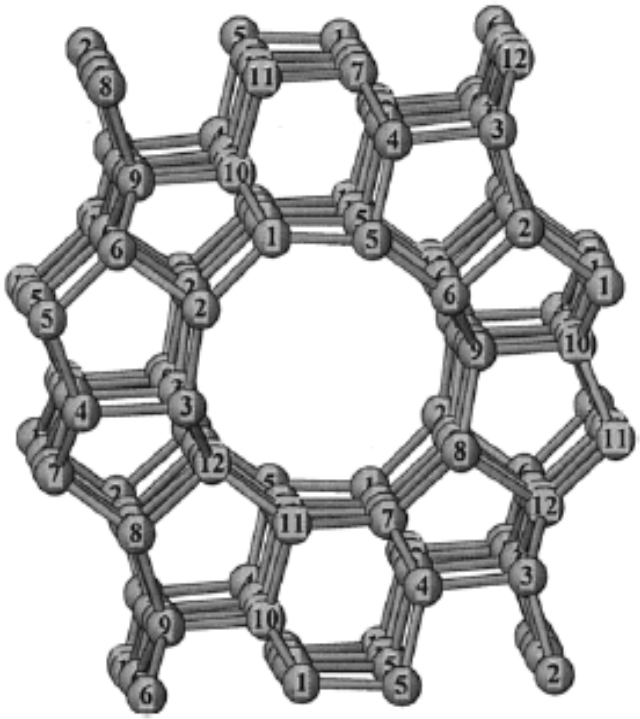

Figure 13 The structure of orthorhombic form of silicalite-1 (MFI type) showing the 12 crystallography distinct T sites. The oxygen atoms have been omitted for clarity. Figure reprinted from ref [57].

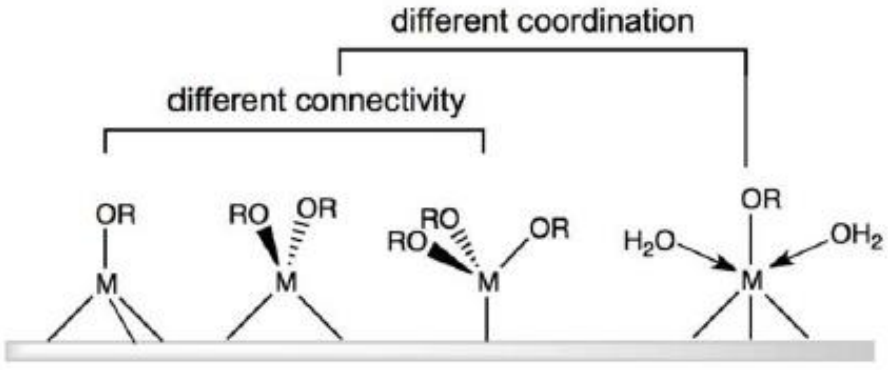

Figure 14 Illustration of the possible mixtures of active sites in grafted titanosilicates.

Table 2 Summary of reaction conditions necessary for reaching high selectivity for the oxidation of TMP to TMBQ.

Reaction Condition	Optimization	Example
Solvent	**Poorly coordinating**	**Acetonitrile**
Temperature	**High**	**80^{0}C**
Substrate Concentration	**Low**	**<0.1M**
H_2O_2 : Ti	**Excesses**	**>3.5 H_2O_2 : Ti**
Substrate to Ti	**Low**	**<10 – 20 TMP : Ti**

Based on these findings, the reaction condition in this work are similar to those presented by Kholdeeva *et.al.*

In addition to optimizing reaction conditions, a second focus of their research was to establish a relationship between mononuclear (a) and dinuclear (b) titanium sites, Figure 15. They investigated the catalytic properties of low Ti weight percent grafted titanosilicates (<2.0 wt.% Ti) and high Ti weight percent grafted titanosilicates (>2 wt. % Ti). They suggest the dinuclear titanium sites are responsible for high selectivity.

General Conclusion of Titanosilicate Catalysts

Since the discovery of Shell's catalyst in the late 20th century, titanosilicates have been extensively studies as pure heterogeneous catalysts. The success of these catalysts can be attributed to the vast number synthetic pathways that allows for the tailoring of their structural and electronic properties. TS-1 was the first example of substituted isolated Ti(IV) site in a silicate matrix. It has shown to be stable in the presence of aqueous hydrogen peroxide, but has a limited substrate range due to its microporosity. The discovery of TS-1 has led to extensive research in the development of other titanosilicates with similar structures but larger pore size, mesoporous materials, such as Ti-MCM-41 and Ti-MCM-48.

These mesoporous materials accept a wider range of substrates, but they lack the stability exhibited by TS-1. These materials are known to leach in the presence of aqueous hydrogen peroxide. Additionally, little is known about the actual catalytic active sites in these materials. Frequently, these catalysts are synthesized using grafting techniques that result in a mixture of

active sites. This lack of homogeneity in the active sites potentially reduces the selectivity of these materials.

TS-1 and other mesoporous titanosilicate have been extensively investigated and shown to incorporate Ti(IV) active site in a tetrahedral geometry. This brings up the question of how such a titanium center could bind substrate when it is encapsulated in a rigid support matrix. It is difficult to visualize how substrate and/or oxidant are able to bind to the active site without disrupting the linkages to the surrounding matrix. If a bond is broken from the active site to the support, the potential for leaching is greatly increased. Therefore, there is still a need for a synthetic methodology that allows for the synthesis of isolated, accessible, single-site, titanosilicates within a mesoporous matrix.

Catalytic Activity

Perhaps the most influential driving force behind catalyst development is improving catalytic performance. Up until recently, the area of heterogeneous catalysis lacked a uniform way to calculate and represent catalytic activity. However, the notion of benchmarking catalytic activity is becoming a more popular concept in catalysis today. Benchmarking refers to the agreed upon protocol to document, share, and reproduce both methods and results.[63]

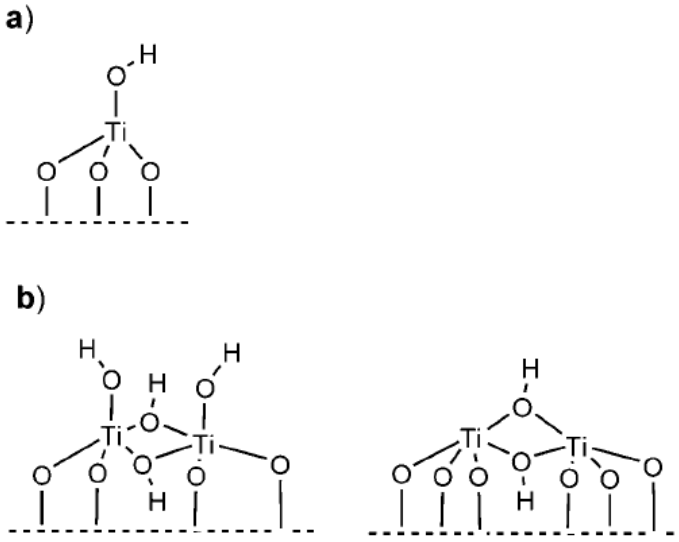

Figure 15 a) mononuclear Ti center, b) dinuclear Ti centers as a result from grafting.

The two key practices of characterizing catalytic performance are activity and selectivity. A catalyst can be advantageous for activity, selectivity, or both. Activity denotes the rate at which the reaction progresses to chemical equilibrium in response to the catalyst and can be defined in a variety of different ways.

Traditionally, the rate of heterogeneous catalysts is expressed in arbitrary units, frequently conversion vs time at a specific temperature. However, by utilizing arbitrary units, it is nearly impossible to reproduce the work of others. The second way to express rate is through areal rate, or rate per surface area. Today, catalytic activity is often expressed as specific rates, or more explicitly rate per unit mass of catalyst.[64] Unfortunately, specific rate is only an average expression of catalytic activity for many heterogeneous catalysts. This is a direct result of heterogeneous catalysts containing mixtures of active sites. Ideally, catalytic activity should be expressed in terms of the number of active centers. In this sense, catalytic activity can be defined as the amount of product produced per active site as a function of time. This notion of catalytic activity is quantitatively expressed as *turnover number* (TON), Equation 6, and/or *turnover frequency* (TOF), Equation 7, which stem from early research in enzyme catalysis. TON is defined as the amount of reactant consumed per amount of catalyst and frequently defines the maximum rate per catalytic site defined by Michaelis-Menten kinetics.[64] Additionally, TOF, or turnover rate is the TON per unit time, commonly expressed as per second. Generally, initial TON and TOF are used to describe the catalysts rate of reaction.

$$TON = \frac{moles\ of\ reatant\ consumed}{moles\ of\ catalyst} \qquad \text{Equation 6}$$

$$TOF = \frac{TON}{unit\ time} \qquad \text{Equation 7}$$

While TON and TOF are commonly used to describe catalytic activity, they both rely on the consumption of reactant. Additionally, it is possible to characterize catalytic activity in terms of product formation. *Site time yield* (STY), is a derivative of TOF, but instead accounts for the amount of product formed per catalytic site and unit time, Equation 8.

$$\mathrm{STY} = \frac{moles\ product}{\frac{moles\ active\ site}{unit\ time}} \qquad \text{Equation 8}$$

There are several challenges to accurately describing heterogeneous catalytic activity. As previously mentioned, a major challenge in heterogeneous catalysis is that frequently the catalysts have more than one type of active site. Therefore, TON, TOF, and STY are an

approximation of the true catalytic activity because it is very difficult to accurately count the number of sites and determine if each active site is identical. Second, heterogeneous catalytic rates are also functions of temperature, pressure, concentration, and mass transfer.[65] Despite these challenges, expressing catalytic activity along with detailed reaction conditions provides researchers with a way to reproduce and compare catalysts.

Selectivity

Traditionally, *yield* is used to quantify the amount of product formed, Equation 9. However, y*ield* is a measure of mass conservation. Consequently, it is possible to obtain higher than 100% yield because of multiple reactants forming one product, i.e., A + B → C. Therefore, it is advantageous to report productivity in terms of a molar ratio.

$$Yield = \frac{moles\ of\ product}{\Delta\ moles\ reactant} \qquad \text{Equation 9}$$

The second way to characterize catalytic properties is selectivity, Equation 10. While selectivity is generally not included in the theoretical or academic definition of catalysis, in "practical" catalysis it can be of equal or greater importance. *Selectivity* is defined as a catalyst's ability to preferentially distinguish between competing substrates or reaction pathways to achieve one specific product. It can also be defined as a catalyst's ability to produce one product over another.

$$\%Selectivity = \frac{moles\ of\ product}{(intial\ moles\ of\ reactant - moles\ of\ reactant\ consumed)}\ x\ 100\% \qquad \text{Equation 10}$$

Selectivity is one of the most important properties of any catalyst because it is critical to clean processes or green chemistry.[66] It is therefore of interest to consider how one can design selectivity into the function of a catalyst. Historically, the control of selectivity has been inhibited by a lack of understanding of heterogeneous catalysts at the molecular level.[67] Understanding selectivity requires that one consider the active site at the atomic level. Without an understanding of catalysts at the atomic level, it is debatable as to whether existing catalysts will be enhanced or superior new catalysts be established.[39] Improved experimental and theoretical tools are being developed to better understand catalytic processes leading to new synthetic methodologies based upon molecular approaches.[68] Three approaches to understanding catalysts at the

atomic level include: 1) targeted synthesis; 2) new and better characterization tools; and 3) computational modeling.

One way to achieve selectivity is by controlling the size and shape of surface sites or tailoring the sites. By tailoring a site, the catalyst recognizes a specific substrate for a particular reaction above all other possible substrates and reactions. Mainstream heterogeneous catalysts are often metals dispersed on a high surface area supports. These catalysts are frequently synthesized by impregnation of the support with a metal salt followed by oxidative or reductive activation steps. This method of synthesis does not yield active sites that are uniform in either size or shape. It creates a distribution of sites capable of supporting multiple reactions thus limiting control of selectivity.[68]

As mentioned above, another way to enhance selectivity is by controlling the shape of the site. With heterogeneous catalysts tailoring shape can occur in two different phases of the catalyst; the active site or the support. The support material for a heterogeneous catalysts is often thought of as being inert, but it can in fact influence activity along with selectivity. The discovery of zeolites and mesoporous materials has allowed scientists to design catalysts with specific pore shapes to help enhance the selectivity of a desired product. This is done through the use of templating agents, organic functionalization, and atomic layer deposition. As previously mentioned, heterogeneous catalysts frequently contain a number of active sites that exhibit their own energetics, activities, and selectivities.[40]

Leaching

While activity and selectivity play critical roles in the development of new catalysts, it is also important to understand stability. Unlike homogenous catalysts, the issue of leaching must be considered with heterogeneous catalysts. If a heterogeneous catalyst releases its active species into solution, it defeats the concept of heterogeneous and is impractical in an industrial setting. Leaching is a result of solvolysis; either solvent, reactant or product react with the bonds that hold the active catalyst on the support, thereby releasing it. Several factors contribute to the probability of a metal leaching; 1) the type of the transition metal; 2) the reaction solvent; 3) type of oxidant; 4) temperature of the reaction; and 5) the structure of the supporting matrix, e.g., silica tends to be more resistant to leaching than alumina.[69] There are three possible outcomes if/when leaching occurs: 1) The active metal does not undergo solvolysis resulting in a pure heterogeneous catalyst; 2) The metal leaches, but the solutions species is not active and therefore the initial catalytic activity results from the primarily heterogeneous catalyst; or 3) the

metal undergoes solvolysis producing active homogenous catalysts. The observed catalysis then is a mixture of heterogeneous and homogenous catalysts.[70,71]

Leaching is a potential problem under a variety of reaction conditions, but it poses a significant problem for catalysts used in oxidation reactions. This risk of leaching can be attributed to the strong complexing and solvolytic properties of hydrogen peroxide and other organic peroxides in conjunction with their resulting products, for example, alcohols, carboxylic acids, etc.[71] The discovery of TiO_2 on silica by Shell was the first example of a purely heterogeneous catalyst for epoxidation.

An ultimate goal in catalysis science is to develop active sites that are composed of single atoms or small clusters of atoms, which are identical in every aspect relating to their activity, in well-defined molecular supports. [68] One of the goals of the research described here is to develop a well-defined strategy by which single-site heterogeneous catalysts may be prepared. The following chapters introduce the different parts of this strategy as it currently stands.

Overview of Dissertation

Motivation and Goals

The goal of this research was to synthesize and characterizes two different families of isolated, single-site titanosilicate catalysts with mesoporosity for use in selective oxidation reactions. Specifically, we wish to employ a strategy that allows for the tailoring of the number of connections from the titanium active sites to the silicate support. Additionally, we aim to show the geometry of the active centers in each family of catalysts can be altered without disrupting the control of connectivity. To the best of our knowledge, this is the first time a strategy has been designed to tailor both connectivity and geometry of the catalytic active site.

Atomically Dispersed Titanium Centers

Two different families of catalysts have been prepared containing targeted titanium centers with both equilibrium and non-equilibrium geometries. First generation catalysts possess three different titanium connectivities to the matrix referred to as 2-connected (2C-), 3-connected (3C-), and 4-conneccted (4C-) each containing isolated tetrahedral Ti(IV) centers, Figure 16. Catalysts containing isolated, identical titanium metal centers are synthesized using the building block approach and method of sequential additions. Their connectivities and structure are investigated by several independent characterization techniques.

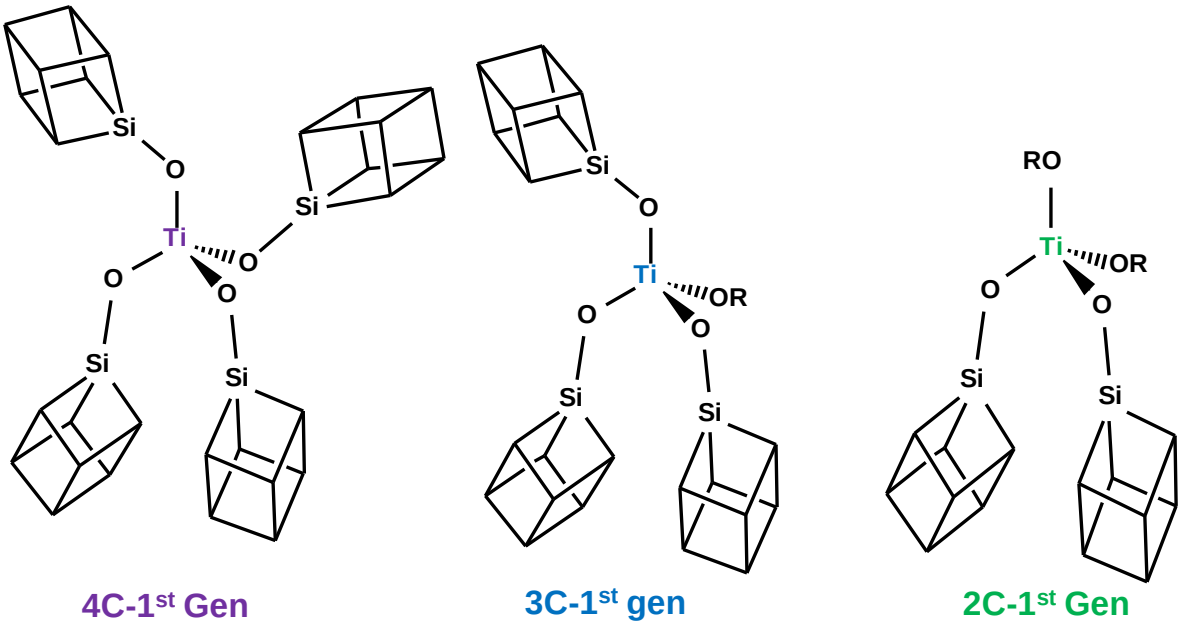

Figure 16 Tetrahedral Titanium centers with different connectivities to the matrix.

In contrast to first generation catalysts, the second family of catalysts or second generation catalysts have non equilibrium geometries around the titanium active site while maintaining the same tailored connections to the matrix. There are two main subcategories to second generation catalysts, those with blocking ligand present (top) and those with blocking ligand removed (bottom), Figure 17. Similarly, these catalysts are synthesized using a silicate building block and method of sequential additions.

Catalytic Properties in Selective Oxidation Reactions

Above all other characterization techniques, catalytic activity is always of primary importance. Therefore, the catalysts synthesized in this work are applied to two different catalytic reactions, hydroxylation and epoxidation. Specifically, the catalytic properties of these materials are investigated in the oxidation of phenols to benzoquinones with aqueous hydrogen peroxide, Figure 18 and cyclohexene to cyclohexene oxide with organic peroxide, Figure 19.

These two different catalytic reactions are thought to proceed by two different mechanisms. Phenols to benzoquinones are suspected to proceed via a radical mechanism, but our understanding of this mechanism is very limited. In contrast, the formation of cyclohexene oxide is the result of an atom transfer mechanism that has been well characterized in the literature.

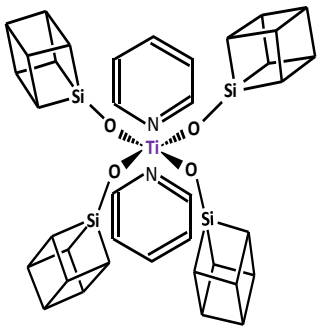

4C-2nd gen with blocking ligand

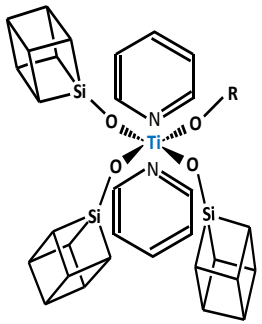

3C-2nd gen with blocking ligand

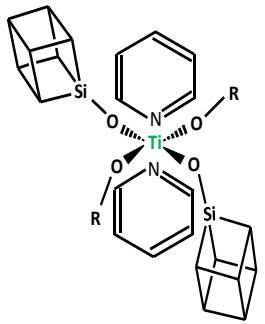

2C-2nd gen with blocking ligand

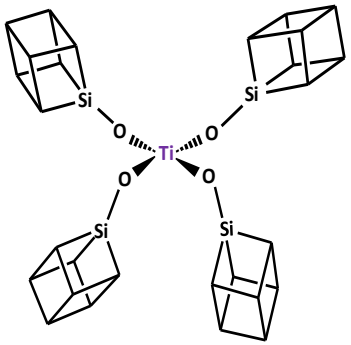

4C-2nd gen without blocking ligand

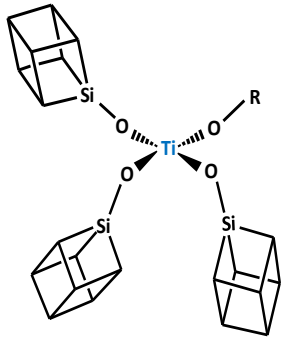

3C-2nd gen without blocking ligand

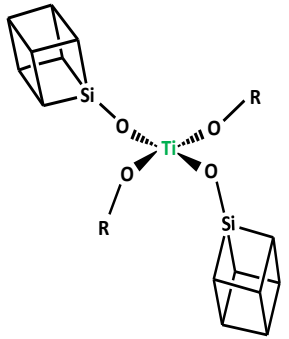

2C-2nd gen without blocking ligand

Figure 17 Second generation titanosilicate catalysts with tailored connectivities and geometries other than tetrahedral.

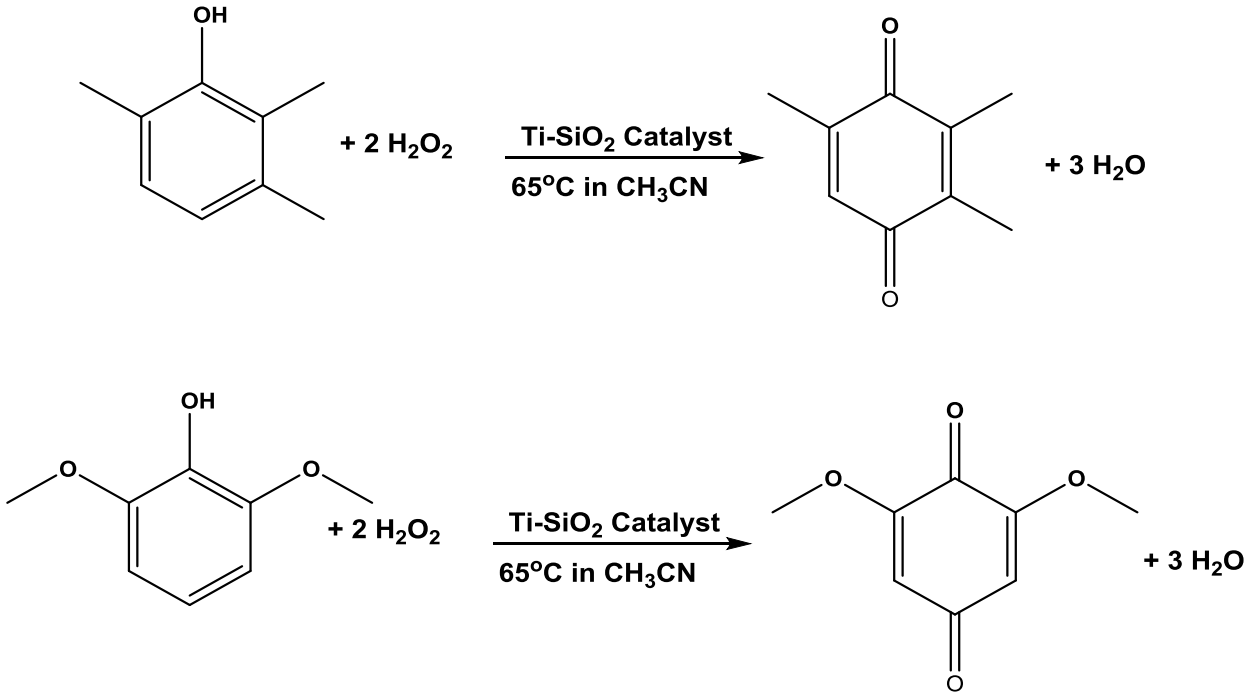

Figure 18 Oxidation of phenols to benzoquinones with aqueous hydrogen peroxide.

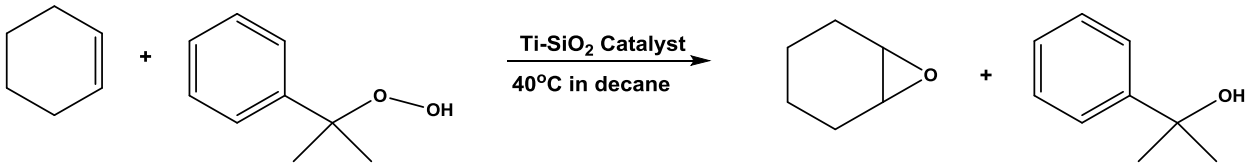

Figure 19 Epoxidation of cyclohexene to cyclohexene oxide with cumene hydroperoxide.

By comparing the observed catalytic activity between the different connectivities and different geometries a structure-function relationship is established. More importantly, to the best of our knowledge, this is the first time a study investigated the relationship of connectivity along with geometry influences the properties of phenol oxidation and epoxidation reactions.

Brief Overview of Chapters

Chapter 2 aims to demonstrate the strategy behind the building block approach and method of sequential additions developed by the Barnes group. This methodology focuses on constructing a robust silicate matrix around the active metal center similar to molecular imprinting. Additionally, a brief introduction and sample preparation protocols are presented for each characterization techniques.

Chapter 3 describes the previous synthesis and characterization of first generation titanosilicates presented by Dr. Nan Chen, a former member of the Barnes research group. There are two unanswered questions that needed to be addressed: 1) Does a methanol passivation step employed to remove trimethyltin groups disrupt or alter the targeted connectivities, i.e., are 4-connected single-sites changed to a mixture of 4-connected, 3-connected, 2-connected, and even 1-connected sites? 2) Do remaining trimethyltin groups play an active role in catalysis? Catalysts are prepared per Dr. Chen's procedures, characterized, and used to answer these questions.

Chapter 4 describes several different passivation strategies that were investigated and their effect on catalysis.

Chapter 5 describes the synthesis and characterization of "new" first generation and second generation titanosilicates. These catalysts are synthesized with the same building block approach and method of sequential additions, but the cross-linker utilized to build the robust supporting matrix was changed to dichlorodimethylsilane instead of silicon tetrachloride previously used by Dr. Chen and in Chapter 3. Additionally, the catalytic activities of these new catalysts are compared to those of previous catalysts by investigating the oxidation of phenols to benzoquinones. Furthermore, stability and recyclability of these catalysts are described.

Chapter 6 describes epoxidation investigations in this research. Both first and second generation catalysts synthesized in Chapter 5 were investigated as potential catalysts in the epoxidation of cyclohexene to cyclohexene oxide. Both catalytic activity and stability were evaluated.

A summary of the work presented along with future work is presented in Chapter 7. While little is known about the mechanism for producing benzoquinones from phenols, evidence suggest that polynuclear titanium centers are needed for high activity and selectivity. The work presented here focuses on atomically dispersed centers, but the strategy employed in this work allows for the possibility of incorporating polynuclear clusters inside the building block matrix. Additionally, the stability shown by both first and second generation catalysts with aqueous hydrogen peroxide in phenol oxidation raises great interest in epoxidation reactions with aqueous hydrogen peroxide.

Chapter II: General Synthesis and Characterization with Experimental Procedures

Building Block Methodology

General Methodology

Over the past decade, the Barnes group has developed a synthetic methodology for producing silicate matrices with isolated, atomically dispersed, identical cationic metal centers.[72] This methodology combines a building block approach with a synthetic strategy that we will refer to as the method of sequential additions. This synthetic strategy is similar to molecular imprinting, but does not require the use of a traditional templating agent. Traditional templating agents are used as a mold during synthesis and then removed from the matrix allowing a substrate to bind in their place. In the building block approach, to make new catalysts, the catalysis metal itself is used as a template for the matrix to build around. The metal(s) and support matrix in the immediate vicinity of those metal centers ultimately become what could be referred to as the catalyst ensemble, Figure 20. This methodology has been previously employed for the synthesis of targeted, atomically dispersed vanadium catalysts.[73]

There are three components to this synthetic strategy; a molecular building block, a linking agent, and a cross-linking reaction. Trimethyltin functionalized silsesquioxane building blocks are utilized as the source of silicon in the silicate matrix. These building blocks are cross-linked by a variety of chemically robust and active linkers to the catalytic metal, typically high valent metal chlorides. Each component will be discussed in more detail in the following sections.

Building Block

The building block plays a critical role in the synthesis of isolated single-site heterogeneous catalysts. The molecular building block used in the Barnes group is a structurally well defined, rigid, cubic silsesquioxane functionalized with trimethyltin groups ($Si_8O_{20}(SnMe_3)_8$) and will be referred to as the "tin-cube." Walzer and Fehrer first described this crystalline spherosilicate.[74] The core of the building block is the cubic arrangement of silicon and oxygen atoms shown in Figure 21. Silicon atoms are on the eight corners of the cube, shown in blue, and are linked to one another by three bridging oxygen atoms, illustrated in red. Each silicon has an additional terminal oxygen atom directed away from the cubic core. All eight of these oxygens are bound to trimethyltin capping groups, represented in green. The trimethyltin groups are highly reactive with high valent metal chlorides and main group chlorides cross-linking cubes together,

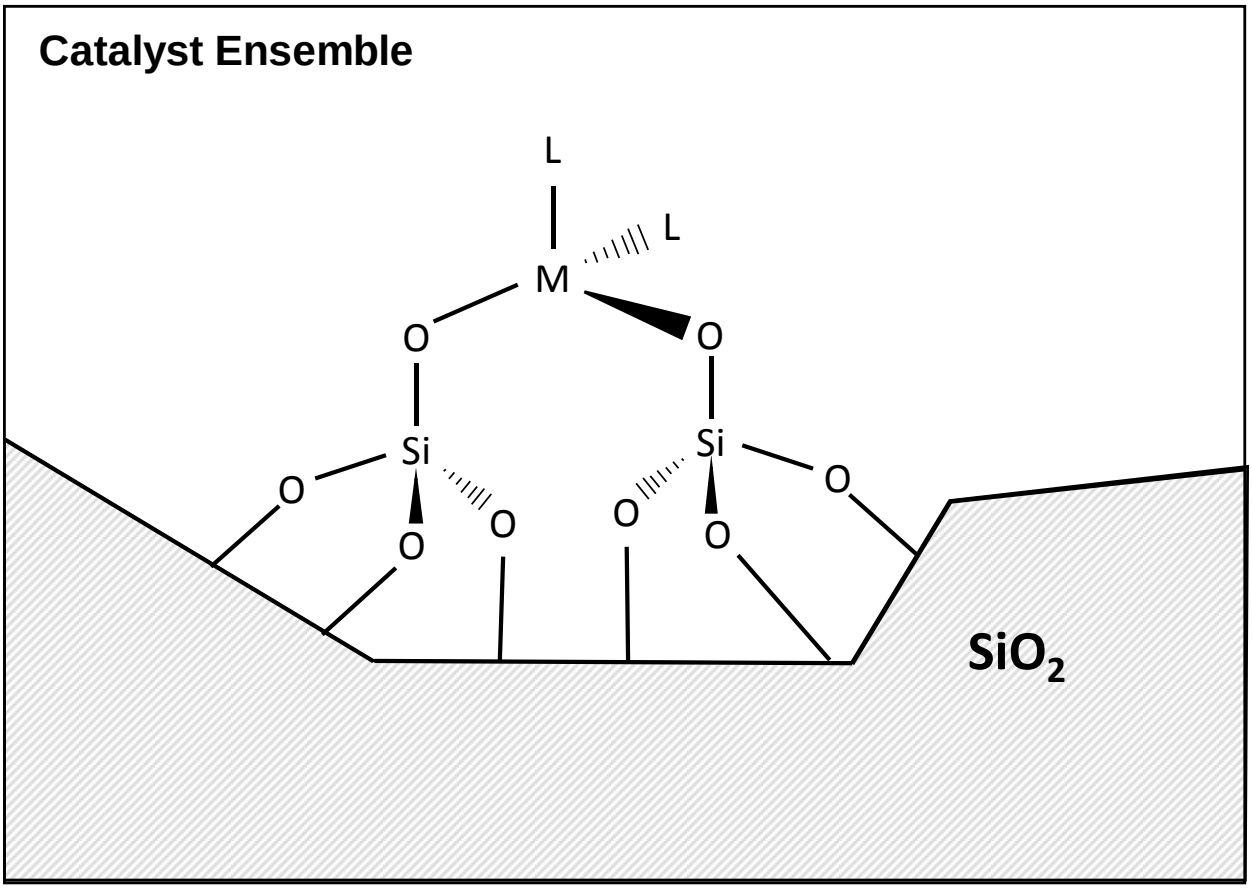

Figure 20 Illustration of catalytic ensemble showing the metal to surface binding, the metal terminating ligands (L) and the support (SiO_2).

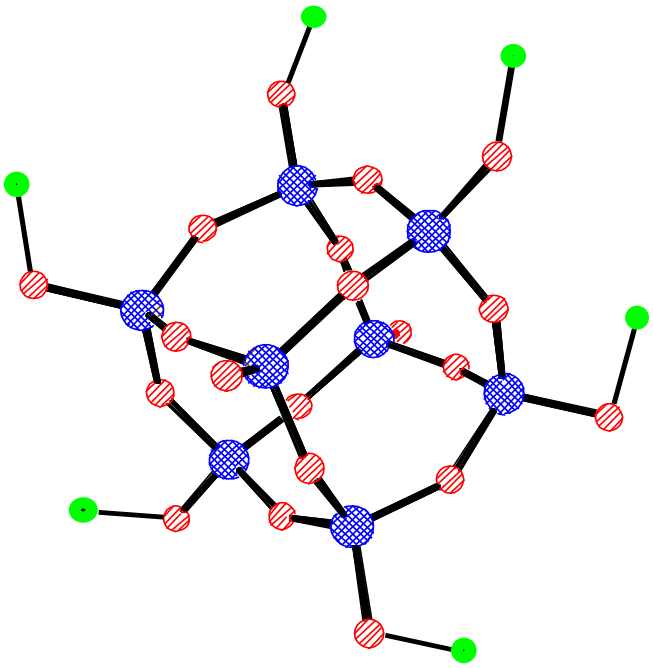

Figure 21 Illustration of the core structure of the tin functionalized building block $Si_8O_{12}(OSnMe_3)_8$ where silicon atoms are blue, oxygen atoms red, and trimethyltin groups green.

via a metathesis reaction in which $ClSnMe_3$ is formed along with a new M-O-Si cube linkage, thereby providing a simple synthetic route to building a silicate matrix based on this building block and these linking agents. Furthermore, having the linking points on the corners of the cubes helps keep each of the active sites isolated from one another preventing aggregation of the catalytic centers. Figure 22 illustrates the spatial separation of terminal oxygen linking points on the tin-cube.

There are several aspects of the tin-cube that make it an ideal building block for the development of highly dispersed single-site catalysts.

1. The tin-cube building blocks are efficiently synthesized in large quantities with high yield.
2. The size of the cube, in the nanometer range (≥1 nm), makes it nearly impossible for the titanium centers on different corners of the building block to come close enough to interact in the matrix. Therefore, it is unlikely for polynuclear titanium groups to be created when mononuclear titanium precursors are employed.
3. The rigidity of the tin-cube and the spatial disposition of the linking groups enforces separation of the trimethyltin groups isolating one active site from another hindering the formation of Ti-O-Ti groups during catalysis.
4. Finally, the thermal stability of the tin-cube makes it an ideal building block. When heated to 400^0 C no obvious changes are seen in various characterization techniques such as NMR, UV-Vis and Infrared spectroscopies.[42]

In addition to advantages, there are several disadvantages that should be addressed.

1. The synthesis of the tin-cube building block is more involved than silica because of the special reactive groups necessary for linking the building block to metal linker.
2. In general, trimethyltin is quite toxic. The toxicity can be circumvented by using tri-n-butyl groups. Previous research has shown that these two capping groups are interchangeable in the synthesis described here. However, the synthesis and characterization of tri-n-butyltin is more difficult than the trimethyltin analogue. Therefore, in work reported here, trimethyltin is used to illustrate the synthetic strategy for making single-site catalysts.

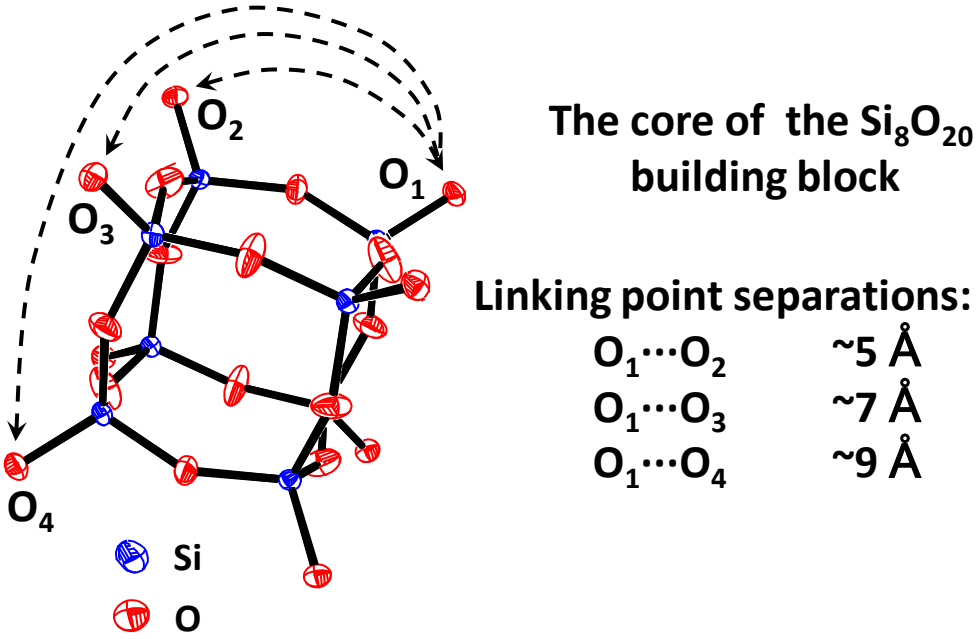

Figure 22 Illustration of the separation distances for the terminal oxygen linking points on the building block $Si_8O_{12}(OSnMe_3)_8$. Figure was obtained from ref [71].

Linking Agents

The second component of this synthetic strategy is a linking agent. There are two different types of linking agents: those that lead to catalytically active sites and those that serve mainly to cross-link the matrix. The active linking agents are used to insert catalytic metal centers into the developing matrix while the inert linking agents are used to cross-link the matrix and create a robust support material. The linking agents are typically high valent metal chlorides and main group chlorides as seen in Table 3. Metal and main group chlorides are commercially available and relatively inexpensive making them suitable linking agents. However, one must be careful when handling these high valent metal and main group chlorides because they can be susceptible to hydrolysis. Therefore, Schlenk techniques and nitrogen atmosphere gloveboxes are necessary during the synthesis of these matrices. While this strategy can be applied to a variety of metal centers, a focus of this research has been placed on incorporating titanium metal centers with targeted connectivities to the matrix as the active sites. Titanium will therefore be the primary example of synthetic strategy shown below.

Table 3 List of inert and catalytically active linkers.

Inert Linkers	Catalytically Active Linkers	
$SiCl_4$	W^{6+}	WCl_6, $WOCl_4$, WO_2Cl_2
$SiCl_4py_2$	V^{5+}	$VOCl_3$
$MeSiCl_3$	Zr^4	$ZrCl_4$
Me_2SiCl_2	Ti^{4+}	$TiCl_4$, $TiCl_4py_2$, $Ti(OiPr)Cl_3$, $Ti(OiPr)_2Cl_2$
Me_3SiCl	V^{4+}	VCl_4
$HSiCl_3$	Sn^{4+}	$SnCl_4$, $BuSnCl_3$, Bu_2SnCl_2
	Al^{3+}	$AlCl_3$
	Ga^{3+}	$GaCl_3$
	P^{3+}	PCl_3
	Au^{3+}	$AuCl_3py$

Cross-linking Reaction

To build a matrix one must have a well-defined linking reaction. The linking agent and building block react in a non-hydrolytic sol-gel forming reaction driven by the oxophilicity of the high valent metals Equation 11.

$$MCl_n + \equiv SiOSnR_3 \rightarrow \equiv SiOMCl_{n-1} + R_3SnCl \qquad \text{Equation 11}$$

The trimethyltin groups on the corners of the tin-cube react with the chloride ligands on the linking reagents producing trimethyltin chloride (Me_3SnCl) and create a new metal siloxane linkage (M-O-Si); in this context M = Ti or Si. This metathesis reaction expands the building block matrix while incorporating the active centers. The number of linkages in the matrix is governed by the number of chlorides on the metal or main group element and the number of available trimethyltin groups in the system. This idea will be discussed in more detail below.

The linking reaction exhibited by the tin-cube and chloride linking reactions is irreversible. Therefore, once a new M-O-Si linkage is formed, it will not revert back to the original Me_3Sn-O-Si and M-Cl bonds nor equilibrate with any other M-O-Si bonds in the matrix. Furthermore, under non-aqueous conditions, the Me_3Sn groups and chloride ligands are complementary functional groups meaning Me_3Sn will not react with another Me_3Sn of an adjacent cube to form $(Me_3Sn)_2O$ and two linking agents will not react to produce Cl_2 and M-M. This concept is illustrated in Figure 23 with a generic building block and linking reagent.

This irreversible cross-linking leads to highly defected, amorphous material with significant voids between building blocks and linkers creating pores in the material. Porosity is an expected consequence of irreversibility in linking reactions. The pores in this material should scale to the size of the building block. Although not a part of this research, porosity can be tailored by the total dose of cross-linking reagent.[75]

There are several advantages to using this building block strategy. Unlike surfactant templating, high temperature procedures and solvent extractions are unnecessary to create porous matrices.[76] Furthermore, site isolation is ensured by the process in which the matrix is built. The matrix is built from Si_8 units instead of single atoms. However, a strategy is needed to employ this building block approach in conjunction with creating “single-site” catalysts.

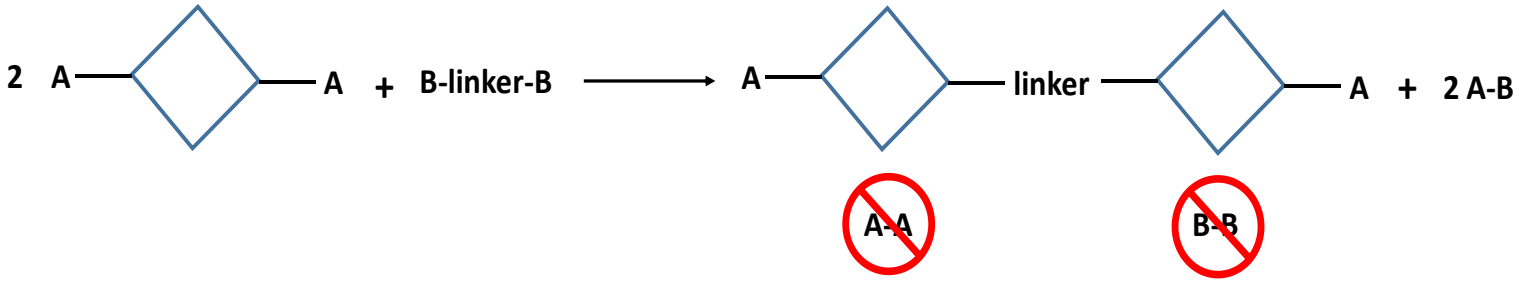

Figure 23 Generic cross-linking reaction between building block and linking agent with complimentary functional groups.

Method of Sequential Additions

In addition to the elements described above, the method of sequential additions is the tactic by which single-site catalysts are obtained. The real "strategy" behind this method is to divide the matrix building into two separate steps. One step focuses on always reaching limiting connectivity between components in the matrix cleanly (this will be discussed in more detail later), while the second step, primarily builds the robust support. In this context, connectivity refers to the number of linkages from the active metal center to the surrounding matrix of building blocks. By having only one specific connectivity to the matrix, the single-site criterion is met. If constrained to using only one linking reagent such as $TiCl_4$ to deliver the active metal to the system, the method of sequential additions can only yield the two extremes with respect to connectivity to the support: surface centers with minimum connectivity to the matrix and embedded centers with maximum connectivity to the matrix (four for titanium). Which of these extremes one obtains depends on the order in which the active linking and inert cross-linking agents are added. Figure 24 illustrates the method of sequential additions obtaining both surface and embedded species.

A matrix containing only surface species may be fashioned by first linking the tin-cube with a small first dose of inert linking agent, such as silicon tetrachloride, silicon tetrachloride bispyridine, or dimethyldichlorosilane (these linking reagents all function identically in this methodology). With an appropriate sized dose that is determined empirically, the cross-linking reaction creates a rigid, robust matrix that contains unreacted isolated trimethyltin groups throughout the matrix. By isolating these unreacted corners, only one connection to the matrix is made with the metal chloride in the second dose as is illustrated in the bottom pathway in Figure 24. However, 1-connected surface sites may not be a practical target in the context of heterogeneous catalysis. The fewer connections to the matrix the greater the probability of the leaching. Therefore, it is more practical to focus on the synthesis of embedded metal centers for heterogeneous catalysis.

A matrix containing only "embedded" metal centers may be obtained by reversing the order of the linking agents (top pathway; Figure 24). Embedded in this context, refers to a catalyst in which the active metal centers have "maximum" connectivity to the surrounding matrix. In the case of titanium, this usually involves four Ti-O-Si linkages to the cube. In the first dose, the tin-cube is reacted with a limiting amount of metal chloride (active linker e.g. $TiCl_4$). Assuming all available chlorides react with Me_3Sn groups as the linking reactions progress, every metal center

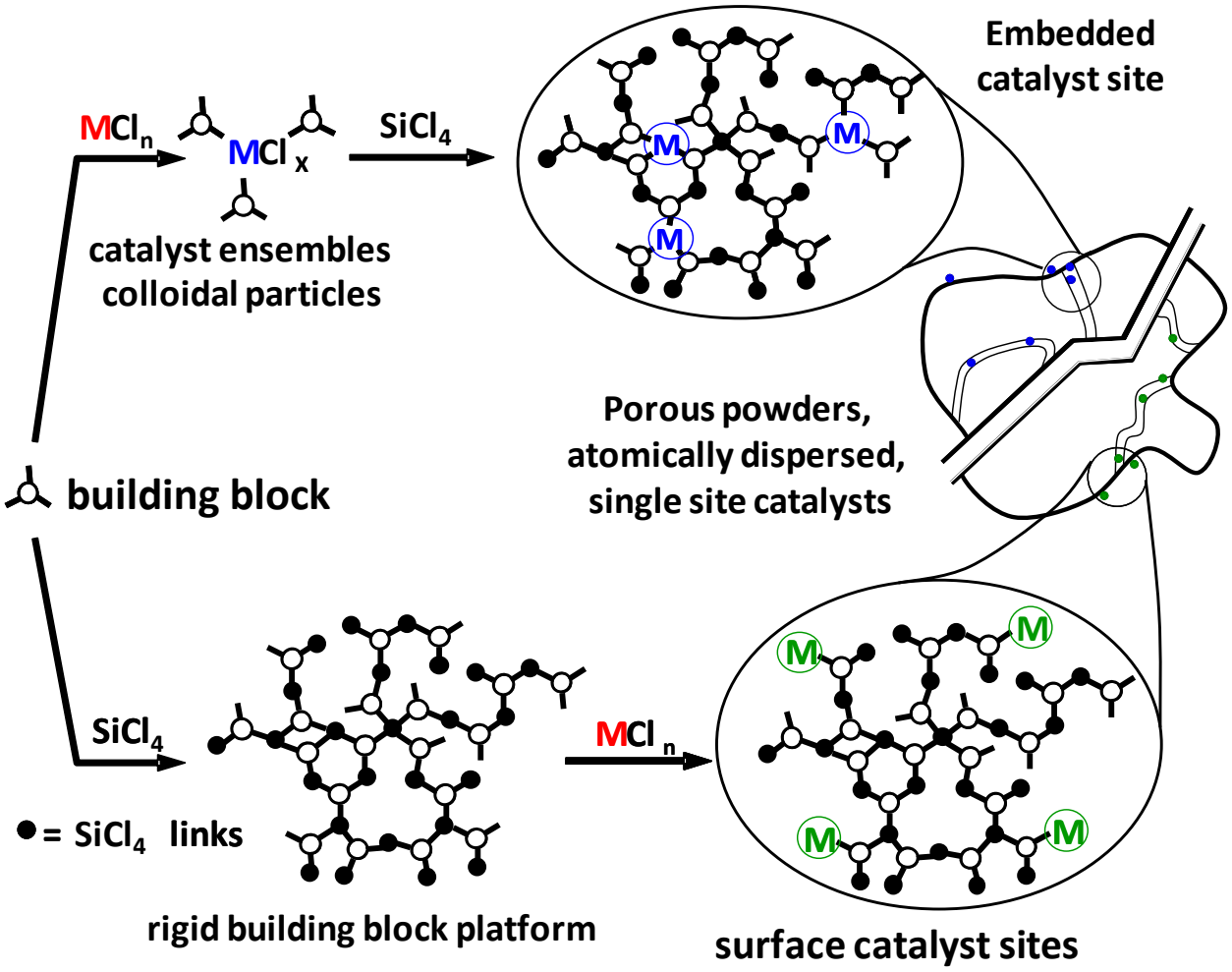

Figure 24 Illustration of the method of sequential additions. Figure was obtained from ref [75].

should achieve the same, maximum connectivity to cubes e.g. 4-connected Ti from $TiCl_4$. In contrast to surface species, the metal center is fully surrounded by building blocks, or zero chloride groups remain on the metal center, Figure *25*. The small oligomers that are formed are then cross-linked with a second dose of inert cross-linking agent such as silicon tetrachloride ($SiCl_4$) or dichlorodimethylsilane (Me_2SiCl_2). The inert cross-linking agent reacts with remaining trimethyltin groups on the building blocks linking the small oligomers from the first dose and securing the surrounding matrix, as illustrated in Figure 26.

It is important to note the active linker, the metal chloride, in the first dose is limiting with respect to the number of tin groups in the reaction. This strategy is the basis for meeting the single-site criterion. By limiting the chloride groups in the first stage of the synthesis, all the chloride ligands on the active linking agent (Ti, Figure *26*) are replaced by bonds to the Si_8-cubes. Thus, all the chlorides on the active linker will react and all Ti centers will have the same connectivity; $TiCl_4$ leads to a fully embedded site with 4 connections to the matrix, i.e., 4C-Ti sites. This ensures an unambiguous connectivity to the matrix. Within the context of this research, all catalyst sites are prepared following the embedded synthetic pathway.

The sequential addition strategy, illustrated for one linking agent, $TiCl_4$, gives the two extreme connectivities, 1-connected (surface sites) and 4-connected (fully embedded sites, Figure 27). Single-site catalysts with intermediate connectivities, 2-connected and 3-connected, may be prepared with the same strategy as 4-connected by using different mononuclear titanium precursors. Figure 28 illustrates the different precursors used during synthesis to create the targeted catalytic sites. The maximum or limiting number of connections to the matrix can be varied by changing the number of chlorides on the precursor**,** $TiCl_n(OiPr)_{4-n}$ (n = 2-4). Ultimately, the desired connectivity is targeted by the number of chloride ligands present on the metal precursor. It has been found that alkoxy groups bound to Ti do not react with the O-$SnMe_3$ corners of cube and therefore function as effective blocking groups in the cross-linking reaction.[42] The entire family of alkoxy chloride complexes, $Ti(OR)_xCl_{4-x}$, where x = 0-4, may be synthesized via simple metathesis reactions from stoichiometric mixtures of the tetrachloride and tetra alkoxide complexes.[77] When these precursors are used in place of $TiCl_4$, for example $TiCl_2(OiPr)_2$, the maximum connectivity achievable is two instead of four. The alkoxide ligands that serve as blocking groups during synthesis may then be removed or exchanged during catalysis. By combining different metal linking reagents and the method of sequential additions, a family of atomically dispersed Ti catalysts with different targeted connectivities can be achieved.

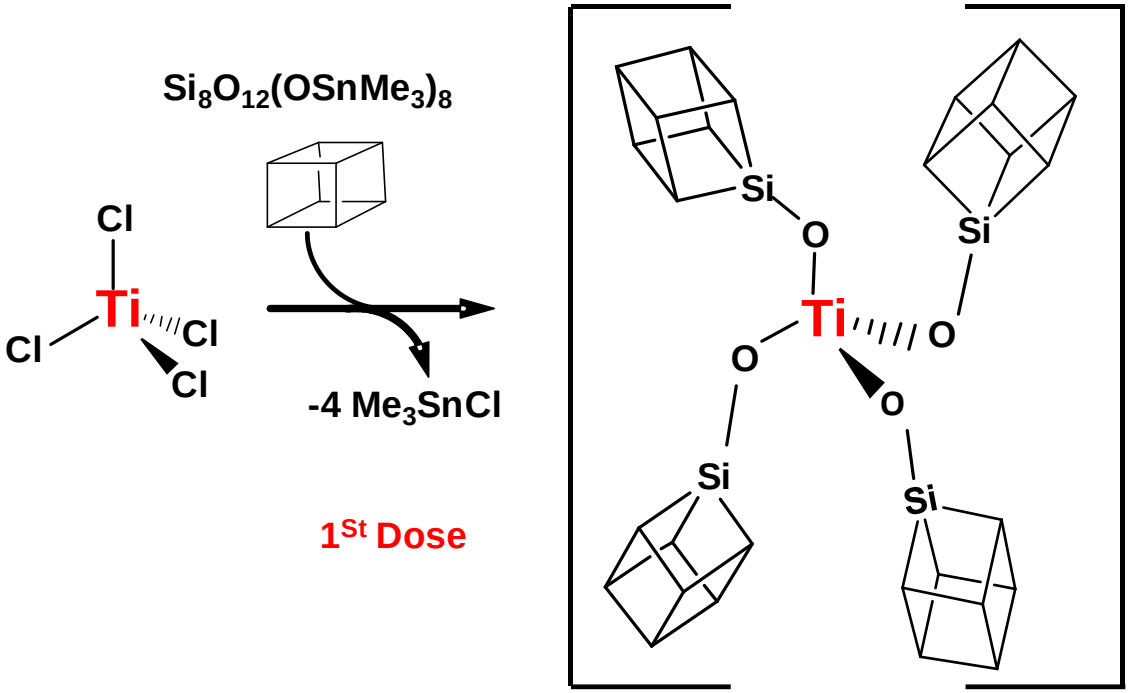

Figure 25 Illustration of the formation of 4-connected embedded titanium center.

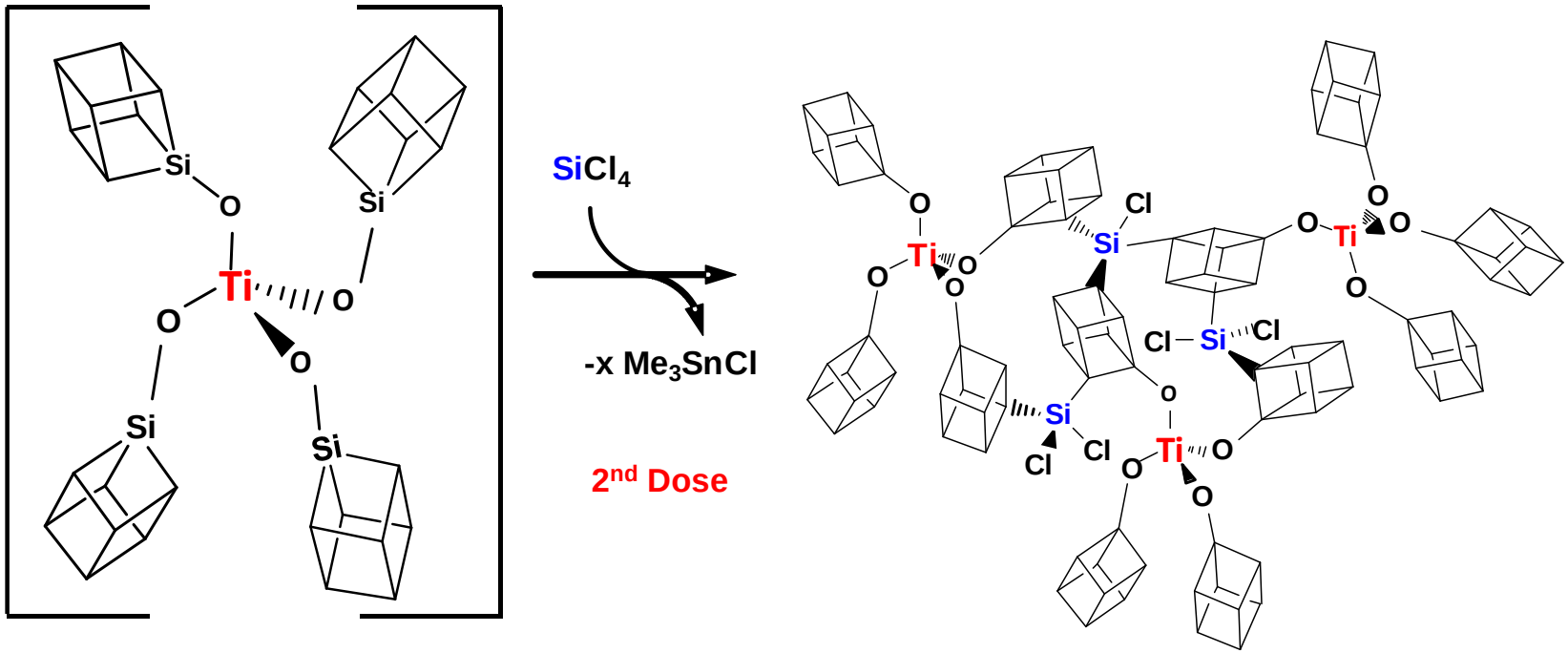

Figure 26 Illustration of the 2nd dose of the method of sequential additions the formation of the matrix by cross-linking the oligomers of the 1st dose.

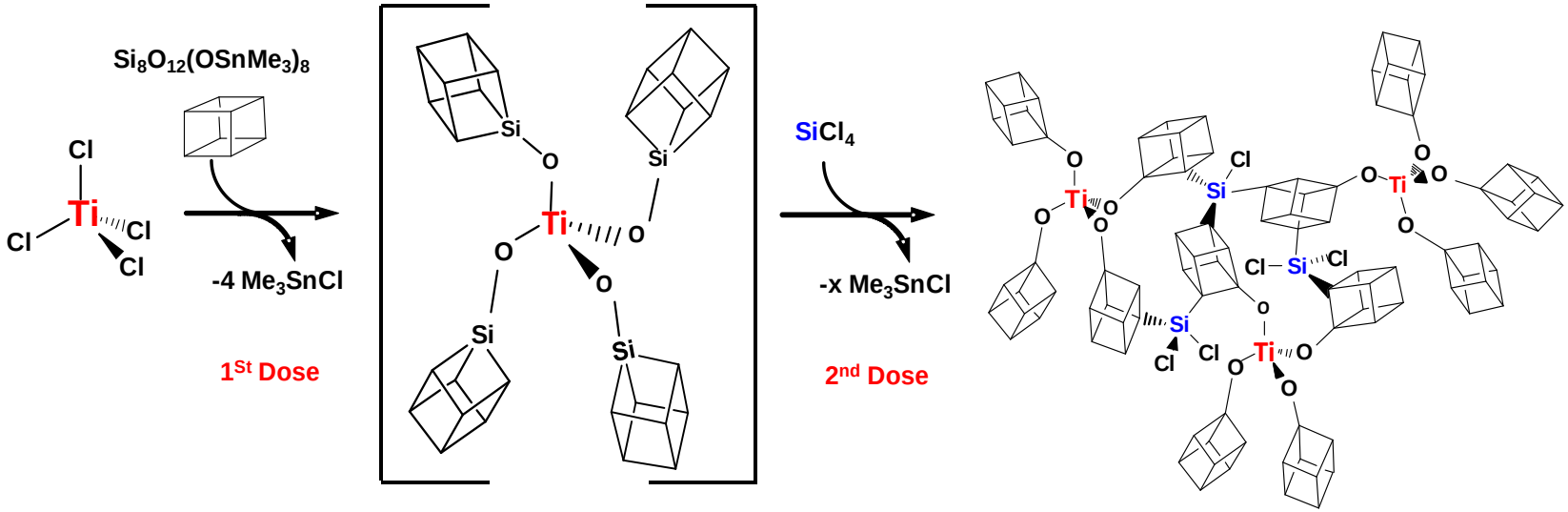

Figure 27 Illustration of the two-dose strategy employed in the method of sequential additions for fully embedded 4-connected titanium centers.

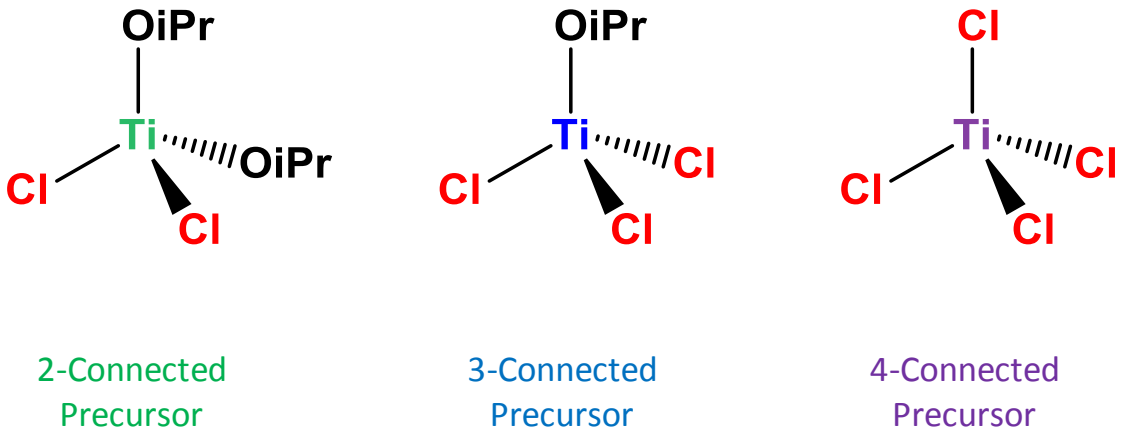

Figure 28 Mononuclear titanium precursors used to target specific connectivities to the matrix; 2-connected (left), 3-connected (middle), 4-connected (right).

Figure 29 illustrates the three unique targeted connectivities for embedded titanium catalysts synthesized using different mononuclear precursors and the method of sequential additions.

Once the connectivity of the active site is established in the first dose and the remaining matrix is cross-linked with an inert linker in the second dose, unreacted silyl chlorides may also remain in the matrix. When exposed to water these silyl chloride groups rapidly hydrolyze producing HCl and silanols. There is a possibility that HCl could disrupt the targeted connectivities by breaking the Ti-O-Si linkages. The resulting catalyst would then no longer be homogenous in connectivity and a mixture of sites with multiple connectivities would develop. Figure 30 illustrates the matrix of a 2-connected catalyst after the second dose. As the silyl chlorides react with water, HCl can be produced *in situ* and disrupt the sites creating a mixture of catalytic centers. In order to make the catalyst air stable, several methods for removing remaining silyl chloride groups have been investigated. These methods will be discussed in further detail in Chapter 3s and 4.

General Conclusion

In conclusion, the synthetic strategy which we refer to as the method of sequential additions, leads to the synthesis of well defined, isolated, single-site, heterogeneous catalysts. This notion of single-site has been brought up repeatedly because of its importance in heterogeneous catalysis. By having only one type of active site, the chances of having multiple products is reduced. In theory, multiple sites can produce different products reducing the selectivity toward the desired product. The complexity of determining the reaction mechanism is also reduced with single-site catalysts. When multiple active sites are present, the desired product can be produced by multiple mechanisms from different sites making these processes difficult to unravel and characterize. Additionally, having one type of active site makes spectroscopic techniques, such as XAS, easier to interpret because each active center gives rise to the same signal, not overlapping or interfering signals. While titanium was presented here as an example, it is important to remember that this approach can be applied to a wide variety of metal centers for numerous catalytic reactions.

Characterization

Introduction

Traditionally, a major drawback to heterogeneous catalysis is lack of knowledge about the active site. This can be attributed to traditional synthetic protocols producing multiple active sites combined with the lack of techniques available to distinguish one catalytic site from another.

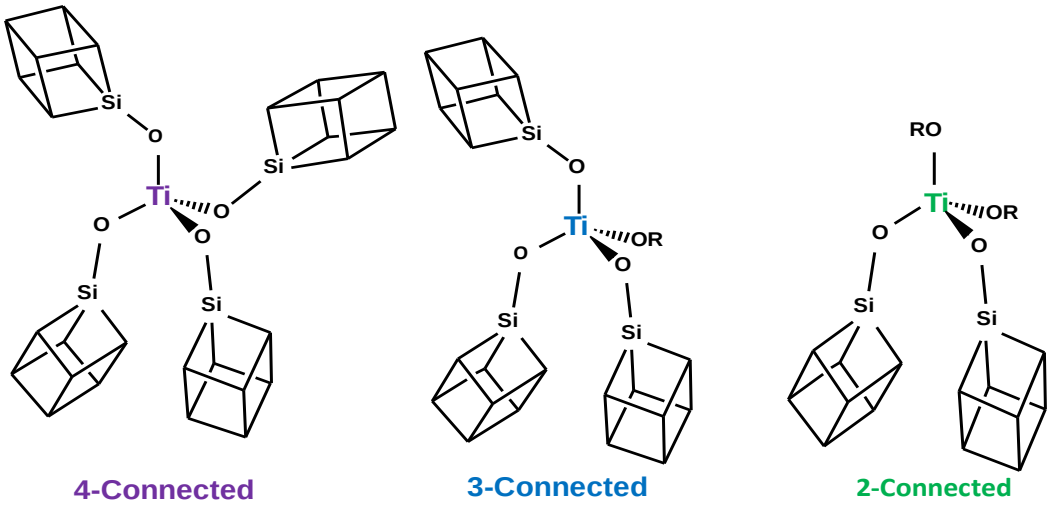

Figure 29 Illustration of three different titanium connectivities to the silicate

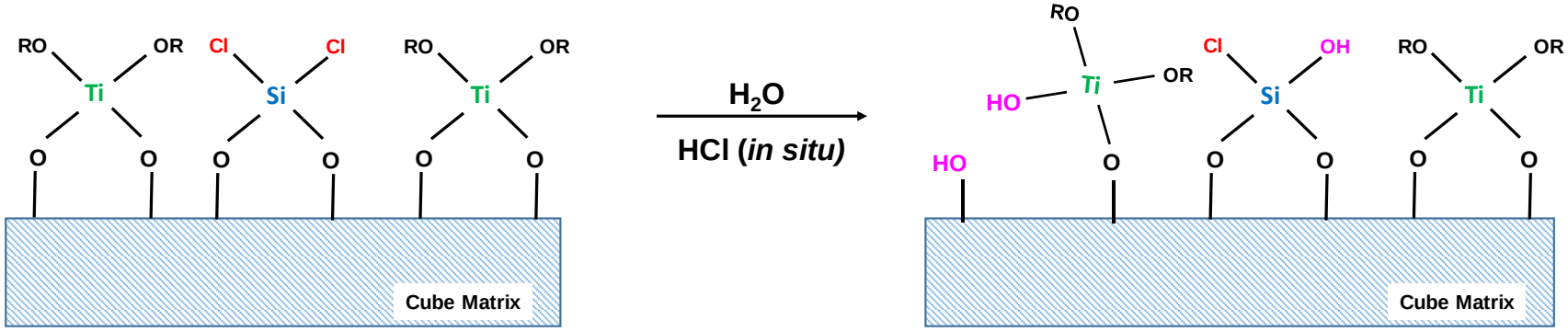

Figure 30 Illustration of a 2-connected matrix after second cross-linking illustration silyl chloride groups remain and pose the risk of disrupting the targeted connectivities.

Homogeneous catalysts are traditionally single-site in nature and are characterized using both x-ray crystallography and solution nuclear magnetic resonance spectroscopy (NMR). By utilizing the building block approach and method of sequential additions single-site heterogeneous catalysts are synthesized but lack long range order. Due to the amorphous and insoluble nature of these catalysts, traditional characterization techniques via diffraction and solution NMR are not available. However, they are still ideal heterogeneous catalysts for investigating the active site on the atomic level through the use other characterization techniques. While one technique alone may not provide all the information necessary, the combination of several techniques can provide enough detail to determine what the active site is at the atomic scale. Therefore, much effort has been spent on probing the active site using the following characterization techniques: gravimetric analysis, NMR, Fourier Transform Infrared spectroscopy (FTIR), inductively coupled plasma optical emission spectroscopy (ICP-OES), diffuse reflectance uv-visible spectroscopy (DRUV), x-ray absorption spectroscopy (XAS), and Brunauer-Emmett-Teller surface area analysis (BET. The following sections will provide a brief introduction to each characterization technique and their specific applications in this work.

Gravimetric Analysis

Connectivity, within this context, is defined as the number of titanium linkages to the silica matrix (Ti-O-Si). Traditional synthesis of heterogeneous catalysts leads to active sites with multiple connectivities. In order to claim our catalysts are single-site and different than literature catalysts, their connectivities must be defined. An experimentally simple and accurate way to indirectly determine connectivity is through gravimetric analysis.

Gravimetric analysis is defined as the chemical analysis based on a weight change that can be used to determine the extent to which a chemical reaction has occurred. In this context, gravimetric analysis can be used to provide two types of information. First, it defines the exact stoichiometry of the overall reaction. Second, it indirectly defines the local environment around the active site. The irreversible metathesis reaction that occurs between the trimethyltin groups of the building block and the highly reactive chloride groups of the titanium or silicon precursors produces defined amounts of trimethyltin chloride ($ClSnMe_3$), which are directly related to the number of bonds formed in the matrix. During the first dose, the mass lost is associated with the loss of the volatile byproduct $ClSnMe_3$. Consequently, by measuring the mass before and after the reaction, the amount of $ClSnMe_3$ can be determined and corresponds directly to the number Ti-O-Si linkages formed, Equations 12-14

$$TiCl_4 \ + \ 4\ cube \rightarrow 4\ ClSnMe_3 \ + \ Ti-(-O-Si)_4 \quad \text{Equation 12}$$

$$TiCl_3OiPr \ + \ 3\ cube \rightarrow 3\ ClSnMe_3 \ + \ PriO-Ti-(-O-Si)_3 \quad \text{Equation 13}$$

$$TiCl_2(OiPr)_2 \ + \ 2\ cube \rightarrow \ 2\ ClSnMe_3 \ + \ (PriO)_2-Ti-(-O-Si)_2 \quad \text{Equation 14}$$

According to the equation above, the number of Ti-O-Si linkages formed is equivalent to the number of $ClSnMe_3$ equivalents lost. Ultimately, the connectivity can be calculated according to Equation 15, by knowing the amount of titanium in the reaction and taking its ratio to the amount of tin lost.

$$Connectivity = \frac{[Ti-O-Si]}{[Ti\ centers]} = \frac{[ClSnMe_3]\ (mmol)}{[Ti](mmol)} \quad \text{Equation 15}$$

The weight change is directly and quantitatively proportional to the bonding environment around the active site and gravimetric analysis provides indirect characterization of the titanium connectivity.

Nuclear Magnetic Resonance Spectroscopy

While NMR spectroscopy plays a crucial role in the direct characterization of homogenous catalysts, it is difficult to directly characterize heterogeneous catalysts with this technique. Many heterogeneous catalysts are metals bound to solid supports that are not soluble in NMR solvents. There are several NMR active nuclei that allow for solid state NMR (ssNMR) techniques, but in the case of this work, Ti is not a viable nucleus. ^{29}Si is available, but it is not very sensitive and it would only characterize the matrix not the actual catalytic active site. Even though NMR is not a viable characterization technique in the traditional sense, it is very important in the characterization of the catalytic reaction itself.

Two important aspects in catalysis are concentration and purity of reactants and products. One way to evaluate these properties is through the use of quantitative nuclear magnetic resonance spectroscopy (qNMR). Here the focus will primarily be on the use of proton NMR, ^{1}H, but this concept of quantitative NMR could in theory be applied to any active nuclei. In NMR, the intensity of each signal is directly proportional to the number of corresponding resonance nuclei (spins), assuming that there are no overlapping or underlying signals. In contrast to other techniques, response factors are not dependent on molecular properties thus only require the internal standard to a have a different molecular structure than the analyte.[78] The fundamental relationship of qNMR expressed by Equation 16.[79]

$$I_x = K_s N_x \quad \text{Equation 16}$$

In this equation, I_x is the signal response, K_s is a spectrometer constant, and N_x is the number of spins. Since the primary focus here will be on the use of proton NMR, ^{1}H, the equation has been modified to H_x instead of N_x to represent the number of protons proportional to a specific signal, Equation 17.

$$I_x = K_s H_x \qquad \text{Equation 17}$$

When acquisition parameters are optimized, mainly relaxation delay, K_s is an identical constant for each resonance line within the same spectrum. Therefore, the ratio of two resonance lines from two different molecules within the same spectrum can be obtained, Equation 18. The relaxation delay should be long enough so that all protons relax fully before the next pulse. An in depth discussion on optimizing acquisition parameter has been previously discussed by Malz *et.al.[79]*

$$\frac{I_x}{I_y} = \frac{H_y}{H_x} \qquad \text{Equation 18}$$

Consequently, the molar concentration (C) of x to y can be directly calculated, Equation 19.

$$\frac{C_x}{C_y} = \frac{I_x H_y}{I_y H_x} \qquad \text{Equation 19}$$

This notion of qNMR allows for a simple and relatively fast method for following the kinetics of catalytic reactions through the use of an internal standard. With the addition of a substance whose resonance lines do not interfere with any resonance lines of the reactants and products of the reaction, qNMR can be used to determine concentrations at any point in time during the reaction. It is important to use an internal standard that is not effected by the catalytic reaction in question. qNMR was the main technique used to follow the kinetics of the reactions in this thesis.

Fourier Transfer Infrared Spectroscopy

Infrared (IR) spectroscopy has become a staple in the characterization of heterogeneous catalysts because of its sampling versatility, high resolution, and it is not limited by pressure and temperature.[80] It has been widely used in the literature for the characterization of titanosilicates. Frequently, it is used to follow the adsorption and desorption of weakly bound water molecules in titanosilicates such as TS-1. Figure 31 shows the gradual loss of the broad adsorption feature at 3700 – 2500 cm^{-1} in correspondence with the dehydroxylation of TS-1 at high temperatures.[81] Figure 32 shows the IR spectrum of the tin-cube building block and is

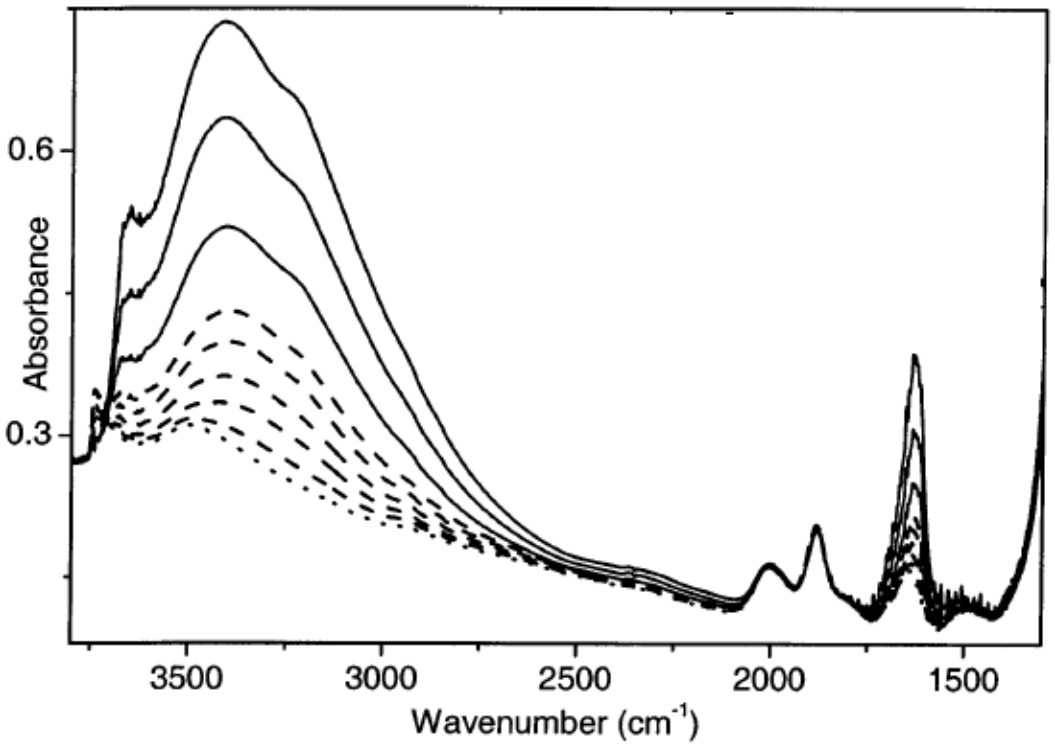

Figure 31 FTIR spectra following the dehydration of TS-1, low H_2O absorption dotted lines, high concentration solid lines. Figure modified from ref [56].

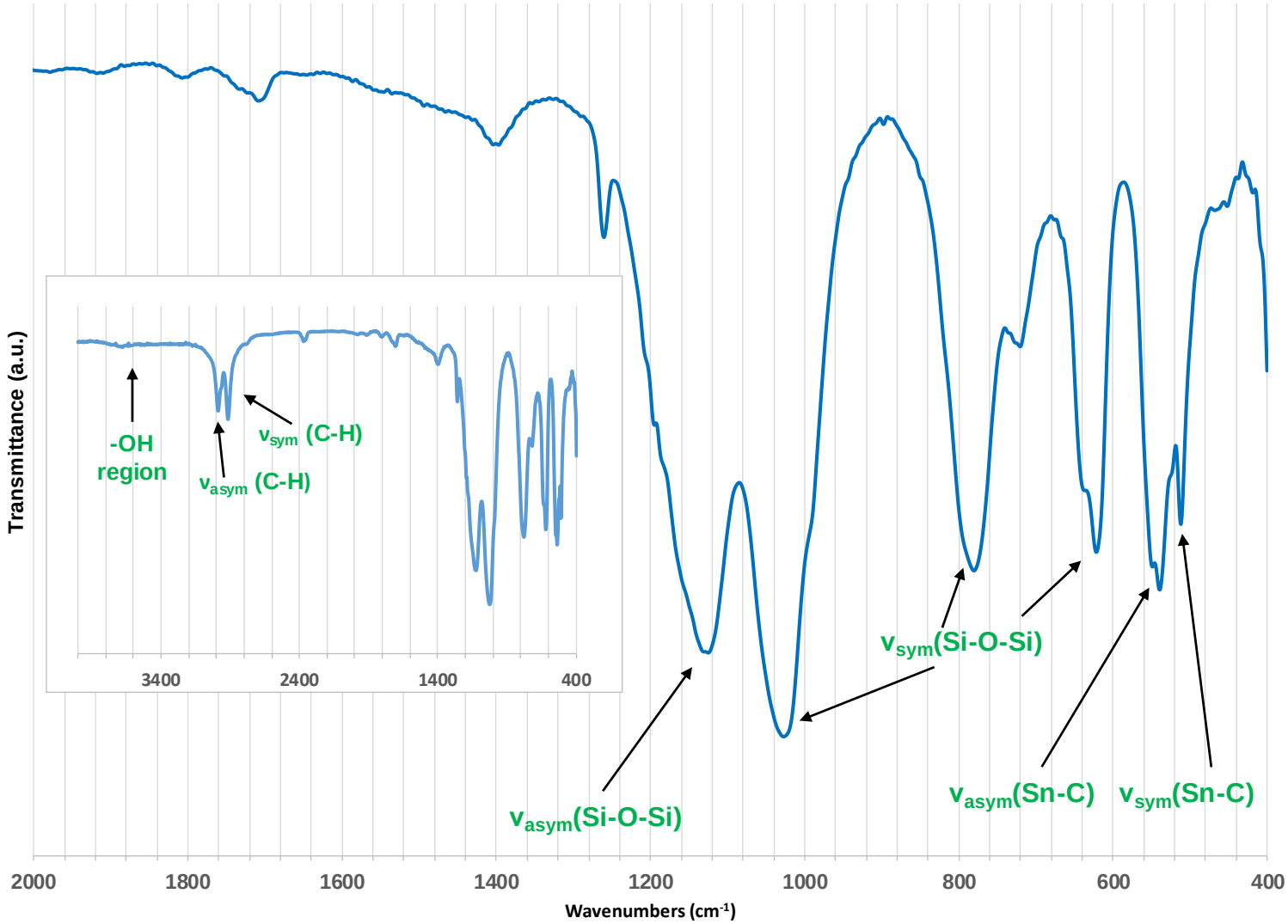

Figure 32 FTIR spectrum of the tin-cube building block illustrating the fingerprint regions used for characterization.

labelled to illustrate the different regions used to characterize the catalysts and matrices synthesized in this work.

Possibly the most convenient way to determine if titanium has been incorporated into a silica matrix is through infrared spectroscopy. In this work, IR spectroscopy is used as a fingerprint technique in characterizing both first and second generation titanosilicates. The IR spectrum can be broken down into several key characterization regions/features. Perhaps the most important region or in this case feature is located at 960 cm^{-1}.[82] This Ti-O-Si vibrational band is indicative of titanium centers incorporated into a silicate lattice. In pure silicate matrices, there is no visible band at 960 cm^{-1} but in titanosilicates a feature at 960 cm^{-1} is present and has been attributed to the stretching mode of SiO_4 units that are bonded to a Ti ion, Figure 33.[81,83]

The second region of importance is the aliphatic region, 2800 – 3000 cm^{-1}. In this region, stretches corresponding to both the methyl groups of trimethyltin and the hydrocarbon chains of the isopropoxide groups can be seen. The IR spectrum can be used to qualitatively observe the loss of the trimethyltin features as cross-linking of cubes occurs with the loss of trimethyltin chloride.

In addition to the aliphatic region, at slightly higher wavenumbers, 3400 cm^{-1} – 3800 cm^{-1}, the presence of silanols groups can be monitored. The presence of a broad feature around 3600 cm^{-1} indicates the presence of –OH in the matrix and is evidence of catalyst exposure to air at some point in its synthesis.

Lastly, the IR can be used to identify other ligands present in the catalytic ensemble. For example, pyridine ring stretches absorb in the 1400 – 1700 cm^{-1} region. Not only can pyridine be identified, but the IR stretches correspond to nature of the sites present in the system, Lewis acid sites, BrØnsted sites, or silanols.[84] Figure 34 depicts the different modes of pyridine binding in an aluminosilicate matrix. Each type of site has one unique absorption feature and has been highlighted to illustrate their differences. Other small molecules can also be identified via signature features.

Sample Preparation and Data Collection FTIR

All IR spectra are obtained using a Thermo Nicolet IR100 located inside a nitrogen atmosphere glovebox (Braun LabMaster) to reduce the exposure and absorption of water, Figure 35. Each spectrum is prepared and analyzed according to the following procedure (unless

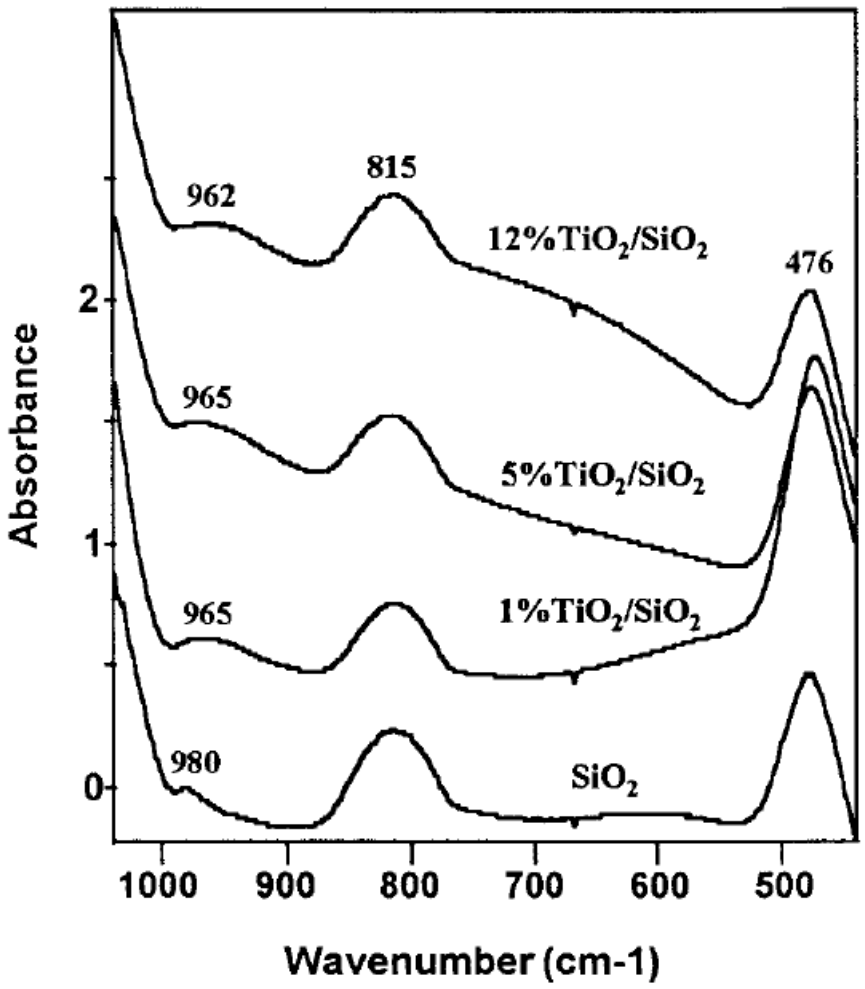

Figure 33 FTIR spectra of pure SiO_2 (bottom) and TiO_2 showing the absence of the 960 shoulder when Ti is not present in the matrix. Figure was obtained from ref [82].

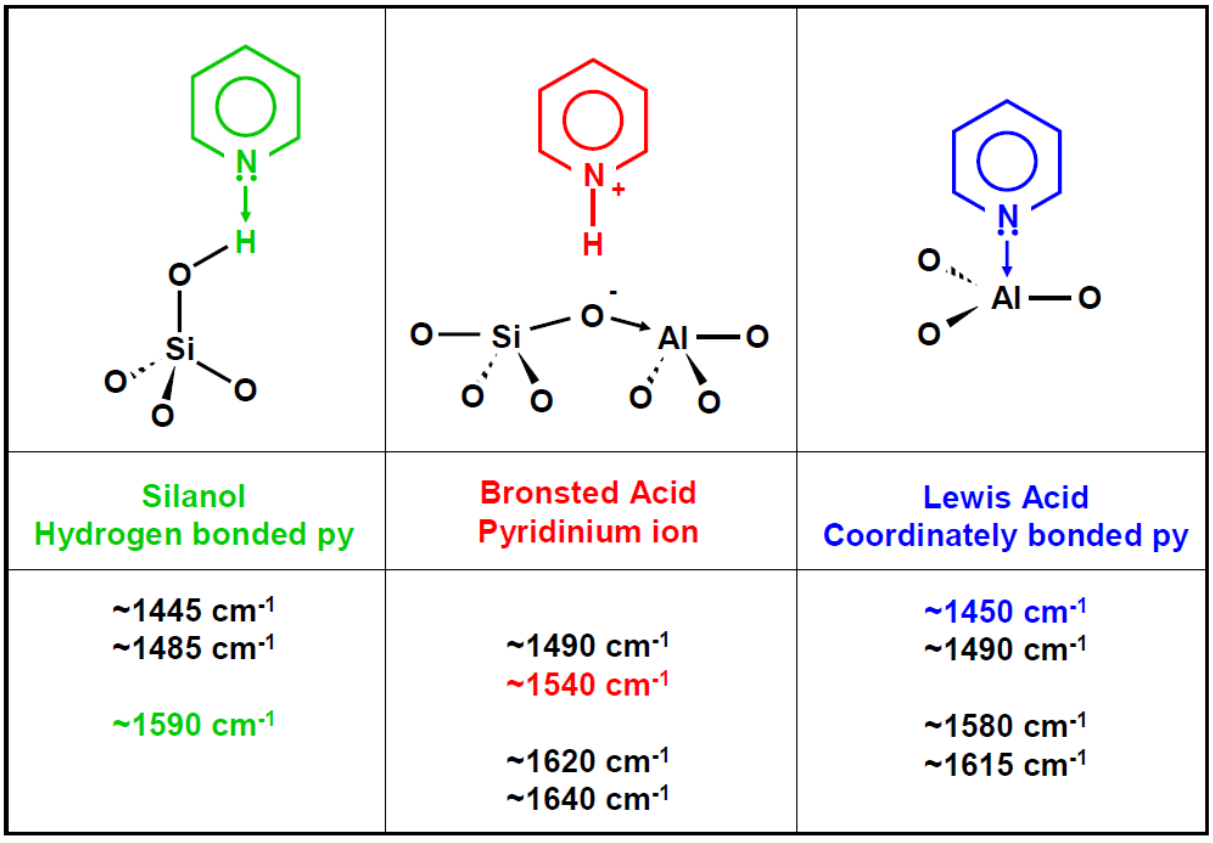

Figure 34 Modes and frequencies of pyridine binding on aluminosilicates (left) silanols, (middle) Brønsted, (right) Lewis.

Figure 35 Photograph of the IR spectrometer located inside a nitrogen atmosphere glovebox.

otherwise noted): Approximately 40 mg of dry KBr is pressed into a pellet and analyzed as a background; 32 scans are collected with a 4 cm^{-1} resolution ranging from 400 – 4000 cm^{-1}. Once the background is collected, a ~1 – 2 wt% of sample is pressed into the same KBr background pellet and the data collected under the same conditions.

Inductively Coupled Plasma Atomic Emission Spectroscopy

Atomic spectroscopy is a useful technique in the identification and quantification of trace metals. In atomic spectroscopy samples are first digested in strong aqueous acids (1:1 HF:HNO_3 vol) and then atomic ions are created in a plasma. Each specific element is identified by its characteristic wavelength corresponding to the absorption or emission of ultraviolet or visible radiation. There are three different categories of atomic spectroscopy: 1) absorption, 2) emission, and 3) fluorescence. In the work described here, atomic emission spectroscopy is used exclusively.

As previously mentioned, one way to characterized the activity of heterogeneous catalysts is by expressing the substrate concentration per number of catalyst sites, turn over number. Hence, it is of utmost importance to accurately determine the weight percent titanium (Ti wt. %) for each catalyst synthesized. In traditional synthesis methods, weight percent is not a viable measurement of the amount of active catalyst because there is often a mixture of sites present and the actual number of active sites in unknown. On the contrary, by using the building block approach and method of sequential additions only one type of active site should be present in the matrix. Ideally, this strategy converts 100% of the titanium from the precursor to identical active centers and Ti wt. % allows one to calculate activity on a per site basis, i.e., TON.

Sample Preparation and Data Collection ICP-OES

Elemental analysis for titanium is obtained via a Perkin Elmer Optima 2100 DV Inductively Coupled Plasma – Optical Emission Spectrometer equipped with a Scott spray chamber. A calibration curve is obtained by preparing six solutions containing different known concentrations of titanium using standard solutions for ICP (1000 mg/L, Fisher Scientific), in ultrapure water, ranging from 2 ppm to 100 ppm. The solutions are then measured according to the method presented in Table 4. A Beer's Law plot (intensity vs. concentration) is automatically generated by the instrument, Figure 36. While it is possible to save calibrations for future use, a new

Table 4 Summary of ICP-OES parameters.

Delay Time	**60 seconds**	
Sample flow rate	**1.50 mL·min^{-1}**	
Replicates	**3**	
Flush time	**0**	
Plasma view	**Axial**	
Points per peak	**7**	
Emission Lines	**Wavelength (nm)**	**Integration regions (nm)**
	334.940	**334.794 – 335.086**
	336.121	**335.996 – 336.276**
	337.279	**337.126 – 337.432**
	334.903	**334.757 – 335.049**

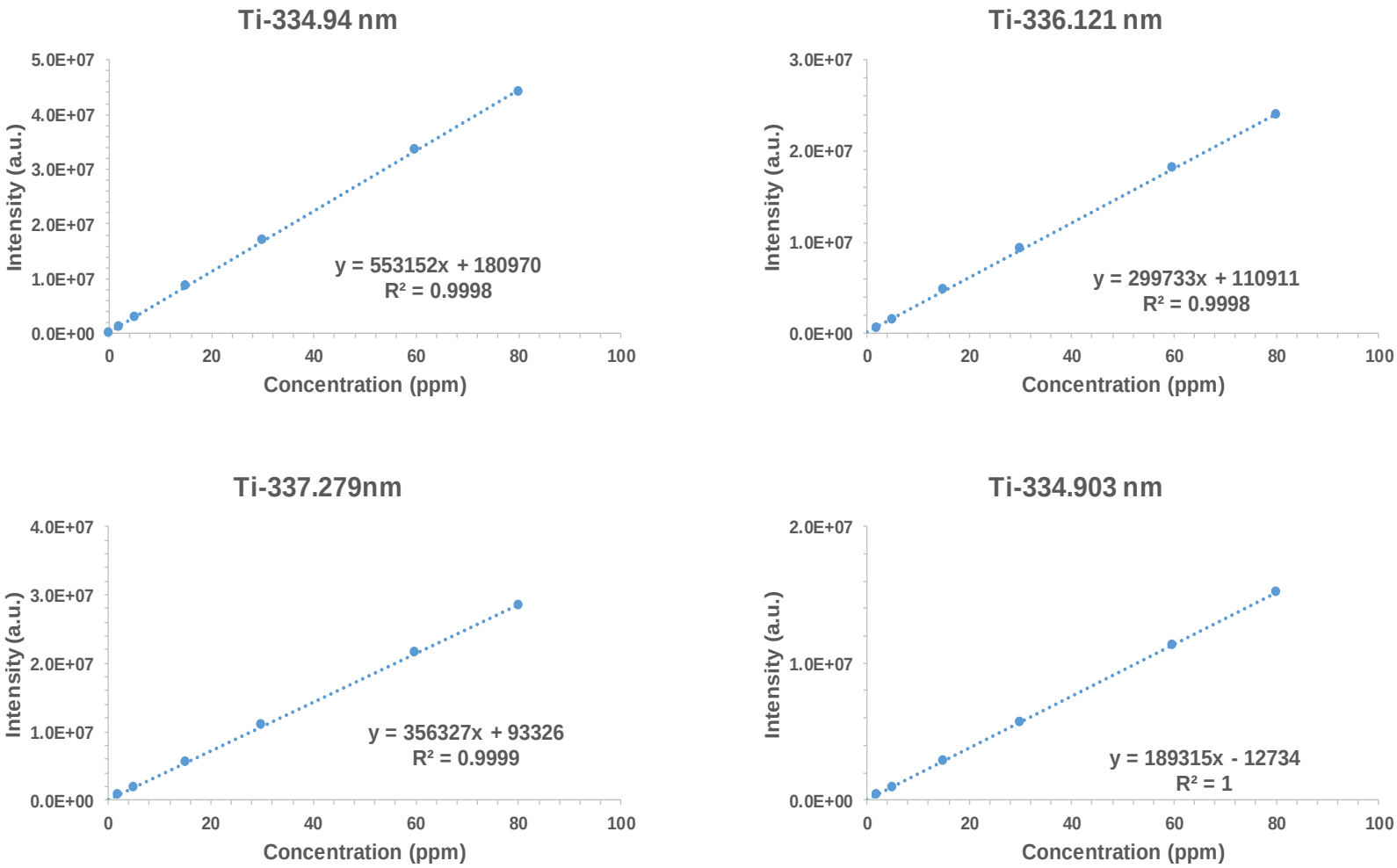

Figure 36 Illustration of the calibration curves obtained for each titanium wavelength.

calibration curve from “fresh” standard solutions is obtained each time to account for any changes in the instrument that may have occurred over time.

Sample solutions are prepared according to the following procedure: empty polypropylene bottles are weighed with caps and taken into a nitrogen atmosphere glovebox. Approximately 10 – 30 mg of sample powders are added to the bottles, capped, and reweighed outside of the glovebox to obtain an accurate weight. The sample powders are then digested overnight in a mixture of concentrated nitric acid (~1 mL) and hydrofluoric acid (~1 mL). The exact amount of acid is not crucial to determining the concentration of the solution; only the total mass of the solution must be known. Once the samples have been completely digested, the samples are diluted to ~50 g total weight with ultrapure water and the final concentration of the solution, in ppm, is calculated using Equation 20.

$$[Sample] = \frac{mass\ of\ catalyst\ (g)}{total\ mass\ of\ solution}\ x\ 10^6 \qquad \text{Equation 20}$$

The samples are analyzed under the same parameters described above. In order to achieve a more accurate weight percent, each sample was prepared and analyzed in triplicate and the average value reported. The actual titanium weight percent is determined by Equation 21.

$$wt\%\ Ti = \frac{Ti\ Concentration\ ICP\ (ppm)}{total\ sample\ concentration\ (ppm)}\ x\ 100\% \qquad \text{Equation 21}$$

In addition to determining initial Ti wt.%, ICP was also used to test for leaching of Ti during catalytic reactions as will be further discussed in Chapters 3 and 5.

Diffuse Reflectance UV-Visible Spectroscopy

Diffuse reflectance UV-Visible spectroscopy (DRUV) has become a key characterization technique for finely ground powders including titanosilicates. Surface reflected-electromagnetic radiation is collected analyzed to obtain a reflectance spectrum. Reflectance can be divided into two different types: regular (specular) and diffuse reflections. If a surface has a glossy or mirror like surface, the reflections are often considered specular. Specular reflectance is a result of reflection occurring at the surface of the sample without any transmittance into the sample.[85,86] Consequently, the angle of reflections is equal to the incidence angle, Figure 37. Spectroscopic information of materials that produce only spectral reflectance can often be obtained using simpler techniques such as external and internal reflectance measurements.[86]

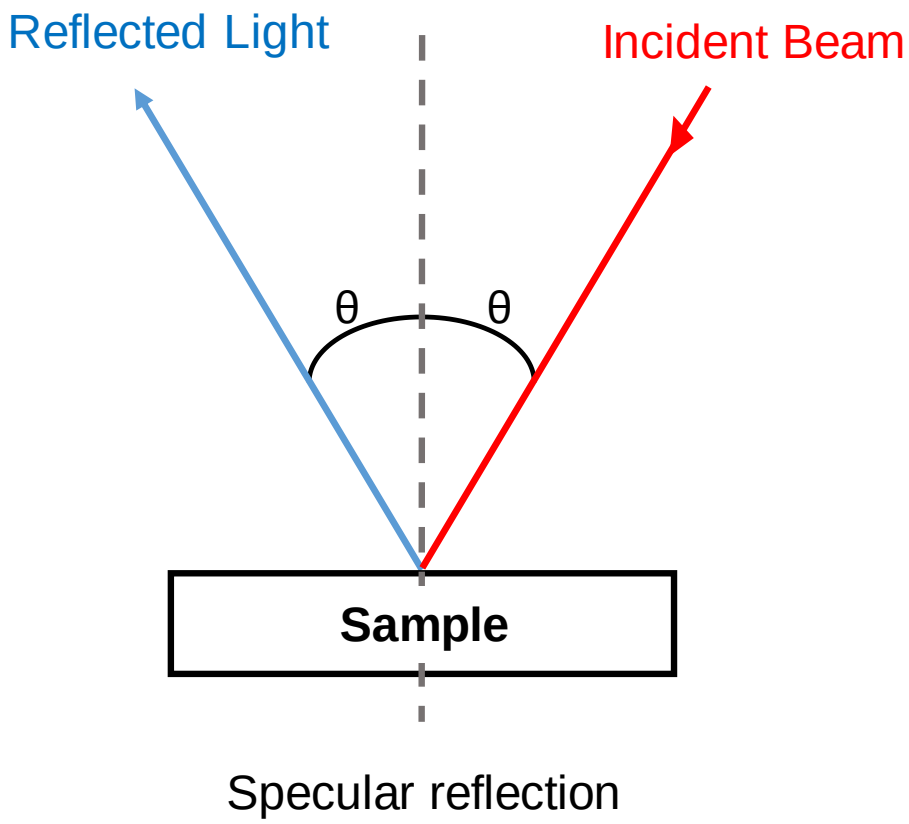

Figure 37 Illustration of specular reflection showing the incident angle is equal to the reflectance angle.

In contrast, diffuse reflections are often associated with powders whose surfaces are considered to be dull or mat. Diffuse reflections are a result of multiple scattering patterns: diffraction, reflection, and refraction. In addition, some of the radiation is partially absorbed by the sample at specific wavelengths or frequencies.[85] Therefore, the angle of reflection of the emitted radiation is independent of the angle of incidence, Figure 38.

It is important to understand that diffuse reflections can also have specular components and thus increasing the complexity of data treatment. Therefore, it is crucial to limit the specular reflection which can be done by tailoring sample preparation and the instrument. More information on alleviating specular reflection will be presented later.

The most widely used theory in treating diffuse reflection was developed by Kubelka and Munk.[85] Several assumptions are made in the Kubelka-Munk theory; 1) there is no specular component in the reflections detected; 2) the particle sizes are much smaller than the sample thickness, 3) the sample is infinitely thick. In other words, the incident beam never completely penetrates the sample reaching the sample holder; 4) the incident beam is smaller than the sample diameter to avoid interfering optical effects. The Kubelka-Munk theory can be expressed by Equation 22.

$$F(R_\infty) = \frac{(1-R_\infty)^2}{2R_\infty} = \frac{k}{s} \qquad \text{Equation 22}$$

Where R_∞ is the diffuse reflectance of an infinitely thick sample, k is the molar absorption coefficient of the sample, and s is the scattering coefficient. However, it is impractical to measure absolute reflectance therefore R_∞ can be represented similar to transmittance, Equation 23

$$R'_\infty = \frac{R_{\infty\, sample}}{R_{\infty\, standard}} \qquad \text{Equation 23}$$

The Kubelka-Munk equation operates under the assumption that no specular reflection occurs. This assumption becomes valid when samples are diluted with a non or low absorbing powder so that the specular reflections resemble those of the standard and are therefore canceled out of the equation.[86]

Similar to Beer's law in transmission spectroscopy, a linear relationship between analyte concentration and reflectance can be quantitated by the following relationship, Equation 24

$$F(R_\infty) = \frac{(1-R_\infty)^2}{2R_\infty} = \frac{K}{S} = \frac{2.303\,\varepsilon C}{S} \qquad \text{Equation 24}$$

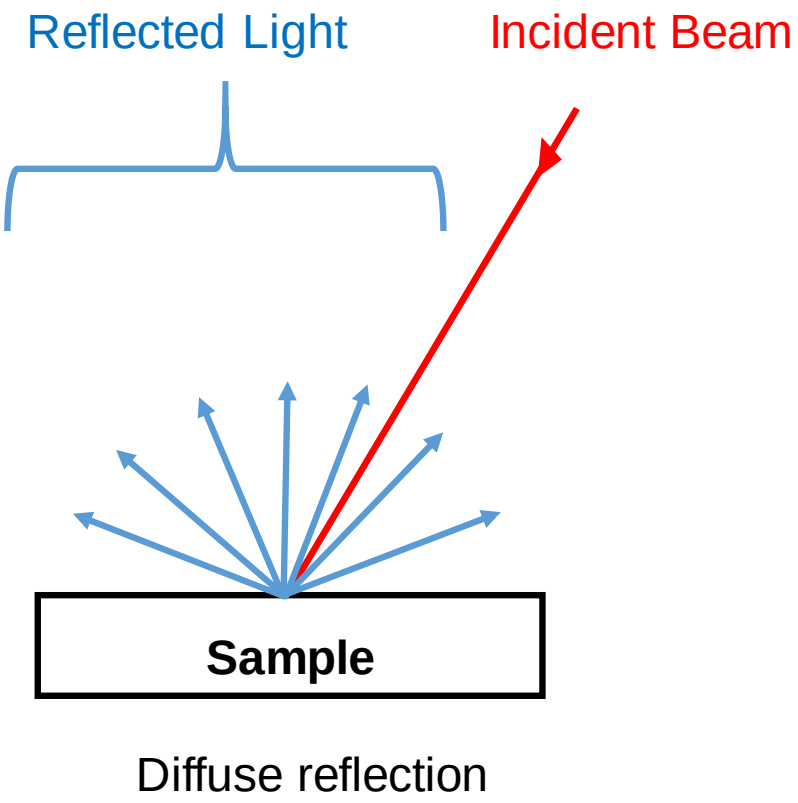

Figure 38 Illustration of diffuse reflections where the incident angle does not equal the reflected angles.

Here, K is twice the Beer's law absorption coefficient, S is twice the scattering coefficient, ε is the extinction coefficient, and C is the molar concentration. Like Beer's law in absorption, deviations from linearity are observed indicating the presence of specular reflectance at high sample concentrations.[85]

One-way diffuse reflectance can be presented is as a plot of the log of $F(R_\infty)$ as a function frequency or wavelength, Equation 25.

$$log\, F(R_\infty) = log\, \varepsilon + log \frac{2.303\, C}{S} \qquad \text{Equation 25}$$

In order to relate diffuse reflectance to absorption or transmittance, it is more frequently represented as "apparent absorbance" or log ($1/R_\infty$) vs frequency or wavelength.

Applications for Diffuse Reflectance UV-Visible Spectroscopy

A challenge in heterogeneous catalysis is the identification of oxidation states and coordination environment of transition metal active sites.[87] By using DRUV, both d-d transitions and charge transfer transitions can be probed to learn about the oxidation and coordination state of transitions metals. For this reason, in the last few decades DRUV has become an important characterization technique for heterogeneous catalysts, especially titanosilicates. DRUV has been used to obtain information about the first and second coordination sphere of titanium.[82] Ligand to metal charge transfer (LMCT) between the coordinating ligands (X = H-O^-, Ti-O^-, Si-O^-, etc.) and the empty d orbitals of Ti^{4+} can be determined according to the following equations:

$$\bar{\nu}(cm^{-1}) = 30\,000[\chi_{opt}(X) - \chi_{opt}(Ti)] \qquad \text{Equation 26}$$

$$\bar{\lambda}(nm) = \frac{1}{\bar{\nu}} * 10^7 \qquad \text{Equation 27}$$

The coordination number of titanium plays an important impact on $\chi_{opt}(Ti)$. According to literature $\chi_{opt}(Ti)$ increases as the titanium site moves from a tetrahedral to an octahedral complex; from 1.82 to 2.05 respectively.[82] Therefore, the octahedral sites are expected to absorb at a higher wavelength than their corresponding tetrahedral sites. While a clear red shift in wavelength can be seen between tetrahedral and octahedral titanium site, there are other factors that affect the wavelength. For example, both TS-1 and 1.5 wt% TiO_2 – SiO_2 mixed oxide contain tetrahedral sites, but exhibit different absorptions peaks, Figure 39.

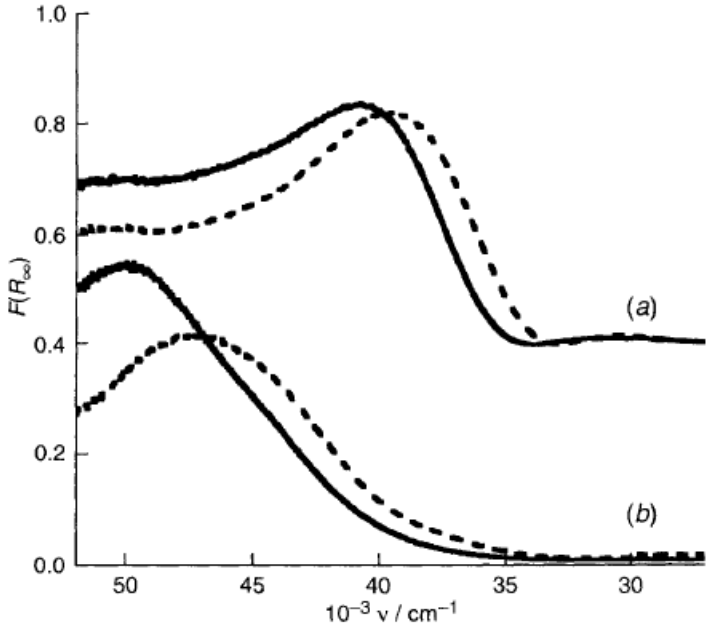

Figure 39 DRUV spectra for dehydrated (-) and hydrated (- -) TiO2 (a, offset by 0.4) and TS-1 (b). Figure was reprinted from ref [87].

Dehydrated TS-1 presented three deconvoluted components centered at 199 nm, 227 nm, and 248 nm while $TiO_2 – SiO_2$ was centered at 250 nm, 50 nm higher than TS-1. It is argued that the difference in the Ti-O-Si bond angles for TS-1 and $TiO_2 – SiO_2$ is responsible for the changes in LMCT transition energy.[88] The Ti-O-Si bond angle in the mixed oxide is 159^0 compared to 163^0 in TS-1 resulting in lower π donation and decreasing transition energy. The difference in bond angles has been proposed to be a result of open and closed titanium sites, $Ti(OH)(OSi)_3$ and $Ti(OSi)_4$ respectively, Figure 40.[88]

DRUV Spectra and Interpretation

Heterogeneous catalysts often possess a mixture of titanium sites, each presenting their own absorption feature in the UV-Vis spectrum. This often leads to overlapping signals and the need for spectral deconvolution is often necessary. Frequently, the overlapping signals combined with the complex factors affecting the LMCT energy leads to different interpretations of DRUV data. Therefore, DRUV should be used in tandem with other spectroscopic techniques.[87]

Sample Preparation and Data Collection

In this research, the titanium wt% for all samples ranges from 1.80 – 15.5%. Each sample was then diluted with KBr to between 50 wt% – 100 wt%, of the original sample concentration to make sure the absorbance is on scale (0 – 1)

Inside a nitrogen atmosphere glovebox, anhydrous KBr is added to a polystyrene vial containing the sample of interest and a 3/8 in. Plexiglas® ball. To prepare Homogenous samples after the addition of KBr the vial is capped and the samples are mixed using a Wig-L-Bug®. By homogenizing the samples, reliability and reproducibility of the samples are ensured. Spectral reflection interference is reduced by decreasing particle size due to smaller bandwidths and enhanced relative intensity. This mixture is then pressed into the well of an UHMW Polyethylene (McMaster-Carr) plate.[89] Careful precautions were taken to make sure the sample was as smooth and flat as possible. A quartz cover slip was placed over the sample and secured using Scotch tape around all edges, left Figure 41. Tape was used to prevent the sample from exposure to atmosphere. To avoid possible reflectance signals from the tape, a window is cut in a sheet of black construction paper to the size of the sample blocking any signal from materials other than the sample, right Figure 41 . A blank sample containing only KBr is prepared and used as the background spectrum. Additionally, a spectrum of the construction paper is

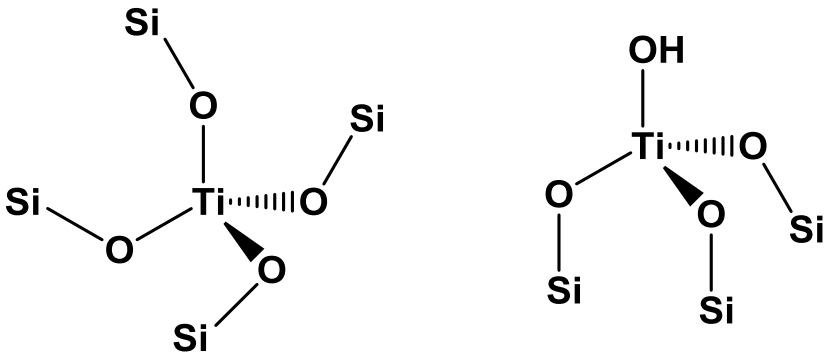

Figure 40 Illustration of the two different types of tetrahedral titanium sites found in titanosilicates, closed (left) and open (right).

Figure 41 Photograph of the DRUV sample cell prepared inside a nitrogen atmosphere glovebox, left-without cover, right-with black cover to mask the tape.

obtained. The construction paper did not contribute its own reflectance spectrum. Percent reflectance spectra are collected on a Cary 5000 equipped with an integrating sphere under the following parameters:

- Accessory – 150 nm Integrating Sphere (DRA)
- Data interval – 1.1 nm
- Slit bandwidth – 2 nm
- Averaging time per nm – 0.16 sec
- Scanning rate – 400 nm/min
- Reduced slit
- Beam mode – double
- Baseline correction – yes
- Range nm – 190 – 800

An additional Ti-free building block platform spectrum is obtained. The remaining tin groups of the tin-cube building block contribute to an absorption feature close to the absorption feature for tetrahedral titanium. Thus, the Ti-free platform is used as a secondary DRUV background for the titanium catalysts presented in this work. In order to correct for the influence of tin, the Ti-free spectrum function is multiplied by an arbitrary coefficient (0.1 – 0.9) depending on the concentration of tin sites remaining in the matrix. This corrected spectrum is then subtracted from the raw sample data resulting in the final DRUV spectra. A more detailed discussion of secondary background subtraction is presented in Chapter 5.

X-ray Absorption Spectroscopy

Introduction

X-ray absorption spectroscopy (XAS) is a direct method to investigate the local atomic environment within approximately 6 Å of the absorbing atom. X-ray absorption is the result of an atom absorbing the energy of an x-ray leading to the ejection of a core electron to a higher unoccupied energy orbital or into the continuum, Figure 42. The atom is now said to be in an excited state where one of the core electron levels is empty. Following excitation, typically within a few femtoseconds, the excited state decays as an electron from a higher energy level fills the empty core shell. As the core hole is filled, an x-ray with welled defined energy is admitted corresponding to the specific atom. This phenomenon is known as fluorescence, Figure 43. Therefore, XAS can be measured in either transmittance or fluorescence mode.

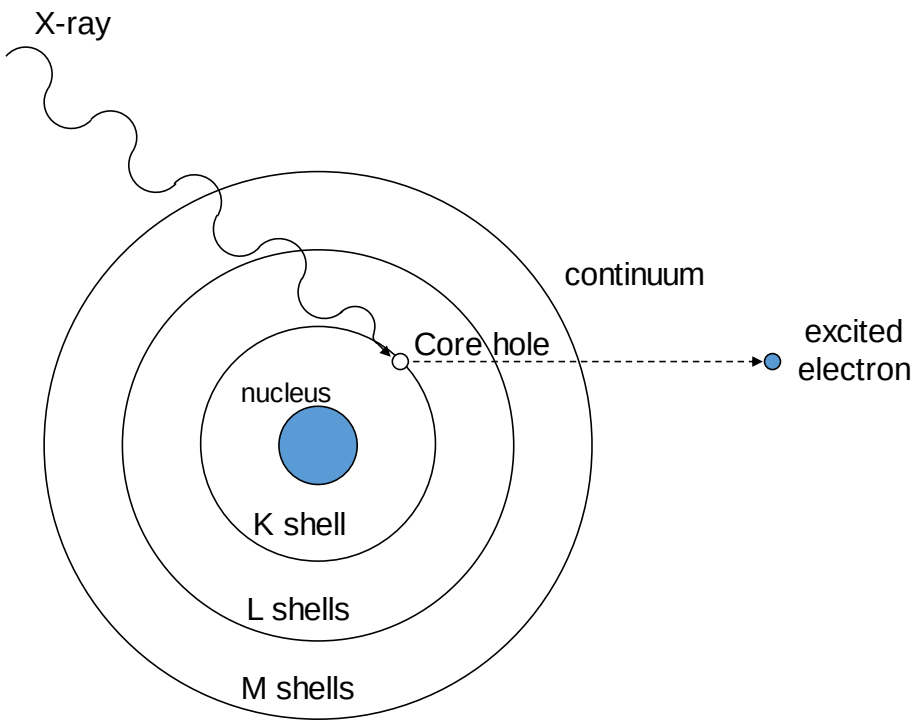

Figure 42 A core electron is excited by a X-ray photon of the proper energy.

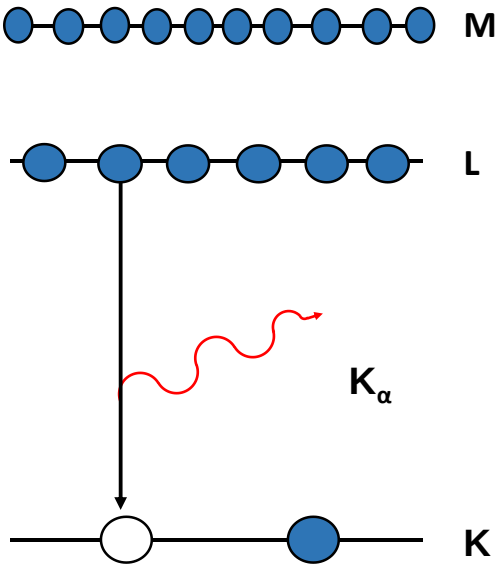

Figure 43 Fluorescence decay of the excited state.

Table 5 summarizes the specific absorption edge for x-ray transitions while Figure 44 correlates the energies of the absorption edge with the atomic number of the absorbing atom.

XAS spectra are sensitive to the formal oxidation state, coordination number, site-symmetry, distance and type of neighboring atoms. As a result, XAS can be used to determine the chemical state and local structure about a specific site at the atomic level. In contrast to single crystal x-ray diffraction, crystallinity is not required and thus XAS has become a vital tool for the characterization of amorphous materials.[90]

Traditionally, XAS is divided into two regions for interpretation, Figure 45: 1) x-ray absorption near-edge structure (XANES); and 2) extended x-ray absorption fine-structure (EXAFS). XANES is sensitive to oxidation state and coordination geometry of the absorbing atom. On the other hand, EXAFS is used to determine the local bonding parameters such as distances, coordination number, and types of adjacent atoms. XAS is an element specific technique which increases its selectivity. In theory, for metal complexes, the x-ray incident beam can be tuned to the binding energy of any atom. Therefore, information can be obtained about either the metal itself or the coordinated ligands. The focus presented here will be specifically on the titanium K-edge.

X-ray Absorption Near Edge Structure (XANES)

The XANES region of XAS, -50 to +100 eV, includes the pre-edge feature, the absorption edge itself, and features on or just above the edge. The pre-edge is a result of dipole-allowed transitions, in the case of titanium 1s → 3d transition. Because this is a bound transition, the excitation process must follow Laporte selection rules; thus the pre-edge feature is sensitive to the coordination symmetry of the titanium site. A Ti^{4+} d^0 center has ground states A_{1g} and A_1 for octahedral and tetrahedral geometries, respectively. The excitation of the 1s electrons to the empty 3d orbitals of first row transition metals with an octahedral or psuedooctahedral geometry is Laporte forbidden. The symmetry operator for an octahedral Ti^{4+} complex is T_{1u} therefore 1s (A_{1g}) → 3d (T_2g) or 1s (A_{1g}) → 3d (E_g) results in ungerade symmetry forbidden. Hence, no pre-edge feature is expected for a Ti^{4+} octahedral complex. However, a low intensity pre-edge feature is frequently observed, due to the hybridization of 4p and 3d orbitals Figure 46.[91,92]

On the other hand, the symmetry operator for tetrahedral Ti^{4+} complex is T_2 therefore the electronic transitions of the 1s (A_1) → 3d (T_2) and 1s (A_1) → 3d (E) are Laporte allowed. Consequently, a strong pre-edge feature is expected for tetrahedral Ti (IV) complexes, Figure 46.

Table 5 Summary of the nomenclature for specific X-ray absorption transitions (X-ray absorption edges).

Edge	Excited Core Electron
K	**1s**
L_1	**2s**
L_2	**$2p_{1/2}$**
L_3	**$2p_{3/2}$**
M_1	**3s**
M_2	**$3p_{1/2}$**
M_3	**$3p_{3/2}$**

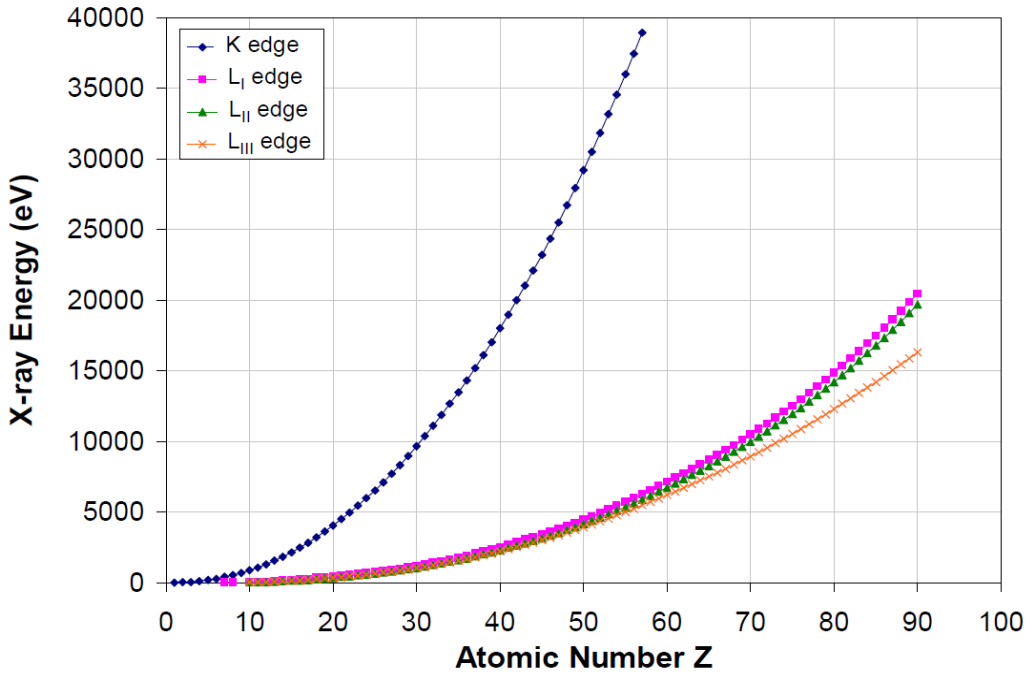

Figure 44 Plot of X-ray absorption energies as a function of atomic number.

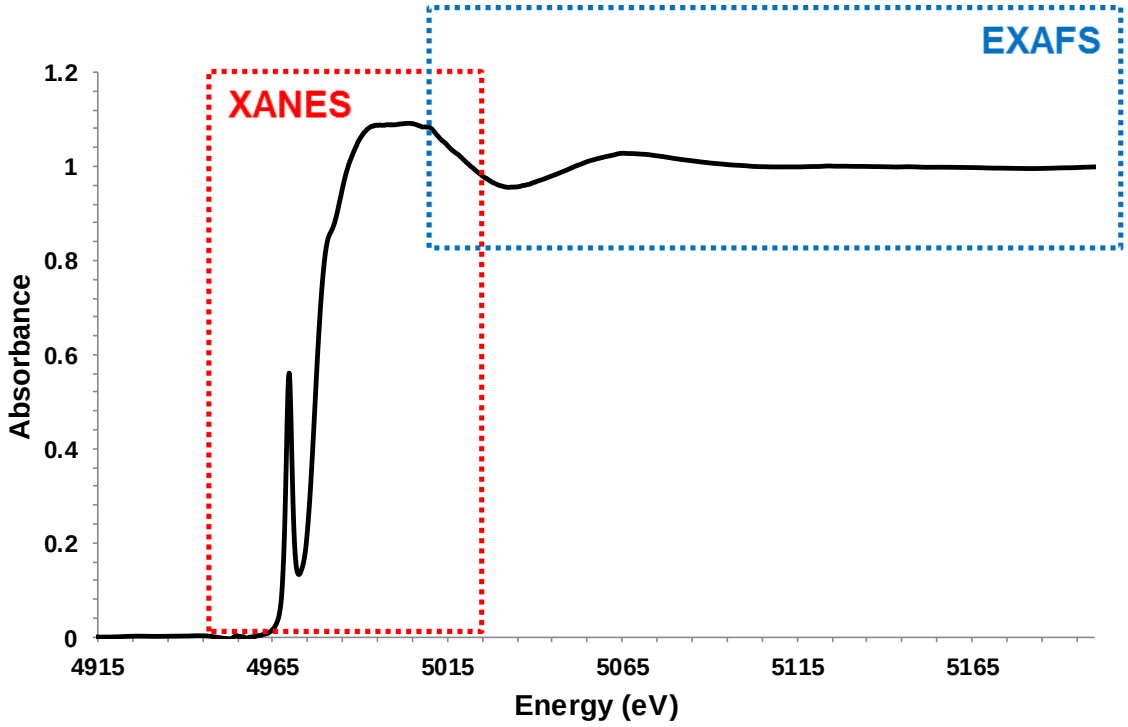

Figure 45 XAS spectrum of Ti K-edge illustrating the two distinct regions, XANES (red) and EXAFS (Blue).

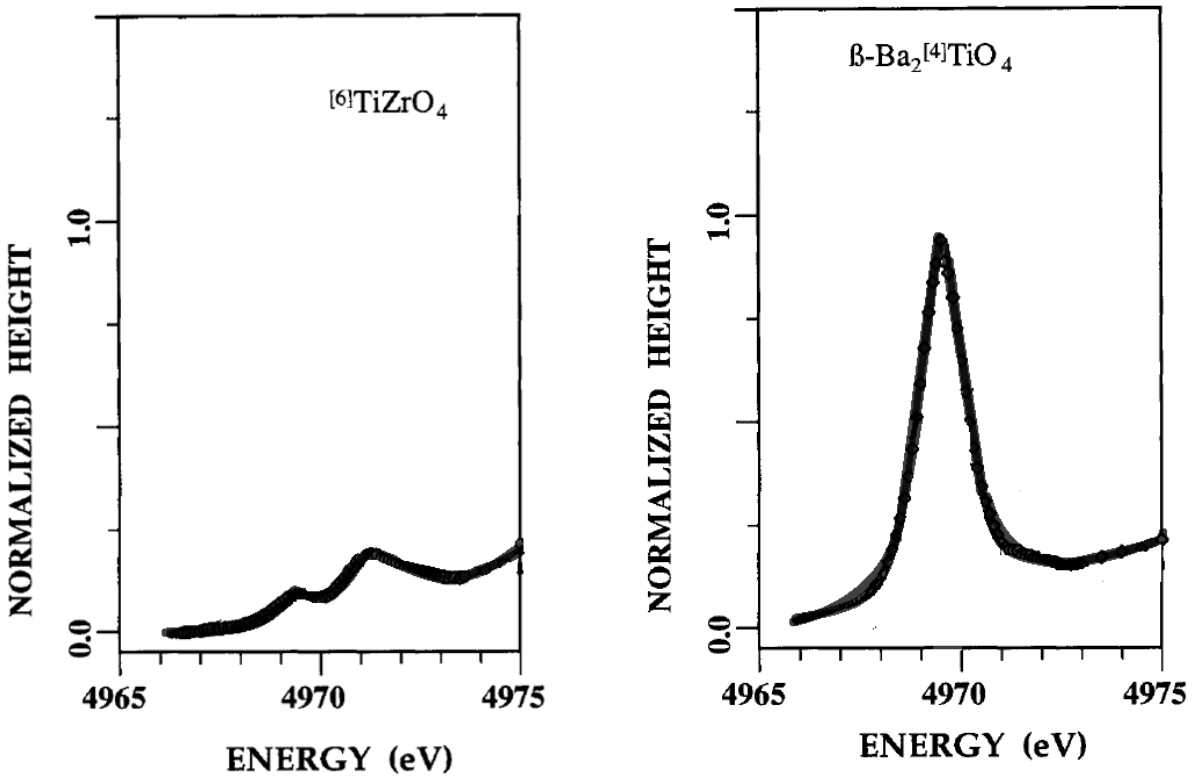

Figure 46 Illustration of the pre-edge feature of a 6-coordinate titanium species (left) and a 4-coordinate complex (right) in the XANES region of XAS. Figure modified from ref [93].

In addition to intensity, the pre-edge feature is also sensitive to shifts in energy depending on the coordination of the absorbing atom. The pre-edge feature in 4-coordinate tetrahedral Ti^{4+} is shifted to lower energy by approximately 2 eV compared to a 6-coordinate octahedral complex, Figure 47.[93]

The position of the absorption edge (E_0) is typically defined as the point of inflection or at half the maximum of the main edge jump. This position is sensitive to both oxidation state and the ligands surround the absorbing atom.

Extended X-ray Absorption Fine Structure (EXAFS)

In contrast to XANES, the EXAFS region provides information about the number and type of coordinated ligands to the absorbing atom. The EXAFS region ranges from ~+20 eV to +1000 eV and contains fine structures super imposed on the absorption edge backgrounds. These fine structures are a result of backscattering between the ejected photoelectron wave and the electron density of neighboring nuclei, Figure 48. At energies higher than the absorption edge, the electrons are no longer promoted to a higher unoccupied orbital, they are now completed ejected in to the continuum. The energy is released as a photoelectron which interacts with the neighboring atoms producing oscillations dependent on the distance and energy of the neighboring atoms. Each atom in the same shell contributes to the same EXAFS signal. Shell refers to coordination sphere, i.e., the first coordination sphere contains atoms directly bound to the absorber, the second contains atoms once removed and so forth, Figure 49.

There are two different types of scattering paths, single scattering and multiple scattering, Figure 50. A single scattering path is between the absorber atom and one shell of atoms while a multiple scattering path occurs between the absorbing atom and multiple shells.[94]

Unlike XANES, an analytical theory has been developed for the EXAFS region and therefore the information obtained can be mathematically determined. An in-depth discussion of the theory behind EXAFS computations can be found in “XAFS for Everyone” by Scott Calvin. [95] Ultimately, the EXAFS signal is defined as $\chi(k)$ which can be defined as the sum of signals from each scattering path, Equation 28 and each scattering path can be defined as $\chi_i(k)$, Equation 29.

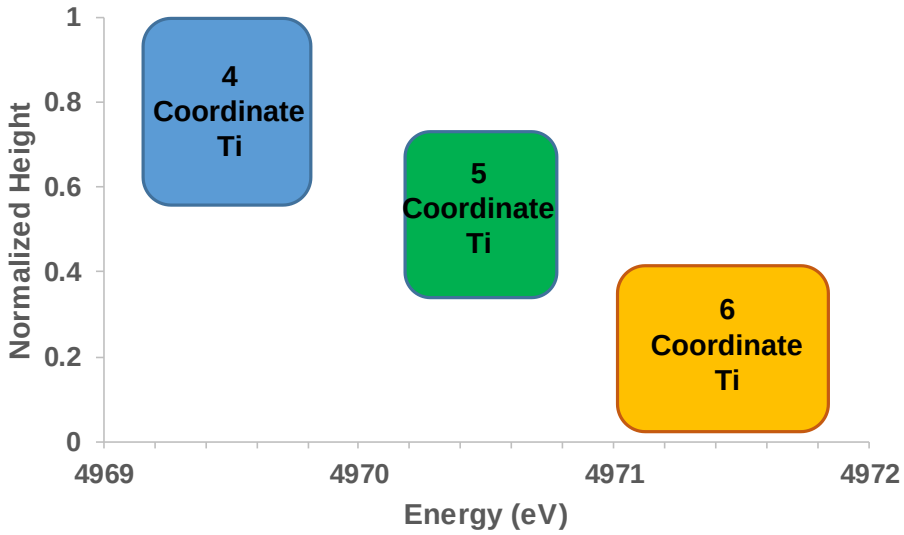

Figure 47 Illustration of how coordination geometry influences the Ti pre-edge intensity and peak position. Figure was reprinted from [107].

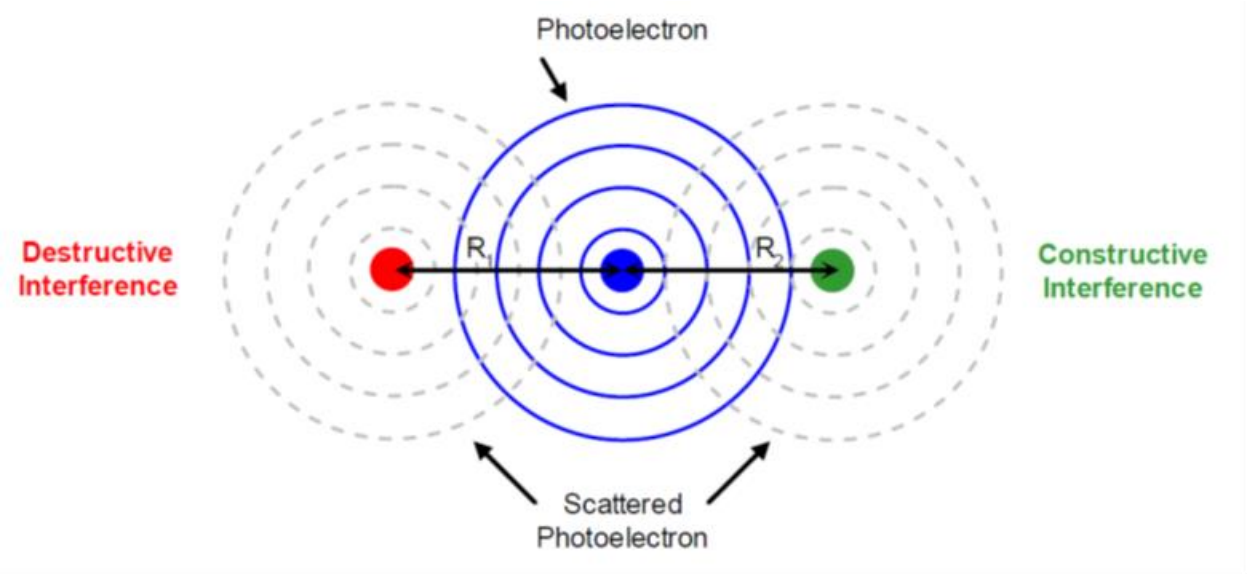

Figure 48 Illustration of deconstructive (left) and constructive (right) interface, absorbing atom is blue and the backscattering atoms are red and green.

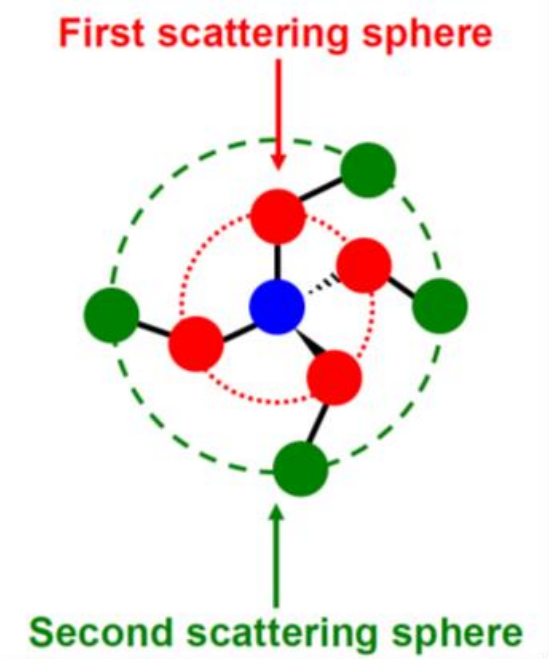

Figure 49 Illustration of the scattering spheres.

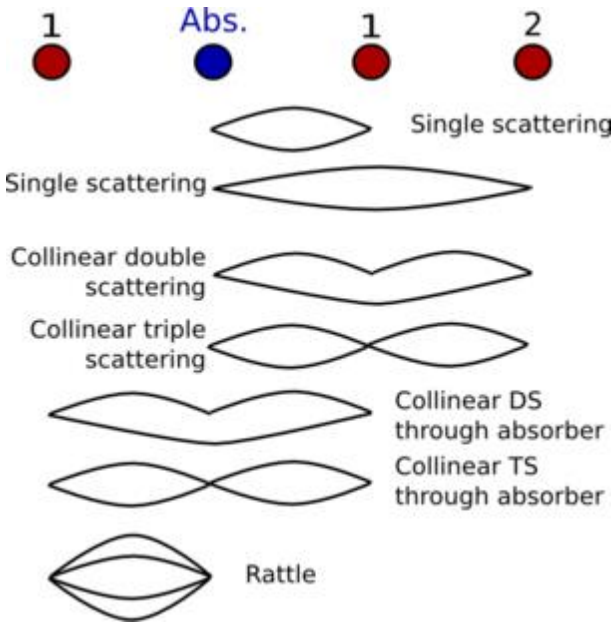

Figure 50 Illustration of the different types of scattering paths. Figure obtained from ref [94].

$$(k) = \sum_i \chi_i(k) \qquad \text{Equation 28}$$

$$\chi_i(k) = \frac{(N_i S_0^2) F_{eff_i}(k)}{kR_i^2} \sin[2kR_i + \varphi(k)] e^{-\sigma_i^2} e^{\frac{-2R_i}{\lambda(k)}} \qquad \text{Equation 29}$$

Where N_i is the coordination number of i[th] shell of backscattering atoms and R_i is the distance between the absorbing atom and the backscattering atom, S_0^2 is the amplitude reduction factor, $F_{eff}(k)$ is the effective scattering amplitude, φ_0^2 is the effective scattering phase shift, σ_i^2 is the Debye-Waller factor, and λ (k) is the mean free path of the electron.[96] These parameters are used in EXAFS modeling software to optimize the data fitting which will be discussed below.

Sample Preparation and Data Collection

To obtain XAS data, tunable x-rays with high flux are necessary. In order to meet these requirements a synchrotron light source is required. Currently, there are three primary facilities in the United States that have the capability of producing the hard x-rays essential for exciting the core electrons of transition metals: The Advanced Photon Source (APS) at Argonne National Laboratory, National Synchrotron Light Source II (NSLS-II) at Brookhaven National Laboratory, and the Sandford Synchrotron Radiation Laboratory (SSRL) at the Stanford Linear Accelerator Center. While there are other synchrotron light sources in the United States, the do not have enough flux for XAS analyses of titanium. However, before the opening of NSLS-II in 2015, the National Synchrotron Light Source (NSLS) was operating at Brookhaven National Laboratory. The data collected for this work was obtained at NSLS prior to its closing in September of 2014.

An UHMW polyethylene (McMaster-Carr) plate containing three 15 mm x 7 mm x 1 mm rectangular wells is used as the sample holder. Polypropylene windows are taped to the polyethylene plate with double-sided transparent tape to seal the sample cell, Figure 51

All samples are ground into fine powders using a Wig-L-Bug prior to sample loading. The samples are then mixed with a minimal amount of mineral oil in order to hold the fine powders together. Dilution of the titanosilicate samples is not necessary

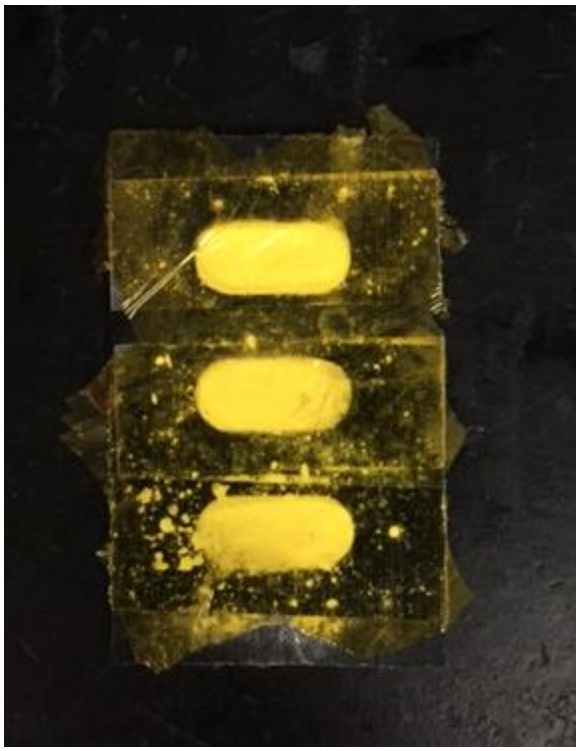

Figure 51 UHMW polyethylene plate loaded with samples and sealed with polypropylene windows.

because of their generally low titanium weight percent. However, pure complex precursors are diluted by 50% with graphite and prepared the same way. All samples were prepared in a nitrogen atmosphere glovebox.

In this work, titanium is the absorber atom and the spectra are collected in fluorescence mode on beam lines X19A and X19B at NSLS. Titanium foil presents a pre-edge feature at 4966 eV and is used as a reference sample for calibration. A solid-state passivated implanted planar silicon (PIPS) detector is used at a 45^{o} angle to the sample in order collect fluorescence data. The PIPS detector is placed as close to the front face of the sample as possible without obstructing the incoming x-ray beam. As much of the diffuse fluorescence radiation as possible is captured by the PIPS detector. A Si (111) double crystal is monochromator was used to obtain tunable monochromatic light.

XAS data collection can be divided into four regions: pre-XANES (-150 to -15 eV), XANES (-15 to +75 eV), EXAFS near the edge (+75 to +550 eV), and EXAFS far from the edge (+550 to +1000 eV). Each region is determined by its energy range relative to the absorption edge position. The intensity of the EXAFS signal decreases as the energy of the x-ray beam increases above the absorption edge. The integration time and step sizes for each region are dependent on the energy range interest: pre-XANES 5 eV, XANES 0.3 – 1.5 eV, EXAFS near edge 1.5 – 4.5 eV, and EXAFS far edge 4.5 – 6.1 eV. In the XANES region, the step size should be as small as possible to accurately record subtle pre-edge features and edge structures that develop in this region. On the contrary, signals in the EXAFS region, far from the absorption edge, are broad and require much fewer measurement points to accurately define them. Therefore, the step size is increased along with the integration time to decrease the signal to noise ratio. The step size refers to movement of the Si crystals in the monochromator. Table 6 presents the specific collection parameters for the data presented in this work.

Table 6 List of collection parameters for XAS measurements.

Energy Range (eV)	Step (eV)	Integration Time (s)
-200 to -15	5	1
-15 to +75	0.5	2
+75 to +550	1.5	3
+550 to +1000	5	4

Analysis of XAS Data

Generally, there are two methods for analyzing x-ray absorption data: 1) simple comparison of unknowns to literature or "standard" spectra; 2) fitting the experimental spectrum of the sample with a theoretical spectrum derived from a structural model. Typically, a combination of these two methods is used for the analysis of EXAFS data. It is important to note that modeling is traditionally not attempted for the XANES region of XAS. The analyses presented in this work use both methods and the modeling component is discussed below.

While there are several computational programs capable for EXAFS modeling, IFEFFIT data analysis (Athena and Artemis) is used in this work.[90,97,98] Athena is used to process the raw data obtaining XANES spectra and extraction of the EXAFS from the smooth edge background. This work followed a standard XAS data processing protocol described in the literature.[97-99] The main steps of data processing in Athena are as follows:

1. Glitch removal
2. Truncating and aligning the spectrum
3. Defining the absorption edge energy (E_0): the position of the absorption edge provides crucial information on the oxidation state of the absorbing atom. In this work, E_0 is determined to be the energy at the half height of the normalized absorption edge.
4. Setting the pre-edge and post-edge lines:
5. Normalization of the spectrum
6. Background subtraction and Fourier transform
7. Averaging and Merging multiple scans

These steps are critical for accurately fitting the data to the theoretical models. Once the data is processed in Athena, the data can be imported along with a structural model to Artemis and a theoretical model can be obtained. The experimental data is then compared to the function generated from the structural model. When fit parameters converge to stable and acceptable values, the fitting procedure is complete. An in-depth

discussion of EXAFS modeling can be found in Fundamentals of XAFS by Matthew Newville.[90]

Nitrogen Adsorption/Desorption

Materials that possess high surface area with pore sizes in the mesoporous range are desirable in industry due to the high activity per unit volume observed.[17] Therefore, surface area and pore size analyses are critical parameters in the characterization of porous materials in many applications. Adsorption/desorption measurements are used to characterize the type porosity associate with the material. The instrument does a known amount of gas (typically, nitrogen) into a known volume with sample. The sample is then allowed to equilibrate for some time. The instrument then measures the volume of gas absorbed at varying pressures. By plotting amount of gas absorbed verse relative pressure, isotherm plots can be generated and used to identify the porosity of the material. Figure 52 illustrates the different types of isotherms.[100] Table 7 summarize the porosity associated with each isotherm.[101]

While there is not a technique capable of providing an absolute surface area, the Brunauer-Emmett-Teller (BET) method is the most widely used, Equation 30.

$$\frac{1}{n[\left(\frac{P_0}{P}\right)-1]} = \left(\frac{1}{n_m C}\right) + \left[\frac{(C-1)}{n_m C}\right]\frac{P}{P_0} \qquad \text{Equation 30}$$

In Equation 30 P/P_0 is the relative pressure, C is the BET constant, n is the amount of amount of absorbed gas, and n_m is the monolayer capacity.

Experimental

The surface areas for all catalysts presented in this work are determined using a Quantachrome® Asiqwin™. The samples included both first and second generation atomically dispersed titanium catalysts synthesized with dichlorodimethylsilane as the inert cross-linking agent along with MCM-41 purchased from ACS Materials to validate the BET protocol. Approximately 100 mg of sample powder is used to determine the surface area and pore volume. The sample is added to a 6 mm cell and capped with a non-elutriating plug. The sample is then degassed for two hours at 150 ^{0} C. BET surface area is calculated using adsorption data over the relative pressure range of 0.05 – 0.35 and average pore size distribution determined using the BJH method. The surface area and average pore size of MCM-41 are determined to be

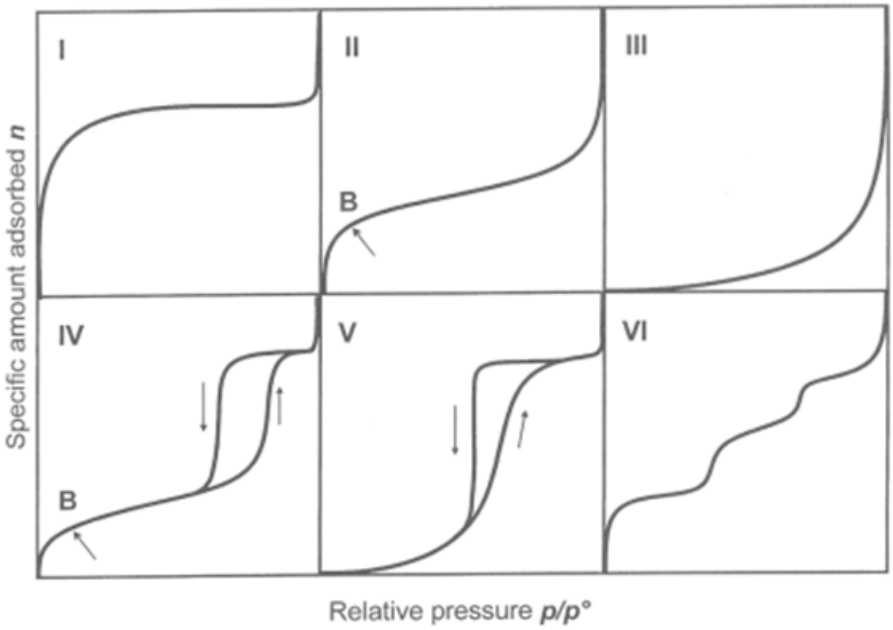

Figure 52 IUPAC description of adsorption/desorption isotherms. Figure was obtained from ref [100].

Table 7 Summary of porosity based on isotherm type.

Isotherm Type	Porosity
Type I	**Microporous**
Type II	**Macroporous**
Type III	**Nonporous**
Type IV	**Mesoporous**
Type V	**Mesoporous (uncommon)**
Type VI	**Layered**

848 m^2/g and 3.7 nm which is consistent with the surface area and pore size distribution presented by the manufacturer, surface area > 800 m^2/g and 3.5 – 4 nm respectively. Both first and second generation catalysts exhibited type IV isotherms consistent with mesoporous materials. Figure 53 shows the isotherm obtained for a 2-connected first generation catalysts and is representative of the typical type IV isotherm exhibited by all catalysts in this work.

The surface areas for the materials synthesized using the building block approach and method of sequential additions ranged from 300 – 600 m^2/g depending on the ratio of inert cross-linker to tin-cube used during synthesis. The Barnes group has shown that by varying the ratio of tin-cube building block to linker, the surface area of these materials can be tailored.[75] Additionally, the average pore size distribution for the catalysts was determined to be 3.0 – 4.0 nm confirming mesoprosity.

General Conclusion

The above characterization techniques are a combination of spectroscopic and analytical techniques. Individually, these techniques provide only small pieces of information about the active site, but when used collectively, a picture of the active site and its local environment can be constructed. In addition to these characterization techniques, catalytic activity can be used as secondary characterization.

Secondary Characterization

Catalytic activity

A reoccurring issue with heterogeneous catalysts is the lack of knowledge about the active site. While it is of utmost importance to fully understand the physical characteristics of an active site, it is of little interest if the catalyst is not active.

Catalytic oxidation plays a key role in a variety of vital chemical reactions including the production of fuels and fine chemicals. In the past, soluble metal salts and clean inexpensive oxidants such as molecular oxygen, hydrogen peroxide, and organic peroxides were largely utilized in liquid phase oxidation reactions. Today, heterogeneous catalysts are advantageous due to their easy of separation and recyclability.

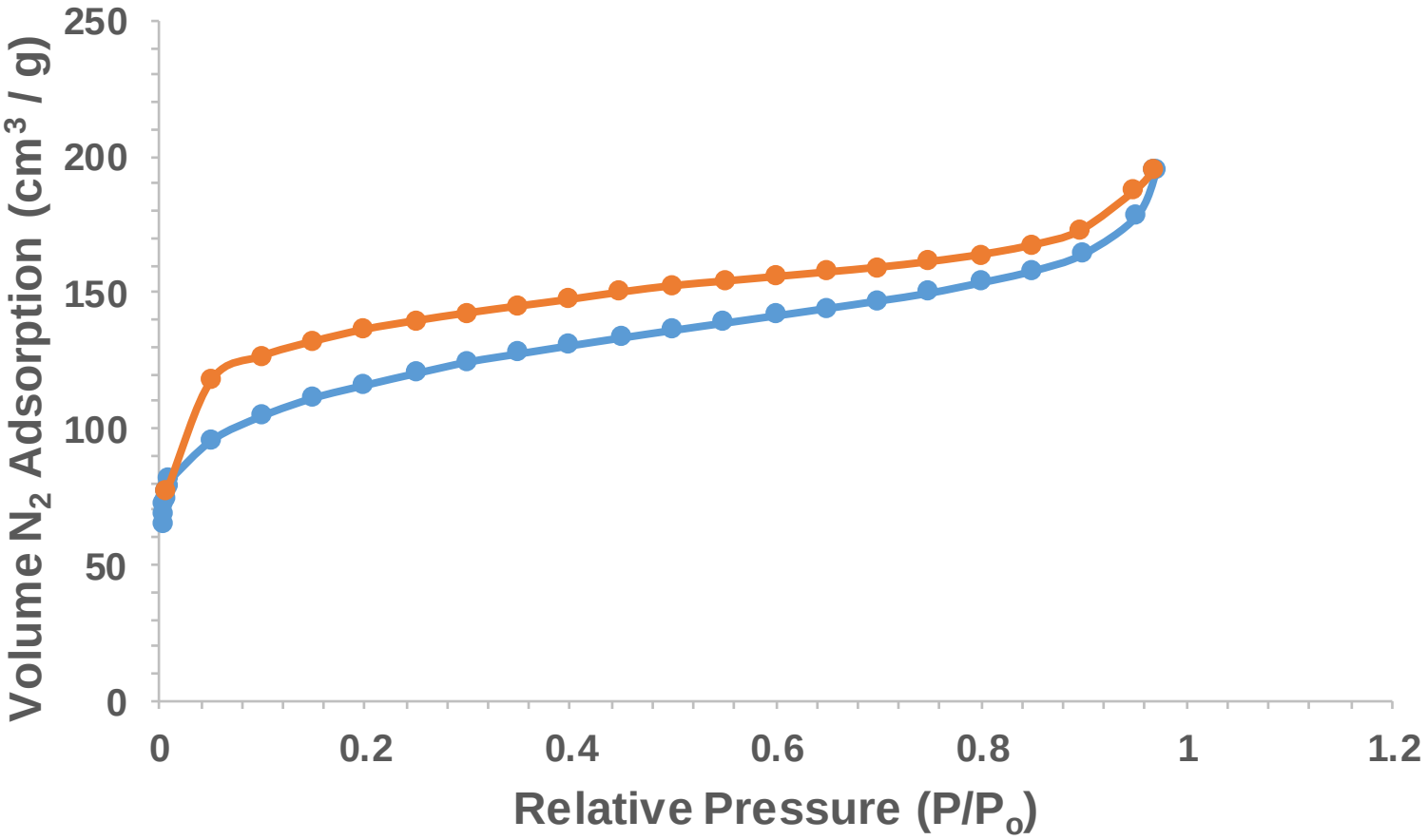

Figure 53 Nitrogen adsorption/desorption isotherm for 2-connected first generation catalysts (blue is adsorption branch and orange is desorption branch).

The materials in this worked are investigated as catalysts in the oxidation of phenols to benzoquinones. Khlodeeva *et. al.* have extensively studied the oxidation of 2, 3, 5-trimethylphenol (TMBQ) to 2, 3, 6-trimethylbenzoquinone (TMBQ) with mesoporous heterogeneous catalysts.[61] However the catalysts presented in literature do not meet the single-site criterion. The synthetic strategy presented in this work may have potentially overcome the issue of multiple sites. Therefore, the oxidation of two different phenols TMP and 2,6-dimethoxyphenol (DMOP) to 2,6-dimethoxybezoquinone (DMOBQ) are investigated. The catalytic procedure described below has been developed based on catalytic protocols presented by Kholdeeva *et. al.*

Alkylphenol Oxidation Catalytic Protocol

A 9 dram (~ 33 mL) vial containing a 10 mm stir bar and septa cap is weighed, tared, and taken into a nitrogen atmosphere glovebox. Approximately 40 mg of catalyst is added to the empty vial which is taken out of the glovebox, and reweighed to obtain an accurate measure of the amount of catalyst present. It is important to note that the initial amount of catalyst (weighed in the glovebox) is not important because all values and ratios are adjusted once the final weight of the catalyst is obtained. Once the initial mass of catalysts is obtained along with the actual Ti wt% determined via ICP, calculations are carried out to determine the appropriate amount of acetonitrile, substrate and oxidant necessary to acquire the following mole ratios: Ti : substrate : oxidant, initial concentration of Ti; 1 : 20 : 250, 3.9 mM of Ti. Acetonitrile (~5 mL) is added to the reaction vial via syringe through the septum. Once the catalyst is covered with solvent, approximately 25.0 mg of internal standard (4,4'-dimethoxybenzophenone) is added followed by the addition of substrate. Once all reactants except oxidant are added to the vial, the reaction is placed into an oil bath at 65 ^{0} C. The reaction mixture is then allowed to equilibrate to temperature inside a submerged aluminum metal block for 30 minutes with constant stirring at 500 rpm, Figure 54. Once the reaction reached equilibrium temperature, the first 50 µL aliquot was taken, t=0. The aliquot is added to a NMR tube containing both $MgSO_4$ and 500 µL deuterated chloroform ($CDCl_3$). The NMR tube is then capped, shaken, and immersed into a dry ice/isopropanol bath to quench the reaction.

To initiate reaction, the septum cap is removed and 250 molar equivalents, typically 600 µL, of 40% aqueous hydrogen peroxide (oxidant) is added to the reaction mixture via a calibrated Wheaton™ Socorex Acura™ 835 pipet. The aqueous hydrogen peroxide is purchased from Fisher Scientific as 50 wt/v% and the actual concentration is determined using a standard

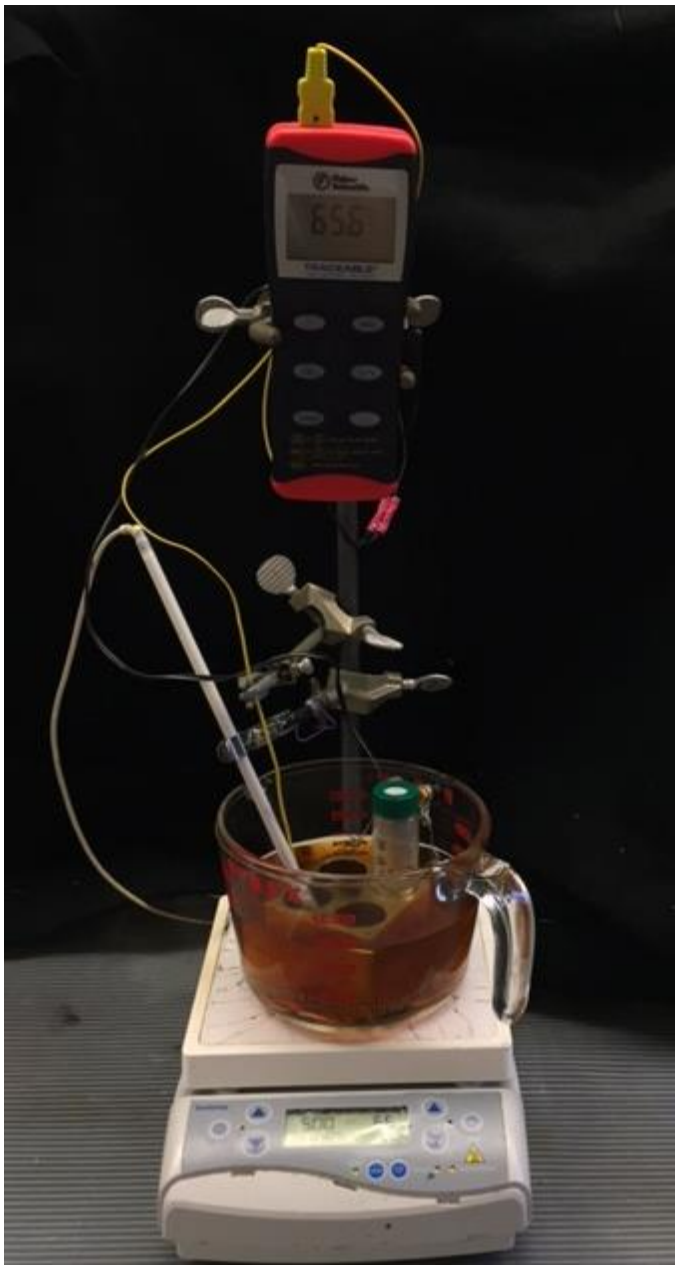

Figure 54 Picture of catalysis set up.

permanganate titration method. It is not necessary to bring the hydrogen peroxide to reaction temperature for two reasons: 1) the volume change due to the addition of hydrogen peroxide was negligible compared to the initial volume; 2) hydrogen peroxide is known to decompose with exposure to light and temperature. A stop watch is then started, septum cap replaced, and additional aliquots are taken in the same fashion at the following time intervals: 2, 5, 10, 15, 30, 60, 120, and 240 minutes.

Validation of Catalytic Protocol

When developing a catalytic protocol, it is important to ensure reproducibility in all aspects of said protocol. Several experiments are carried out to verify the addition of $MgSO_4$ does not compromise catalysis results, the use of a dry ice/isopropanol bath quenches the reaction, and the internal standard is not affected by the catalyst itself.

$MgSO_4$ is added to each NMR tube as a drying agent. As seen in Figure 55, blue spectrum, a broad feature appears at 6.471 ppm which masks the aromatic and ring proton regions of interest. It is believed that this broad feature results from water exchange. This peak moves significantly on the chemical shift scale, presumably due to hydrogen bonding with peroxide and other species in the reaction mixture. $MgSO_4$ is added to absorb the majority of water in the aliquot. We found the addition of $MgSO_4$ removed this unwanted peak without perturbing the catalytic data of interest, Figure 55, red spectrum.

To investigate the addition of $MgSO_4$ three 50 µL aliquot are taken 10 minutes after the addition of oxidant. Each aliquot is added to one of the following NMR tubes and placed in a dry ice/isopropanol bath: 1) 500 µL $CDCl_3$; 2) 500 µL $CDCl_3$ with ~ 4 mg of $MgSO_4$; 3) 500 µL $CDCl_3$ with ~ 8 mg of $MgSO_4$. NMR spectra are collected and analyzed as described below. Table 8 summarizes the integrations of each aliquot. As $MgSO_4$ is added to the reaction, the integrations do not change indicating $MgSO_4$ does not bind or alter the reactants or products and can be used as a drying agent to prevent proton exchange between water and peroxide and can be used as a viable drying agent.

Because aliquots are obtained without ceasing stirring, it is assumed that each aliquot contains, internal standard, substrate, oxidant, and catalysts and thus potentially allowing the reaction to continue in the NMR tube. Therefore, each NMR tube is submerged in a dry ice/isopropanol bath to quench the reaction halting the conversion of substrate and formation of product. In order to confirm this happens, the quenching of each aliquot in a dry ice/isopropanol

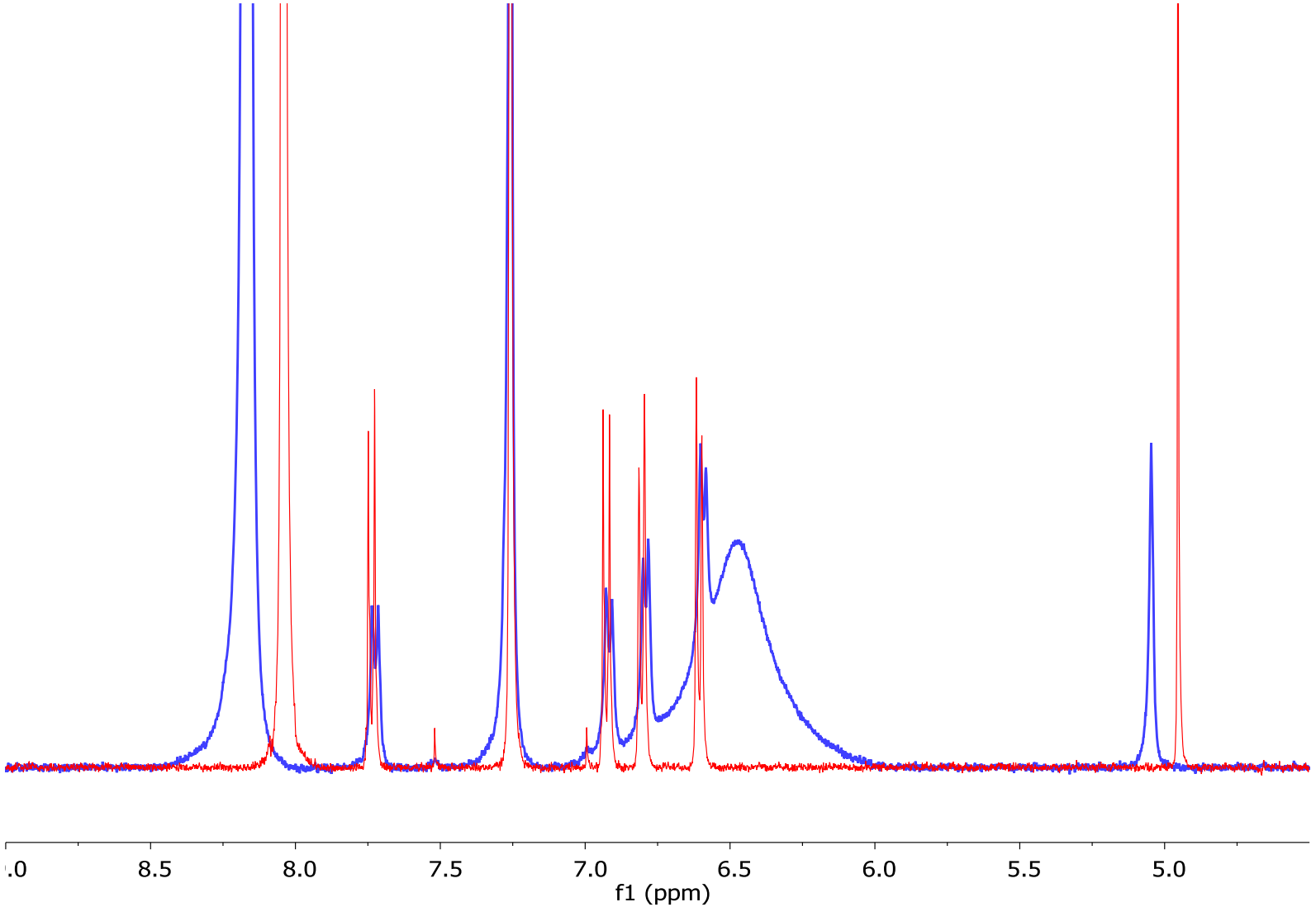

Figure 55 NMR spectra of an aliquot without $MgSO_4$ (blue) showing the presence of a broad feature at ~6.5 ppm and an aliquot with $MgSO_4$ (red) illustrating the absence of the broad feature in the presence of $MgSO_4$.

Table 8 Summary of the integrations without $MgSO_4$, with $MgSO_4$, and with double the amount of $MgSO_4$.

Compound	Peak (ppm)	Integration No $MgSO_4$	Integration with $MgSO_4$ (4 mg)	Integration with $MgSO_4$ (8 mg)
Internal Standard	**7.721**	**1.000**	**1.000**	**1.000**
TMP	**6.619**	**0.867**	**0.868**	**0.866**
TMBQ	**6.510**	**0.065**	**0.066**	**0.065**

bath is also investigated. Two aliquots are taken ten minutes after the addition of oxidant. Both aliquots are added to prepared NMR tubes containing $CDCl_3$ and $MgSO_4$, capped and shaken. Sample A is immersed in a dry ice/isopropanol bath while the NMR spectrum of sample B is immediately obtained. The NMR spectrum of sample A is taken 6 hours after quenching. The NMR integrations for sample A and B are identical indicating a dry/ice isopropanol bath is sufficient for quenching the catalytic reactions.

The internal standard chosen for these studies was found to be completely unreactive in these catalysis reactions.

Characterization of Products

Proton NMR (^1H) spectroscopy is used to characterize each aliquot of the catalytic reactions. The NMR spectra are obtained using a Varian VNMRS 500 MHz under the following conditions: 25 ^{0} C, 16 scans, 10-second relaxation delay, 45^0 pulse. If a 500 MHz NMR is unavailable, spectra are obtained using a Bruker 400 MHz NMR under then following conditions: 25 ^{0} C, 32 scans, 5-second relaxation delay, 30^0 pulse.

The relaxation behavior of the protons in substrate, product and internal standard are explored. On a Varian 500 MHz NMR with a 45^0 pulse, relaxation delays of 10 and 20 seconds are found to give unchanging integrations of all peaks used in the kinetic study. Similar experiments are conducted on a Bruker 400 MHz NMR with a 30^o pulse. The protons integrations remain unchanged between relaxation delays of 5 and 10 seconds. Additionally, the integrations remain unchanged between the spectra obtained on the 500 MHz NMR in comparison to the 400 MHz NMR using the above stated protocol.

Phenol Oxidation Analysis Parameters

Each spectrum was analyzed using MestraNova V10.2. NMR. Work up protocol was carried out in the following manner: 1) window set from 10 ppm to 3 ppm; 2) manually phased; 3) auto baseline corrected (Whittaker Smoother); 4) line broadened (0.3 Hz); 5) manually integrated. Figure 56 illustrates a typically NMR spectrum for the oxidation of TMP to TMBQ. The spectra were integrated over the regions found in Table 9.

The integration regions may vary from spectrum to spectrum due to slight shifts in peak position most likely resulting from changes in solvent polarity and hydrogen bonding. However, the width of the integration window remained constant for all integration regions (a is for TMP to

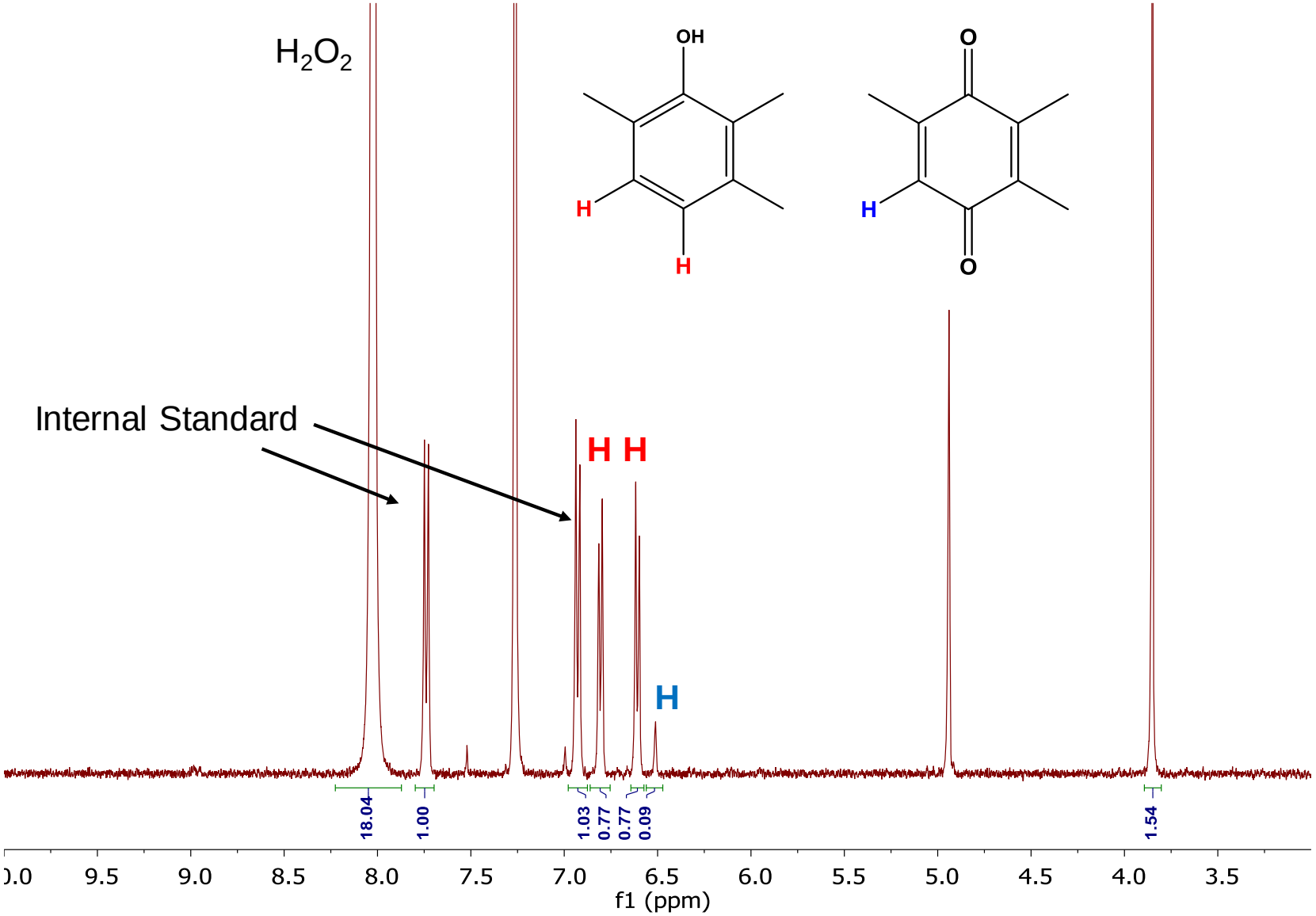

Figure 56 Typical NMR spectrum for the oxidation TMP to TMBQ.

Table 9 List of integration regions used for NMR workup.

Compound	Peak Position (ppm)	# Protons	Approximate Integration Region (ppm)
H_2O_2	8.066	2	8.255 – 7.835
4,4'-dimethoxybenzophenone (IS)	7.721	4	7.779 – 7.692
	6.912	4	6.964 – 6.887
2,3,6-trimethyphenol [a]	6.802	2	6.831 – 6.786
	6.619	2	6.711 – 6.666
2,6-dimethoxyphenol [b]	6.752	1	6.790 – 6.707
	6.551	2	6.588 – 6.485
2,3,5-trimethylbenzoquinone [a]	6.510	2	6.626 – 6.590
2,6-dimethoxybenzoquinone [b]	5.830	2	5.862 – 5.775

TMBQ while b is for DMOP to DMOBQ): 1) 0.087 ppm; 2) 0.42 ppm; 3a) 0.045 and 0.045 ppm, 3b) 0.083 and 0.103 ppm; 4a) 0.036 ppm, 4b) 0.087.

Concentration and Catalytic Activity

From these integrations, the moles and concentration of both the reactant and products are calculated according to Equation 31 where C is concentration, I is the integration, and H is the number of protons. In this context, y represents the internal standard and x corresponds to either the substrate or product.

$$C_x = \frac{I_x H_y C_y}{I_y H_x} \qquad \text{Equation 31}$$

Once the amount of substrate and product are obtained, they are plotted as a function of time along with their sum, Figure 57.

From these data, several key pieces of information can be obtained about the reaction and the catalyst itself such as activity. Activity is the amount of substrate converted per unit time. There are several ways to define activity: percent conversion, turn over number (TON), and turn over frequency (TOF). Percent conversion, Equation 32, is often utilized as a measure of activity because it does not take into account the number of sites and often in heterogeneous catalysis the actual number of active sites is unknown. This can lead to easy manipulation of results by increasing the amount of catalyst present; thus increasing the amount of substrate converted.

$$Conversion\ (\%) = \frac{\Delta\ moles\ substrate}{intial\ moles\ substrate}\ x\ 100\% \qquad \text{Equation 32}$$

More accurate representations of activity are TON, Equation 33, and TOF, Equation 34. TON measures the amount of substrate converted per active site where in this context of single-site catalysts, the total amount of titanium present in the catalyst is the number of active sites. TOF defines the activity of a catalytic site per unit time. TOF plays a critical role in understanding the rate of a reaction at early time points when concentrations of starting material are still close to their initial concentrations. As the reaction progress, TOF becomes an average expression because several variables are changing with concentration. For this reason, TOF is calculated two minutes after the addition of oxidant.

$$TON = \frac{\Delta\ mole\ substrate}{mole\ of\ active\ site\ (Ti)} \qquad \text{Equation 33}$$

$$TOF = \frac{TON}{\Delta\ Time} \qquad \text{Equation 34}$$

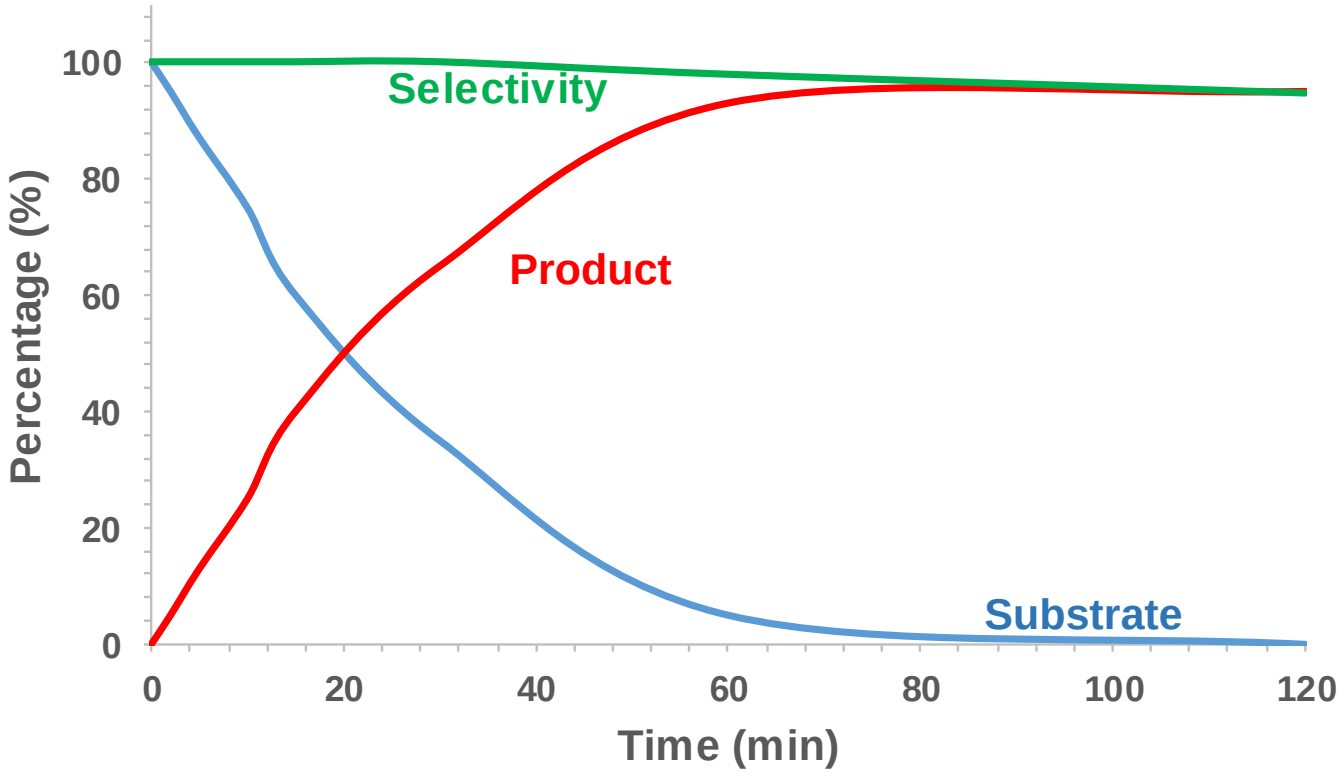

Figure 57 Generic plot of the reaction kinetics, conversion of substrate (blue), formation of products (red), selectivity (green).

By determining TOF at two minutes, apparent kinetic data can be determined. During the initial phase of the reaction, the concentrations of substrate and oxidant are in great excess and are not rapidly changing. Therefore, the catalysis data is completely dependent on the active site alone.

In addition to activity, selectivity is often used to characterize a catalysts productivity. Selectivity, Equation 35, is a measure of how efficient a catalyst produces one product relative to all other possible reactants. It is generally represented as the percent yield at a given percent conversion. In an ideal situation, all of the substrate would be converted to one product leading to 100% selectivity. In this case, when the sum of reactants and products is plotted as a function of time, selectivity remains as a straight line at 100%, Figure 57.

$$Selectivity\ (\%) = \frac{mole\ product\ formed}{moles\ of\ reactant\ converted}\ x\ 100\% \qquad \text{Equation 35}$$

Conclusion

To fully understand the nature of the catalysts synthesized in this work, both spectroscopic and physical characterization techniques are employed. By combining multiple characterization techniques, a more complete picture can be painted about the environment of each active site along with its corresponding catalytic properties. The remaining chapters of this dissertation aim to answer remaining questions about work presented by Dr. Nan Chen (Chapter 3), approaches to overcoming the challenges associated with the production of strong acid (HCl, Chapter 4), designing a rational synthesis for a second generation of titanosilicate and their properties as hydroxylation catalysts (Chapter 5), and the investigation of single-site titanosilicates for epoxidation (Chapter 6).

Chapter III: Synthesis and Characterization of First Generation Passivated Atomically Dispersed Ti Catalysts with $SiCl_4$

Introduction

Dr. Nan Chen, a previous member of the Barnes' research group developed a family of what we will call, "first generation" single-site titanium catalysts. Each titanium center in these catalysts has a specific connectivity to the matrix, 4-connections, 3-connections, or 2-connections, with each titanium active site having tetrahedral coordination geometry. Dr. Chen used the building block approach and method of sequential additions as described in Chapter 2 followed by a passivation step. This passivation step was employed to remove any remaining silyl chloride and trimethyltin groups. However, several questions remained unanswered about this passivation step:

1. Does the production of anhydrous HCl during passivation change the connectivity of the active site?
2. Do trimethyltin groups play an active role in catalysis?
3. Are there alternative techniques to limit or remove remaining silyl chloride groups?

The work presented in this chapter will focus on the first two questions and Chapter 4 will describe investigations into other passivation techniques. The characterization of the first generation catalysts relies heavily on the work presented by Dr. Nan Chan. The FTIR spectra of 2C-Ti, 3C-Ti and 4C-Ti catalysts along with XAS data of the 4C-Ti catalyst obtained in this work directly compare to the work of Dr. Chen and therefore, we believe the characterization data from Dr. Chen applies to the catalysts synthesized in this work.

Titanium Precursors

To obtain atomically dispersed single-site titanosilicate catalysts, mononuclear titanium precursors are essential. In the work described here, the precursors are the following: titanium tetrachloride ($TiCl_4$), isopropoxy titanium trichloride ($TiCl_3(OiPr)$), and diisopropoxy titanium dichloride ($TiCl_2(OiPr)_2$). The alkoxy chlorotitanates are synthesized according to Kamigaito et. al. [77] which involves mixing $TiCl_4$ with titanium isopropoxide ($Ti(OiPr)_4$) in carefully controlled ratios, Equation 36 and Equation 37.

$$TiCl_4 + Ti(OiPr)_4 \rightarrow 2\,TiCl_2(OiPr)_2 \qquad \text{Equation 36}$$

$$3\,TiCl_4 + Ti(OiPr)_4 \rightarrow 4\,TiCl_3(OiPr) \qquad \text{Equation 37}$$

The syntheses for the precursors are as follows (all chemicals are distilled and stored under vacuum in sealed Schlenk bulbs, and all glassware is silylated with trimethylsilyl chloride and kept in an oven at 80°C prior to use):

Initially, $Ti(OiPr)_4$ is added to a silylated Schlenk vessel in a nitrogen atmosphere glovebox. Approximately 25 mL of dry n-hexane is vapor transferred at -80^0 C (dry ice/isopropanol bath). The solution is constantly stirring while $TiCl_4$ is vapor transferred until ratios according to Equation 36 and Equation 37 are obtained. The Schlenk vessel is then covered to exclude light in case the product is photosensitive. The solution is then warmed to room temperature and allowed to react for three hours while stirring. An off white to light yellow precipitate forms almost immediately for both the di- and tri-chloride species. The solvent and other volatiles are then removed under vacuum at room temperature, and the solid residues are allowed to dry under vacuum overnight at room temperature away from light. Finally, the products are purified via sublimation at 55^0 C. The final products are light yellow powders and are stored in a nitrogen atmosphere glovebox to reduce the rate of self-decomposition. Purity was verified by comparison with literature ^{1}H NMR spectra.

Characterization of Titanium Precursors

NMR spectra of both precursors, $TiCl_3(OiPr)$ and $TiCl_2(OiPr)_2$ are collected and compared to the NMR spectrum of pure $Ti(OiPr)_4$, Figure 58. The NMR spectra show signals corresponding to pure $TiCl_3(OiPr)$ and $TiCl_2(OiPr)_2$, provided the ratios of $TiCl_4$ to $Ti(OiPr)_4$ are precisely controlled, 3:1 and 1:1, respectively. The NMR shifts are consistent with the chemical shifts reported in the literature.[77] If the ratios are not precisely controlled, the resulting NMR spectra show a mixture of products, but with further purification via sublimation, the desired products can be obtained.

It is important to note the dichloro and trichloro titanium precursors are very sensitive to decomposition. Visual changes, such as graying of the solids, begins within a week even when carefully stored under nitrogen atmosphere. To minimize degradation of the precursor due to self-decomposition overtime, the alkoxylated chlorotitanates are used within 48 hours of being synthesized.

Synthesis of First Generation Single-Site Titanosilicate Catalysts

As described in Chapter 2, the building block approach combined with the method of sequential additions is the methodology employed to prepare first generation atomically dispersed

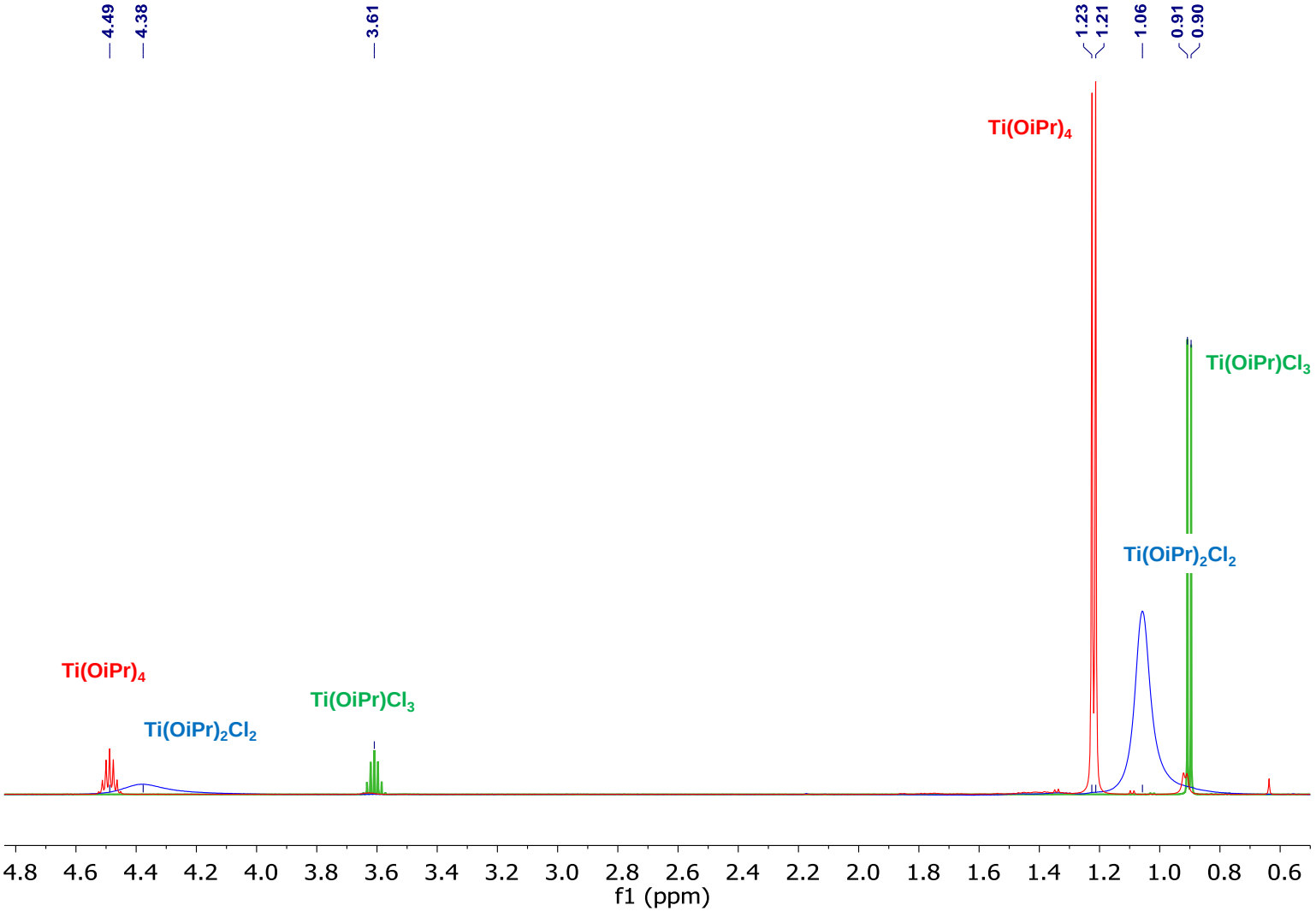

Figure 58 Overlaid ^{1}H NMR spectra of $Ti(Oipr)_4$ (red), $Ti(OiPr)_2Cl_2$ (blue), $Ti(OiPr)Cl_3$ (green).

titanium catalysts. The procedure used to synthesize first generation catalysts was first described by Dr. Nan Chen and Dr. Richard Mayes.[42,73] However, there are several issues with the final matrices that are investigated further in the work reported here.

All vapor transfers are done at dry ice/isopropanol temperature (~ -80^0 C)

The first dose in the method of sequential additions establishes the connectivity of titanium to the matrix. Three different titanium connectivities, 2-connected, 3-connected, and 4-connected, are achieved by using different mononuclear titanium precursors, $TiCl_2(OiPr)_2$, $TiCl_3(OiPr)$, and $TiCl_4$ respectively. Anhydrous tin-cube building block is reacted with the proper mononuclear titanium precursor at 80^0 C for 24 hours using toluene as the solvent. Table 10 shows the ratios of titanium precursor to building block required to obtain the desired limiting connectivities. Toluene and volatiles are then removed under vacuum, the remaining product is dried at 80^0 C overnight, and connectivity calculated via gravimetric analysis. By limiting the amount of precursor, all chlorides remain active and all titanium active sites have an identical tailored connectivity. Figure 59 illustrates the three different targeted connectivities that are achieved using mononuclear titanium precursors.

Once connectivity around titanium is established, the oligomers are further cross-linked by a second dose of an inert linker, silicon tetrachloride ($SiCl_4$). Two equivalents of inert linker to initial starting amount of tin cube building block are added to the original Schlenk vessel in approximately 25 mL of dry toluene. The reaction is then allowed to stir at 80^0 C over 48 hours.

Once the second cross-linking reaction is complete, the remaining volatiles are removed under vacuum and dried at 80^{o}C overnight. The average connectivity of silicon to tin cube is calculated gravimetrically based on the amount of silicon added and the amount of trimethyltin chloride lost, typically 2.3 – 2.7 Si per cube. These catalysts will be referred to as “first generation catalysts.” Each catalyst synthesized as a first generation catalysts will have a targeted titanium connectivity and the titanium active site will be locked in a tetrahedral geometry.

Unlike in the first dose where all Ti-Cl groups react to achieve a targeted titanium connectivity, the second cross-linking has an excess of chloride groups to remaining trimethyltin groups on the tin-cube. Therefore, the measured connectivity for the silyl cross-linker represents an average connectivity of 4-connected, 3-connected, 2-connected, and possibly 1-connected linking groups. Figure 60 shows the first dose creates a targeted connectivity, in this case 4C-Ti, while the second crosslinking with $SiCl_4$ yields a mixture of sites. The remaining silyl chloride groups cause the catalysts to be very acidic in the presence of water. The pH of these catalysts

Table 10 Precursors, Ti: cube ratios, connectivity and titanium weight percent used for synthesizing first generation single site titanosilicates.

Ti Catalyst	Precursor	Ti:Cube = x:1 X value	Desired Connectivity	Actual Connectivity (±-0.1)	Wt.% Ti (ICP)
2-Connected	$Ti(OiPr)_2Cl_2$	1.0 – 1.5	2	1.9	6.2 – 10.2
3-Connected	$Ti(OiPr)Cl_2$	0.7 – 1.0	3	2.9	4.7 – 6.4
4-Connected	$TiCl_4$	0.5 – 0.8	4	4.0	3.5 – 4.6

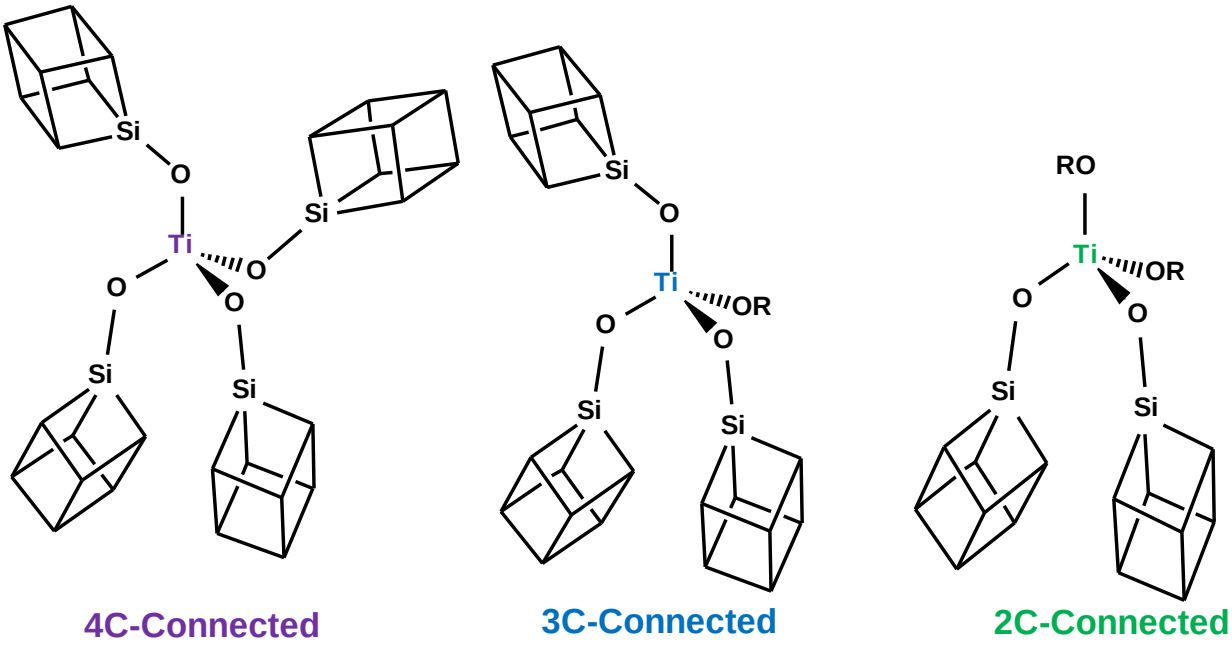

Figure 59 Illustration of the three different targeted connectivities to the matrix, 4C-Ti (left, purple), 3C-Ti (middle, blue), and 2C-Ti (right, green).

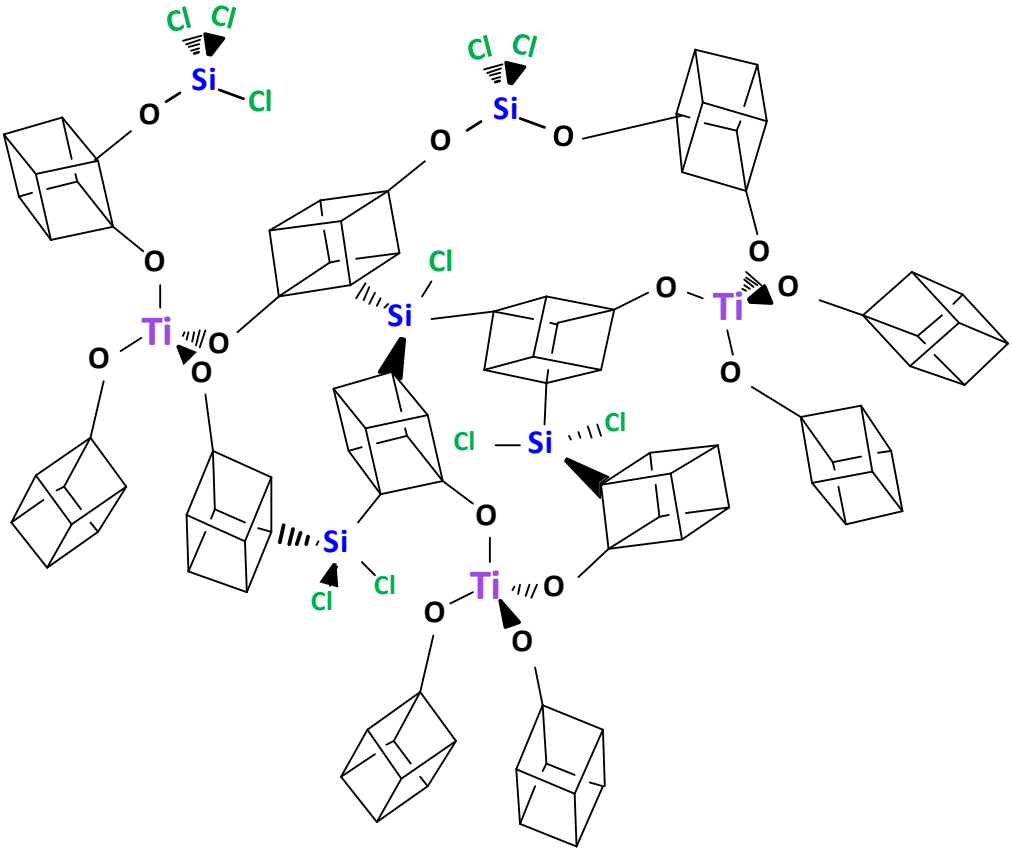

Figure 60 4C-Ti first generation catalyst matrix after the first dose. All titanium centers (purple) have the same connectivity while the silicon centers (blue) have multiple connectivities to the matrix.

is determined to be approximately two. To remove the residual chloride groups and produce more air and moisture stable catalysts, these catalysts are subjected to a passivation step.

Methanol Passivation

Previous work presented by Dr. Nan Chen showed anhydrous methanol to be an effective passivating reagent by reacting with remaining Cl groups producing alkoxysilanes and anhydrous HCl. The HCl generated then reacts with any remaining trimethyltin groups producing trimethyltin chloride (Me_3SnCl) and silanols groups, Figure 61. The byproduct, Me_3SnCl, is volatile and can be removed by heating at 80^0 C under vacuum. After passivating with methanol, virtually all Si-Cl and Si-O-$SnMe_3$ are converted to Si-O-Me and Si-OH. Assuming no other reactions occurs in this step, the resulting catalysts should be relatively air stable and the only possible catalytic active sites that remain are titanium center. The procedure for methanol passivation is as follows:

Methanol is distilled and stored over calcium hydride prior to use. Approximately 25 mL of dry toluene is vapor transferred onto the second dose matrices described above. Excess dry methanol (8 methanol : 1 $SiCl_4$; 2 methanol : 1 Cl) is then vapor transferred and the reaction is allowed to stir for ~16 hours (overnight) at 80^0 C. Volatiles are then removed under vacuum and the resulting catalyst is dried at 80^0 C overnight. The acidity of each catalyst is determined using pHydrion paper (Micro Essentials Laboratory). After methanol passivation, the resulting catalysts are neutral and consequently more air and moisture stable than non-passivated catalysts. In order to reduce adsorption of water to the active titanium sites, catalysts are stored in a nitrogen glovebox. These catalysts will be referred to as “first generation methanol passivated” (Ti-1st Gen $SiCl_4$-MeOH).

In addition to the titanium catalysts, a titanium free platform is synthesized to compare the spectroscopic signals and catalytic active of the matrix and the titanium active site. The Ti-free platform is synthesized according the protocol described above, but instead of using a titanium containing precursor, silicon tetrachloride bispyridine is used as the active linker in the first dose. No other modifications to the protocol are made.

Characterization of First Generation Methanol Passivated Catalysts

In addition to gravimetric analysis, Dr. Chen was able to characterize and compare each targeted connectivity through the use FTIR, ICP, DRUV, and XAS. In accordance with gravimetric analysis, Dr. Chen used elemental analysis, ICP, to determine both the Ti and Sn weight percent

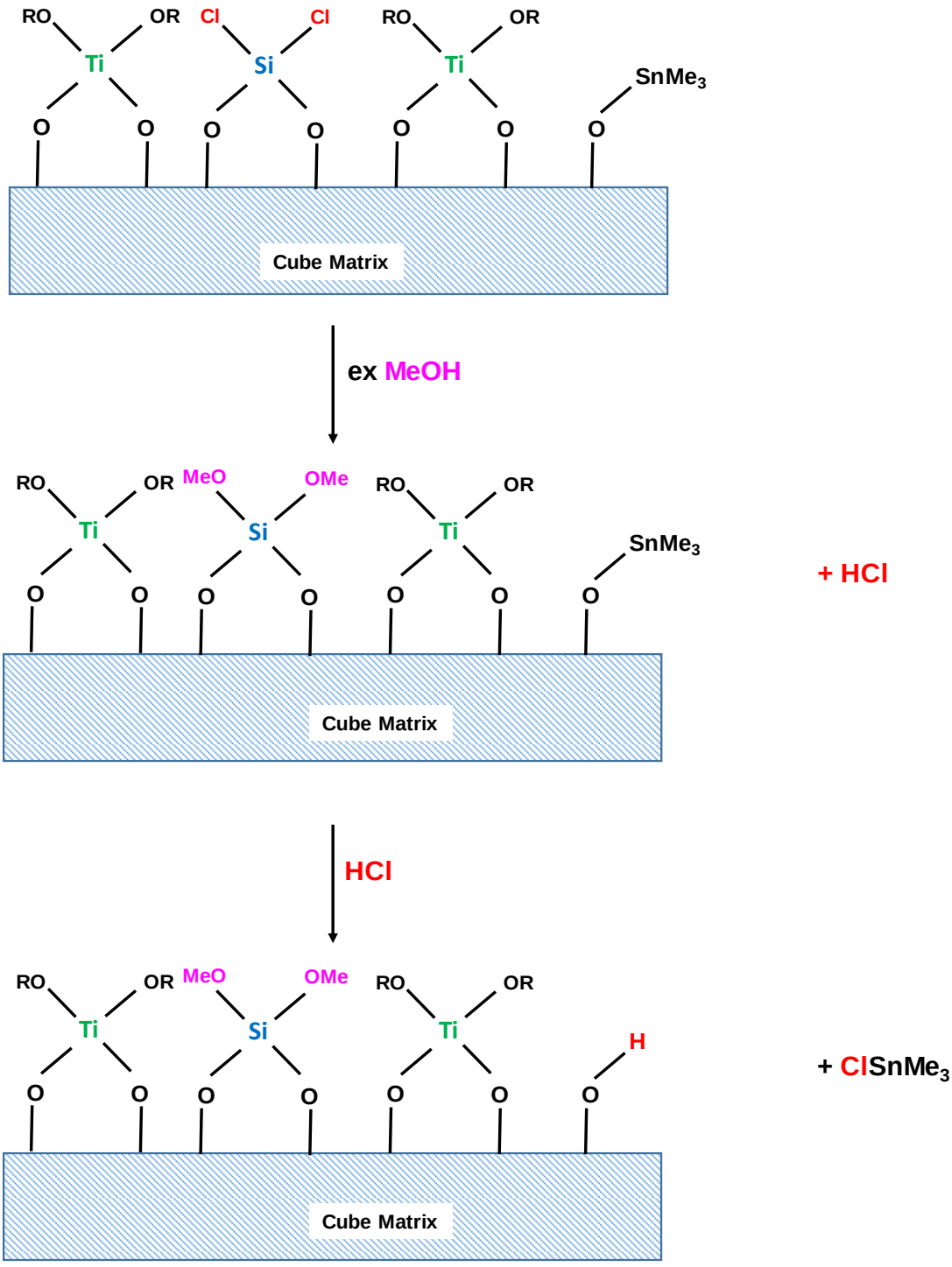

Figure 61 Illustration of methanol passivation reducing the number of silyl chloride groups in the final matrix along with remaining trimethyltin groups.

before and after passivation, Table 11. The consistency in titanium weight percent before and after passivation suggests titanium does not leach from the matrix during the methanol passivation step. In addition, the reduced weight % of Sn after passivation is indicative of the production of HCl followed by a secondary reaction with remaining trimethyltin groups on the unreacted corners of the tin-cube building block. However, while titanium leaching was not observed in the ICP analysis, this does not answer the question whether the connectivity of the titanium centers has been changed. This concern has led to further investigation of methanol passivation which will be discussed in the remainder of this Chapter.

Diffuse reflectance UV-vis has been used to qualitatively assess whether titanium is isolated throughout the support, or if titanium is present in small domains. Dr. Chen was able to show that methanol passivated titanosilicate catalysts contained isolated titanium active sites, not titania domains. Figure 62 shows the overlay of the DRUV spectra for the three different titanium catalysts, 2C-Ti (black), 3C-Ti (red), and 4C-Ti (blue). The lack of absorption above 300 nm is consistent with that titania domains are absent from these matrices. In addition, the broad absorption bands at ~ 220 – 225 nm are assigned to isolated titanium tetrahedron. In comparison to TS-1 (210 nm), the absorption band is broadened and shifted to higher wavelengths. The observed shift in wavelength and broadening of the absorption feature is typical for tetrahedral titanium in these types of amorphous silicate matrices.[42]

Dr. Chen also obtained XAS data as additional evidence that the titanium active site is indeed tetrahedral. Each XANES spectra of the non-passivated titanium catalysts, regardless of connectivity, exhibited a single pre-edge feature with a normalized intensity of ~ 50% relative to the main edge height. Figure 63 shows the XANES spectrum for a 4C-Ti first generation catalysts. The XANES regions for the 2C-Ti and 3C-Ti are nearly identical to that presented for 4C-Ti. The literature suggests that a 4-coordinate tetrahedral titanium center present a single pre-edge feature with an intensity of greater than 70% of the absorption edge height. Unlike the literature catalysts, the titanium silicate matrices presented here are amorphous which may account for the broader pre-edge feature with decreased intensity observed.[102] However, in all cases after passivation, the pre-edge feature decreases to ~ 35% of the absorption edge as well as band broadening. There is a possibility that the coordination number has increased to 5- or 6-coordinate due to coordination of methoxy or hydroxyl groups, but the pre-edge position remained unchanged, 4969.4 eV for both non-passivated and methanol passivated catalysts. Because the pre-edge position remains unchanged and the features broadened as intensity decreased along

Table 11 Summary of the elemental composition of Ti and Sn before and after methanol passivation for a 2C-Ti catalyst. Table obtained from ref [42].

2C-Ti [a]	Ti wt% $_{(grav.)}$ [b] (± 10%)	Ti wt% $_{(ICP-AES)}$ (± 10%)	Sn wt% $_{(ICP-AES)}$ (± 10%)	Ti : Sn (mol)
Before passivation	2.5	2.3	5.1	1.1 : 1
After passivation	2.7	2.6	0.47	14 : 1

[a] 2C-Ti sample was synthesized by reacting 0.6 mmol of $TiCl_2(OiPr)_2$ with 1.0 mmol of bb, and then 3.0 mmol $SiCl_4$

[b] titanium wt% $_{(grav.)}$ is calculated according to the initial amount of titanium added and the mass of the final product

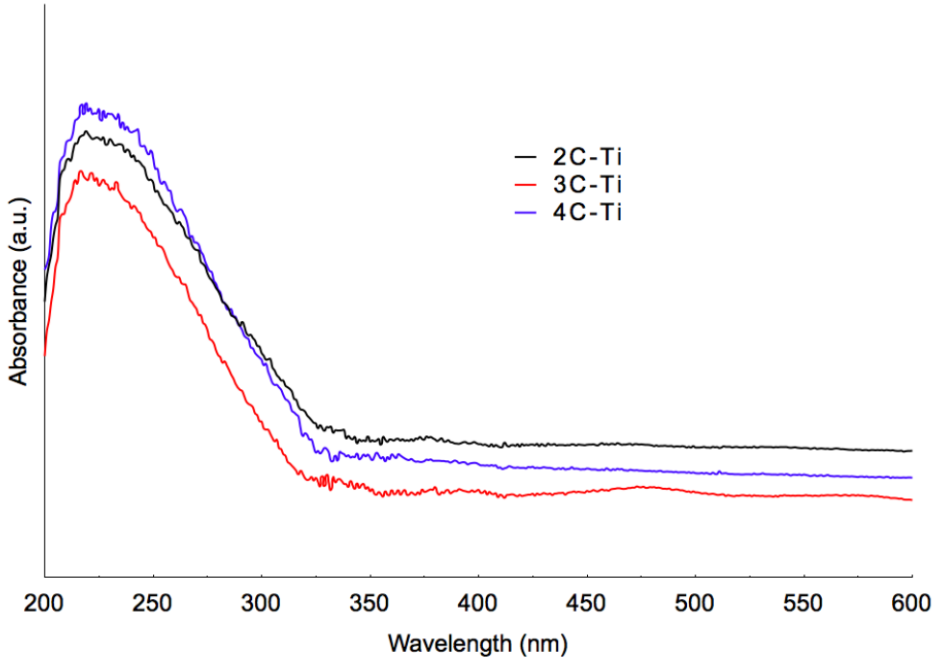

Figure 62 DRUV spectra overlays, 2C-Ti (black), 3C-Ti (red), and 4C-Ti (blue). Figure obtained from ref [42].

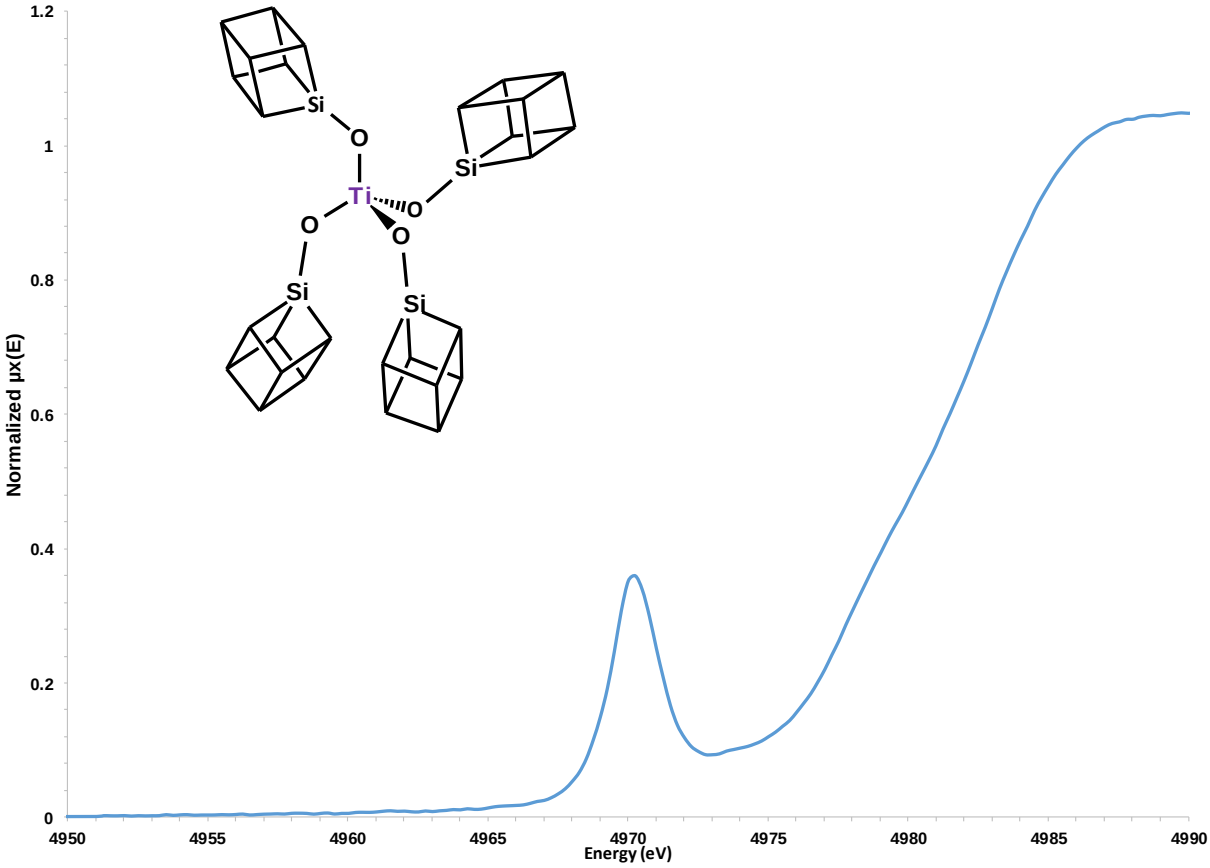

Figure 63 XANES spectrum for 4C-Ti 1st generation catalysts showing a single peak pre-edge feature indicative of 4-coordinate tetrahedral Ti.

with DRUV data, the titanium active sites in both non-passivated and methanol passivated samples are best described as tetrahedral.

Figure 64 shows the infrared spectra for non-passivated first generation catalyst (spectra are obtained after the second cross-linking with $SiCl_4$). All three catalysts, 2C-Ti (black), 3C-Ti (blue), 4C-Ti (orange) exhibit an absorption feature at 960 cm^{-1} characteristics of Ti-O-Si linkages. In contrast, the Ti-free platform (green) lacks this feature indicating titanium has been incorporated into the silicate matrices.

Catalytic Activity of First Generation Catalysts

While spectroscopic characterizations are of vital importance to understanding the active site, they provide little to no information about the connectivity. Therefore, catalytic activity is used as an indirect characterization technique to explore the connectivity of the active site. In this work, the selective oxidation of 2,3,5-trimethylphenol to 2,3,6-trimethylbenzoquinone with aqueous hydrogen peroxide is explored. Table 12 shows the catalytic activity of first generation catalysts analyzed by Dr. Nan Chen. It is noteworthy that the data collected by Dr. Chen were collected using a slightly different protocol than presented in Chapter 2. Dr. Chen's initial aliquot was taken five minutes after the addition of oxidant instead of two minutes. Additionally, the aliquots were characterized via GC-FID not by NMR spectroscopy.

Dr. Chen was able to establish a relationship between connectivity and activity, the fewer connections to the matrix, the more active the catalyst, 2C-Ti-MeOH > 3C-Ti-MeOH > 4C-Ti-MeOH. The different TOFs may be explained by the structural differences between the three catalysts and will be discussed in more detail in Chapters 5 and 6.

Unfortunately, I was unable to reproduce the catalytic results obtained by Dr. Chen. As seen in Table 13, the turnover frequencies (2 min), the percent conversions (1 hr), and the selectivities (1 hr) are virtually the same for all three catalysts. In addition to the titanium catalysts, the catalytic properties of two titanium free platforms are investigate. The first Ti-free platfrom has been passivated according to the methanol passivation procedure described above. In contrast, the second titanium-free platfrom is not passivated and therefore, significants amounts of tin sites remain in the matrix. One concern with remaining trimehtyltin groups is that they will possess their own catalytic activities. From the data presented in table 13, it can be seen that the active of both platforms regardless of the amount of tin in the martix are virtually the same. Both catalysts present very low percent conversion one hour after the addition of oxidant. Furthermore,

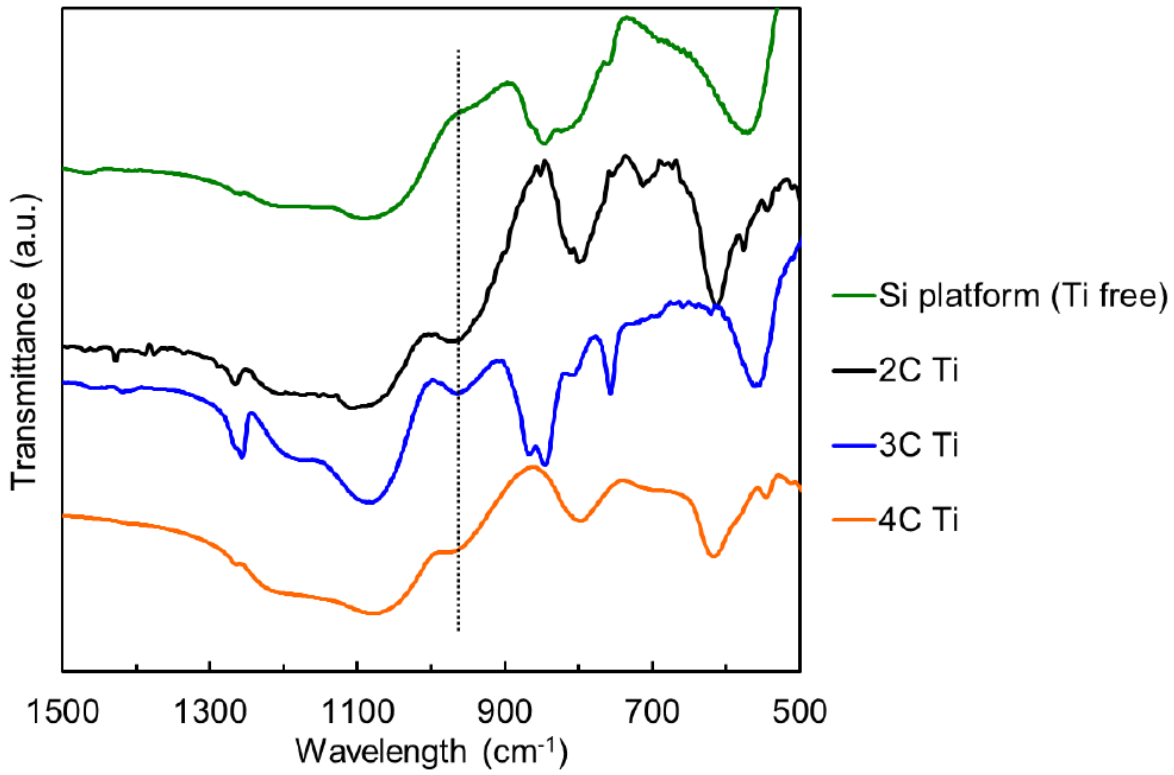

Figure 64 Infrared spectra of 2C-Ti (black), 3C-Ti (blue), 4C-Ti (orange), and Ti free platform (green.) Figure was reprinted from ref [42].

Table 12 Results of catalytic properties of first generation methanol passivated titanosilicates in the oxidation of TMP to TMBQ obtained by Dr. Chen.

Catalyst	TOF (min^{-1}) 5 min	Conversion % 240 min (± 3%)	Selectivity % 240 min (± 3%)	Yield % 240 min (± 3%)
4C-Ti-1st Gen $SiCl_4$ MeOH Passivated	0.35	26	43	11
3C-Ti-1st Gen $SiCl_4$ MeOH passivated	0.51	23	36	8
2C-Ti-1st Gen $SiCl_4$ MeOH passivated	1.58	90	80	73

Table 13 Results of catalytic activity for first generation catalysts synthesized in this work compared to two titanium free catalysts for the oxidation of TMP to TMBQ.

Catalyst	TOF (min^{-1}) 2 min (± 0.05)	Conversion % 60 min (± 3%)	Selectivity % 60 min (± 3%)	Yield % 60 min (± 3%)
Si-Platform MeOH Passivated	**0**	**4.9**	**1.2**	**0.60**
Si-Platform Non-passivated *	**0**	**4.8**	**17**	**0.82**
4C-Ti-1st Gen $SiCl_4$ MeOH Passivated	**0.525**	**100**	**60.6**	**60.6**
3C-Ti-1st Gen $SiCl_4$ MeOH passivated	**0.490**	**100**	**64.6**	**64.6**
2C-Ti-1st Gen $SiCl_4$ MeOH passivated	**0.456**	**83.9**	**65.7**	**55.1**

* Significant amounts of tin remaining in the matrix.

there is no apparent active at the beginning of the reaction. Therefore, it can be said that tin does not act as an active catalyst in the converions of TMP to TMBQ.

A major concern with methanol passivation is the possibility that the connectivity of titanium to the support is altered. The production of anhydrous HCl in the methanol passivation step has the possibility of changing the connectivity resulting in a mixture of 4C-, 3C-, 2C- and even 1C- titanium centers, Figure 65. The similar TOFs presented in Table 13 for all three titanium catalysts leads us to suspect that this unwanted side reaction occurs during passivation.

Confocal Microscopy

In addition to each connectivity presenting similar catalytic activity, a brief qualitative study using confocal microscopy raises additional concerns for methanol passivation. These spectra are collected using a Keyence VK-X250 3D Laser Scanning Confocal Microscopy. Three 2-connected catalysts have been studied: two catalysts are passivated and one non-passivated catalysts: 1) 2C-Ti methanol passivated (as described above), 2) 2C-Ti methyl *tert*-butyl ether passivated (described in Chapter 4), 3) 2C-Ti cross-linked with dicholorodimethylsilane (described in Chapter 5). As seen in Figure 66, the morphology of the methanol passivated catalyst has significantly changed in comparison to the MTBE passivated and the non-passivated catalysts. The 2-connected methanol passivated catalysts, seen in the middle, appears to have a glossy surface while both the non-passivated and MTBE passivated catalysts have a dull or mat appearance vide infra, that of which is expected for amorphous silicates.

In addition, the roughness of both the MTBE passivated and the non-passivated samples are consistent with Figure 67 and are therefore considered comparable. As seen in Figure 68, the particle morphology of the MeOH passivated catalysts has changed in comparison to the MTBE passivated catalyst. This change is consistent with significant surface reconstruction.

General Conclusion of Methanol Passivation

The change in morphology and the observed catalytic activities for methanol passivated catalysts has led to the investigation of other passivation techniques and ultimately the abandonment of the methanol passivation step. Chapter 4 aims to address the third question presented at the beginning of this chapter “Are there alternate techniques that limit or reduce the number of remaining silyl chloride groups?”

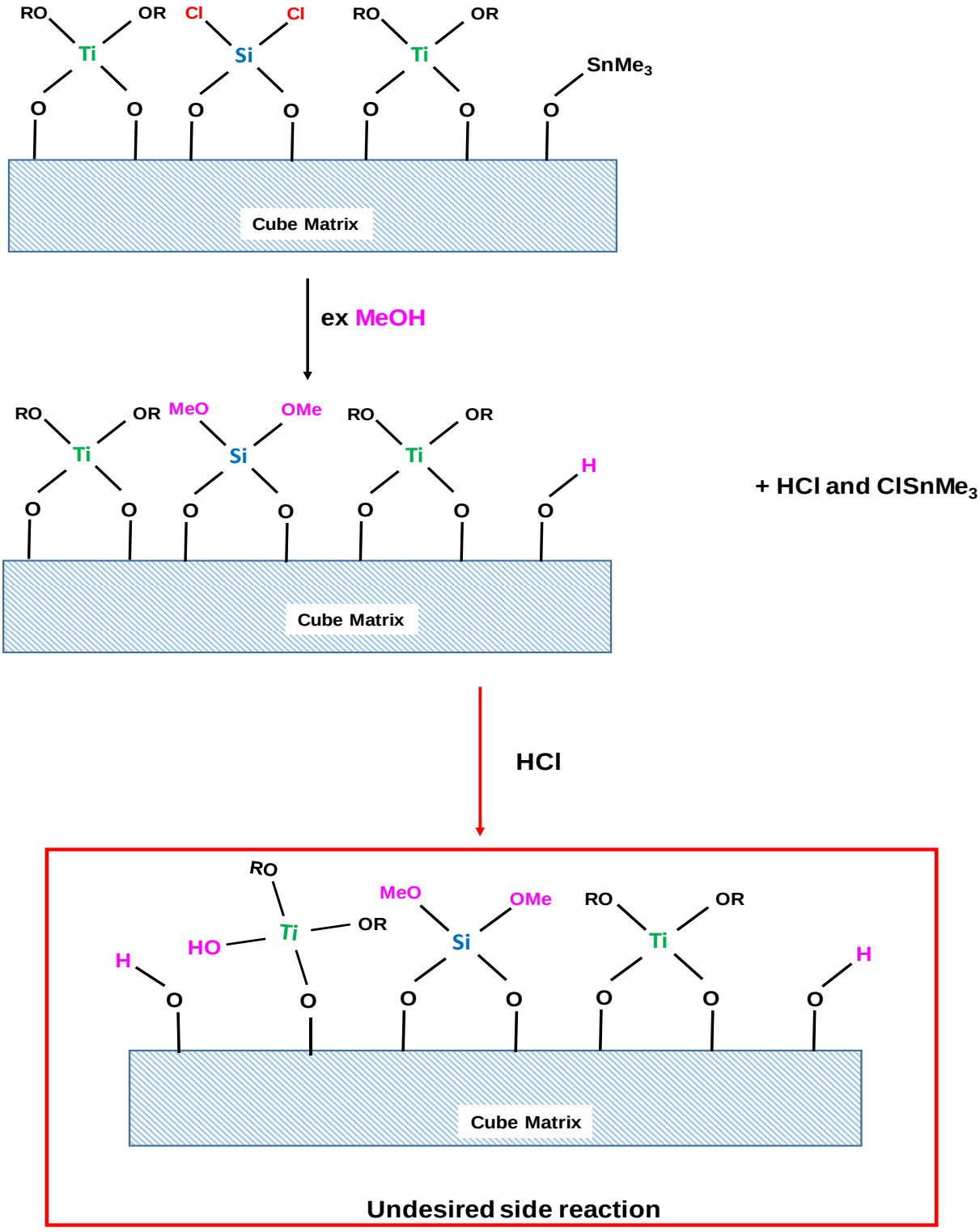

Figure 65 Illustration of unwanted side relation with HCl during methanol passivation leading to mixtures of active sites.

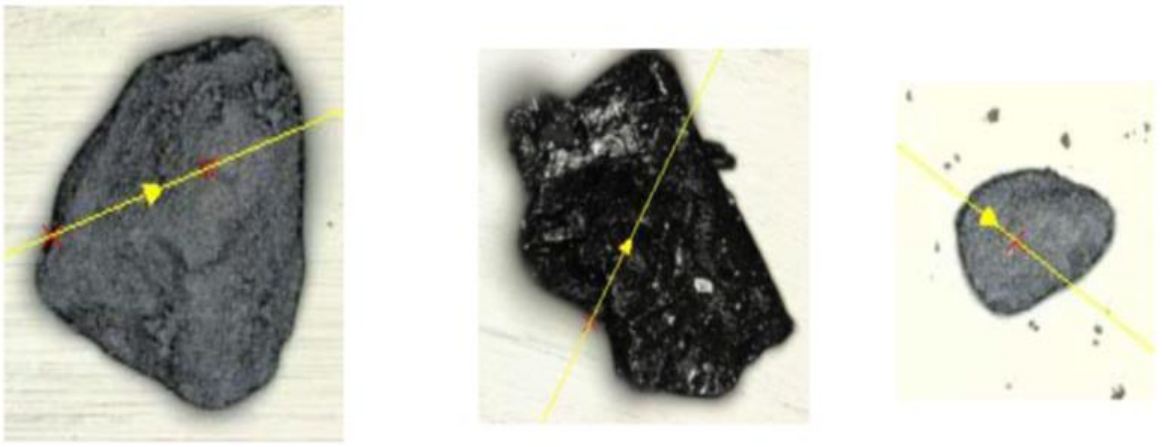

Figure 66 Confocal microscopy images of three different 2-connected first generation titanium catalysts, 2-connected MTBE passivated (left), 2C-MeOH passivated (middle), and 2C-non-passivatd (right).

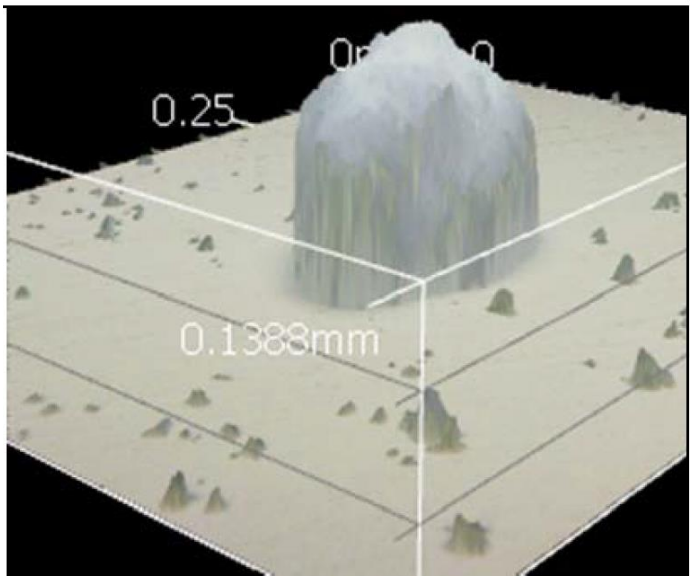

Figure 67 Illustration of the surface roughness for a 2C-Ti-non-passivated catalyst.

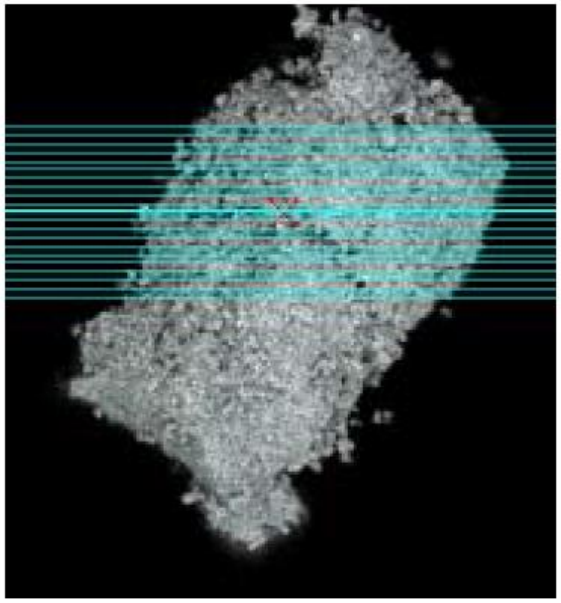

2-connected MTBE Passivated

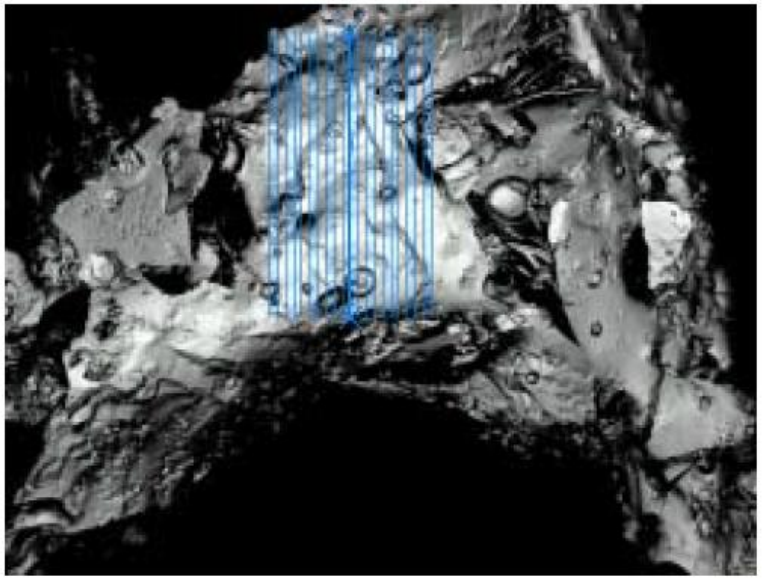

2-connected MeOH Passivated

Figure 68 Optical 3D surface reconstruction of the 2C-Ti-MTBE passivated catalyst (left) and the 2C-Ti-MeOH passivated catalyst (right).

Chapter IV: Problems and Solutions to Methanol Passivation

Based on the contradicting results between Dr. Chen and the work presented here, several alternative approaches to methanol passivation are investigated:

1. Methanol passivation with base.
2. No passivation step.
3. No passivation step but added base to neutralize the reaction.
4. Passivation with methyl-*tert*-butyl ether.
5. Reducing the initial number of chloride groups.

Each technique will be discussed in detail below.1

Methanol Passivation in the Presence of Base

To prevent HCl from reacting with Ti-O-Si, triethylamine (TEA) is added to the reaction flask during methanol passivation. After the second cross-linking reaction with $SiCl_4$, the silicon to cube connectivity is determined to be 2.3 – 2.7 connections on average, indicating 1.3 – 1.7 chloride groups remain per inert silicon linker. Based on the calculated connectivity and the number of remaining chloride groups, approximately 1.5 equivalents of dry TEA are added to the reaction mixture according to the following procedure:

After the second dose with $SiCl_4$, the reaction is dried under vacuum at 80^0 C to remove volatile Me_3SnCl. Approximately 25 mL of dry toluene is then vapor transferred at dry ice/isopropanol temperature followed by 1.5 equivalents of TEA to one1 remaining chloride group. The reaction is allowed to stir while two equivalents of dry methanol are vapor transferred to the same reaction flask. The solution is then allowed to warm to room temperature and heated to 80^0 C for 16 hours with constant stirring. The catalysts are then dried under vacuum at 80^0 C to remove any remaining volatiles. While triethylammonium chloride, $(C_2H_5)_3N \bullet HCl$, remains as a salt in the reaction, it is believed that it will not play an active role in catalysis.

Table 14 summarizes the catalytic results for catalysts passivated with methanol in the presence of base. Unfortunately, the addition of base appears to have poisoned the catalysts. Initially, there is no observed catalytic active, i.e., TOFs are equal to zero. As the reaction progresses, some activity is observed, but the selectivities of these catalysts are poor. In addition,

Table 14 Catalytic results of the oxidation of TMP to TMBQ by first generation methanol passivated in the presence of base.

Catalyst	TOF 2 min	Conversion % 60 min (± 5)	Selectivity % 60 min (± 5)	Yield % 60 min (± 5)
4C-Ti-1st Gen $SiCl_4$ MeOH Passivated w/TEA	0	23	23	5.4
3C-Ti-1st Gen $SiCl_4$ MeOH passivated w/TEA	0	15	15	2.3
2C-Ti-1st Gen $SiCl_4$ MeOH passivated w/TEA	0	10	11	1.1

by 60 minutes, all the aqueous hydrogen peroxide has been consumed and the reaction stops. Figure 69 illustrates that substrate conversion (red) and product formation (blue) halt once oxidant has been consumed. Therefore, the addition of base during passivation is not a practical strategy for synthesizing air stable single-site heterogeneous catalysts.

Non-Passivated Catalysts

The catalysts "as synthesized" with no attempt to removed silyl chloride groups from the matrix are also investigated. These catalysts are referred to as first generation non-passivated (Ti-1st gen $SiCl_4$-NP). Even though the catalysts still contain unreacted chloride groups, during the catalysis reaction the chlorides may react with the aqueous hydrogen peroxide. Table 15 compares the catalytic activity of non-passivated (NP) 2C-Ti-NP, 3C-Ti-NP, and 4C-Ti-NP catalysts. Like methanol passivated catalysts, the TOFs, percent conversions, and selectivities for all three non-passivated catalysts are quite similar. We believe it is likely that aqueous HCl is still breaking Ti-O-Si bonds creating catalysts with a mixture of sites instead of having only one targeted site in the system.

Addition of Base to Non-Passivated Catalysts

Base can also be added directly to the catalysis reaction as an acid scavenger to neutralize the generated acid. The addition of sodium acetate and triethylamine are investigated and give virtually identical results. Therefore, only the sodium acetate procedure will be described.

Sodium acetate is dried under vacuum at 110^0 C and stored in a nitrogen atmosphere glovebox. The IR spectrum of sodium acetate does not show a broad feature at 3600 cm^{-1} indicating the absence of water, Figure 70. These precautions to reduce contact with water are taken to prevent the premature exposure of the non-passivated catalysts to HCl production. A calculated amount of sodium acetate, two equivalents of base to remaining Cl, is added to the reaction vial inside the glovebox prior to the addition of catalyst. Other than the addition of base, the catalytic protocol outlined in Chapter 2 is followed.

Table 16 summarizes the catalytic active of non-passivated first generation catalysts in the presence of sodium acetate. Each connectivity exhibits a distinct catalytic activity 3C > 2C > 4C. According to the literature the oxidation of phenols to benzoquinones is thought to occur at 3-connected Ti sites. The results presented here are consistent with the literature. The selectivities for these non-passivated catalysts in the presence of base is significantly reduced

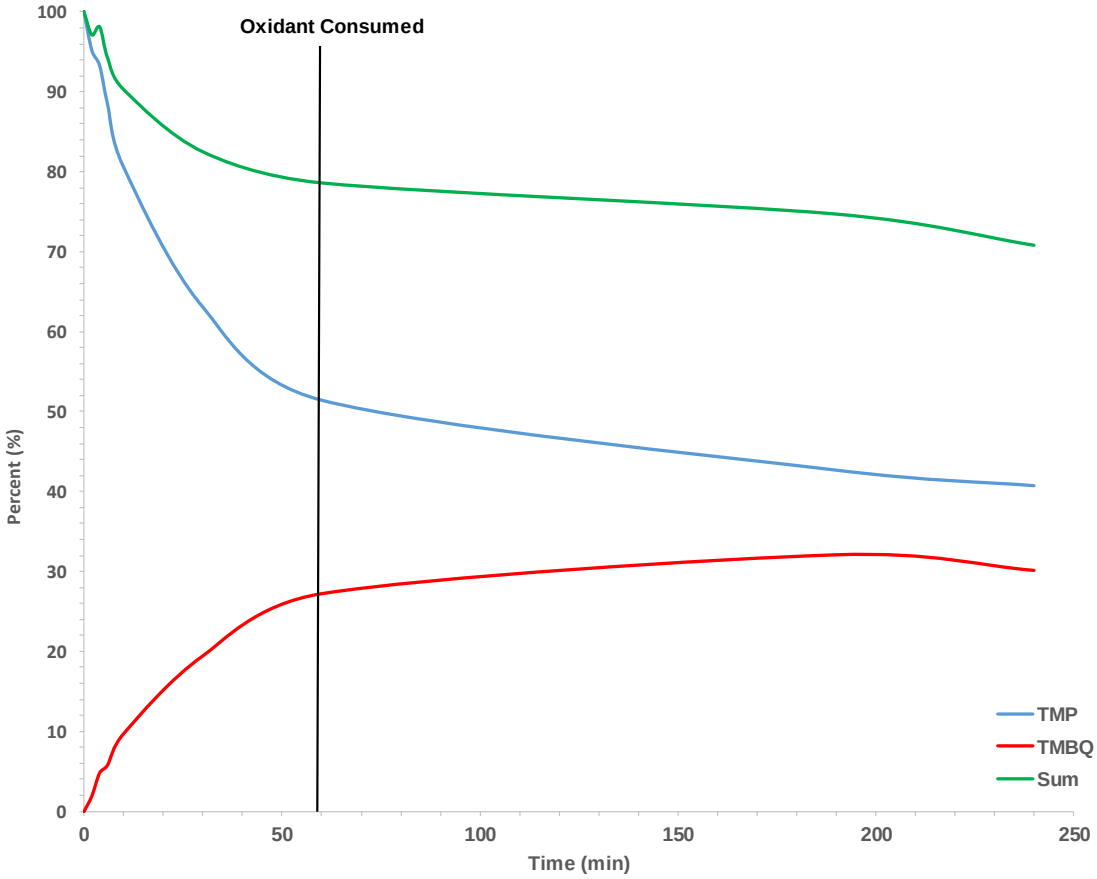

Figure 69 Kinetic plot of the conversion of TMP to TMBQ by 4C-Ti-1st gen MeOH passivated in the presence of base. Hydrogen peroxide has been completely consumed by 60 minutes.

Table 15 Catalytic results of first generation non-passivated titanosilicates in the oxidation of TMP to TMBQ.

Catalyst	TOF 2 min (± 0.2)	Conversion % 60 min (± 5)	Selectivity % 60 min (± 5)	Yield % 60 min (± 5)
4C-Ti-1st Gen $SiCl_4$ NP	2.28	98.9	40.2	39.8
3C-Ti-1st Gen $SiCl_4$ NP	2.49	100	52.1	52.1
2C-Ti-1st Gen $SiCl_4$ NP	2.64	100	46.7	46.7

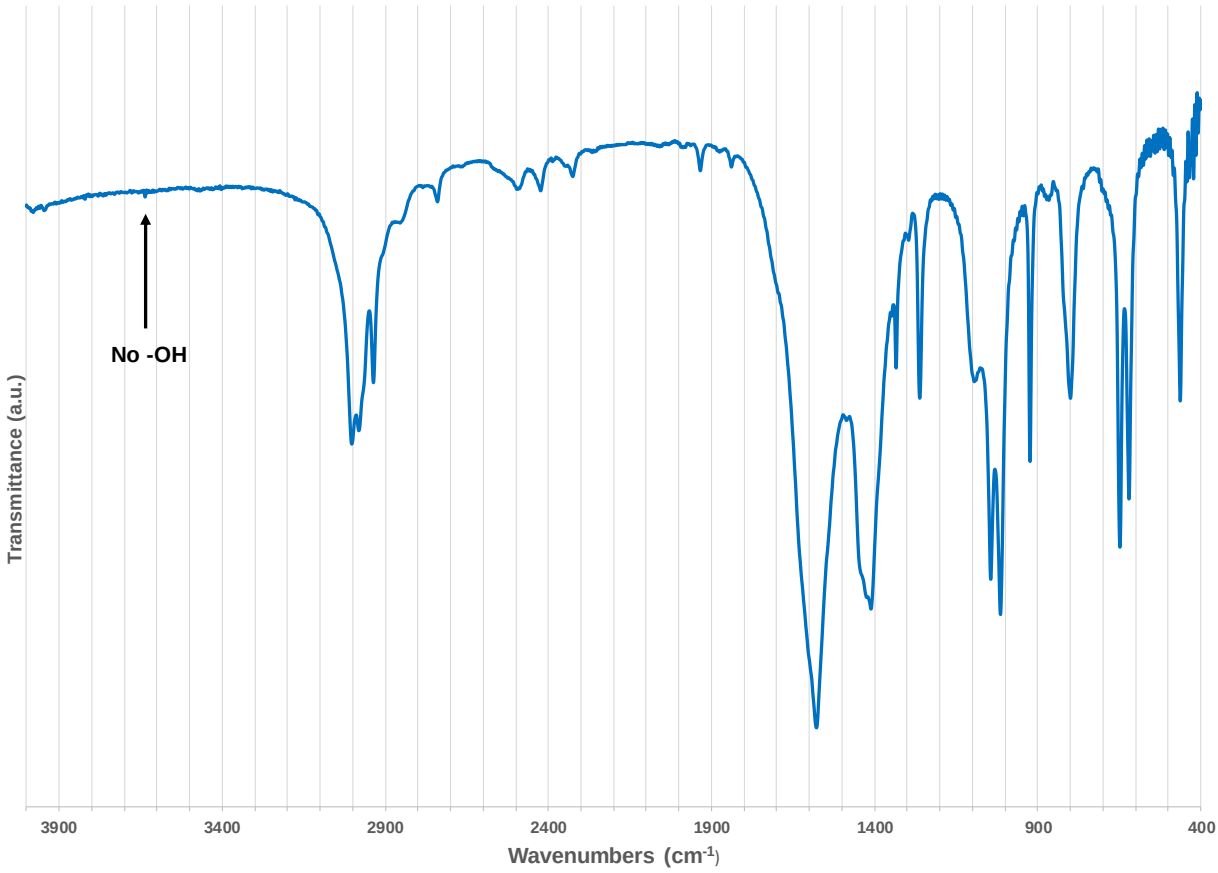

Figure 70 IR Spectrum of dried sodium acetate illustrating water is not present.

Table 16 Catalytic results of first generation non-passivated titanosilicates with added base in the oxidation of TMP to TMBQ.

Catalyst	TOF 2 min (± 0.3)	Conversion % 60 min (± 5%)	Selectivity % 60 min (± 5%)	Yield % 60 min (± 5%)
Si-Platform NP w/$NaC_2H_3O_2$	-	17	30	5.1
4C-Ti-1st Gen $SiCl_4$ NP w/$NaC_2H_3O_2$	0.00	15	10.5	1.26
3C-Ti-1st Gen $SiCl_4$ NP w/$NaC_2H_3O_2$	4.7	35	15	5.05
2C-Ti-1st Gen $SiCl_4$ NP w/$NaC_2H_3O_2$	2.5	43	35	15.5

compared to methanol passivated and non-passivated catalysts without base. This reduction in selectivity severely limits their use as potential oxidation catalysts. Similar to base added during methanol passivation, oxidant is consumed before the reaction is complete preventing 100% conversion of substrate. Furthermore, neutralizing acid with equivalent or excess amounts of base is only viable in an academic setting; this would not be an acceptable method in industry.[103] It is noteworthy that in the absence of catalyst, aqueous hydrogen peroxide is consumed in approximately 60 minutes in the presence of sodium acetate alone. Figure 71 shows the NMR spectra of a catalytic reaction containing solvent, substrate, internal standard, sodium acetate, and oxidant at t = 0 (blue) and t = 60 minutes (pink). The loss of signal at ~ 8 ppm indicates all the hydrogen peroxide has been consumed.

Methyl-*tert*-butyl ether (MTBE) Passivation

According to Wakabayashi *et.al.*[103] asymmetric ethers in the presence of Lewis acid catalysts will react with Si-Cl groups producing a siloxy group and chloroalkane as shown in Equation 38. A Lewis acid is added as a catalyst to promote passivation with asymmetric ether. In this work, the titanium active site of the material being passivated acts as the Lewis acid needed for this reaction.

$$-SiCl + R^1{-}O - R^2 \xrightarrow{MCl_{3\ cat.}\ (M=Bi,Fe,Al)} -SiOR^2 + R^1Cl \qquad \text{Equation 38}$$

Second dose catalysts are passivated with MTBE by a procedure similar methanol passivation. After the second cross-linking with $SiCl_4$ the catalyst is dried and the connectivity calculated, ~25 mL of dry toluene is vapor transferred to the reaction vessel. Approximately, two equivalents of methyl-*tert*-butyl ether to remaining silyl chloride groups are vapor transferred to the reaction vessel with constant stirring. The reaction is then placed in an 80°C oil bath and allowed to react for 16 hours. The catalyst is then dried at 80°C under vacuum and the volatiles are collected and analyzed via NMR spectroscopy. The acidity of each catalyst is qualitatively determined. The pH test indicates these MTBE passivated catalysts are essentially neutral or weakly acidic, pH $\geq$ 6. The catalytic activities of first generation MTBE passivated catalysts are presented in Table 17.

Unfortunately, 2-methylpropene was identified in the NMR and is indicative of the production of HCl during this passivation step, Figure 72. While the different connectivities of titanium to the matrix exhibited individual catalytic properties, passivation with MTBE was abandoned due to.

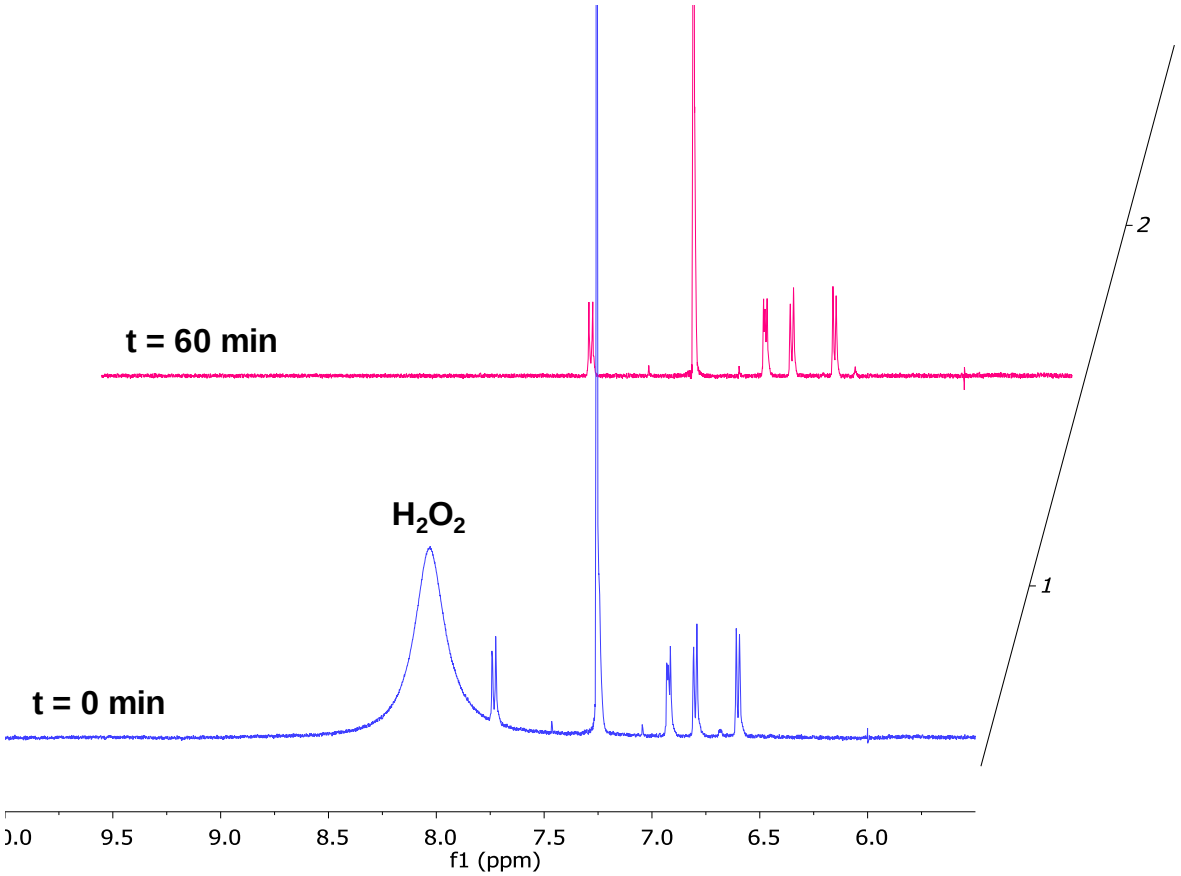

Figure 71 NMR spectra t = 0 minutes (1, blue) and t = 60 minutes (2, pink) illustrating the consumption of H_2O_2.

Table 17 Catalytic results of first generation MTBE passivated catalysts with added base in the oxidation of TMP to TMBQ.

Catalyst	TOF 2 min (± 0.2)	Conversion % 60 min (± 5)	Selectivity % 60 min (± 5)	Yield % 60 min (± 5)
4C-Ti-1st Gen $SiCl_4$ MTBE Passivated	0.590	76.0	43.9	33.3
3C-Ti-1st Gen $SiCl_4$ MTBE-passivated	0.240	49.4	63.6	38.5
2C-Ti-1st Gen $SiCl_4$ MTBE passivated	1.32	100	56.7	56.7

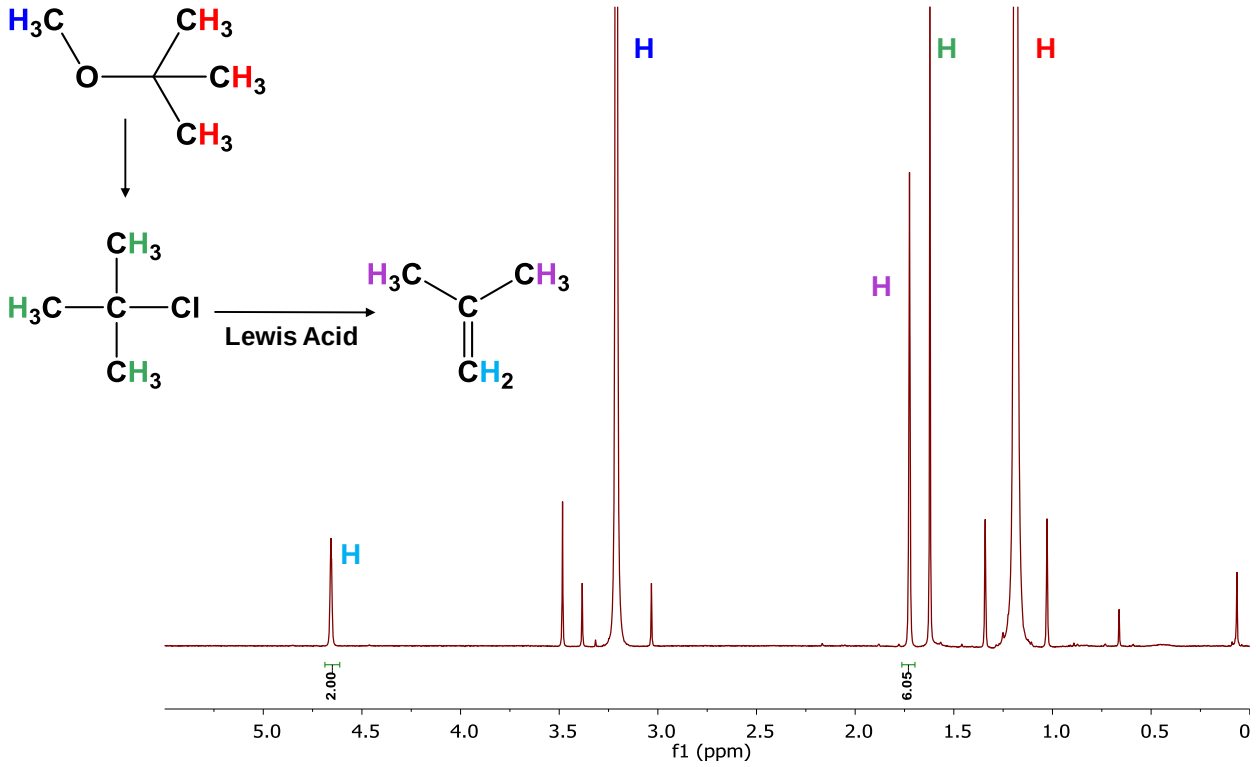

Figure 72 NMR spectrum of the volatiles from MTBE passivation.

evidence of HCl production. Ultimately, passivation with MTBE may be a viable alternative to methanol passivation under optimum reaction conditions and may be worth further investigation.

Changing Inert Linker

After several failed attempts of trying to remove or neutralize the remaining chlorides on the catalyst, a different approach is taken to produce neutral catalysts. On average, the connectivity after the second cross-linking is calculated to be approximately 2.3 – 2.7 connected. Therefore, we chose to investigate a new cross-linking agent which will have a maximum connectivity of 2. Dichlorodimethylsilane (Me_2SiCl_2) has been chosen as the new inert linking agent. Chapter 5 will discuss, in detail, the synthesis and characterization of both first and second generation catalysts synthesized using Me_2SiCl_2 as the inert cross-linking agent.

Chapter V: Synthesis and Characterization of Non-Passivated First and Second Generation Single-Site Titanosilicate Catalysts

Introduction

As has been described in Chapters 3 and 4, the production of HCl has proven to be a significant problem in the passivation step leading to air stable single-site titanosilicate catalysts. After exploring several different passivation strategies, it was decided to try and decrease the number of chloride groups remaining after synthesis to lessen the acidity of the final catalysts and negate the need for passivation altogether.

The precedent for this work was presented by Dr. Richard Mayes, Dr. Nan Chen, and Dr. Joshua Abbott.[42,73,104] During the development of the method of sequential additions, silicon tetrachloride is used to further cross-link the oligomers produced in the first dose and build a robust matrix around the catalytic active site. The average connectivity of silicon to tin cube is determined to be 2.3 – 2.7 Si : tin-cube. The maximum connectivity when using silicon tetrachloride as the second cross-linking agent is four. Therefore, the connectivity measurement indicates there are still several chloride ligands remaining, on average 1.3 – 1.7 Cl per silicon linker, which results in very acidic catalysts. In order to reduce the number of remaining chloride ligands and reduce the acidity of the catalysts, dichlorodimethylsilane (Me_2SiCl_2) is investigated as an alternative cross-linking agent. By changing the cross-linking agent in the second dose, the connectivity of titanium active sites established in the first dose should remain unchanged. Thus, each catalyst will still have a tailored connectivity and a specific imprinted geometry around the titanium active site, but in theory be less acidic and consequently more air and water stable.

These “new” catalysts are synthesized with the same mononuclear titanium precursors as described in Chapter 3, $TiCl_4$, $Ti(OiPr)Cl_3$, $Ti(OiPr)_2Cl_2$. Each precursor is synthesized and used as previously described following the same first dose cross-linking reaction with the tin-cube building block. Gravimetric analysis is initially used to calculate the connectivity to the matrix. However, after determining connectivity several times, it is assumed that under these specific reaction conditions each catalyst reaches its limiting connectivity cleanly.

Experimental

First Generation Cross-linked with Me_2SiCl_2

After the titanium connectivity is established, the reaction is removed from the oil bath and allowed to cool to room temperature. Me_2SiCl_2 is then vapor transferred into the reaction flask in

a 2 : 1 ratio of Si : tin-cube with constant stirring under dry ice/isopropanol conditions. After the addition of Me_2SiCl_2 the reaction is replaced into an 80^0 C oil bath and allowed to react for 72 hours under constant stirring. In contrast to previous catalysts cross-linked with $SiCl_4$, the reaction is heated for an additional 24 hours. The increase in reaction time is to account for fewer silyl chloride groups on the new linking reagent, Me_2SiCl_2. We believe that the chlorides on Me_2SiCl_2 are less reactive than $SiCl_4$. After the second cross-linking reaction, the connectivity of silicon to cube is calculated by gravimetric analysis. The connectivity of the silicon is found to be 2 ± 0.1 in all cases, indicating that the majority, if not all, chlorides present on the inert linker reacted. This addresses the concern about excess Si-Cl groups left in the matrix from the second cross-linking reaction. Based on gravimetric analysis, the maximum silicon connectivity is reached and thus creates a neutral catalyst.

Determining the pH of "New" First Generation Catalysts

To qualitatively determine the acidity of these catalysts, approximately 2.5 mg of first generation catalysts 2C-Ti, 3C-Ti, and 4C-Ti are added to 4mL vials and covered with approximately 250 μL of ultrapure water. The vials are then capped and sonicated for 30 minutes. After sonication, a drop of the solution is placed onto pHydrion paper (Micro Essentials Laboratory) and the pH is found to be neutral. Each catalyst is stored in a silylated 4-dram vial inside a nitrogen atmosphere glovebox to prevent adsorption of water on the titanium active sites.

Characterization of "New" First Generation Catalysts

The catalysts are then characterized using several different techniques: gravimetric analysis, ICP, FTIR, BET, DRUV, and catalytic activity. The catalysts presented in Chapter 3 synthesized with $SiCl_4$ were additionally characterized by XAS. Unfortunately, XAS beam time was not allotted for the characterization of these new Me_2SiCl_2 cross-linked catalysts. However, it can be assumed that the data collected for non-passivated $SiCl_4$ catalysts are identical for catalysts synthesized with Me_2SiCl_2. The absorber atom investigated by XAS in Chapter 3 was the titanium active site. Changing the inert cross-linker does not alter the connectivity or geometry established during the first cross-linking reaction. Hence the assumption made is that the XAS data applies to both sets of catalysts, $SiCl_4$ and Me_2SiCl_2. Figure 73 compares the final matrix of non-passivated 4C-1^{st} gen-Ti-$SiCl_4$ and the new first generation 4C-Ti-Me_2SiCl_2 catalysts. The only difference is the terminating ligands of the silicon linkers.

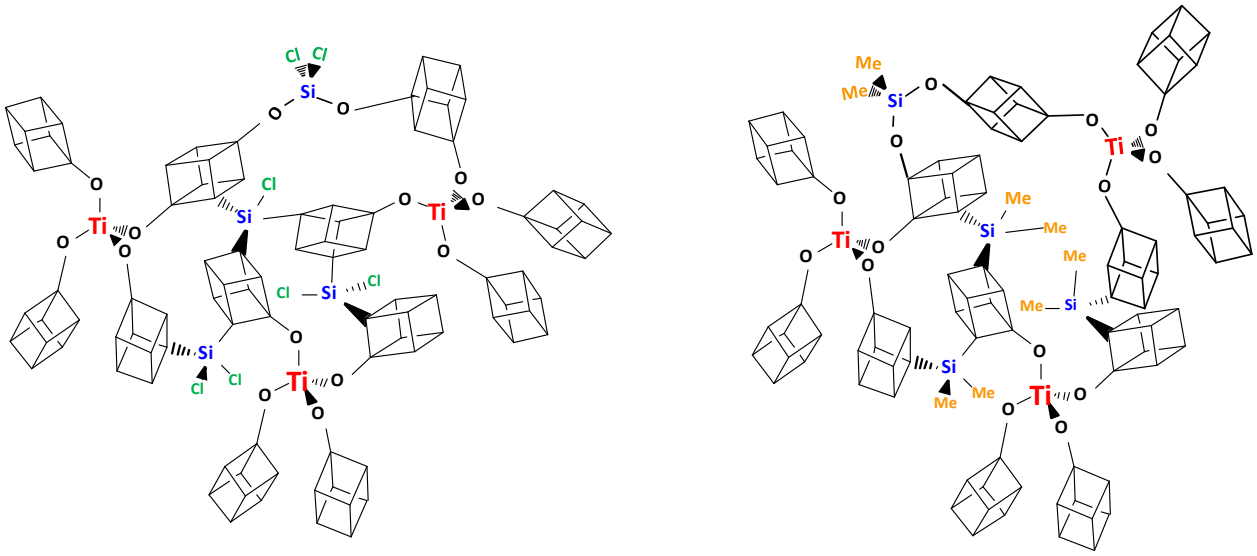

4C-Ti-1st gen $SiCl_4$ **4C-Ti-1st gen Me_2SiCl_2**

Figure 73 Final matrix of first generation catalysts left cross-linked with $SiCl_4$ and right cross-linked with Me_2SiCl_2.

Elemental Analysis

Gravimetric analysis is used to determine both the connectivity of the Ti active site and the approximate weight percent of Ti in the samples. The actual weight percent of Ti are obtained via ICP-OES. Table 18 summarizes the connectivity and weight percent calculated for the family of Ti-1st gen Me_2SiCl_2 catalysts. The differences observed in Ti wt% between gravimetric analyses versus ICP-OES analyses are the result of loss sample during drying and/or loss of silicon grease over the course of the reaction. While precautions are taken to avoid loss of sample during the drying process, it is virtually impossible to ensure zero loss of sample. Therefore, the ICP weight percent is always determined and used as the actual weight percent of the sample.

Infrared Spectroscopy

Similar to first generation catalysts synthesized with $SiCl_4$, these new first generation catalysts are characterized using IR spectroscopy. The same signature bands observed in the FTIR spectra for first generation $SiCl_4$ catalysts for Si-O-Si and Ti-O-Si are present in catalysts synthesized with Me_2SiCl_2. Figure 74 compares the IR spectrum of 4C- first generation $SiCl_4$ non-passivated (blue) and 4C- first generation Me_2SiCl_2 non-passivated (purple) catalysts. From the IR spectrum it can be seen that that while the peak shape are slightly different, the same fingerprint features present in Chapter 3 are still present when the inter linker is changed. The same trend is seen for 2C- and 3C- catalysts.

Figure 75 presents an overlay of the infrared spectra of the 2C-Ti-1st gen Me_2SiCl_2 (green), 3C-Ti-1st gen Me_2SiCl_2 (blue), 4C-Ti-1st gen Me_2SiCl_2 (purple), and Ti-free platform (yellow). All four of the samples synthesized with Me_2SiCl_2 as the inert cross-linker present similar features that are assigned to the Si-O stretching modes. From the spectra, two absorption peaks can be seen at ~1080 cm^{-1} and 1200 cm^{-1}.[105] In this case, the former represent the Si-O stretches of silicon tetrahedron on the inner surfaces of the matrix while the latter is assigned to the external Si-O stretches on the outer surface of the material.[106] These two features correspond to the internal and external anti-symmetric Si-O stretching vibrations of silicate matrices. In addition to these two features, a third feature is present in all four samples at ~800 cm^{-1} which corresponds to the symmetric stretching of the Si-O bonds.

Table 18 Comparison of gravimetric and ICP-OES weight percent.

Catalyst	Connectivity	Weight % (Gravimetric) (± 0.3%)	Weight % (ICP) (± 0.1%)
4C-1st gen-Me_2SiCl_2	4.0 (± 0.1)	2.0 – 2.9	1.9 – 3.0
3C-1st gen-Me_2SiCl_2	3.0 (± 0.1)	3.2 – 6.3	2.9 – 5.9
2C-1st gen-Me_2SiCl_2	1.9 (± 0.1)	5.8 – 8.9	5.3 – 8.7

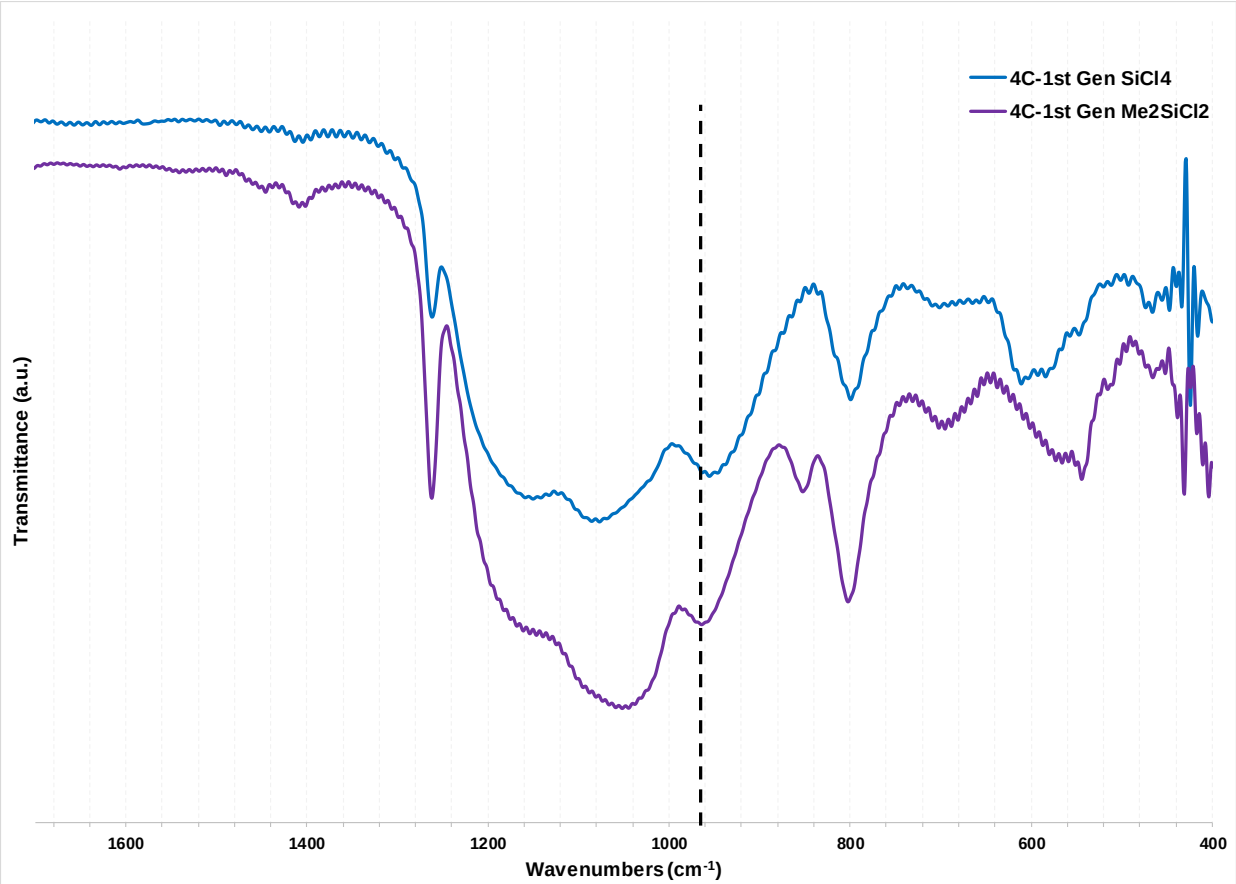

Figure 74 Overlay of FTIR spectra of two non-passivated 4C-Ti catalysts, cross-linked with $SiCl_4$ (blue) and cross-linked with Me_2SiCl_2 (purple).

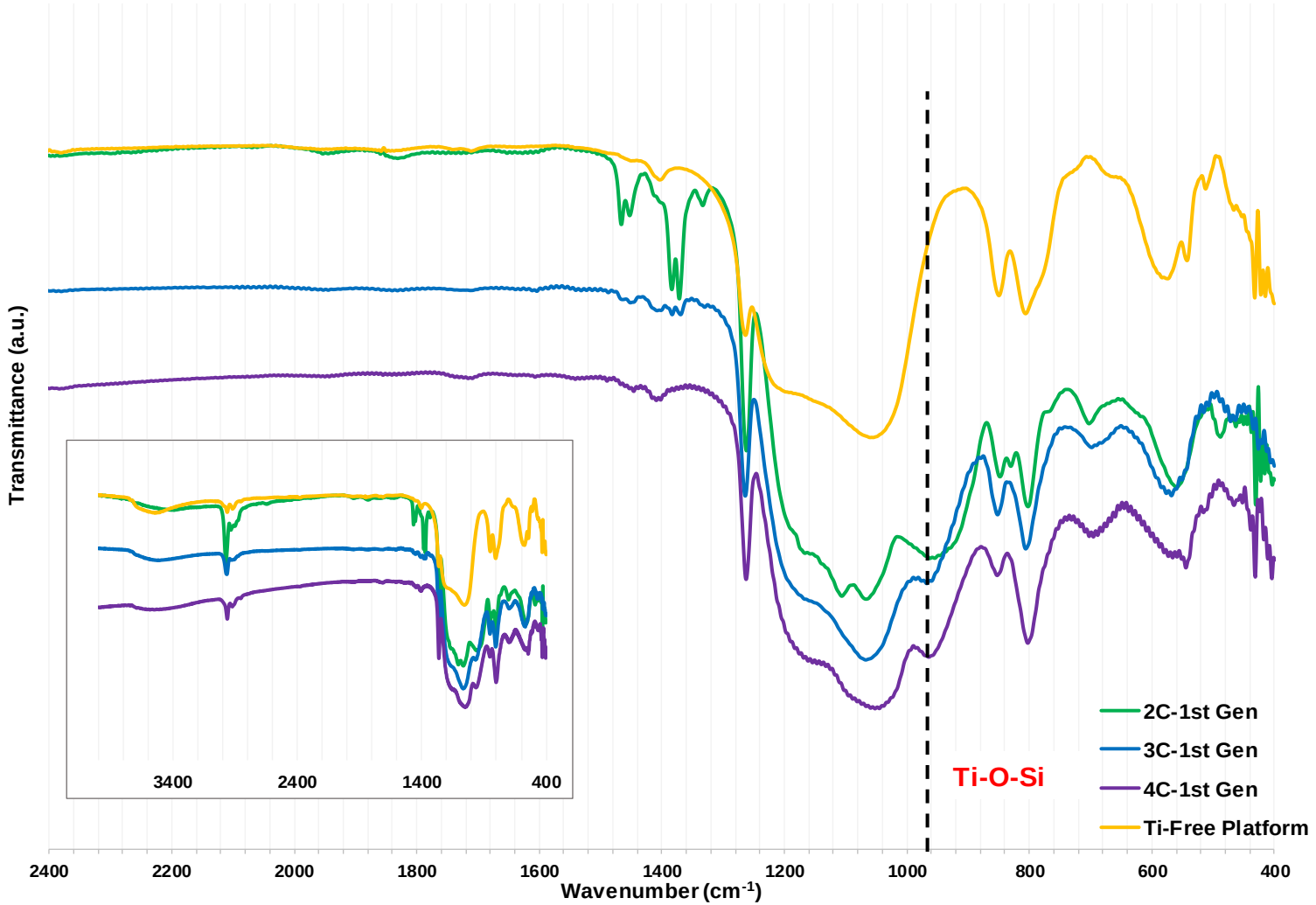

Figure 75 FTIR spectra overlay for first generation catalysts cross-linked with Me_2SiCl_2, 2C-Ti (green), 3C-Ti (Blue), 4C-Ti (purple), and Ti-free platform (yellow). The inlay is the full FTIR window.

The three titanium containing spectra exhibit an additional absorption feature as a shoulder to the Si-O band at ~ 960 cm^{-1}. This band is a signature feature for Ti-O-Si linkages specifically assigned to the Si-O vibrations of Ti-O-Si bonds. [56,82] The lack of this shoulder in the Ti-free platform is expected. Additionally, the absence of an appreciable absorption feature beyond 3500 cm^{-1} indicates the lack of hydroxyl groups in these matrices.

Diffuse Reflectance UV-Visible Spectroscopy

In contrast to traditional titanosilicates, the catalysts presented here are synthesized with a tin functionalized building block. The remaining tin groups contribute their own absorption features at ~200-212 nm. Therefore, a titanium free platform is prepared and measured according to the DRUV procedure outlined in Chapter 2, Figure 76. To correct for tin absorption, the Ti-free platform is multiplied by an arbitrary corrections factor, between 0.1 and 1, and subtracted from the raw data obtained for the titanium containing samples. The multiplier is chosen to provide the best qualitative peak shape. Figure 77 shows the tin corrected DRUV spectra for first generation catalysts. The lack of absorption features above 300 nm indicates these catalysts are isolated Ti(IV) centers and not polynuclear Ti centers (Ti-O-Ti). The absorption region of interest is between 200 – 225 nm. Camberti *et al.[107]* assign the range for tetrahedral Ti(IV) centers as 210-225 nm depending on the type of site, i.e., open or closed. While there is a second feature at approximately 260 nm in these spectra, it is also observed in the Ti-free platform. At this time, we have no definitive explanation for this feature and therefore only the first feature, attributed to Ti(IV), will be discussed. Table 19 summarizes the absorption wavelength maxima for first generation catalysts. It can be seen that all first generation titanium catalysts present a maximum absorption below 225 nm suggesting all three catalysts, regardless of connectivity, have tetrahedral Ti(IV) active sites.

Catalytic Activity of First Generation Catalysts

The titanosilicates synthesized in this work possess several desired properties for heterogeneous catalysts: 1) the synthetic methodology incorporates 100% of the titanium present in the precursor into active sites in the matrix; 2) by targeting connectivity, the active sites have high site homogeneity; 3) the size of the building block isolates each active site preventing dimerization; and 4) the materials are mesoporous allowing for a wide library of substrates.

Under identical reaction conditions, outlined in Chapter 2, the catalytic activity of first generation catalysts synthesized with Me_2SiCl_2 are investigated for the oxidation of 2,3,5-

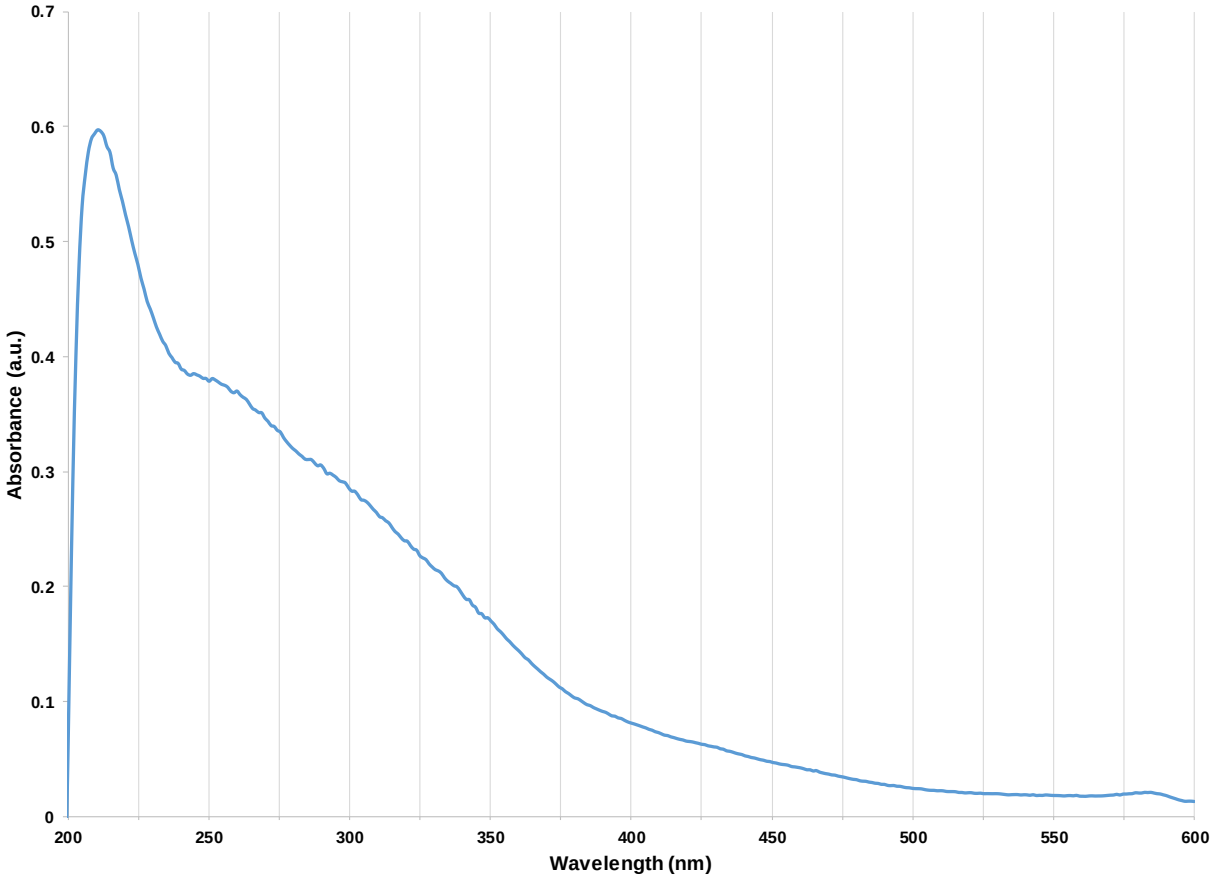

Figure 76 DRUV spectrum of titanium free platform.

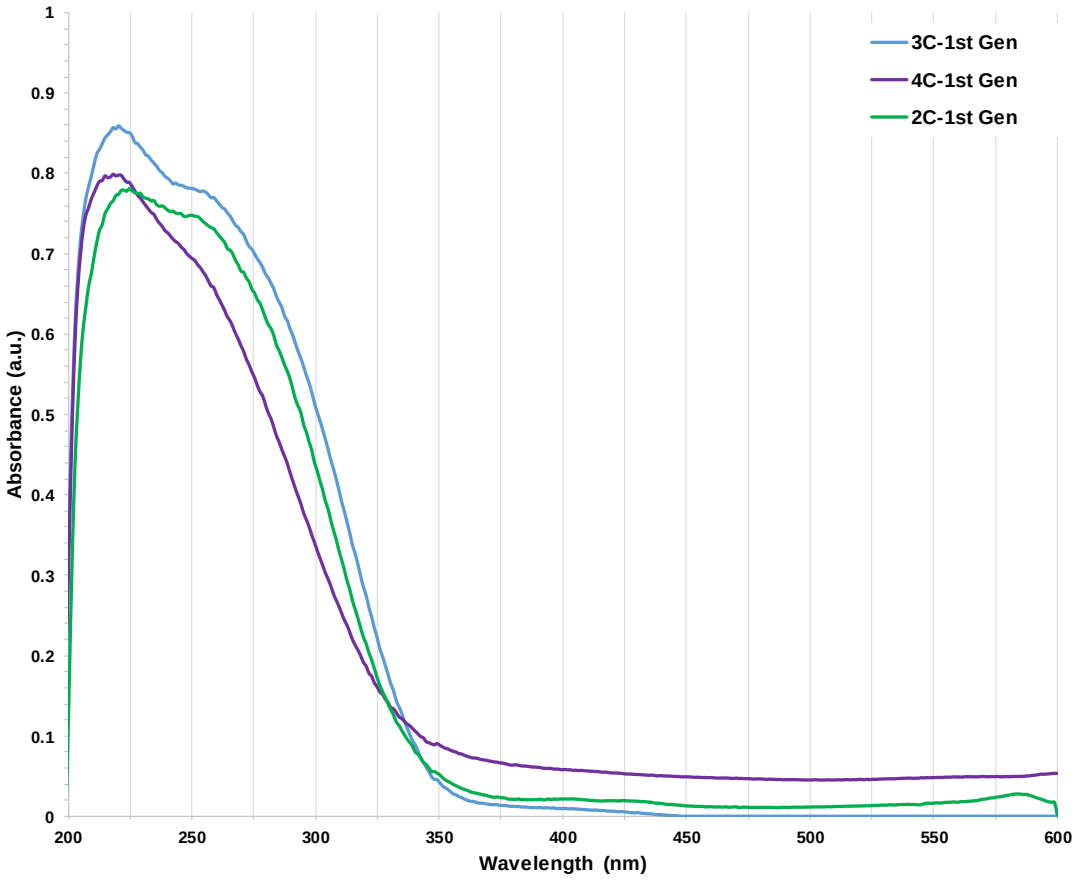

Figure 77 DRUV spectra of 2C-Ti-1st gen, 3C-Ti-1st gen, and 4C-Ti-1st gen after the tin correction.

Table 19 DRUV absorption wavelength maxima for first generation catalysts.

Catalyst	Max Wavelength (nm) (± 0.5)
2C-1st Gen Me_2SiCl_2	225
3C-1st Gen Me_2SiCl_2	222
4C-1st Gen Me_2SiCl_2	219

Trimethylphenol (TMP) to 2,3,6-trimethylbenzoquinone (TMBQ) and 2,6-dimethoxyphenol (syringol, DMOP) to 2,6-dimethoxylbenzoquinone (DMOBQ). The catalytic activity of these reactions are monitored via NMR spectroscopy. Figure 78 shows a typical spectrum for the oxidation of TMP to TMBQ and Figure 79 illustrates DMOP to DMOBQ. In contrast to titanium free platform, upon addition of either substrate to suspensions of these catalysts in solvent (acetonitrile), the color of the titanium catalysts changes from white to yellow (TMP) and orange (DMOP), consistent with substrate binding to the titanium active site. Immediately after the addition of H_2O_2, the solution lightens followed by an increase in color intensity within five minutes. The final solutions, regardless of substrate, are a deep yellow color as a result of the formation of TMBQ and DMOBQ. In comparison to titanium containing catalysts, the titanium free reactions do not exhibit color changes in the solid or the reaction solutions qualitatively demonstrating the lack of substrate binding to silicon which is accompanied by no production of quinone.

The activities of two literature catalysts, TS-1 and grafted Ti-MCM-41, are also investigated. These catalysts are prepared per standard literature procedures.[44,108] TS-1 is described as an ideal example of single-site catalysts and has shown to be an effective heterogeneous catalyst under aqueous conditions. However, in contrast to the catalysts synthesized in this work, TS-1 is microporous and thus mass transport issues play a key role in the lack of conversion observed for TMP and DMOP. Grafted Ti-MCM-41, is a mesoporous silicate in which titanium sites have been grafted to the surface post synthesis. After calcination Ti-MCM-41 has exhibited good catalytic activity, but there is little known about the active site. In the process of grafting, mixtures of active sites are incorporated into the matrix. Therefore, the true catalytic active site cannot be determined and the turnover frequency is not valid because the true amount of active titanium is unknown. In addition, titanium centers in Ti-MCM-41 are known to leach in the presence of aqueous hydrogen peroxide.[71] Leaching is also observed in the work described here and therefore, it is unknown if the active catalyst is the leached species, the remaining heterogonous catalyst, or a combination of both. In contrast to the literature catalysts, the Ti-1st gen Me_2SiCl_2 catalysts are mesoporous which are not limited by mass transfer problems and the catalyst are single-site; therefore, their TOFs represent their true catalytic activities.

The quantitative results presented in Table 20 for the oxidation of TMP to TMBQ, and in Table 21 for the oxidation of syringol to 2,6-dimethoxybenzoquinone are consistent with the qualitative observations made above. The lack of conversion observed for titanium free platform, and a catalyst free blank, indicates titanium is the true active site for the oxidation of

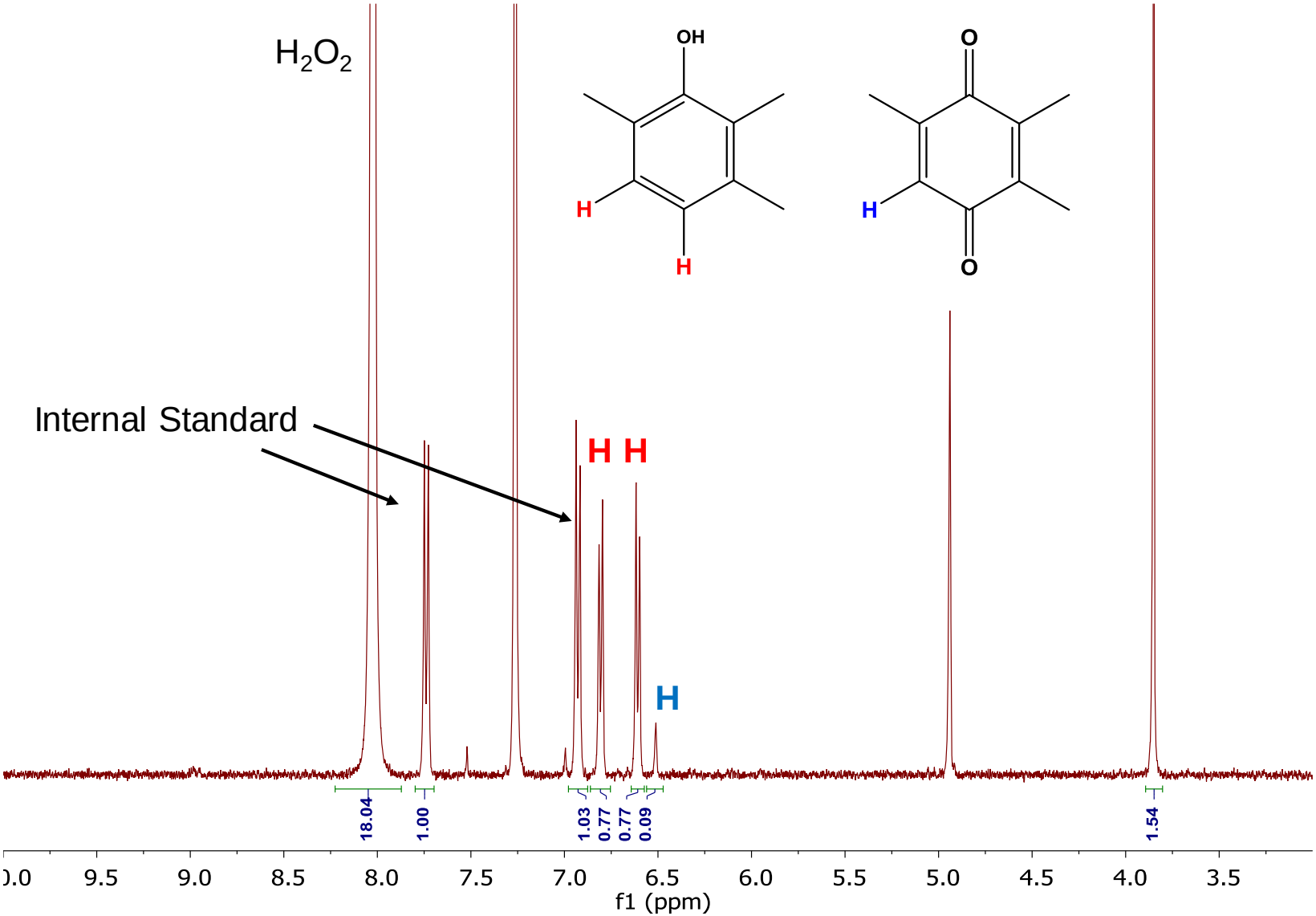

Figure 78 Typical NMR spectrum used for the characterization of catalytic activity for the oxidation of TMP to TMBQ.

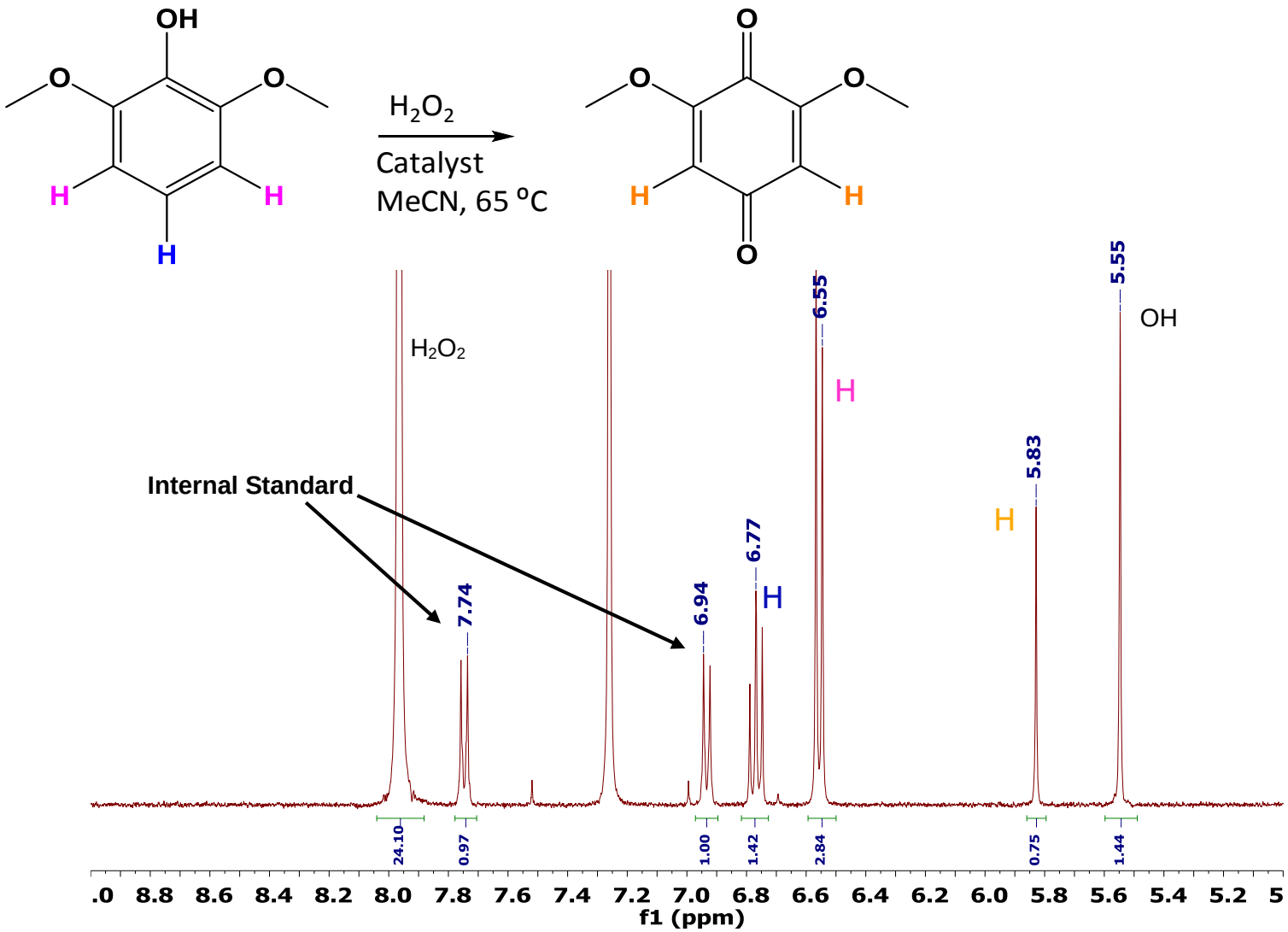

Figure 79 NMR Spectrum of a typical oxidation reaction for the conversion of DMOP to DMBQ.

Table 20 Results of catalytic activity for first generation titanosilicates, two control reactions, and two literature catalyst for the oxidation of TMP to TMBQ.

Catalyst	TOF 2 min	Conversion % 60 min (± 5)	Selectivity % 60 min (±4)	Yield % 60 min (±4)
TMP + H_2O_2	n/a	0	0	0
Si-Platform Me_2SiCl_2	n/a	0	0	0
4C-Ti-1st Gen Me_2SiCl_2	0.75 (±0.03)	63	62	39
3C-Ti-1st Gen Me_2SiCl_2	0.90 (±0.1)	87	66	57
~~2C-Ti-1st Gen Me_2SiCl_2*~~	~~1.27 (± 0.06)~~	~~100~~	~~40~~	~~40~~
TS-1	0	6	0	0
G-Ti-MCM-41*	n/a	100	50	50

* These catalysts leach during catalysis and are not pure heterogenous catalysts.

Table 21 Results of catalytic activity for first generation, two control reactions, and two literature catalyst for the oxidation of DMOP to DMOBQ.

Catalyst	TOF 2 min	Conversion % 60 min (± 5)	Selectivity % 60 min (±4)	Yield % 60 min (±4)
DMOP + H_2O_2	n/a	3	5	0.15
Si-Platform Me_2SiCl_2	n/a	9.4	6.8	0.64
4C-Ti-1st Gen Me_2SiCl_2	0.23 (± 0.03)	50	77	39
3C-Ti-1st Gen Me_2SiCl_2	1.04 (± 0.06)	100	59	59
~~2C-Ti-1st Gen Me_2SiCl_2*~~	~~1.6 (± 0.2)~~	~~100~~	~~64~~	~~64~~
TS-1	0	6	13	0.78
G-Ti-MCM-41*	n/a	100	61	61

* These catalysts leach during catalysis and are not pure heterogenous catalysts.

phenols to benzoquinones. Under the current reactions conditions, neither the tin sites of the unreacted building blocks nor the porous silica matrices catalyze the oxidation of phenols. In addition, hydrogen peroxide is ineffective for oxidizing phenols to benzoquinones alone. In contrast, all catalysts containing titanium show evidence of phenol conversion.

Based on the TOFs presented in Table 20 and Table 21 different catalytic activities are observed for each of the catalysts. 2C-Ti is more active than 3C-Ti which is more active than 4C-Ti. However, while 2C-Ti exhibited the highest activity, it also presented with the lowest selectivity. This is not a surprising result because it is often found in literature that the more active a catalyst, the lower the its selectivity.

One explanation for the observed differences in the catalytic activity may be a result the structural differences between the three catalysts, 2C-Ti-1st gen, 3C-Ti-1st gen, and 4C-Ti-1st gen, Figure 80. All first generation catalysts in this work have been synthesized using the same building block, and the same method of sequential additions. However, the metal precursors employed to target the connectivity are structurally different. The 2C-Ti material has two alkoxy ligands that are not locked to the matrix and are able to move or exchange allowing substrate to bind to the active site. The 3C-Ti catalyst has three Ti-O-Si linkages and one unconstrained alkoxy ligand, while the 4C-Ti catalyst is completely embedded in the matrix by four Ti-O-Si bonds restricting substrate binding. The differences in catalytic activity may be attributed to the accessibility of the titanium sites.

In addition to the direct influence of the ligands coordinated to the titanium, the silicon atoms in the vicinity of the active site can also affect accessibility. The additional building blocks linked to the 4C- catalysts, Figure 81, in comparison to the 3C- and the 2C- catalysts produce a more sterically congested active site. In contrast to the 4C- fully embedded catalysts, the energy barriers for substrate binding to active sites of the 3C- and 2C- catalysts are expected to be significantly lower as a result of fewer Ti-O-Si linkages. A mechanism that has been proposed for phenol oxidation involves the formation of a free radical after the binding of substrate and oxidant to the titanium active site.[59,109,110] It has been hypothesized that in order for phenol oxidation reactions to be catalyzed by titanium, the initial step involves the simultaneous of breaking a Ti-O-Si bond while coordinating either water or peroxide, Figure 82. Based on sterics and electronics, this proposed step has a high energy associated with it and the energy barriers to disrupting subsequent linkages are expected to be lower increasing the possibility of leaching.

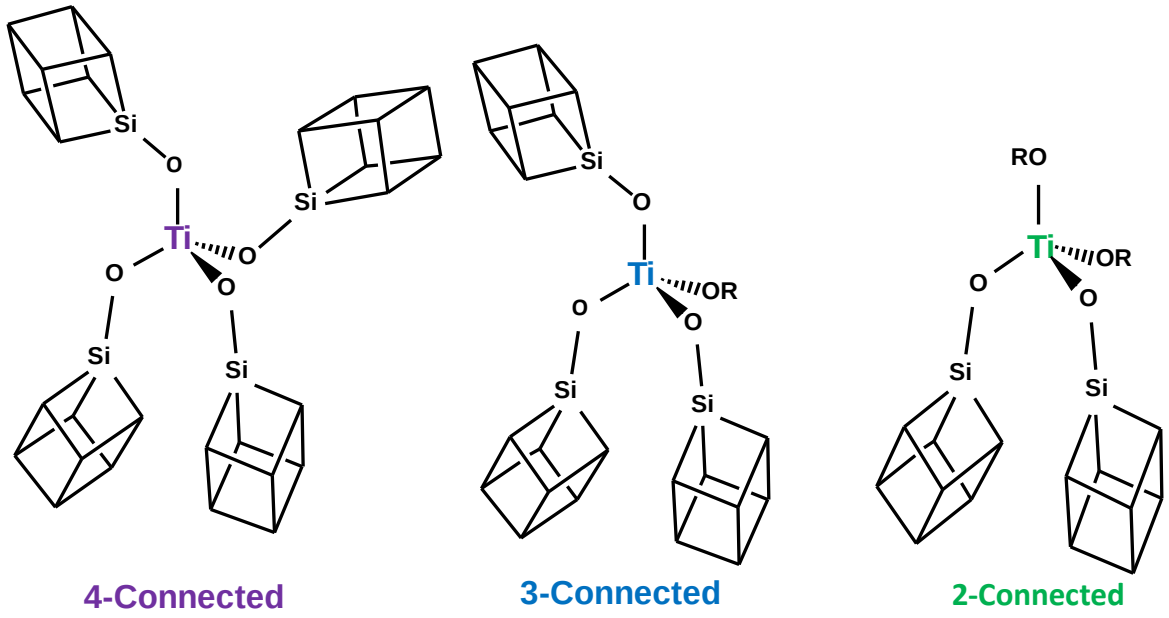

Figure 80 Illustration of the three different active sites.

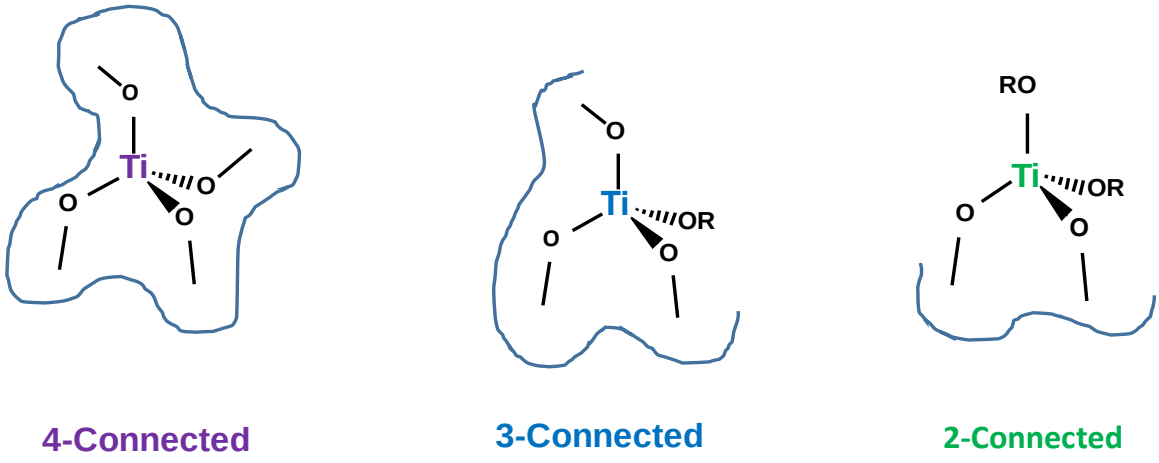

Figure 81 Illustration of how the surrounding matrix effects the accessibility of substrate to the active site.

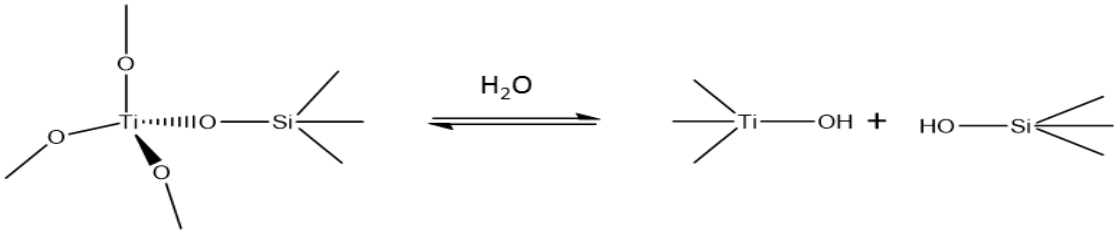

Figure 82 Illustration of the proposed open the 4C-Ti active site.

Leaching

Leaching of the active metal from a support can be one of the severest tests that a heterogeneous catalyst faces. This is certainly the case with many metals on supported silica including titanium. Most titanosilicate materials, regardless of synthesis method, show signs of leaching when exposed to aqueous peroxide solutions. TS-1 is one of the very few catalysts that are stable to aqueous conditions.

Unfortunately, 2C-Ti-1st gen Me_2SiCl_2 catalysts exhibit leaching and therefore are not viable heterogeneous catalysts. In contrast, both 3C-Ti-1st gen Me_2SiCl_2 and 4C-Ti-1st gen Me_2SiCl_2 catalysts do not exhibit leaching and remain as active heterogeneous catalysts as will be discussed in more detail later. The notion of both 3C-Ti-1st gen and 4C-Ti-1st gen being stable under aqueous hydrogen peroxide is very promising. Few literature titanosilicates are stable under aqueous conditions.

The idea behind first generation catalysts was to create a family of single-site titanosilicate catalysts that had uniform connectivities from the active site to the matrix, i.e., 2-connections, 3-connections, and 4-connections. At the same time, all of these catalysts have the same geometry around the titanium active site, namely tetrahedral. The structural differences between the 4-connected, 3-connected, and 2-connected catalysts allows for one to visualize potential problems with the 4-connected catalysts. Unlike the 2-connected and 3-connected catalysts, the 4-connected catalysts are completely embedded inside the silicate matrix, Figure 81. It is hard to propose a low energy pathway that allows substrate to bind to the active site of a fully embedded metal site with rigid tetrahedral geometry without altering the connectivity of the matrix.

An extension of the original goal of this research is to take the idea of targeted connectivity and apply it to design a second family of single-site catalysts with new geometries about the metal center. These "second generation" catalysts are to have the same targeted connectivities as first generation, 2C-Ti, 3C-Ti, and 4C-Ti, but the geometries of the active sites will be different potentially increasing their catalytic activities. The second generation sites may be altered by adding additional ligands to the titanium precursors during synthesis and then removing the ligands after the site's connectivity has been defined and the surrounding matrix secured. This simple extension of first generation catalysts potentially leads to completely new active sites that we believe will be different from those previously synthesized. The second half of this chapter focuses on the synthesis and characterization of these new atomically dispersed single-site titanosilicate catalysts.

Second Generation Single-Site Catalysts

The tetrahedral active sites of "first generation" catalysts presented in this work, regardless of inert linker or passivation, were established by the geometry of the titanium precursors, $Ti(OiPr)_2Cl_2$, $Ti(OiPr)Cl_3$, and $TiCl_4$. If the coordination geometry of the active site precursor can be changed from tetrahedral and the surrounding matrix locked in place so that the immediate coordination sphere of the metal is preserved, a completely new catalyst could effectively be made. There are several advantages to altering the geometry of the active site:

1. Different coordination geometries should produce different reactivity, i.e., make completely new catalysts.

2. Non Td geometries should be less stable and possibly more reactive than traditional tetrahedral sites. This could lead to more active catalysts, or it could potential render them inactive.

3. Creating non-equilibrium coordination geometries in homogenous metal complexes requires much effort in designing and synthesizing special constrained ligands, e.g., ansa-Cp systems. In the solid state, this is potentially much easier if we can template, or imprint, the geometry of the site as it is being built. Additionally, after the site is imprinted and the local matrix is rigidly cross-linked and set, a change in the coordination sphere of the metal can be affected (e.g., remove a place holding ligand) to create a new geometry that is not able to relax back to the most stable 4-coordinate geometry, i.e., Td.

4. By forcing the active sites of second generation catalysts to higher coordination than first generation, the geometry and spatial disposition of the coordinating ligands should increase activity. In theory and observed with structures of four and six coordinate titanium complexes, the metal to ligand bond distances should increase with increasing coordination number.[111] Addition of ligands to a metal center increases the electron density around the metal and thus increases the M-L bond lengths.

5. Place holding ligands will also take up more room in the immediate area of the active site similarly imprinting the surrounding matrix. During synthesis, the blocking ligands act as a templating agent altering the way the matrix forms around the active site. When blocking ligands are removed, the matrix is robust and rigid and thus retains the original shape. There is now more space, larger pores, for larger substrates. Figure 83 illustrates the imprinting of the matrix by the blocking ligands. In the case of a 4-connected tetrahedral active site, there is virtually no access to the Ti center without disrupting the linkages to the matrix. However, by imprinting the active site, the surround matrix is also imprinted resulting in a more open site.

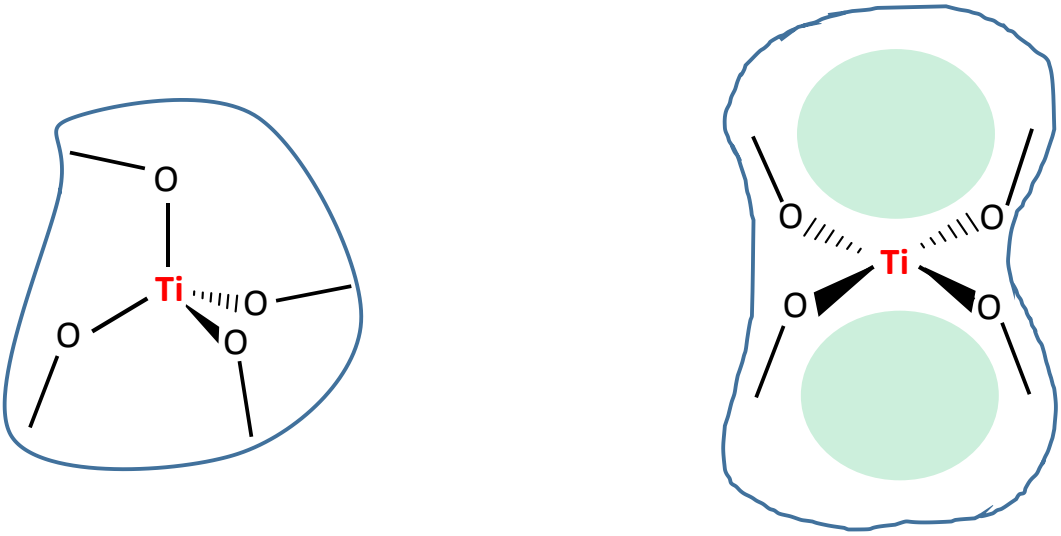

Figure 83 Illustration of the accessibility of two fully embedded 4-connected catalysts, first generation tetrahedral (left) and second generation square planar after imprinting ligand removed (right).

The work presented in the next section of this chapter will discuss the synthesis and characterization of second generation catalysts with three tailored connectivities, 2C-Ti, 3C-Ti, and 4C-Ti. Like first generation catalysts, second generation catalysts are synthesized using the building block approach and method of sequential additions. To obtain tailored connectivities characteristic of first generation catalysts, different mononuclear titanium precursors are employed. With this idea in mind, second generation catalysts are synthesized with mononuclear precursors that exhibit alternative geometries to first generation, but the same number of chloride linkers, i.e., 4 Cl, 3 Cl, or 2 Cl. An important factor in this discussion is how elastic the surrounding matrix is and how far it might be able to relax and reestablish the preferred geometry. Therefore, several variations of second generation catalysts will be discussed. Figure 84 shows a flow chart as an overview for the synthesis of these new second generation catalysts. There are three main families of catalysts, first generation, second generation, and third generation catalysts. First generation catalysts are synthesized with a tetrahedral precursor and result in tetrahedral active sites. Second generation catalysts are synthesized with six-coordinate precursors and have active site geometries other than pure tetrahedral. In contrast, third generation catalysts are synthesized with tetrahedral precursors and then the geometries are altered after the connectivity to the matrix has been established. Third generation catalysts are predicted to have similar properties of second generation catalysts. In addition, if second generation catalysts are heated during the first dose to remove the imprinting ligand, they should behave like first generation catalyst. The synthesis and characterization of the three families of catalysts will be discussed in the remainder of this chapter. It is noteworthy that third generation catalysts have not been heated to removed blocking ligands, but should be considered in future work.

Second Generation Precursors

Titanium tetrachloride is a Lewis acid which makes it ideal for forming six coordinate complexes with different oxygen and nitrogen containing bases. In the case of monodentate ligands, smaller ligands with lower donating ability generally form *cis* complexes, e.g., tetrahydrofuran (THF) and acetonitrile (MeCN). In contrast, *trans* configuration complexes result from larger ligands with stronger donating abilities, such as pyridine, Figure 85. While it is possible to form 1:1 complexes with smaller ligands, it has been found that the 1:2 complexes are more stable.[112]

Second generation single-site catalysts are prepared using modified mononuclear precursors derived from first generation catalysts. As previously mentioned, 4-connected, 3-

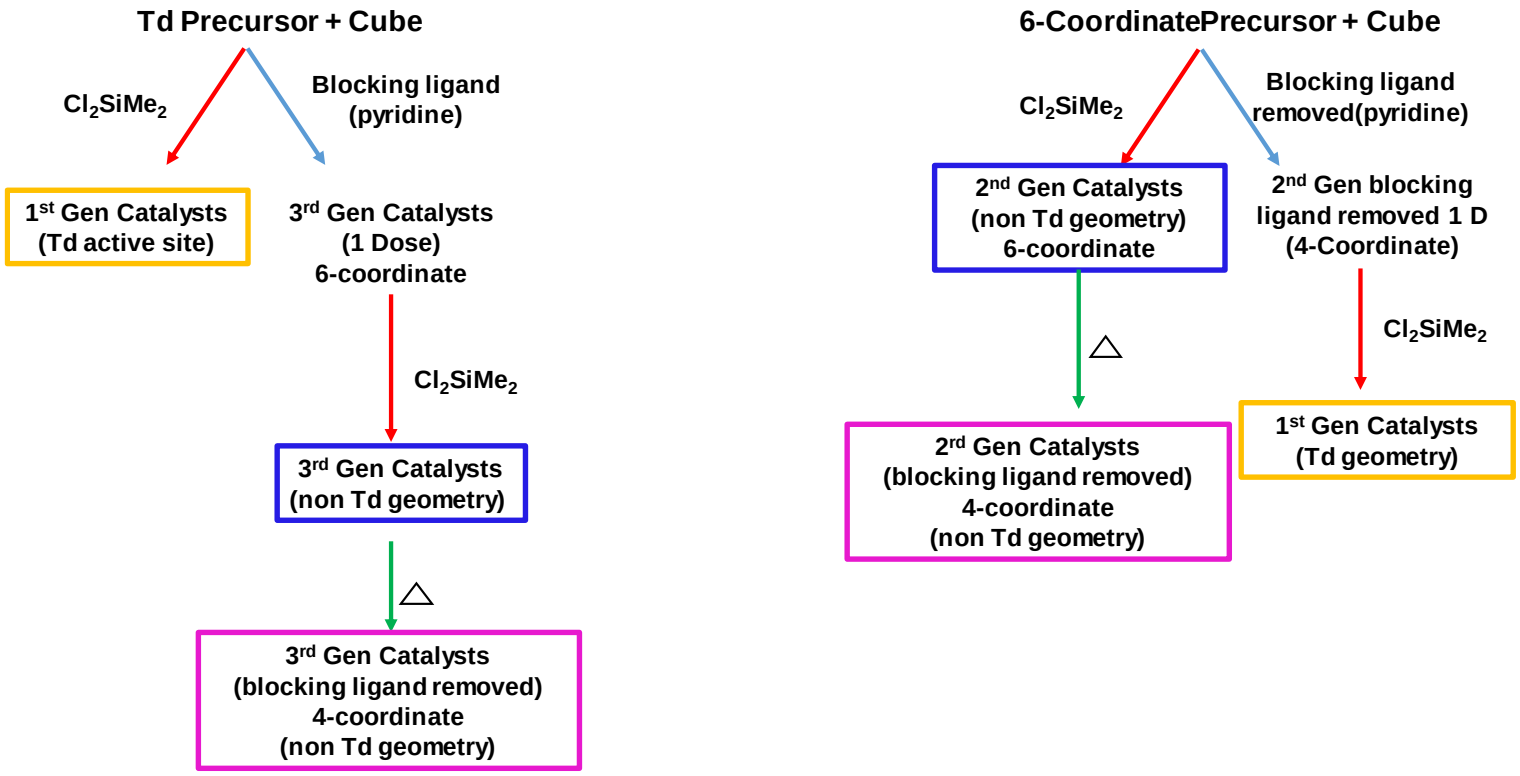

Figure 84 Flow chart illustration the modification of the Ti active site. Blue arrows indicate first dose, red arrows indicate second dose, and green arrows indicate heating. Boxes of the same color represent catalysts predicted to have the same active site but different synthetic pathways.

connected, and 2-connected first generation catalysts are synthesized using tetrahedral precursors, $TiCl_4$, $TiCl_3(OiPr)$, and $TiCl_2(OiPr)_2$ respectively. In order to tailor the geometry of the active site, the geometry about the precursors must be altered. Second generation precursors are prepared per the following Equations 39 – 43:

$$TiCl_4 + 2\ THF \rightarrow TiCl_4THF_2 \qquad \text{Equation 39}$$

$$TiCl_4 + 2\ CH_3CN \rightarrow TiCl_4(CH_3CN)_2 \qquad \text{Equation 40}$$

$$TiCl_4 + 2\ py \rightarrow TiCl_4py_2 \qquad \text{Equation 41}$$

$$TiCl_3(OiPr) + 2\ py \rightarrow TiCl_3(OiPr)py_2 \qquad \text{Equation 42}$$

$$TiCl_2(OiPr)_2 + 2\ py \rightarrow TiCl_2(OiPr)_2py_2 \qquad \text{Equation 43}$$

Synthesis of Titanium Tetrachloride Bisacetonitrile

Titanium tetrachloride ($TiCl_4$, 99%, Sigma-Aldrich) is distilled and stored under vacuum in a Schlenk vessel prior to use. Acetonitrile (MeCN, 99.9%, Fisher Scientific) is distilled over calcium hydride and stored under vacuum in a Schlenk vessel. Approximately 1 mL (9.1 mmol) of $TiCl_4$ is vapor transferred into a clean, dry, silylated Schlenk vessel followed by ~ 25 mL of dry hexane. With constant stirring, 5 equivalents of MeCN are added to the solution and allowed to stir and warm to room temperature for 30 minutes. A yellow precipitate forms and the volatiles are removed under vacuum at room temperature overnight. Visible changes such as discoloration of the solid sample begin within a week of synthesis even when stored under nitrogen atmosphere. Therefore, the precursor is used within 48 hours of synthesis.

Figure 85 Illustration of the *trans* (left) and *cis* (right) metal chloride complexes.

Characterization of $TiCl_4(MeCN)_2$

Figure 86 shows the IR spectrum of $TiCl_4MeCN_2$. Through comparison of the adduct and the pure acetonitrile, several key features are present indicating the coordination of acetonitrile to $TiCl_4$. Two absorption bands are present at ~ 2992 cm^{-1} and 2926 cm^{-1} corresponding to the C-H vibrational stretches present in acetonitrile. At a first glance there appears to be two features, one at ~ 2313 cm^{-1} and ~2284 cm^{-1} assigned to the C≡N stretching frequencies, but after careful examination, it can be seen that both absorption bands are actually split into two sets of two, 2313 cm^{-1} and 2306 cm^{-1}, and 2284 cm^{-1} and 2280 cm^{-1}, which can be explained by the Fermi resonance.[113] In addition, the two features at 1401 cm^{-1} and 1358 cm^{-1} are assigned to the asymmetric bending modes of the CH_3 group of acetonitrile.[113] While difficult to observe, the broad feature at the lower limit of the IR spectrum is indicative of Ti-Cl. Additional splitting for the other absorption features indicates the molecules has low symmetry.[112] Therefore, acetonitrile coordinated to $TiCl_4$ is best described as a *cis* complex.

Synthesis of Titanium Tetrachloride Bistetrahydrofuran

The synthesis of tetrachloridebis(tetrahydrofuran)titanium(IV), $TiCl_4(thf)_2$, follows a modified synthetic procedure outlined by Lis and coworkers.[114] Tetrahydrofuran (THF, 99%, Fisher Scientific) and dichloromethane (99%, ACS grade, Fisher Scientific) are distilled over NaK and stored under vacuum in Schlenk vessels. To a silylated Schlenk flask equipped with a magnetic stir bar, 1 mL (9.1 mmol) of $TiCl_4$ is vapor transferred followed by ~ 25 mL of dry dichloromethane. Under constant stirring, 5 equivalents of THF are vapor transferred to the solution and warmed to room temperature for 30 minutes. A bright yellow precipitate immediately forms and the volatiles are removed under vacuum at room temperature overnight. The remaining solid is then washed three times with dry pentane (~50 mL) and dried at room temperature for four hours. The solid is stored in a silylated vial in a nitrogen atmosphere glovebox.

Characterization of $TiCl_4THF_2$

The IR spectrum for $TiCl_4(thf)_2$, Figure 87 shows a sharp peak at 990 cm^{-1} and a strong broad feature around 830 cm^{-1} which are two characteristic features in the fingerprint region of the IR spectrum for THF coordinated to titanium.[115] Additionally, a large set of bands seen from 2850 cm^{-1} – 3000 cm^{-1} correspond to the aliphatic C-H groups of THF.

Figure 88 illustrates the XANES regions of XAS which can be used to determine the coordination number of titanium along with the two possible structures of $TiCl_4(THF)_2$. The pre-

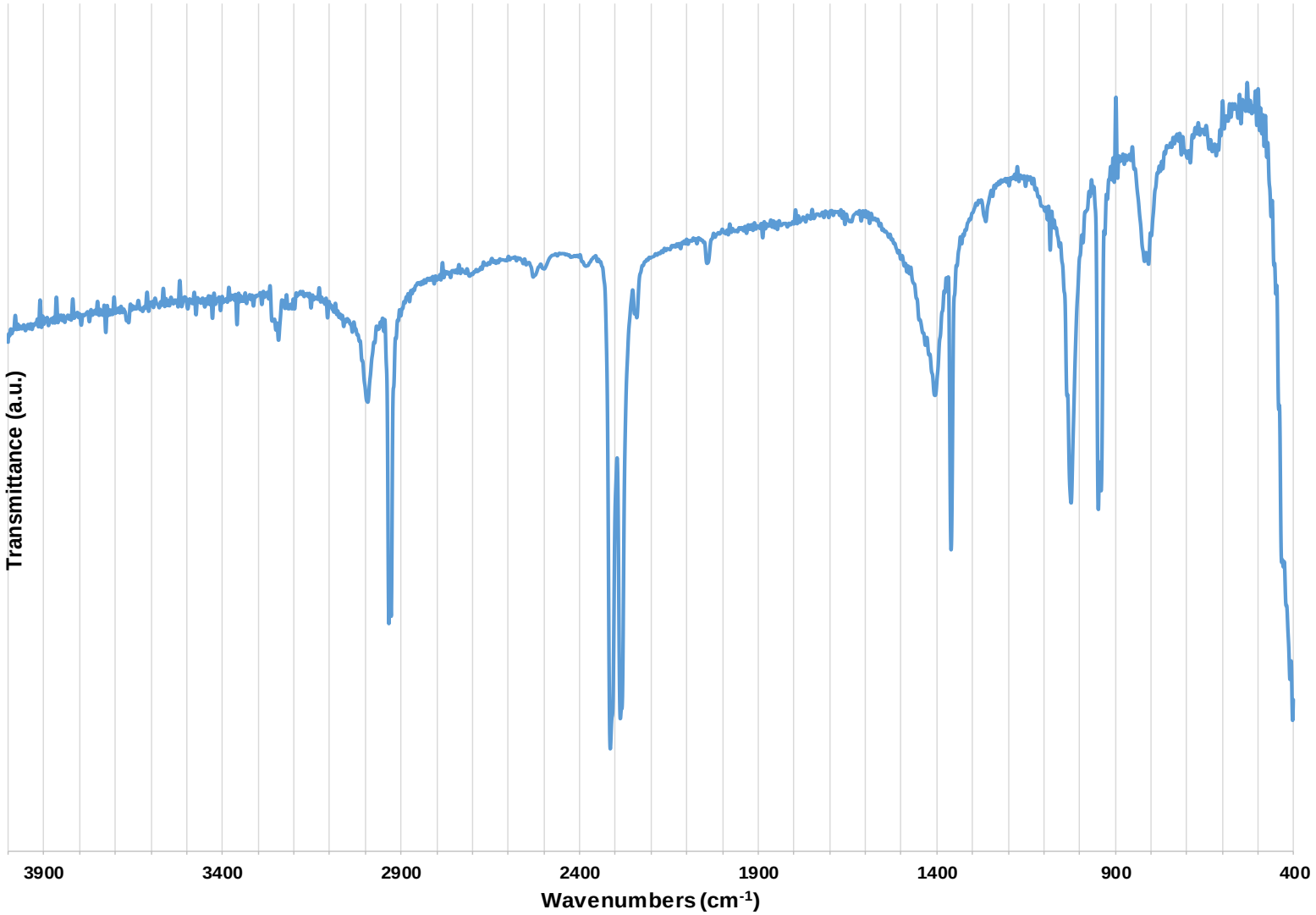

Figure 86 FTIR Spectrum of cis $TiCl_4(MeCN)_2$.

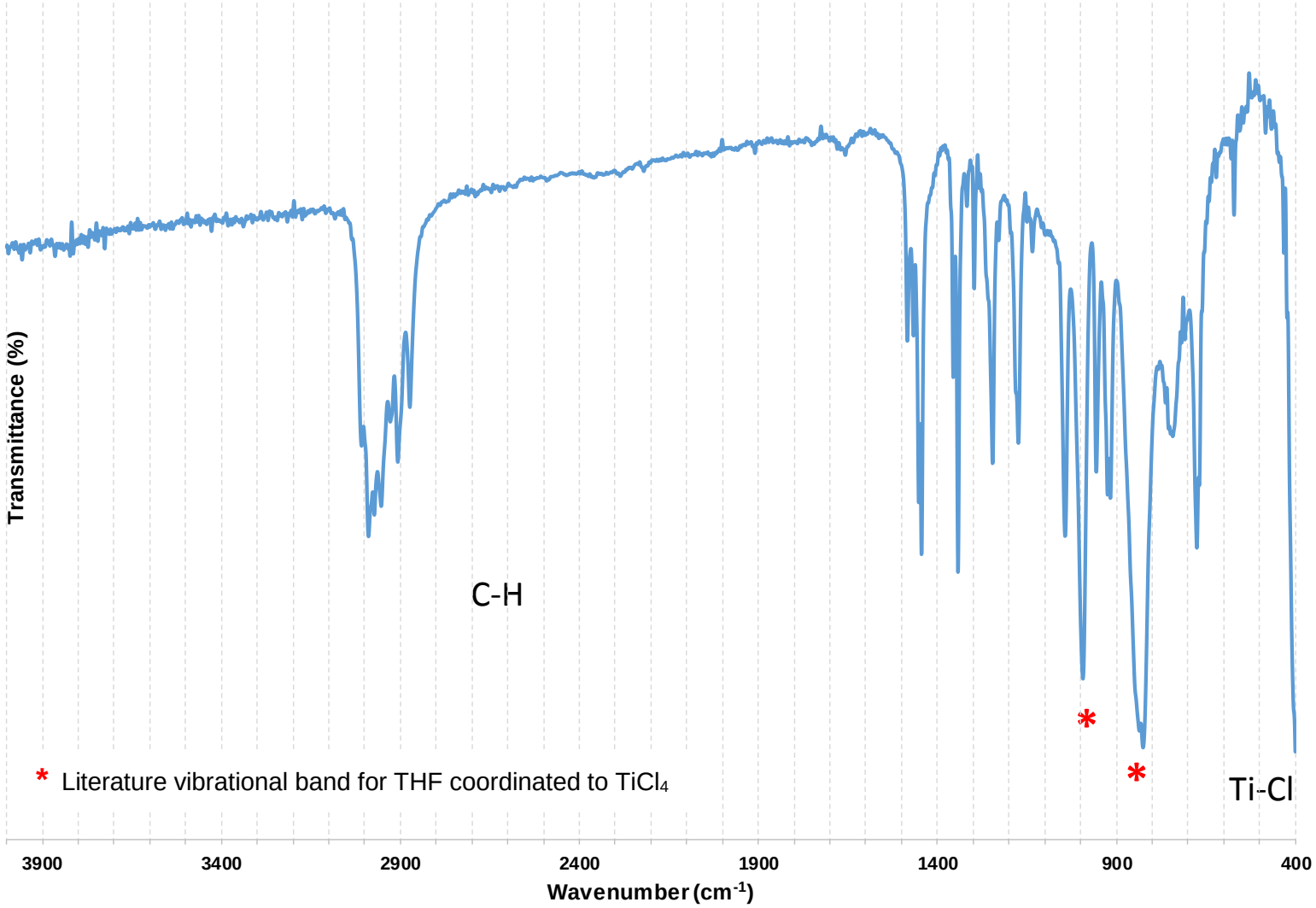

Figure 87 FTIR spectrum of $TiCl_4(THF)_2$.

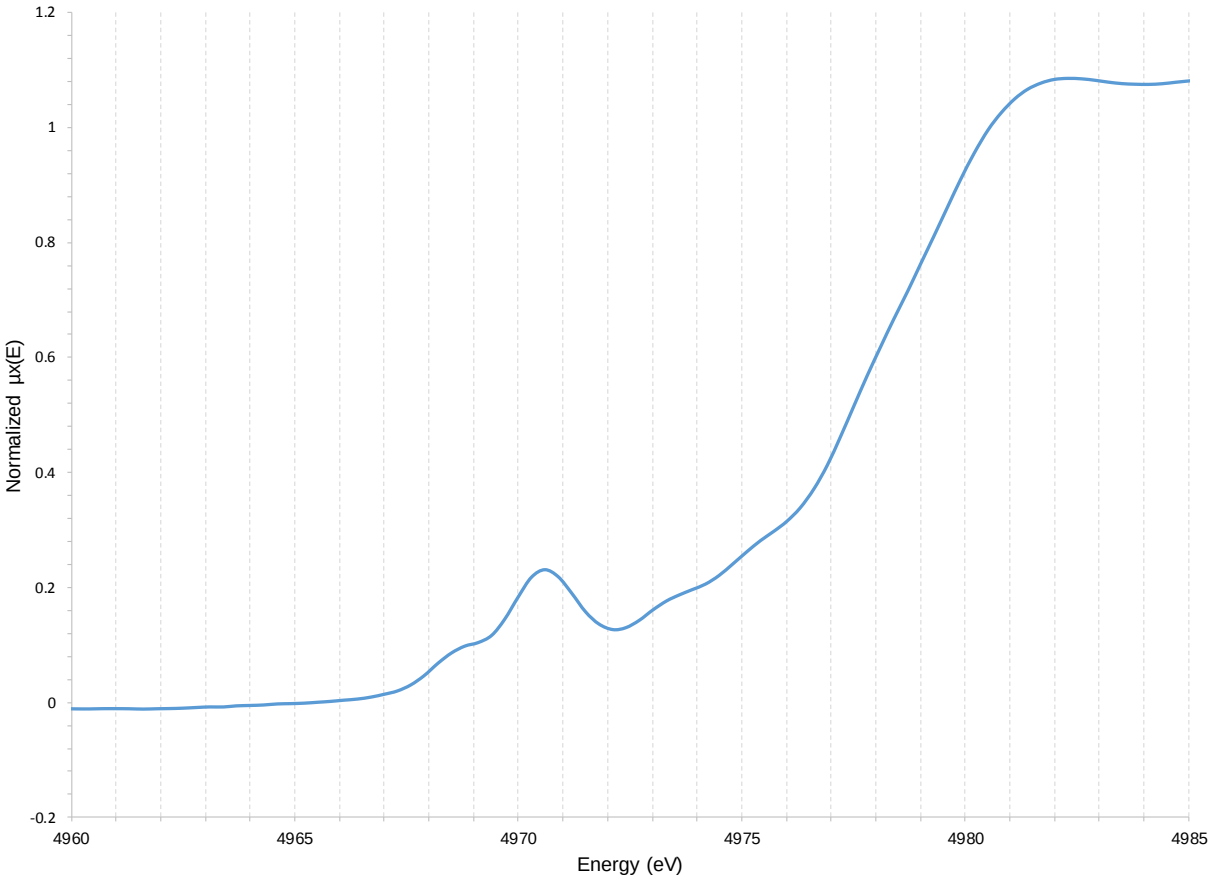

Figure 88 XANES spectrum for $TiCl_4(THF)_2$.

edge features shows a low intensity, 23% of the normalized edge height, along with a three band pattern centered around 4970.6 eV. The decrease in intensity along with a peak shift to higher energy in comparison to tetrahedral Ti centers at 4967 eV is consistent with a six coordinate titanium complex.[116]

The XANES and IR spectra for the adduct of titanium tetrachloride and tetrahydrofuran suggest the adduct is a six coordinate complex. To further understand the symmetry about the titanium active site and the coordination number of neighboring atoms, EXAFS data is modeled. FEFF multiple scattering theory is used to derive theoretical phase and amplitude functions for single and multiple scattering paths used to model the EXAFS data. Figure 89 displays the $\chi(k)$, $q(k)$, and R space plots overlaid with the fits for *trans* $TiCl_4(THF)_2$. The model gives reasonable fits to the data and the structural parameters are summarized in Table 22. To be considered a good fit the R factor should be less than 0.05.[117] Based on the analyses of FTIR, XANES, and EXAFS spectra, the $TiCl_4(THF)_2$ complex is best described as a six coordinate *trans* complex. EXAFS modeling of the *cis* adduct did not result in accurate fits.

Synthesis of Titanium Tetrachloride Bispyridine

Pyridine (py, 99%, Sigma-Aldrich) is distilled and stored under vacuum over calcium hydride in a sealed glass Schlenk vessel prior to use. Glassware is silylated with trimethylsilyl chloride and kept in an oven at 80^0 C. First, $TiCl_4$ is vapor transferred into a Schlenk vessel cooled in a dry ice/isopropanol bath. Approximately 0.1 – 0.2 mole equivalents of pyridine are then transferred to the same reaction vessel. The vessel is then allowed to warm to room temperature and the mixture is stirred for approximately 30 minutes. A bright canary yellow precipitate forms immediately. This first addition of pyridine reacts with any HCl present from the reaction of $TiCl_4$ and trace residual water.[118] The unreacted $TiCl_4$ is then vapor transferred into a new Schlenk vessel followed by ~25 mL of dry hexane. Approximately 2.5 – 3 molar equivalents of pyridine are then vapor transferred to the reaction flask with constant stirring. Finally, the reaction is allowed to warm to room temperature, and a yellowish green precipitate immediately forms (very exothermic reaction). The excess pyridine and hexane are removed under vacuum at room temperature for 4 hours. The final product is stored in a nitrogen atmosphere glovebox. The idea for this synthesis and purification of $TiCl_4py_2$ was developed based on the work of Hulme et. al. with silicon tetrachloride bispyridine.[118].

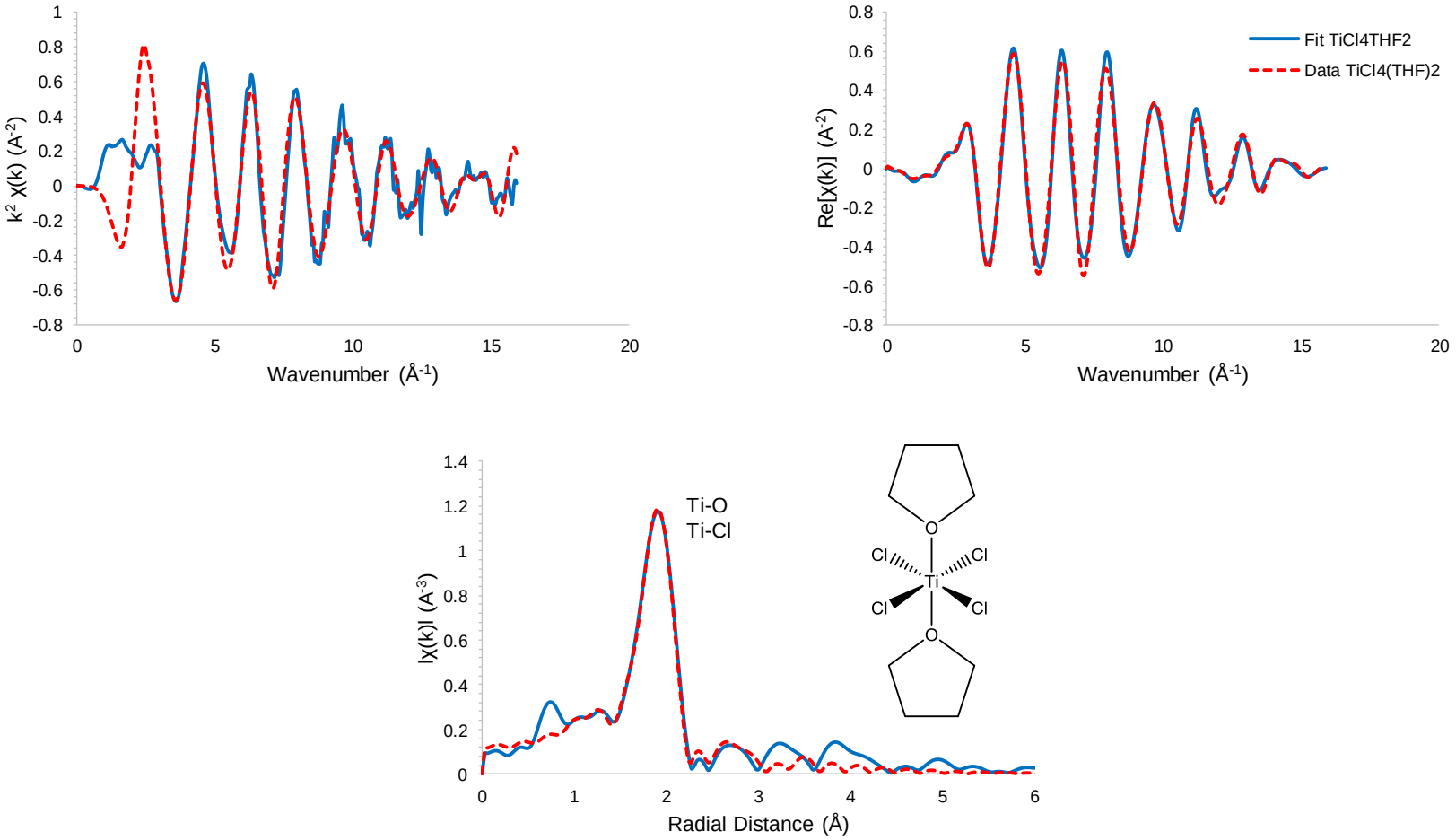

Figure 89 EXAFS spectra (blue) overlaid with fits obtained from FEFF modeling (red) for k space (top left), q space (top right), and R space (bottom center) for trans $TiCl_4(THF)_2$.

Table 22 List of structural parameters obtained from FEFF calculations for *trans* $TiCl_4(THF)_2$.

	Ti – O	Ti – Cl	Ti – C	Ti – O – C
Coordination number (set)	**2**	**4**	**4**	**8**
R (Å)	**1.80 ± 0.02**	**2.27 ± 0.007**	**3.02 ± 0.02**	**3.76 ± 0.08**
σ2	**0.44**			
S_0^2	**0.01**	**0.003**	**0.004**	**0.01**
E_0 (eV)	**-1.32 ± 1.1**			
Reduced χ^2	**177.7**			
R factor	**0.020**			

Characterization of $TiCl_4py_2$

The IR spectrum after the first addition of pyridine shows the presence of both Lewis (~1606, 1489, and 1444 cm^{-1}) and weak Brønsted (~1633, 1532, and 1489 cm^{-1}) pyridine, seen in Figure 90. However, the IR spectrum of the $TiCl_4py_2$ precursor after the second dose of pyridine (the purified $TiCl_4$) shows only peaks corresponding to Lewis bound pyridine, Figure 91. ICP analysis of the $TiCl_4py_2$ precursor confirms the Ti weight percent is consistent with the calculated Ti weight percent based on the molecular formula, 13.76%. The $TiCl_4py_2$ precursor has proven to be stable under nitrogen atmosphere, but readily reacts with moisture due to the reactivity of Ti-Cl groups. When exposed to moisture, the IR spectrum shows absorption peaks consistent with both Lewis and Brønsted pyridine, Figure 92.

While it was not possible to obtain a crystal structure, the literature reports that the titanium tetrachloride bispyridine species has *trans* coordination, but the other titanium halogen complexes, TiF_4py_2 and $TiBr_4py_2$, have *cis* conformations. Based on IR and Ramen data, when pyridine is coordinated in the cis geometry, several bands are split indicative of a lower symmetry (C_{2v}) structure.[112,119,120] In the case of $TiCl_4py_2$, the absorption bands are not split, Figure 93, indicating a symmetrical (D_{4h}) *trans* complex. Additionally, the shift in the Ti-Cl frequency from 482 cm^{-1} observed in pure $TiCl_4$ to 434 cm^{-1} in the bispyridine adduct suggests the coordination geometry of titanium has increased, thus weakening the Ti-Cl linkages.

XAS Analysis of $TiCl_4py_2$

Along with IR data, data obtained from XAS has been used to characterize the $TiCl_4py_2$ precursor. The symmetry of the local environment around the absorber atom effects the intensity, the position, and the shape of the pre-edge feature in the XANES regions of XAS. Similar to the THF adduct, the XANES region for $TiCl_4py_2$ shows a low intensity three band pre-edge feature indicative of a six-coordinate complex, Figure 94.

Athena is used to process the raw EXAFS data where the phase corrected R plot for the bispyridine adduct shows a large broad feature at 2.18 Å which is a result of two unresolved features, one for Ti-Cl and the other for Ti-N. In order to obtain a clearer understanding of the two individual bond lengths, Artemis is used to develop a structural model for the complex. Figure 95 show the overlays of the experimental data and the FEFF model for the *trans* bispyridine adduct in k-space (top left), q-space (top right) and R-space (bottom). According to the literature, the Ti-N bond is slightly longer than the Ti-Cl bond and as seen in Table 23 the modelled data correlates with this trend, 2.28 Å Ti-Cl and 2.34 Å Ti-N.[112] Based on gravimetric analysis, ICP,

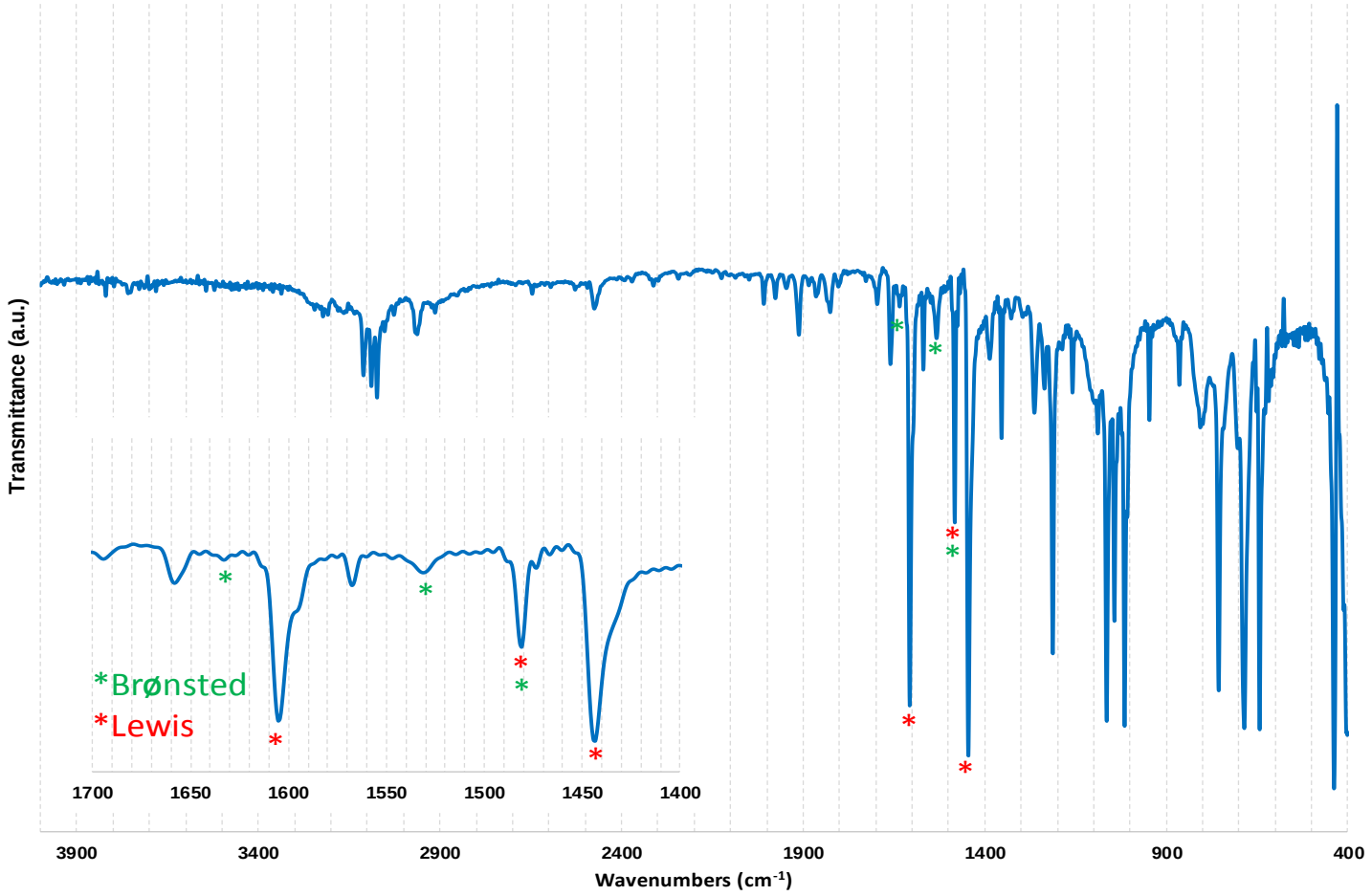

Figure 90 FTIR spectrum of $TiCl_4py_2$ after the first addition of pyridine (purification step). The inlay is a blow up of the pyridine finger print region illustration both Brønsted and Lewis pyridine are in the material.

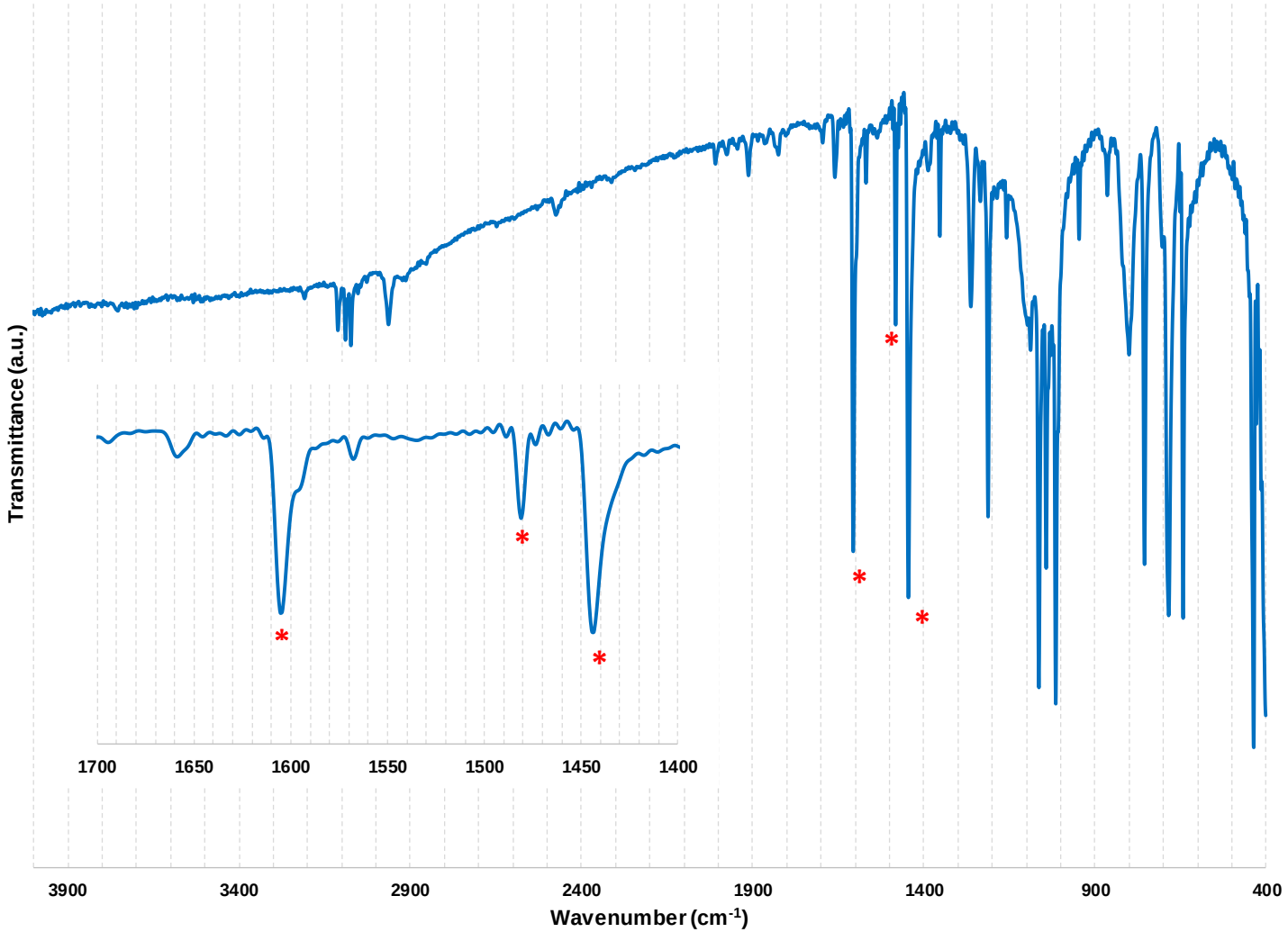

Figure 91 FTIR spectrum of purified $TiCl_4py_2$ showing only Lewis pyridine.

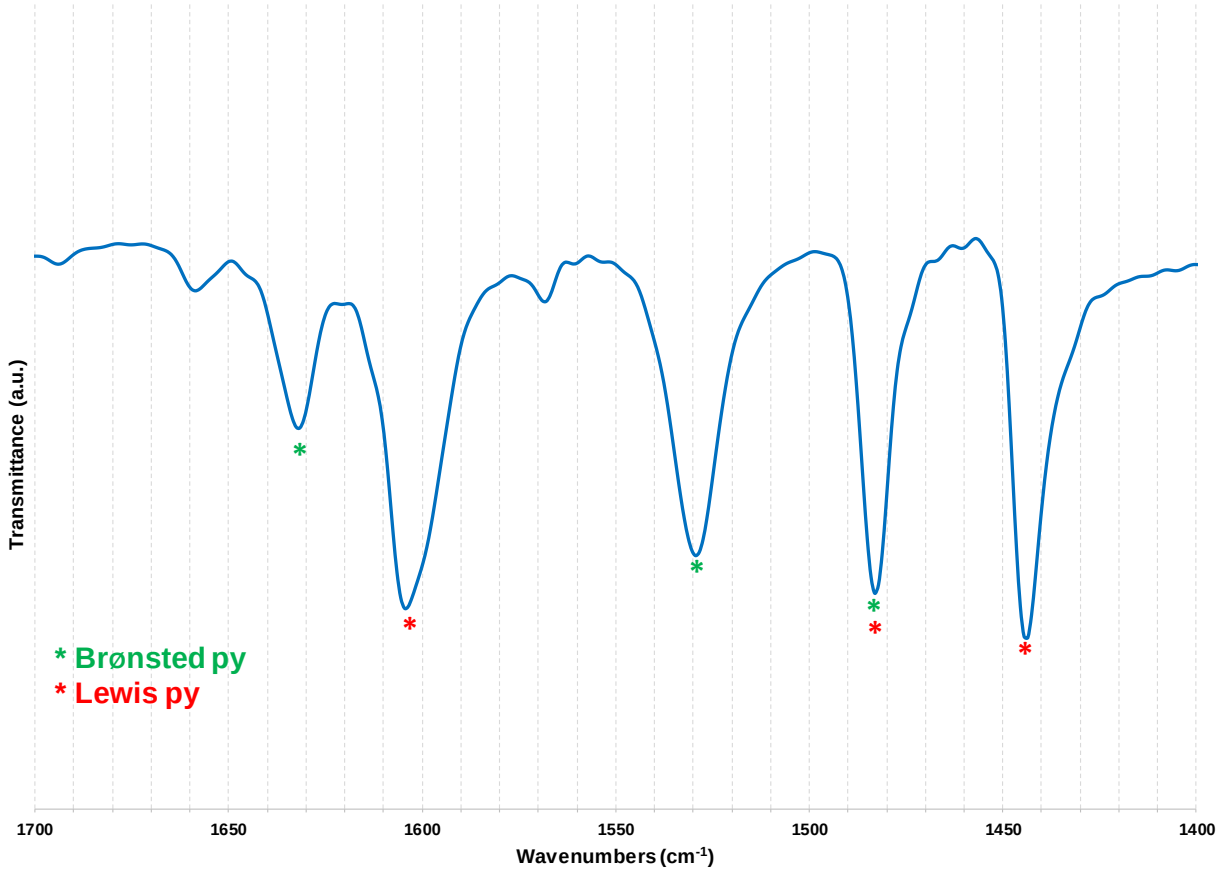

Figure 92 FTIR spectrum showing the pyridine fingerprint region of $TiCl_4py_2$ after being stored for six months.

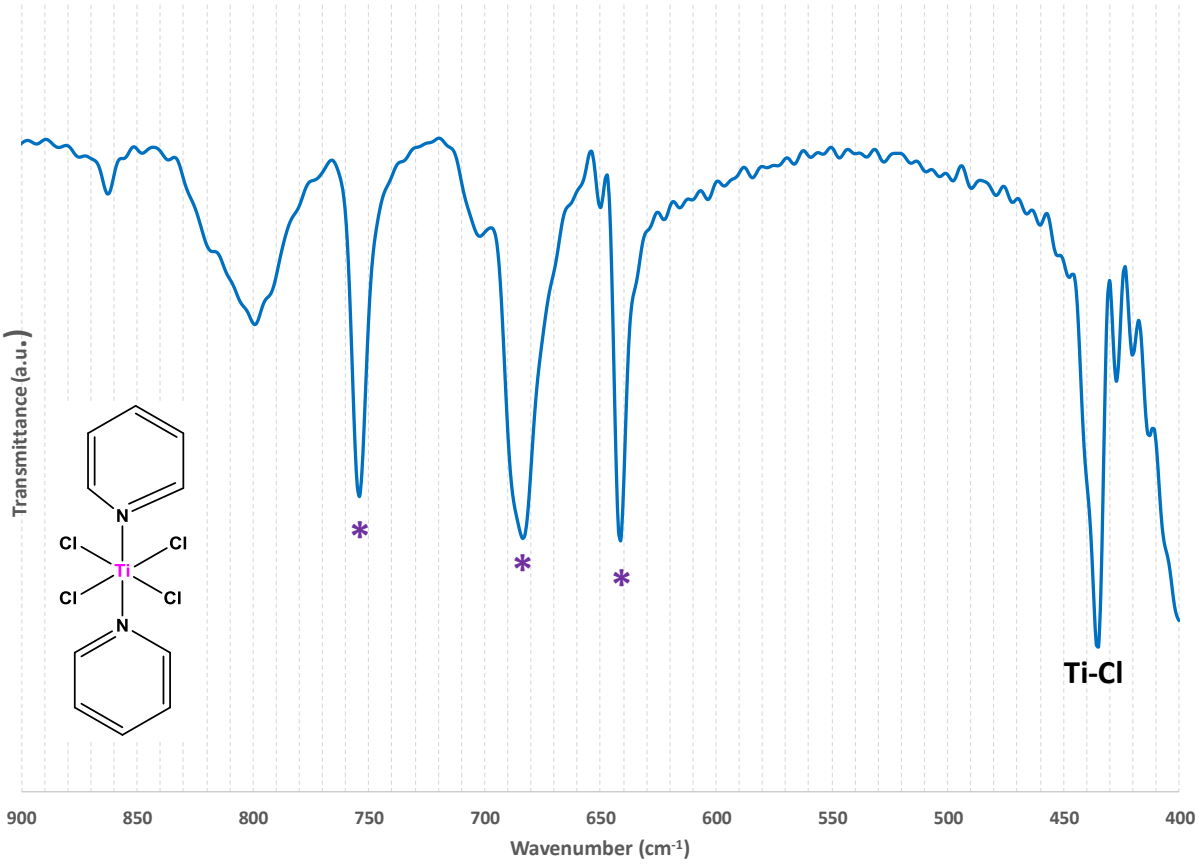

Figure 93 FTIR spectrum of $TiCl_4py_2$ illustration the absorption bands are not split indicating this complex has D_{4h} symmetry.

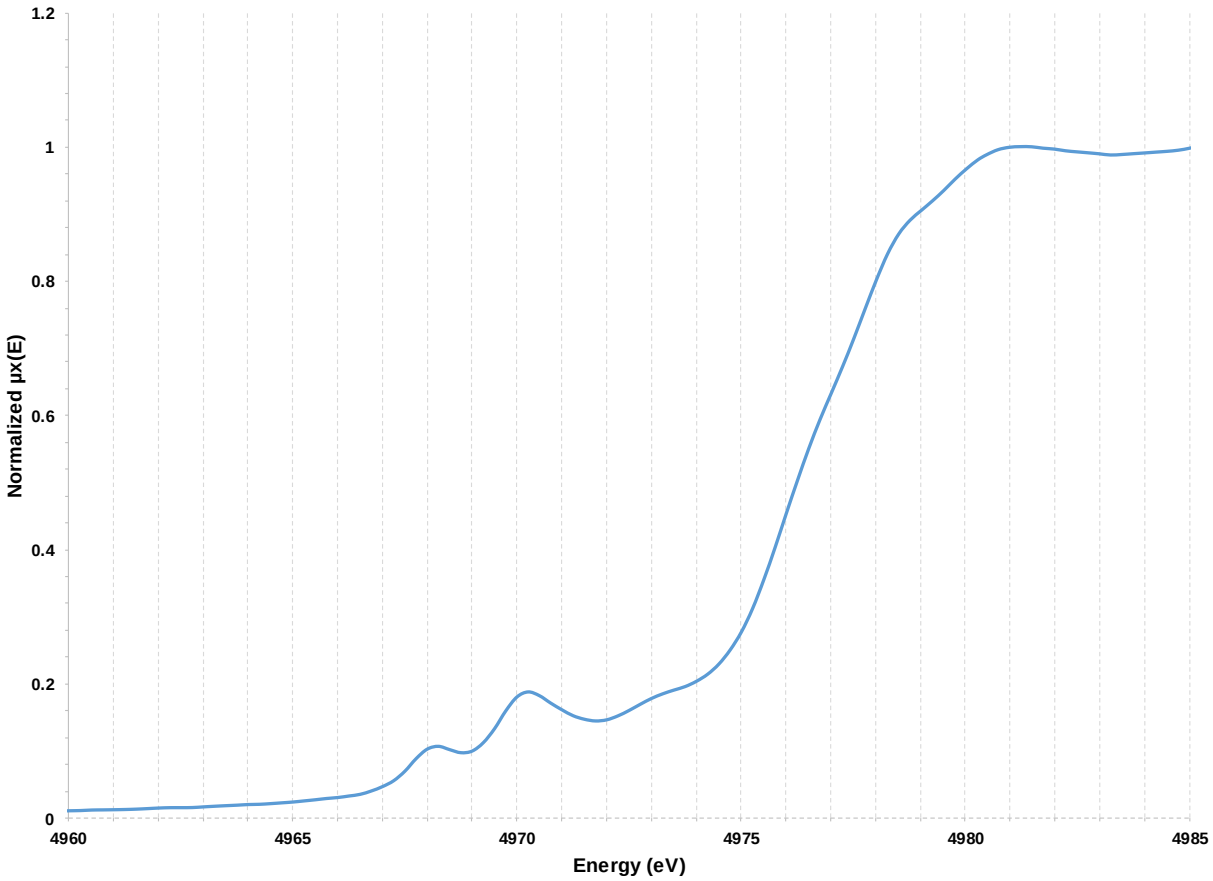

Figure 94 XANES spectrum of trans $TiCl_4py_2$.

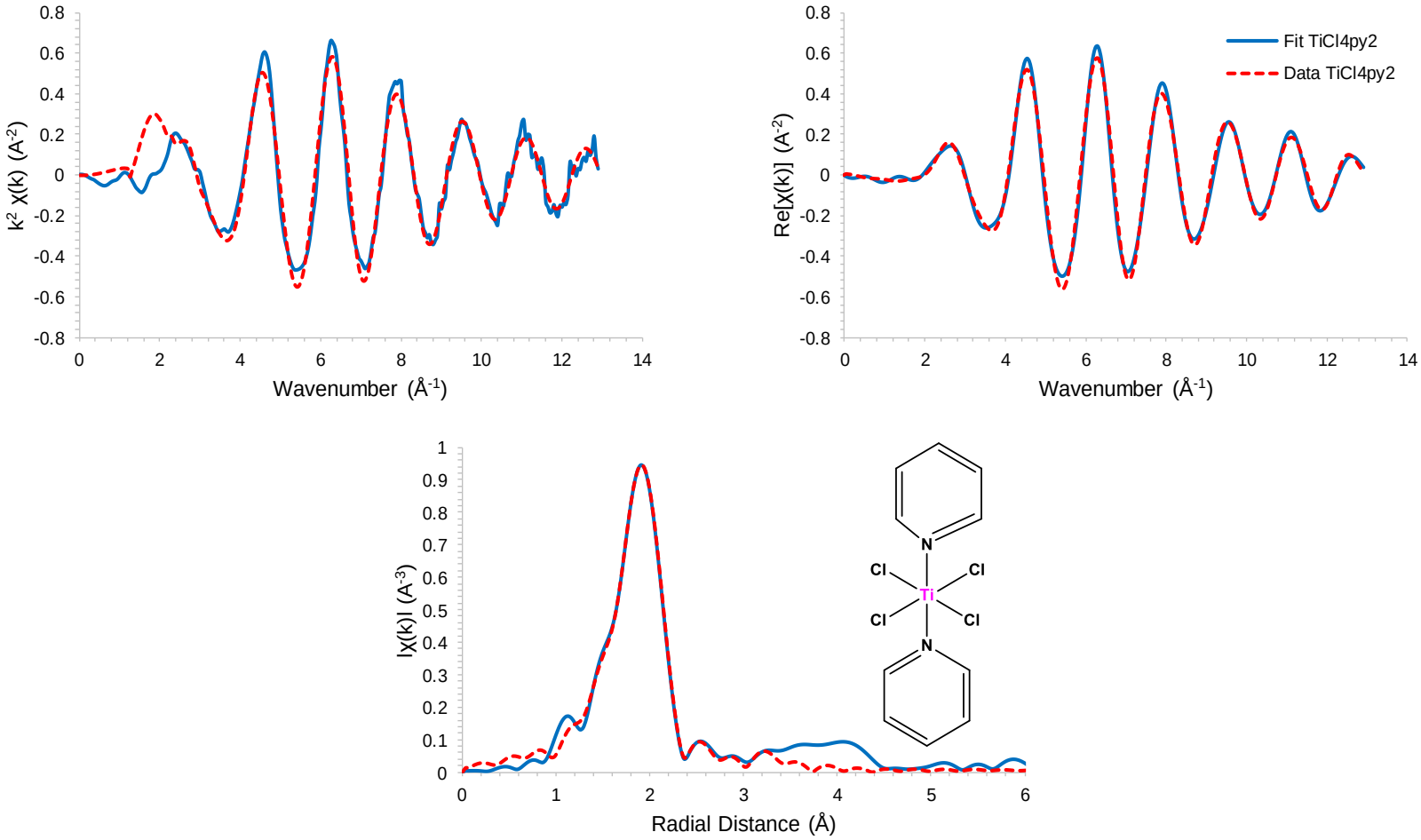

Figure 95 EXAFS spectra (blue) overlaid with fits obtained from FEFF modeling (red) for k space (top left), q space (top right), and R space (bottom center) for trans $TiCl_4py_2$.

Table 23 List of structural fit parameters obtained from FEFF calculations for *trans* for $TiCl_4py_2$.

	Ti – N	Ti – Cl	Ti – C	Ti – N – C	Ti-C_2
Coordination number (set)	**2**	**4**	**4**	**8**	**4**
R (Å)	**2.22 ± 0.09**	**2.32 ± 0.03**	**2.53 ± 0.07**	**2.89 ± 0.06**	**3.99 ± 0.06**
σ2			**0.44**		
S_0^2	**0.005**	**0.005**	**0.013**	**0.006**	**0.014**
E_0 (eV)			**5.23 ± 1.6**		
Reduced χ^2			**229**		
R factor			**0.014**		

IR, XANES, and EXAFS data analyses, the structure of $TiCl_4py_2$ is consistent with a *trans* six coordinate titanium species. It is noteworthy that structural modeling of the *cis* complex has been investigated, but the model is inconsistent with the experimental data.

Synthesis Alkoxy Chlorinated Titanium Bispyridine Precursors

The previously mentioned precursors can potentially be used to imprint four connected titanium centers and are expected to have the most significant influence on the active site geometry. However, the geometry of the 2C-Ti and 3C-Ti centers have the possibility to be altered as well. Assuming the trichloroisopropoxy and dichlorodiisoproxy titanium precursors exhibit the same overall structures with pyridine as $TiCl_4$, the bispyridine adducts can be synthesized according to Equation 44 and 45.

$$TiCl_3(OiPr) + 2\ py \rightarrow TiCl_3(OiPr)py_2 \qquad \text{Equation 44}$$

$$TiCl_2(OiPr)_2 + 2\ py \rightarrow TiCl_2(OiPr)_2py_2 \qquad \text{Equation 45}$$

Isoproxy titanium trichloride ($TiCl_3(OiPr)$) and di-isopropoxy titanium dichloride ($TiCl_2(OiPr)_2$) are synthesized according to the literature procedure by Kamigaito and outlined in Chapter3.

The $TiCl_3(OiPr)$ or $TiCl_2(OiPr)_2$ precursor is added to a silylated Schlenk vessel which is then cooled to dry ice/isopropanol temperature with constant stirring. Excess pyridine is then vapor transferred to the reaction vessel. The reaction is brought to 55°C and allowed to reflux for 30 minutes. The excess pyridine is removed under vacuum overnight at room temperature. Because the chloroalkoxy titanium species have shown to be unstable, the bispyridine adducts are used within 48 hours of synthesis to avoid self-decomposition.

Characterization of $Ti(OiPr)Cl_3py_2$ and $Ti(OiPr)_2Cl_2py_2$

The volatiles from drying the precursors are carefully analyzed. The NMR spectra of the volatiles shows only the loss of pyridine, no evidence for the loss of isoproxide ligands is observed. ICP analyses indicate the Ti weight percent of both $TiCl_3(OiPr)py_2$ and $TiCl_2(OiPr)_2py_2$ are consistent with the calculated Ti weight percent based on the molecular formulas, 12.88% and 12.11% respectively.

Figure 96 compares the IR spectra of $Ti(OiPr)_2Cl_2$ (blue) and $Ti(OiPr)_2Cl_2py_2$ (green) and Figure 97 compares the IR spectra of $Ti(OiPr)Cl_3$ (Red) and $Ti(OiPr)Cl_3py_2$ (blue). Each spectra contains an inlay of the pyridine finger print region. By comparing the two spectra, the only new features correspond to pyridine. The IR spectra of both $TiCl_3(OiPr)py_2$ and $TiCl_2(OiPr)_2py_2$ show absorption peaks corresponding to only Lewis bound pyridine, ~ 1606, 1489, and 1444 cm^{-1}. In addition, a new set of absorption bands appears above 3000 cm^{-1} and correspond to the aromatic stretches of the pyridine ring. No further purification steps are necessary. Since $TiCl_4py_2$ has *trans* py coordination, it was assumed that both the tricholo and dichloro species also exhibited *trans* py coordination.

Synthesis of Second Generation Single-Site Titanosilicate Catalysts

Second generation single-site titanosilicate catalysts are synthesized using the building block approach and method of sequential additions outlined in Chapters 2, 3, and the beginning of this Chapter2. However, two minor but critical adjustments have been employed. First, the solvent is not removed between the first and second dose. Second, catalysts are initially dried at room temperature after the second cross-linking reaction. Both modifications are employed to prevent premature loss of the blocking ligands. Each step of synthesis is carefully investigated and the observations that ultimately led to these modifications are described in following sections.

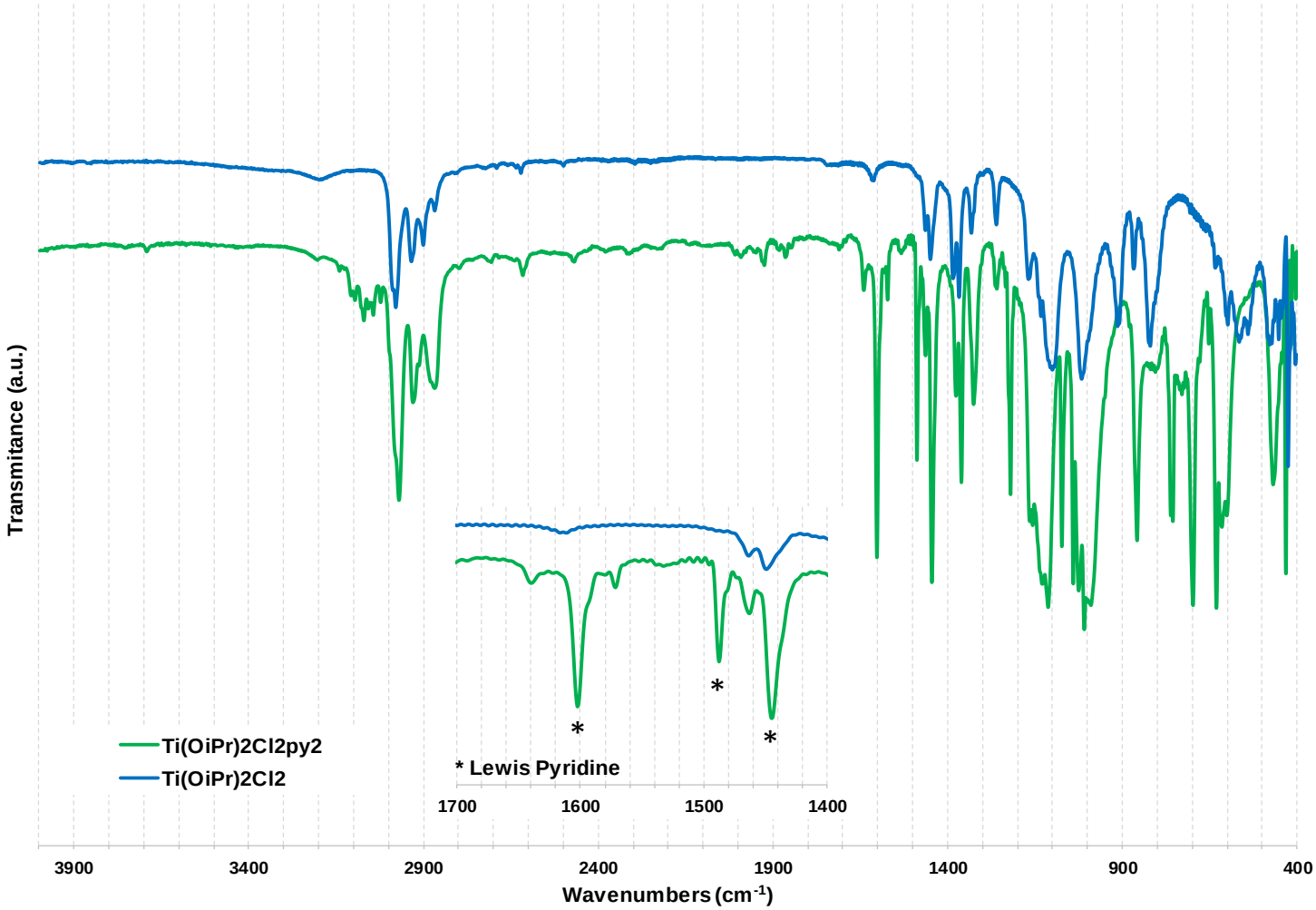

Figure 96 FTIR comparison of the 2C-1st generation precursor ($Ti(OiPr)_2Cl_2$, blue) and the 2C-2nd generation precursor ($Ti(OiPr)_2Cl_2py_2$, green) with an inset of the pyridine fingerprint region.

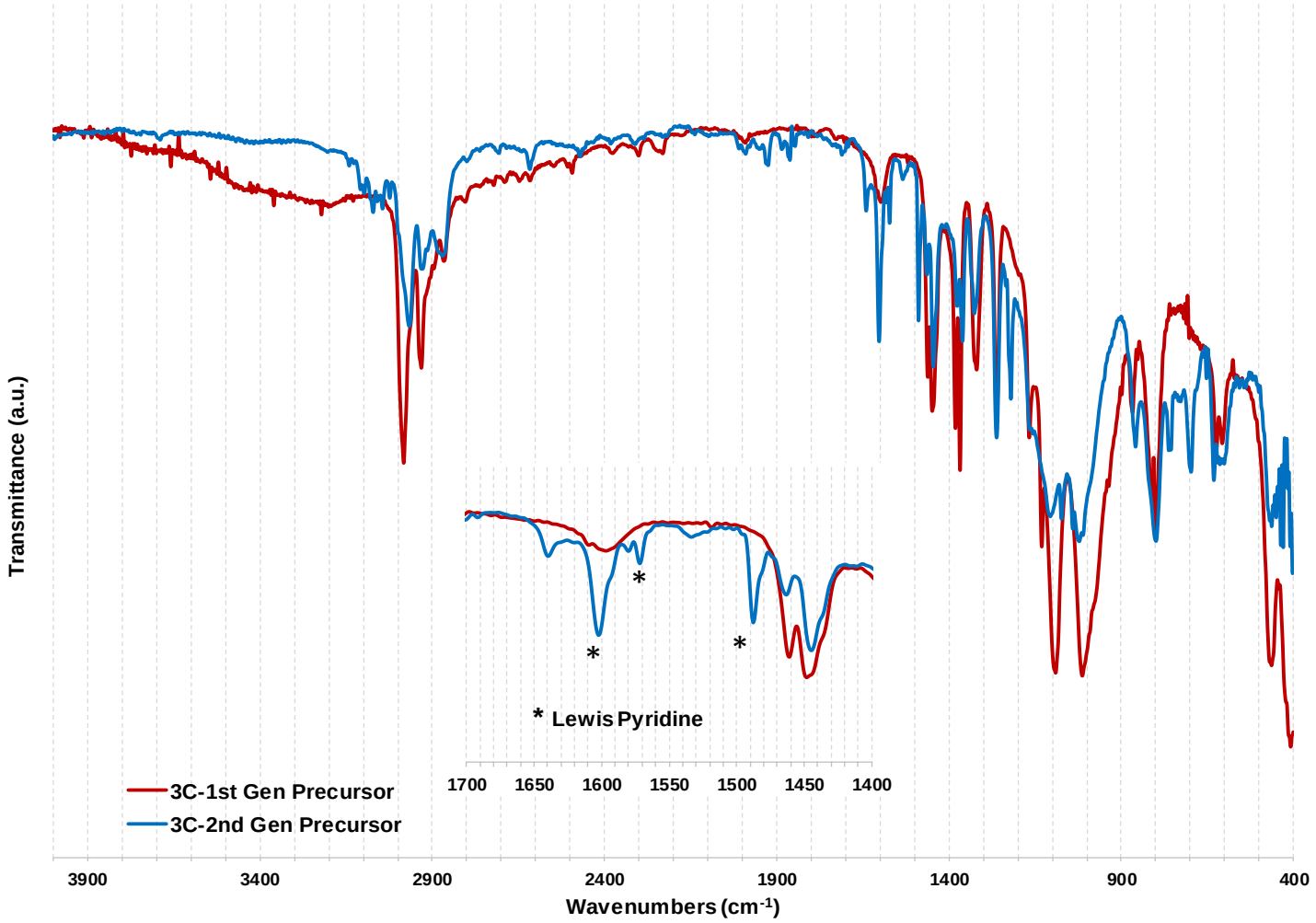

Figure 97 FTIR comparison of the 3C-1st generation precursor ($Ti(OiPr)Cl_3$, blue) and the 3C-2nd generation precursor ($Ti(OiPr)Cl_3py_2$, green) with an inset of the pyridine fingerprint region.

Blocking Ligands and the First Dose

During the synthesis of first generation catalysts, the solvent and trimethyltin chloride byproduct are removed after the first cross-linking reaction by heating at 80°C under vacuum to calculate the connectivity of titanium to the matrix. However, with second generation catalysts, there is a possibility that the neutral Lewis base ligands on the titanium site will be lost during this heating step. Therefore, to ensure these blocking ligands remain on the active site throughout synthesis, the volatiles are not removed after the first dose.

It is important to note however that connectivity has been verified for the second generation catalysts. Each connectivity was initially confirmed by drying after the first dose at 80^0 C to remove the volatile trimethyltin chloride byproduct. $TiCl_4py_2$, $TiCl_4THF_2$, and $TiCl_4MeCN_2$ produce four equivalents of trimethyltin chloride ($SnMe_3Cl$); $TiCl_3(OiPr)py_2$ produces three equivalents of $SnMe_3Cl$; and $TiCl_2(OiPr)_2py_2$ produces two equivalents of $SnMe_3Cl$ when reacted in a limiting amount with the tin cube building block. Unlike first generation catalysts, the calculation of connectivity is more complex for the second generation catalysts. As suspected, after the first cross-linking reaction, loss of imprinting ligands is seen in the NMR spectra of the volatiles. In order to calculate the connectivity of the Ti to tin-cube, NMR ratios combined with gravimetric analysis are factored together

From the data presented in Table 24 it can be seen that the majority of blocking ligand is lost during drying at 80°C under vacuum for four hours for all the complexes studied. This loss of blocking groups raises several questions. The first question is how much blocking ligand is lost after the first dose while drying at room temperature under vacuum. It can be concluded, that the loss of blocking ligands, in this case pyridine, correlates to the connectivity of the active site and ultimately the number of isoproxide ligands. In the case of the 2C-Ti-2^{nd} gen py_2 sites, approximately 75 % of the initial amount of blocking ligand is lost at room temperature. In the process of losing pyridine, the two isopropoxy ligands should be able to move while remaining coordinated to titanium. Ultimately, when both pyridine ligands are lost, the di-isopropoxide ligands can rearrange their positions to achieve an overall pseudo tetrahedral geometry around titanium.

In contrast to 2C-Ti-2^{nd} gen py_2, it is expected to be more difficult to lose pyridine from the 3C-2^{nd} gen py_2 sites. In the 3C-Ti-2^{nd} gen py_2 sites, three of the coordinating ligands are siloxy ligands which are more or less fixed to their right angle relationships by the rigidity of the Si_8O_{20} building blocks. While the single isopropoxide ligand is still free to move about the titanium center

Table 24 Summary of the amount of blocking ligand lost after the first cross-linking reaction at both room temperature and 80 ^{0} C.

Precursor	Connectivity (± 0.1)	% Blocking Ligand Lost (1st dose Room Temp) (± 4 %)	% Blocking Ligand Lost (1st dose 80 ^{0}C) (± 4 %)
$TiCl_4(THF)_2$	3.9	-	100
$TiCl_4(MeCN)_2$	3.8	-	100
$TiCl_4py_2$	4.0	39	71
$Ti(OiPr)Cl_3py_2$	3.0	52	71
$Ti(OiPr)_2Cl_2py_2$	1.9	76	95

as pyridine is lost, the three siloxy ligands remain relatively fixed. Thus, one would predict the resulting 4-coordinate Ti center, along with the energy barrier involved in pyridine loss, will be higher than the 2C-Ti-2nd gen py_2, consistent with what is observed.

Unlike both 2C-Ti-2nd gen py_2 and 3C-Ti-2nd gen py_2, the 4C-Ti-2nd gen py_2 does not have any free alkoxy ligands that can move around the titanium active site as the pyridine blocking ligands are lost. Instead, the four coordinating ligands other than the pyridine on the titanium active site are siloxy ligands which are fixed to their right angle relationships by the robust Si_8O_{20} building block matrix similar to 3C-2nd gen py_2. The lack of free ligands around titanium should result in an increase in the energy barrier involved with the loss of blocking ligands which is consistent with the results in Table 24. The differences in the amount of blocking ligand lost after the first dose at room temperature is additional indirect evidence that the unique precursors result in different targeted connectivities, 2C-Ti, 3C-Ti, and 4C-Ti.

FTIR and XAS Investigation into the First Dose

Second generation 4C-Ti centers have the potential to be influenced the most by altering their geometry in relation to first generation. Therefore, they have been studied in more detail and are presented as models for the second generation catalysts. In addition to NMR evidence, the loss of pyridine blocking ligands is followed by both FTIR and XAS studies. Figure 98 shows the pyridine fingerprint region in the IR spectrum of 4C-2nd gen py_2 after heating at 80^{o}C overnight following the first dose. The lack of absorption features in this region confirms the pyridine blocking ligands can be removed from the titanium active site after the first dose.

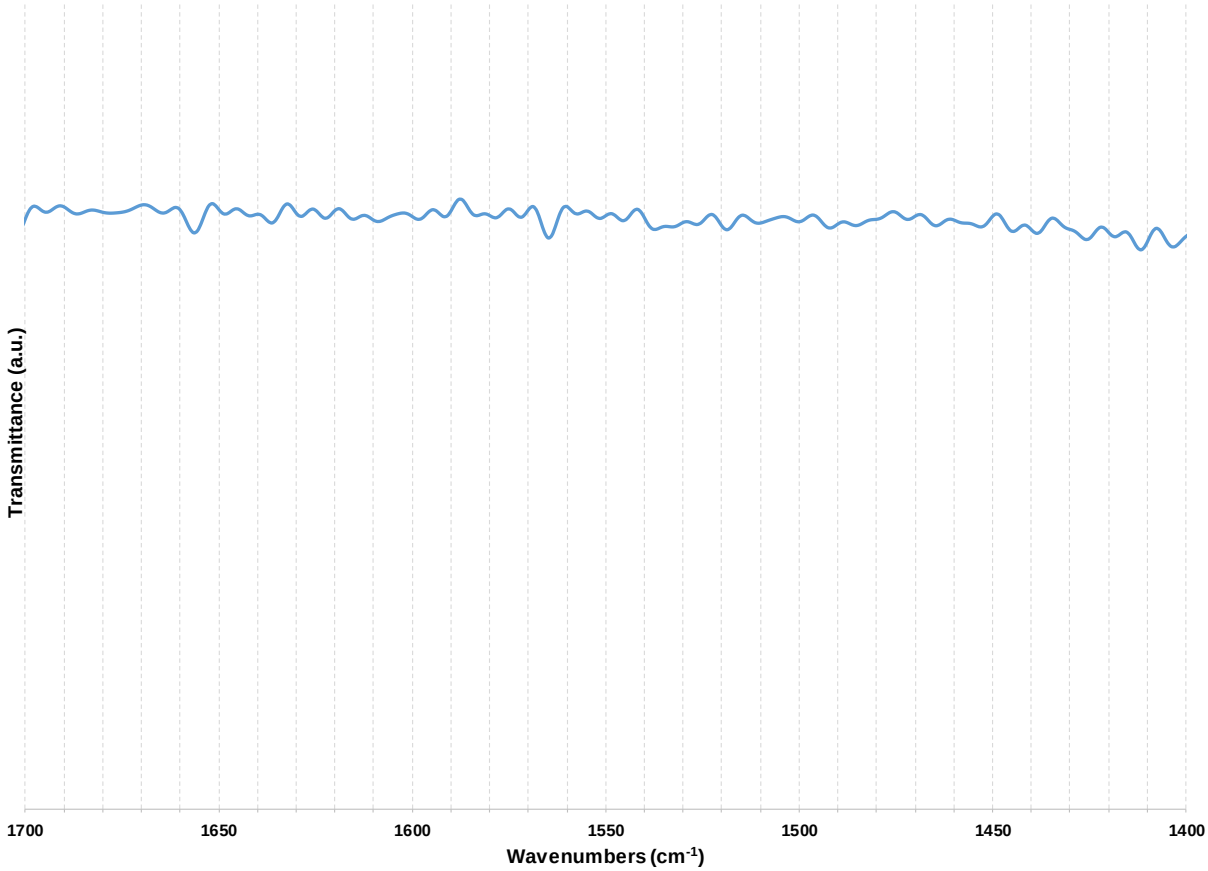

Figure 98 FTIR spectrum of a 4C-2nd gen Ti catalyst heated to 80 ^{0} C after the first dose to remove the pyridine blocking ligand.

The XANES spectrum of this 4-connected catalyst with blocking ligand removed shows a single high intensity pre-edge feature indicative of a four coordinate tetrahedral complex, Figure 99. During the first dose, oligomers are formed with specific connectivities to the matrix, but the robust matrix around the active centers is not established until after the second cross-linking. The notion that the titanium sites in 4C-2nd gen catalysts can relax to tetrahedral geometries when blocking ligands are removed during the first dose is evidence that the oligomers are not locked into a specific geometry leading to a second question about the active site after first dose.

Blocking Ligand Added after the First Dose – Third Generation

Can blocking ligands be added, after connectivity is established in the first dose, to imprint the geometry around the titanium active site but before the matrix has been locked into place in the second cross-linking? In the method of sequential additions, the first dose establishes the connectivity of the active center by reaching maximum connectivity. During the first dose, oligomers are formed that have the potential ability to be modified, e.g., six coordinate active site being modified to a four coordinate active site, which is presented in the data above. Under the same conditions that pyridine can be removed, it also has the potential to be added. In order to investigate this notion of altering the active site after connectivity has been established, first generation catalysts are exposed to pyridine after the first dose. To distinguish between first generation catalysts, and traditional second generation catalysts, these catalysts will be called third generation (geometry imprinted after connectivity is established in the first dose).

Synthesis of Third Generation Catalysts

$TiCl_4$, $Ti(OiPr)Cl_3$ and $Ti(OiPr)_2Cl_2$ are reacted with tin-cube in limiting amounts according to the same ratios presented in Table 10 in Chapter 3 with toluene as the solvent. The reaction is allowed to proceed at 80^{o}C overnight under constant stirring. The reaction is then dried at 80^{o}C under vacuum overnight and the connectivity verified by gravimetric analysis. After the connectivity is determined, approximately 25 mL of dry toluene is vapored transferred to the reaction vessel followed by five equivalents of pyridine to titanium. The reaction is then allowed to react at 80^{o}C for two hours. Two equivalents of dichlorodimethylsilane per tin-cube are then added to the reaction flask to further cross-link the reaction and build the rigid robust matrix around the titanium active site. The reaction is allowed to proceed for 72 hours at 80^{o}C followed by subsequent drying at room temperature under vacuum.

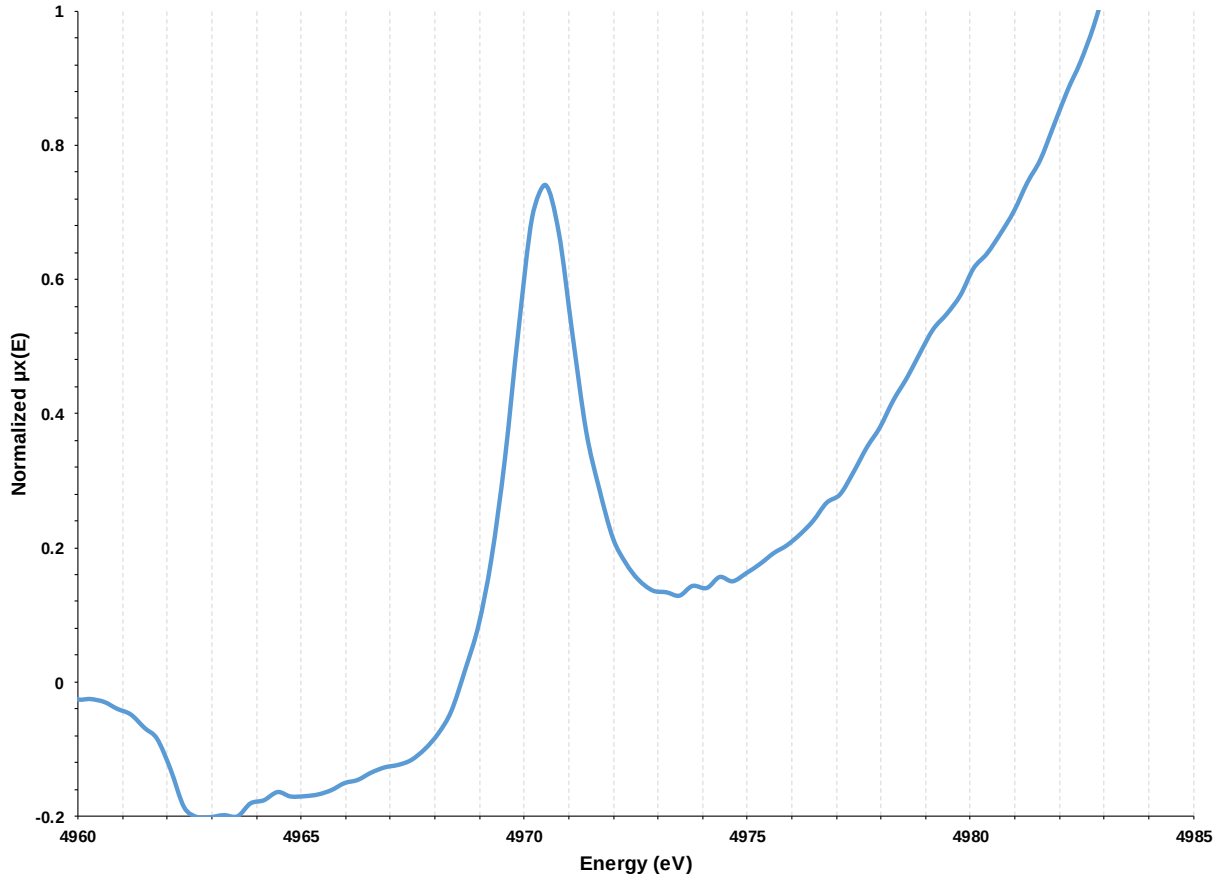

Figure 99 XANES spectrum for a 4C-Ti-2nd generation catalysts with blocking ligand removed after the first dose.

Characterization of Third Generation Catalysts by FTIR and XAS

The IR spectra for 4C-Ti-3rd gen (purple), 3C-Ti-3rd gen (blue), and 2C-Ti-3rd gen (green), after the second dose show evidence for only Lewis bound pyridine on titanium. While it is possible for pyridine to bind to Si sites, a Ti-free platform is synthesized under the same conditions. In contrast to the to the third generation titanium catalysts, no evidence for pyridine binding to the silicon platform is seen, Figure 100. Hence, the only place pyridine occurs is on the titanium sites present in the matrices.

In contrast to 4C-1st Gen and 4C-2nd Gen py_2 removed after the first dose, the XANES spectrum of 4C-3rd gen shows a clear difference in the pre-edge intensity and the peak shape. Figure 101 compares the pre-edge features of 4C-1st gen (green), 4C-2nd gen py_2 removed after the first dose (blue), and 4C-3rd gen (red). The intensity of the pre-edge feature has decreased and the peak shape has changed from a single feature to a distinct three band pattern suggesting the coordination number has increased. The differences observed indicate the geometry around the third generation catalysts is indeed different than both the 4C-Ti-1st gen and 4C-2nd gen py_2 removed after the first dose. In contrast, the 4C-Ti-2nd gen pyridine removed after the first dose looks similar to the 4C-Ti-1st gen catalyst. Therefore, it can be concluded that the oligomers synthesized during the first dose can be modified and made to adapt different geometries by adding or removing imprinting ligands.

It is noteworthy that the XAS studies presented here were conducted on catalysts synthesized with $SiCl_4$ as the inert cross-linking reagent. However, these catalysts were not passivated therefore the data is assumed to be representative of both families of catalysts: those synthesized with $SiCl_4$ or Me_2SiCl_2. The absorber atom, titanium is unaffected by the second cross-linking reaction hence the data obtained is valid regardless of the inert cross-linker.

Blocking Ligand and the Second Dose

Evidence for the ability of a blocking ligand to be added and/or removed after the first dose has led to the modification of the synthetic protocol, in that solvent is not removed after the first dose. A second modification to the synthetic protocol occurs after the second dose; the solvent and volatiles are initially removed under vacuum at room temperature instead of 80°C as in first generation catalysts. After the first dose, evidence for loss of blocking ligand was seen at both room temperature and 80°C. Therefore, drying at room temperature after the second dose is employed to ensure minimal loss of blocking ligand. Unfortunately, when both $TiCl_4(THF)_2$ and $TiCl_4(MeCN)_2$ are embedded in the matrix, there is no evidence in the IR spectra of imprinting

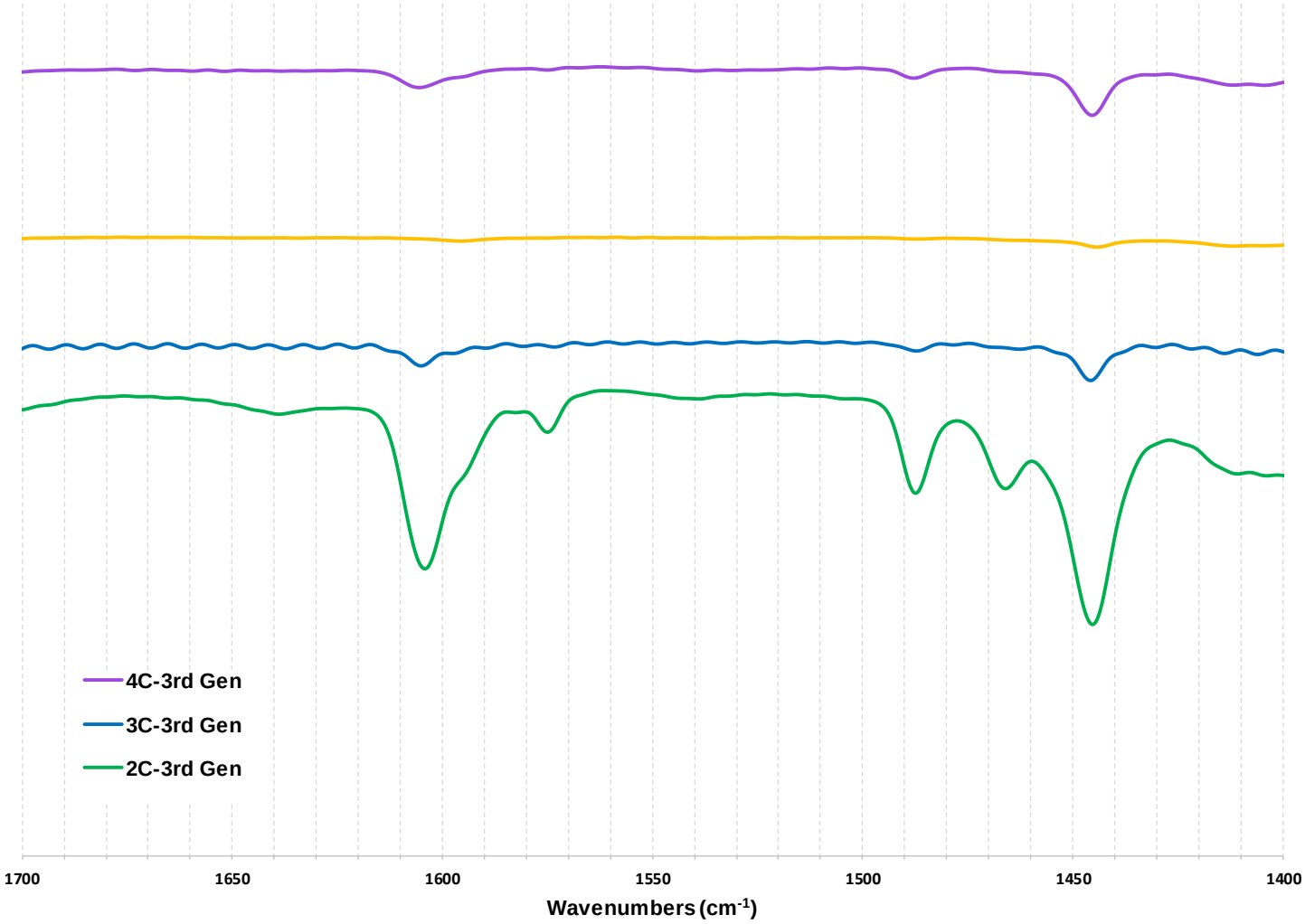

Figure 100 FTIR spectra showing only the pyridine finger print region for 3rd generation catalysts, 2C-Ti-3rd gen (green), 3C-Ti-3rd gen (blue), 4C-3rd gen (purple), and a titanium free platform (yellow).

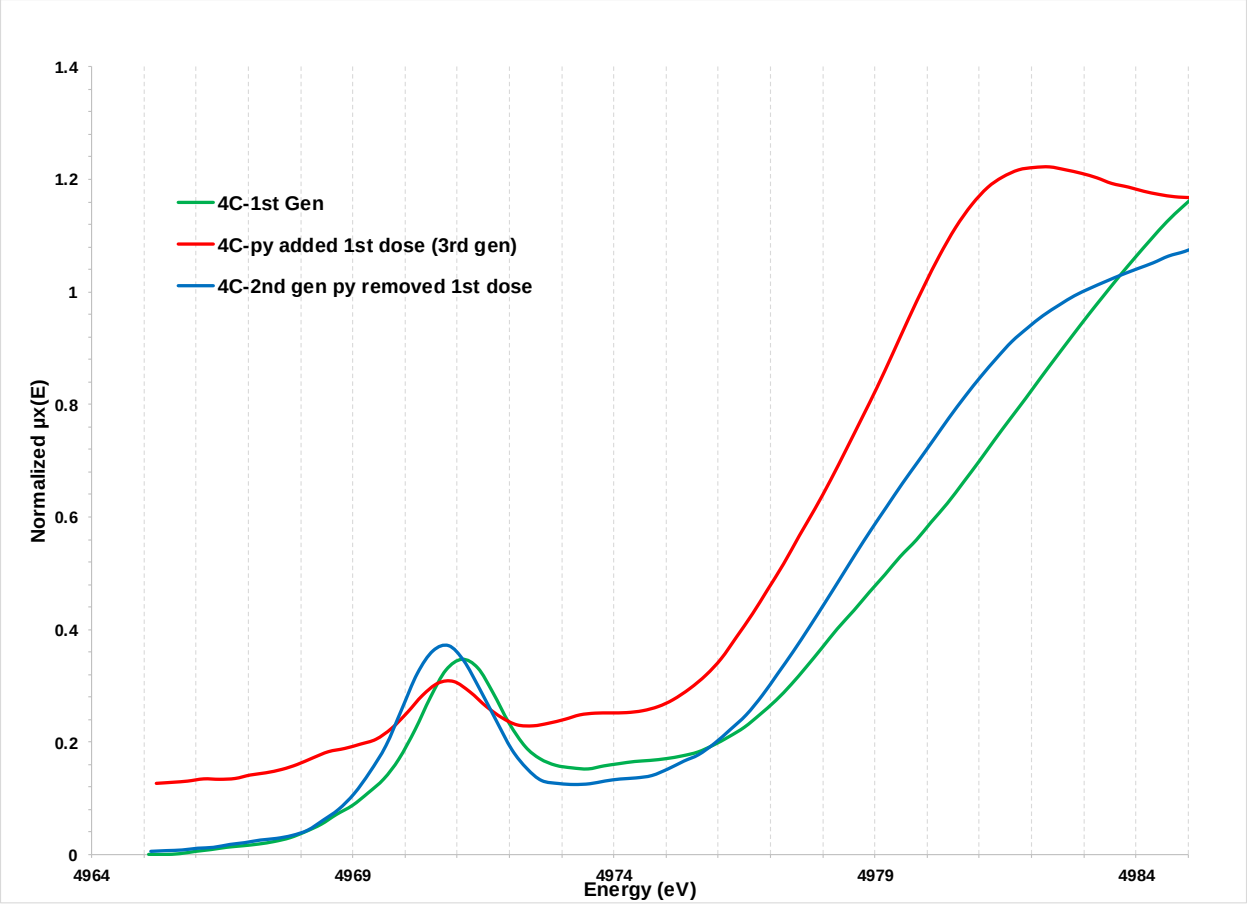

Figure 101 XANES spectra comparing 4C-1st gen (green) to 4C-3rd gen (red) and 4C-2nd gen pyridine removed after the first cross-linking (blue).

ligands after the second dose even when dried at room temperature. Figure 102 and Figure 103 show the IR spectra for 4C-Ti-1st gen overlaid by 4C-Ti-2nd gen THF_2 and 4C-Ti-2nd gen $MeCN_2$ catalysts both dried at room temperature. While the two peaks assigned to $TiCl_4(THF)_2$ are present in the spectrum, there are other peaks in the first generation spectrum at these wavenumbers; therefore, they cannot be used to confirm the presence of THF. In addition, there is little evidence for strong features at 1340 cm^{-1} and 1444 cm^{-1} seen in the $TiCl_4(THF)_2$ precursor. In the case of second generation catalysts synthesized with $TiCl_4(MeCN)_2$, the absence of the C≡N feature at 2300 cm^{-1} indicates the loss of acetonitrile during synthesis. Additionally, in both cases, signals for the blocking ligands are present in the NMR spectra of the volatiles.

To stabilize the imprinting ligands on titanium, THF and MeCN are employed as the reactions solvents instead of toluene for the synthesis of 4C-Ti-2nd gen THF_2 and 4C-2nd gen $MeCN_2$ respectively. Figure 104 shows the two dose 4-connected second generation catalyst synthesized in THF. Evidence for imprinting ligand is present at 1340 cm^{-1} and 1444 cm^{-1} indicating THF is in the matrix, however it is very difficult to determine if this signal is a result from residual solvent or if THF is truly bound to the titanium active site. In contrast, there is no evidence for acetonitrile present in the system.

After careful inspection of the volatiles via NMR spectroscopy and the catalyst matrices via IR spectroscopy it has been concluded that the binding energies of both acetonitrile and THF to titanium are too weak to be used as imprinting ligands for the synthesis of second generation catalysts with altered geometries. In contrast to these observations, catalysts synthesized with pyridine as the imprinting ligand show evidence of blocking ligand present after drying the catalysts at room temperature after the second dose in the IR spectrum, Figure 105. Additionally, only Lewis bound pyridine is present in the matrix. Therefore, the remainder of the work presented here will focus on the use of pyridine as an imprinting agent for second generation catalysts. In addition to FTIR evidence, XAS data shows evidence for pyridine bound to the Ti active site.

XAS Data First and Second Generation

Figure 106 overlays the XANES spectra for 4C-1st gen and 4C-2nd gen with pyridine after drying at room temperature following the second cross-linking. It can be seen that the 4C-2nd gen catalyst yields a lower intensity pre-edge feature, relative to 4C-1st gen, with a slight indication of a three band pattern. Additionally, the pre-edge feature is shifted to slightly higher energy. These changes in the XANES region of XAS are consistent with an increase in coordination geometry when 4C-Ti catalysts are synthesized with $TiCl_4py_2$.

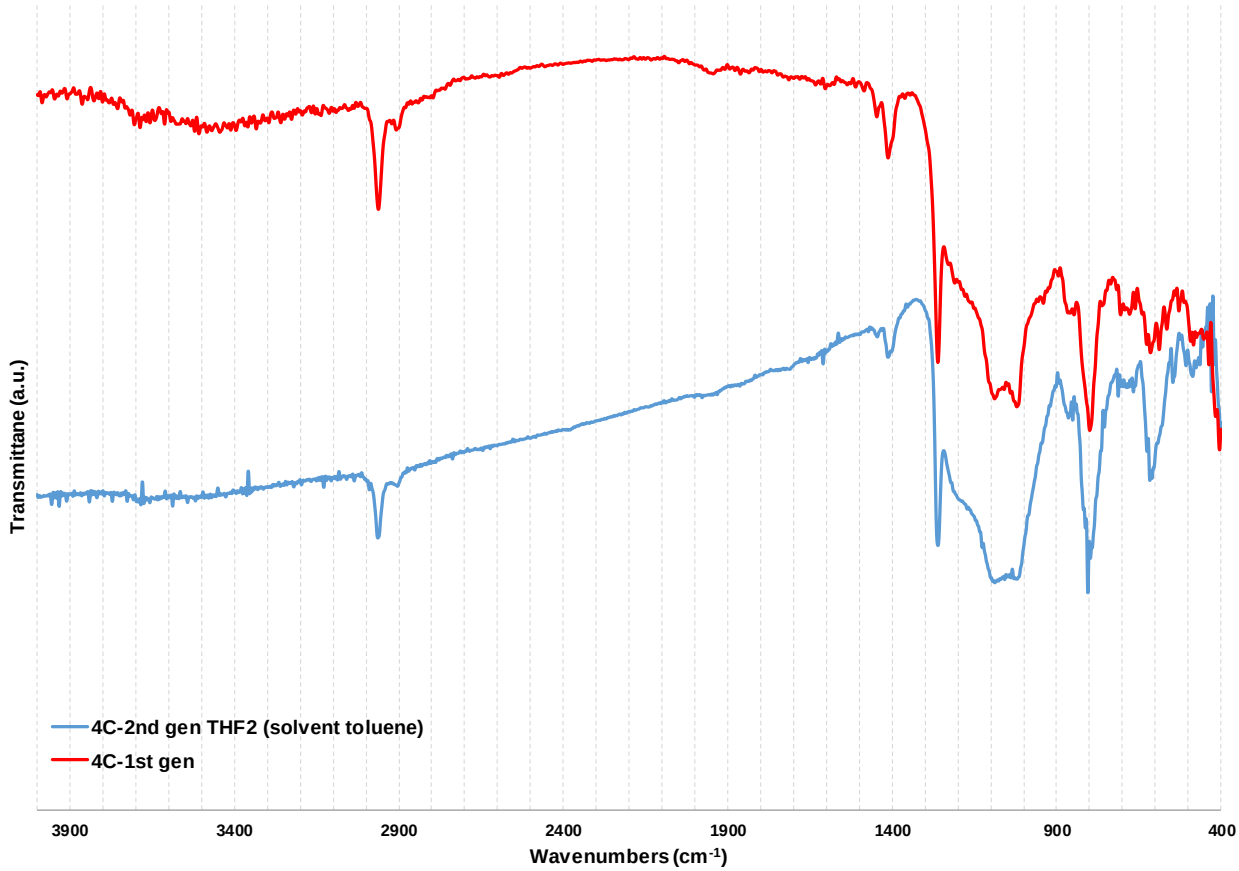

Figure 102 FTIR spectra of 4C-1st gen (red) and 4C-2nd gen with THF_2 (blue).

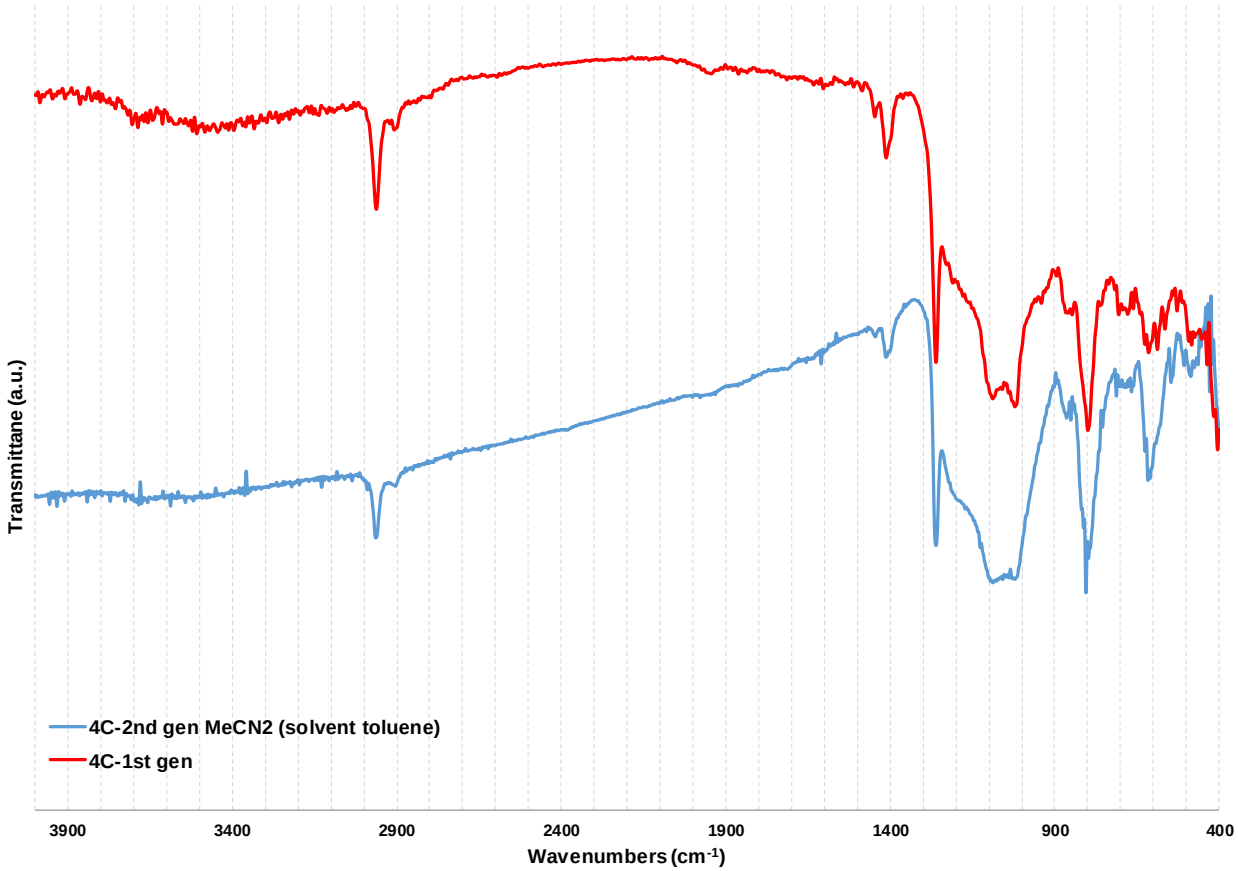

Figure 103 FTIR spectra of 4C-1st gen (red) and 4C-2nd gen with $MeCN_2$ (blue).

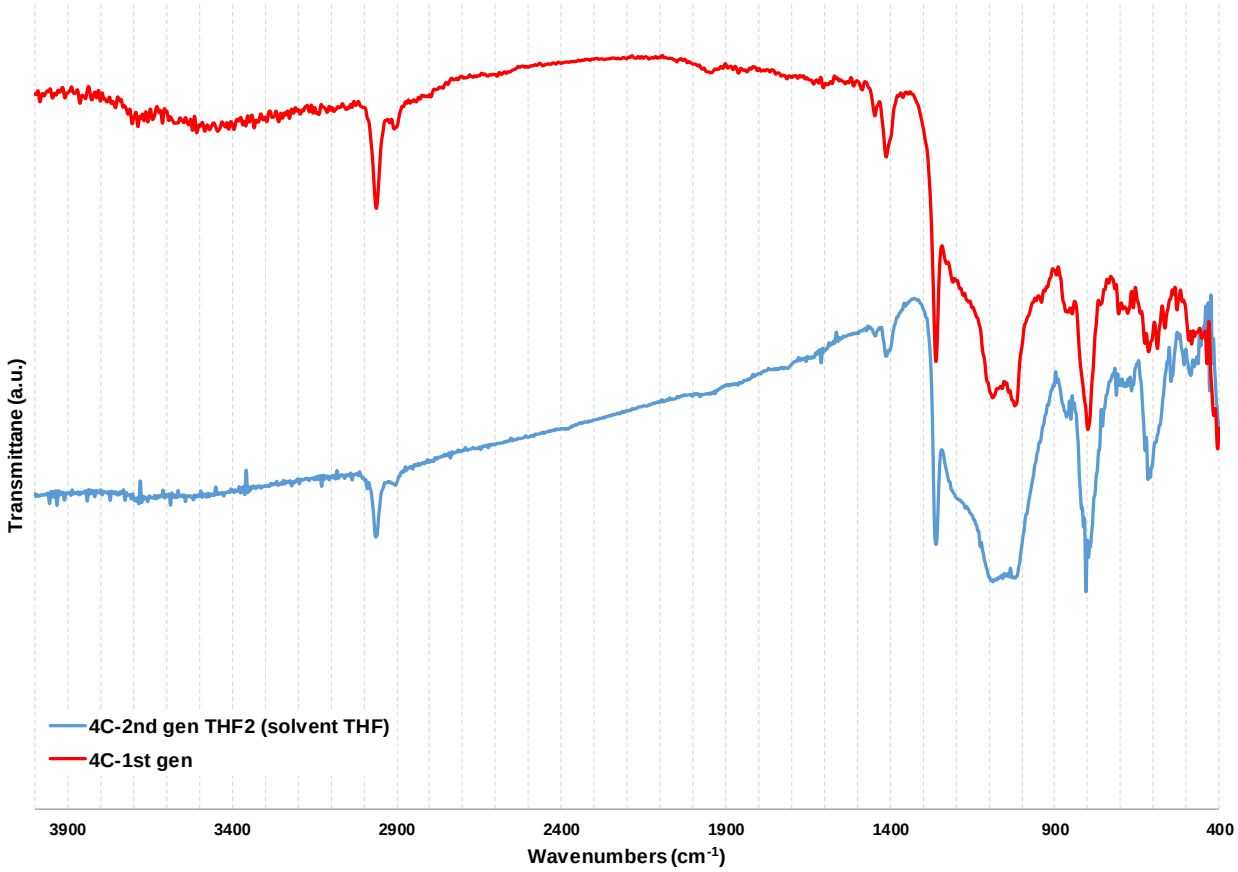

Figure 104 FTIR spectra of 4C-1st gen (red) and 4C-2nd gen with THF2 (blue) with THF as the reaction solvent.

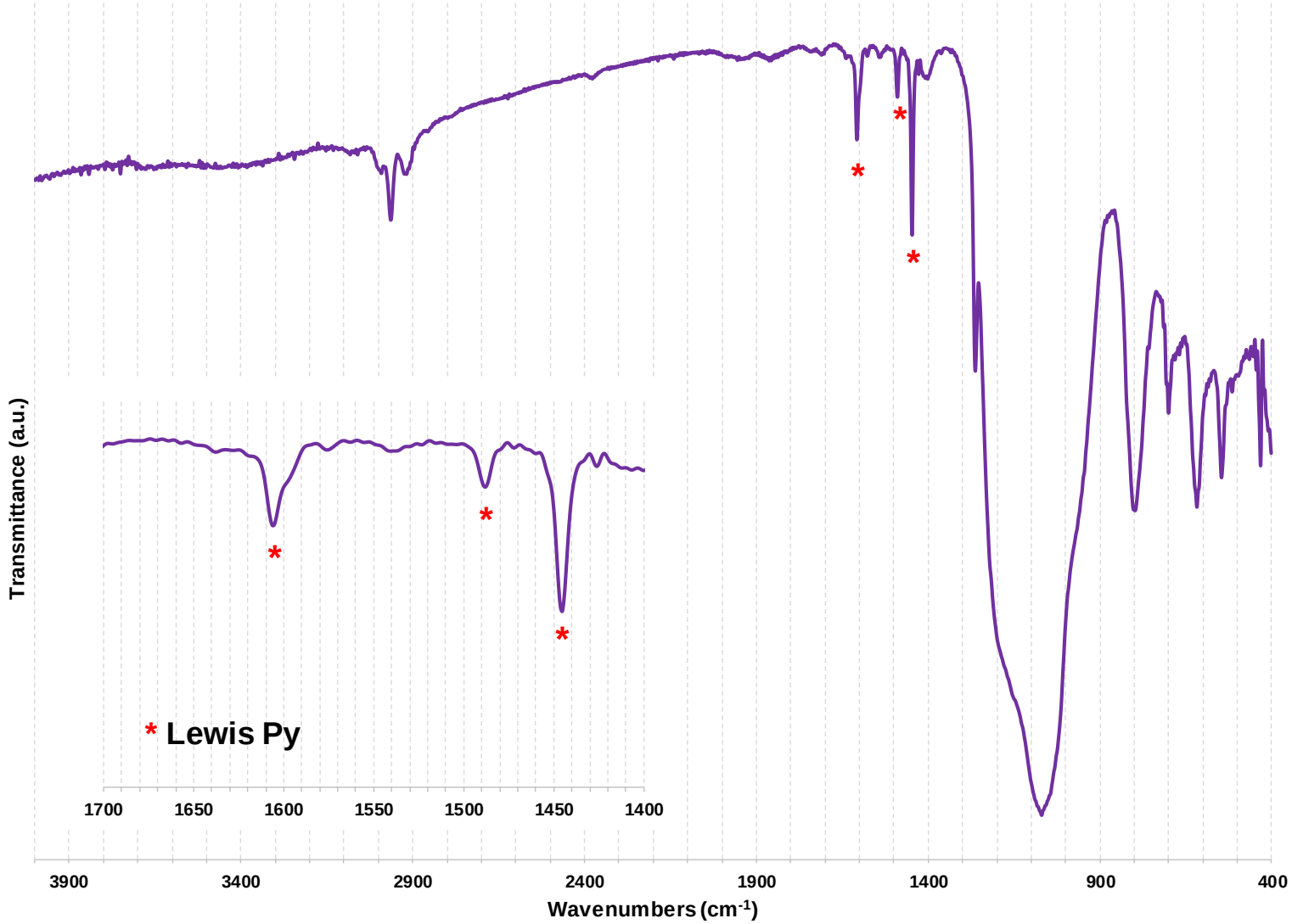

Figure 105 FTIR spectrum of 4C-2nd gen with py_2 dried at room temperature after the second cross-linking. The inset is a blowup of the pyridine fingerprint region illustrating only Lewis absorption bands.

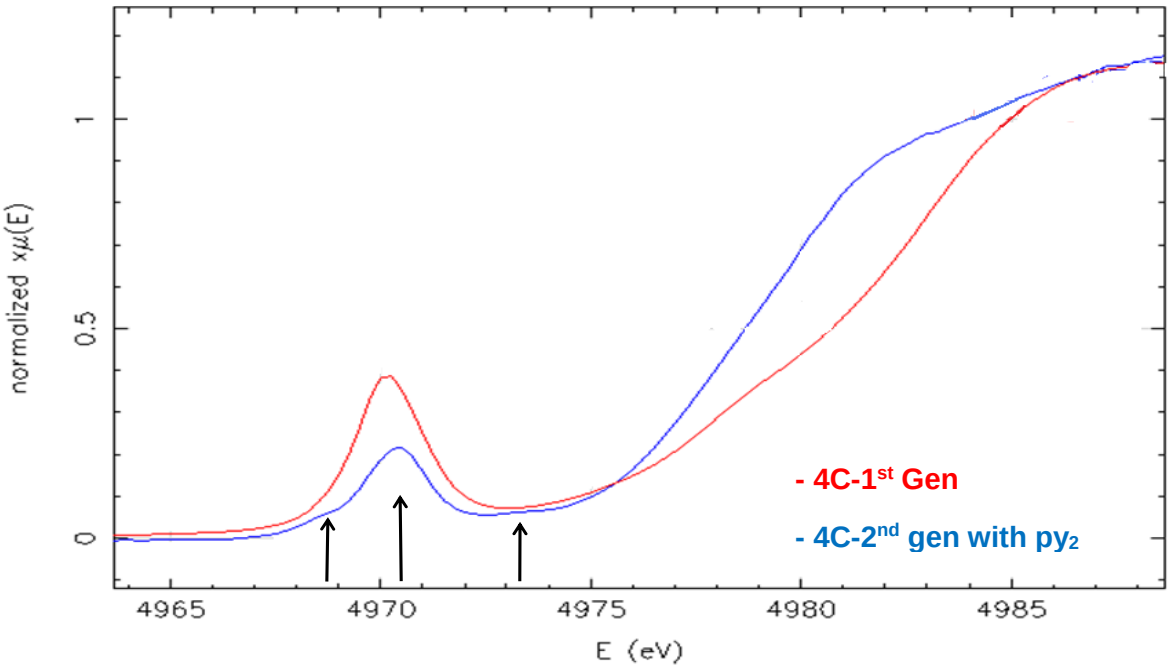

Figure 106 XANES spectra of 4C-1st Gen (red) and 4C-2nd Gen with py_2 (blue).

Furthermore, Figure 107, illustrates the phase corrected R plot of the EXAFS region for the 4C-2nd gen with pyridine catalyst. There are two distinct features. The first feature is at roughly 1.8 Å consistent with Ti-O bonds. The second feature has a slightly longer bond distance, 2.2 Å and corresponds to Ti-N. While modeling of the EXAFS data has been attempted, the fits did not converge. However, the appearance of a second bond distance consistent with Ti-N bond lengths suggest pyridine is still bound to the titanium active site.

Characterization of Second Generation 3C-Ti and 2C-Ti Catalysts

While 4C-2nd gen catalysts have been presented as model catalysts, it is important to characterize the 3C-2nd gen with py_2 catalysts as well as the 2C-2nd gen with py_2 catalysts Figure 108 shows the IR spectra of both 3C-2nd gen with py_2 and 2C-2nd gen with py_2 after drying at room temperature following the second cross-linking. Only Lewis pyridine is present in the both matrices suggesting pyridine remains coordinated to titanium throughout the reaction.

Characterization of the Reaction Volatiles After Second Cross-linking

While precautions for ensuring minimal loss of blocking groups are employed during synthesis, there is evidence for some loss of imprinting ligands in the NMR spectra of the volatiles after drying the second dose at room temperature under vacuum, Figure 109. Similar to drying after the first dose, the amount of blocking ligand lost correlates to the connectivity of the matrix. In Table 25 it can be seen that after drying at room temperature for four hours, the 2C-Ti catalysts lose approximately half of the initial amount of pyridine present at the beginning of the reaction. In contrast, the 3C-Ti and 4C-Ti centers lose less than 15% indicating the majority of the pyridine blocking ligands remain bound to the titanium sites and thus persist as a six coordinate complexes.

The different amounts of pyridine lost after the second dose can be explained in the same manner as the loss of blocking ligand after the first dose. The energy barriers for the loss of ligands for both 3C-Ti and 4C-Ti are higher than that of the 2C-Ti centers. The two free alkoxy ligands are able to move around the active site while remaining coordinated to the 2C-titanium center. In contrast, the 3C-Ti and 4C-Ti catalysts have three and four siloxy ligands, respectively, which are more or less fixed around titanium by the rigidity of the Si_8O_{20} building blocks and the 3D-cross-linikng between them established during the second cross-linking with Me_2SiCl_2. By fixing the Ti-O-Si linkages, one would predict the corresponding energy barriers involved in the loss of pyridine ligands will be high, consistent with the data presented in Table 25.

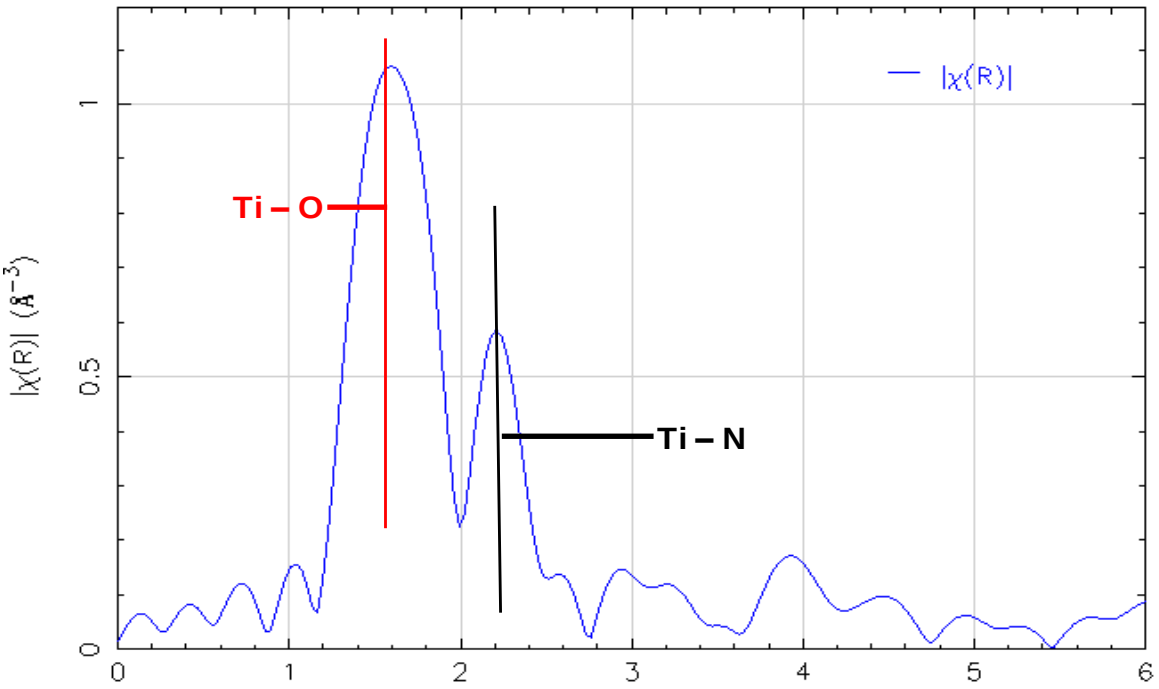

Figure 107 R plot for 4C-2nd gen with py_2 after the second cross-linking reaction illustration two different coordination ligands.

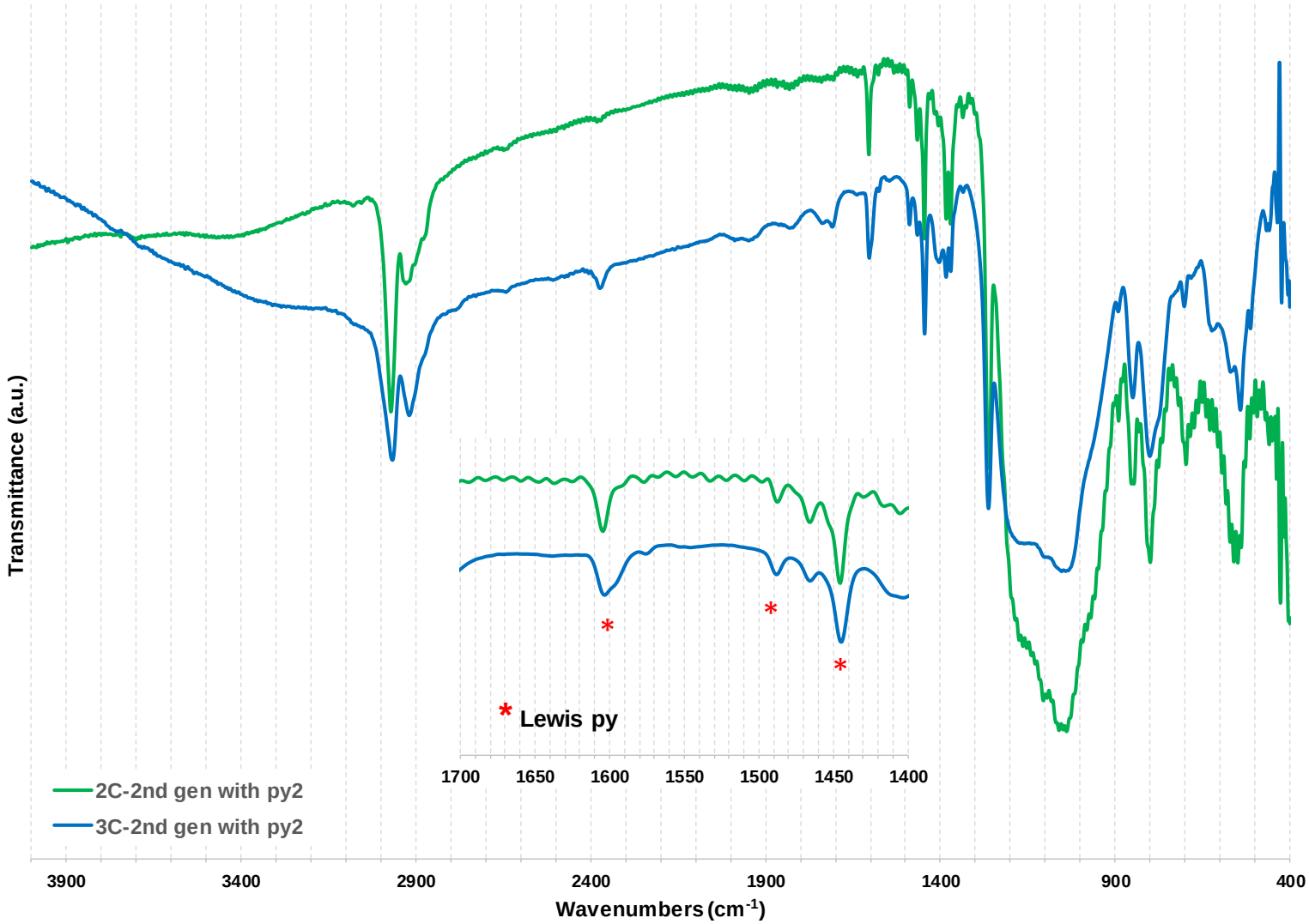

Figure 108 FTIR spectra of 2C-2nd gen with py_2 (green) and 3C-2nd gen with py_2 after the second cross-linking reaction.

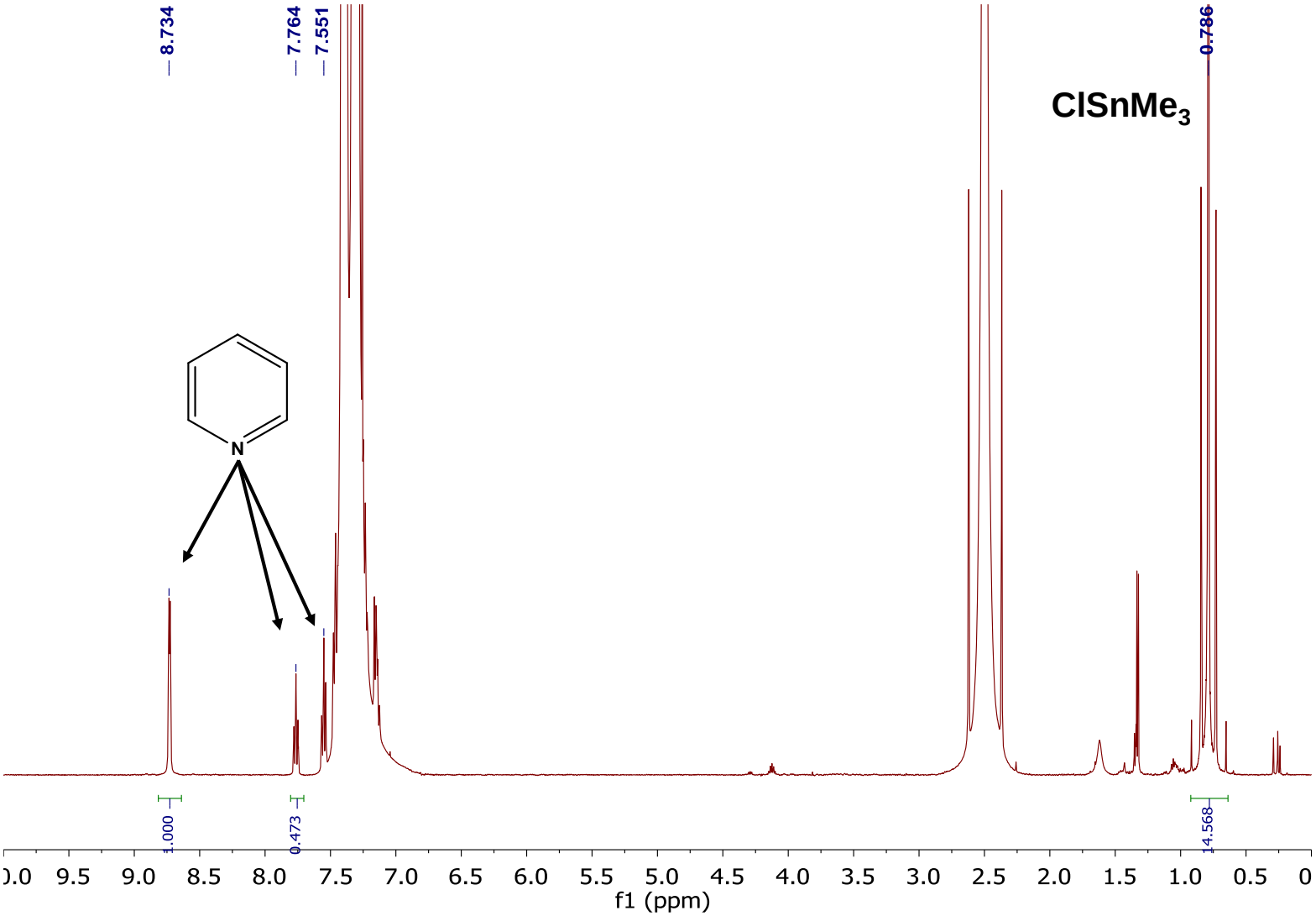

Figure 109 NMR spectrum of the volatiles after drying 2C-2nd gen with py_2 at room temperature after the second dose.

Table 25 Summary of the precursor, connectivity, percent blocking ligand lost, remaining ratio of pyridine to titanium after the drying the catalysts following the second cross-linking reaction.

Precursor	Connectivity (± 0.1)	% Blocking Ligand Lost (2^{nd} dose Room Temp) (± 4 %)	Py : Ti (± 0.1)
4C-Ti 2^{nd} Gen	4.0	<10	1.8 : 1
3C-Ti 2^{nd} Gen	3.0	15	1.7 : 1
2C-Ti 2^{nd} Gen	1.9	55	1.0 : 1

In addition to the differences seen between the loss of pyridine of 2C-Ti, ,3C-Ti, and 4C-Ti, there is a difference in loss of blocking ligands between the first and second dose. Table 26 compares the amount of pyridine lost after the first and second dose for each connectivity.

During the first dose, oligomers with specific connectivity to the matrix are established, but the robust rigid matrix is not fully established until these oligomers are further cross-linked in the second dose. Thus, allowing the blocking ligands to leave more readily than after the second dose. The titanium active sites are able to relax back to a lower energy confirmation stabilizing the loss of blocking ligand. In contrast, after the second dose the Ti-O-Si bonds are fixed to the matrix not allowing for rearrangement of the titanium active site as easily as the first dose.

Second Generation Catalyst with Blocking Ligands Removed

While much effort has been spent on preventing the premature loss of blocking groups the pyridine imprinting ligands ultimately need to be removed after the matrix has been established in order to open the active site of these new Ti-2^{nd} gen with py_2 catalysts, Figure 110. To remove the remaining blocking ligands, the catalysts are heated for four hours at a specific temperature optimized for each individual connectivity, Table 27. The difference in temperatures needed to remove 100% of the blocking ligands is an additional piece of evidence indicating the structural differences between the 2-connected, 3-connected, and 4-connected titanium centers. The 2-connected titanium sites readily release blocking ligands from the matrix. The two alkoxy ligands are not bound to the rigid matrix and can easily rearrange to the tetrahedral equilibrium geometry. While the two alkoxy ligands are free to relax, the two remaining Ti-O-Si linkages are locked into the matrix and may prevent from complete relaxation; therefore the geometry may be distorted tetrahedral. In contrast, the 4-connected fully embedded titanium site takes relatively much higher temperatures to remove the blocking ligands. The rigidity of the Ti-O-Si bonds secured by the

Table 26 Summary of the amount of blocking ligand lost after the first dose and after the second dose.

Precursor	Connectivity (± 0.1)	% Blocking Ligand Lost (1st dose Room Temp) (± 4 %)	% Blocking Ligand Lost (2nd dose Room Temp) (± 4 %)
4C-Ti 2nd Gen	4.0	39	<10
3C-Ti 2nd Gen	3.0	52	15
2C-Ti 2nd Gen	1.9	76	55

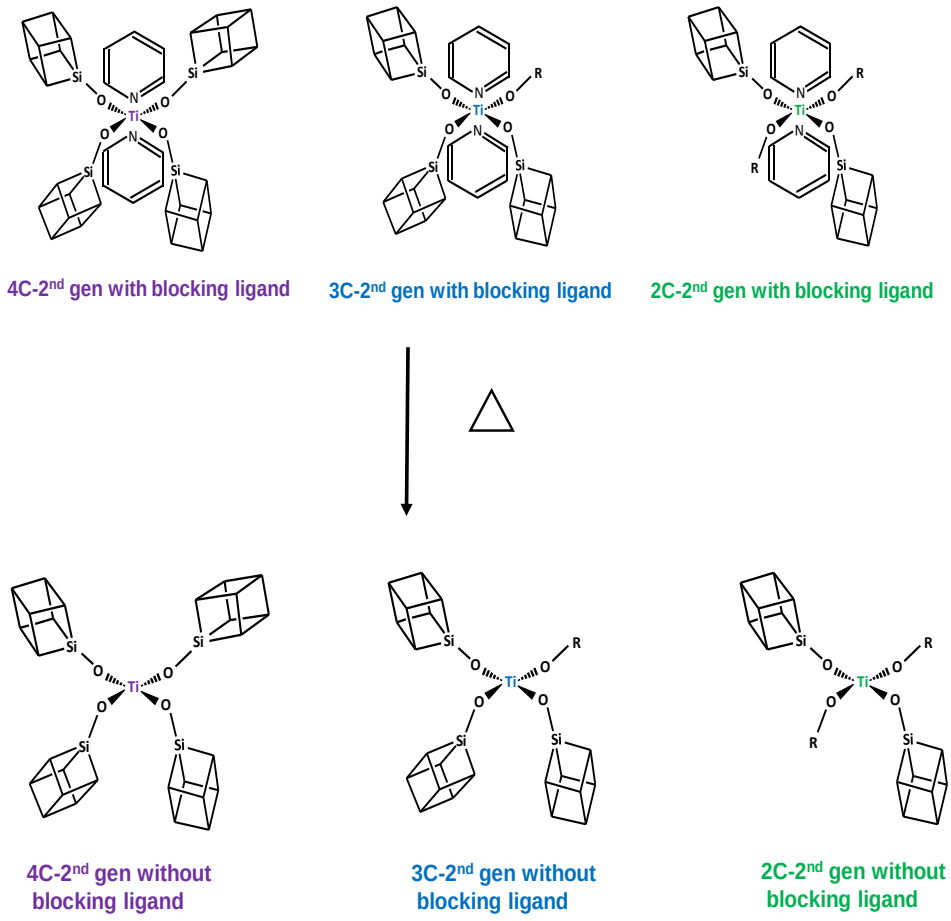

Figure 110 Illustration of heating 2nd gen with py_2 catalysts to create 2nd gen py removed catalysts and thus opening the active sites.

Table 27 Temperature needed to remove 100% of the pyridine blocking ligands after the second cross-linking reaction.

Precursor	Connectivity (± 0.1)	Temperature (^{0} C)
4C-Ti 2nd Gen	4.0	170
3C-Ti 2nd Gen	3.0	125
2C-Ti 2nd Gen	1.9	80

robust building block matrix are expected to resist change locking the matrix into a four coordinate geometry other than Td, most likely a distorted square planar geometry. In contrast to both the 4C-Ti and 2C-Ti sites, the 3C-Ti center poses the most interesting geometry. While there is one alkoxy ligand coordinated to the Ti center that is able to move freely around the active site to stabilize the loss of the pyridine imprinting ligand, the other three siloxy linkages are expected to be fixed in their right angle relationships. Therefore, it is hard to predict the exact geometry of this active site.

The presence and absence of pyridine blocking ligands is characterized primary by FTIR. Figure 111 shows the IR spectra 3C-2nd gen py-removed. The absence of absorption peaks at 1444, 1483, and 1604 cm^{-1} indicates pyridine ligands are no longer bound to the titanium active site. The IR spectra of 2C-2nd gen py-removed and 4C-2nd gen py-removed are identical to the 3C-2nd gen py-removed spectrum.

XAS Analysis for 4C-2nd Gen Catalysts without Pyridine

In addition to FTIR, XAS is used to monitor the presence and absence of pyridine. Figure 112 illustrates the XANES region of the 4C-2nd gen py-removed catalyst. The absorption feature has changed in comparison to 4C-2nd gen with py_2. The pre-edge feature is now a single finger with higher intensity. This increase intensity and loss of the three band pattern suggest the Ti active site is now four-coordinate. In addition, Figure 113 shows the R plots for 4C-2nd gen with py_2 (left) compared to 4C-2nd gen py-removed (right). After heating, the disappearance of the second feature at 2.2 Å suggest pyridine is no longer bound to the titanium center.

DRUV Analyses of Second Generation Catalysts

Like first generation catalysts, second generation catalysts are characterized using diffuse reflectance UV-vis. Figure 114, Figure 115, and Figure 116 show the DRUV spectra overlays for the families of 4C-Ti, 3C-Ti, and 2C-Ti catalysts, respectively. All first generation catalysts are shown in blue, second generation catalysts with pyridine are in red, while second generation catalysts with pyridine removed are illustrated in green. Like first generation, these catalysts exhibit two features below 300 nm indicating isolated Ti(IV) sites. Again, only the first feature will be discussed. The larger feature at ~262 nm of the second generation catalysts with pyridine is assigned to the aromatic pyridine ligands coordinated to titanium. While this does not give direct information about the titanium site, it confirms the presence of pyridine in the matrix. Table 28 summarizes the maximum absorption wavelength for the 2C-Ti (green), 3C-Ti (blue), and 4C-Ti (purple) catalysts. As you add pyridine to the system, the wavelength of the absorption maximum

Figure 111 Pyridine finger region of the IR spectrum of the 3C-2nd gen py removed catalyst.

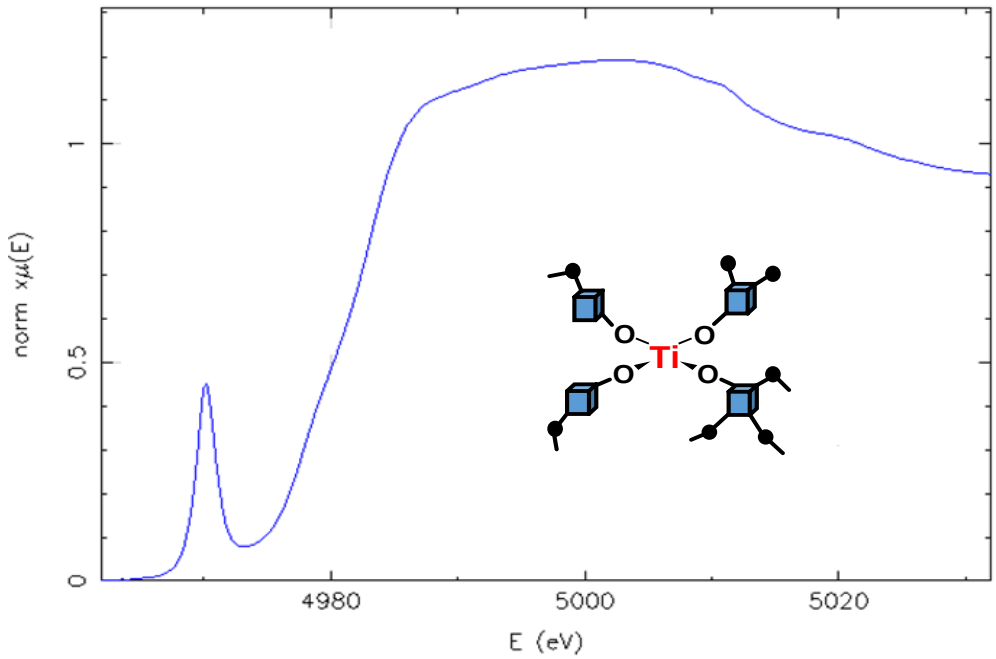

Figure 112 XANES spectrum for 4C-2nd gen py removed.

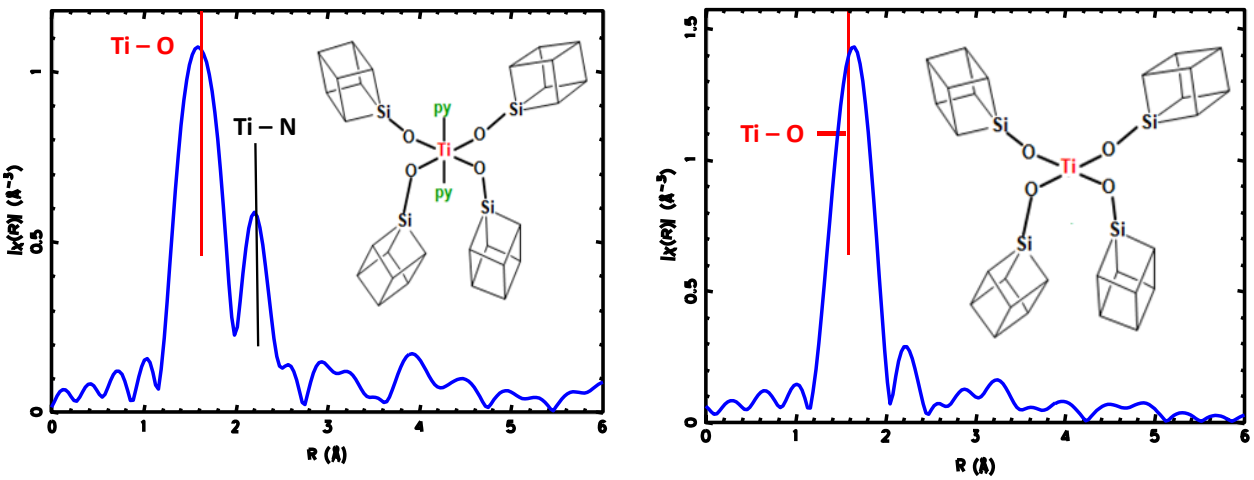

Figure 113 R plots for 4C-2nd gen with py_2 (left) and after heating to remove blocking ligands, 4C-2nd gen py-removed (right).

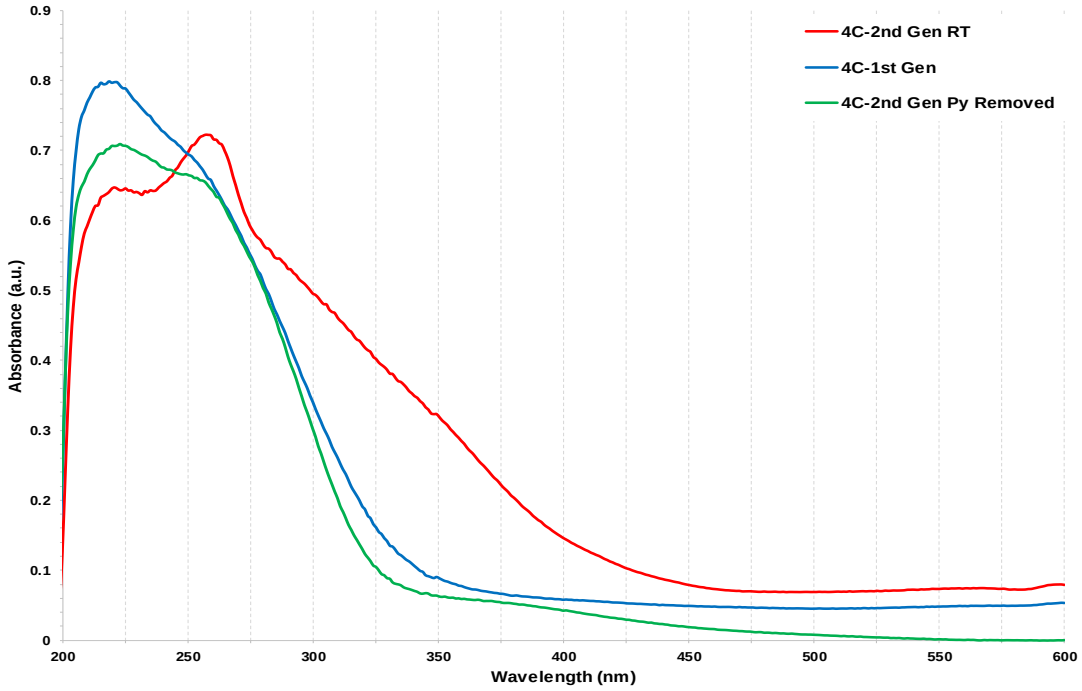

Figure 114 DRUV overlays for 4C-Ti catalysts.

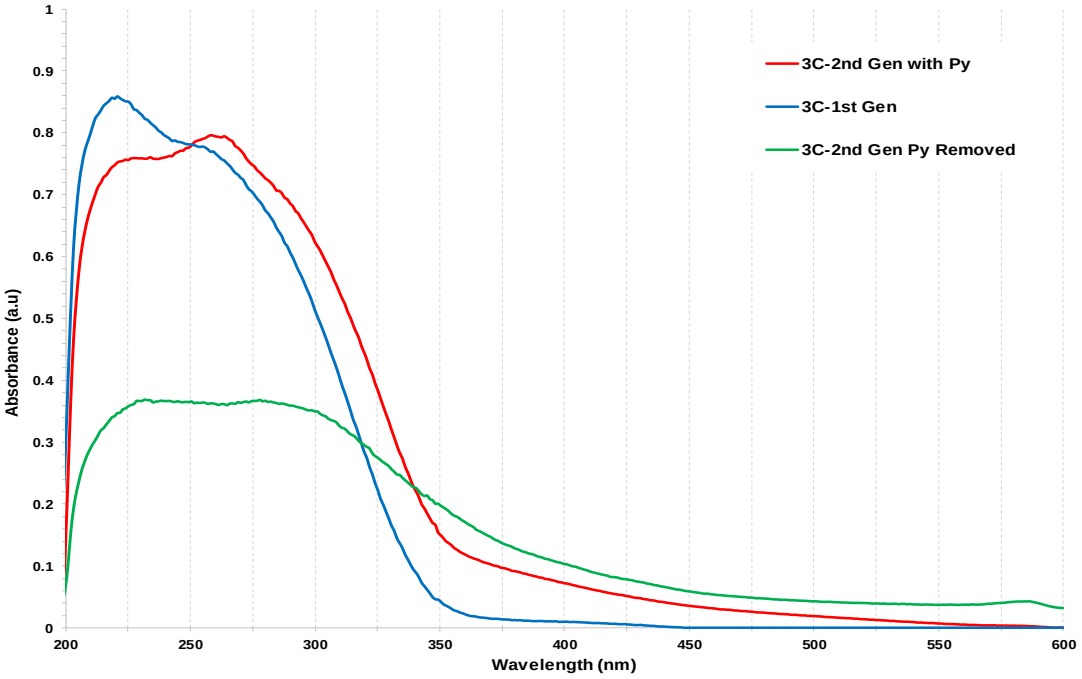

Figure 115 DRUV overlays for 3C-Ti catalysts.

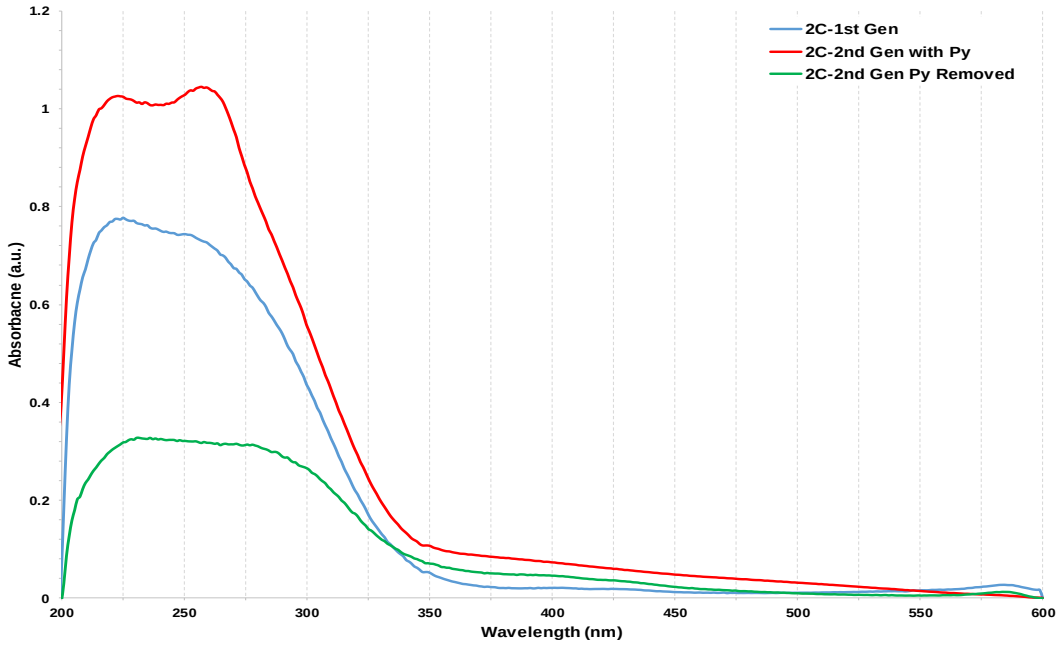

Figure 116 DRUV spectra for 2C-Ti catalysts.

Table 28 Summary of DRUV wavelength absorption maxima.

Catalyst	Max Wavelength (nm) (± 0.5)
2C-1st Gen Me2SiCl2	225
2C-2nd Gen with Py	232
2C-2nd Gen Py-Removed	232
3C-1st Gen Me2SiCl2	222
3C-2nd Gen with Py	228
3C-2nd Gen Py Removed	235
4C-1st Gen Me_2SiCl_2	219
4C-2nd Gen with Py	223
4C-2nd Gen Py Removed	226

increases. This trend is consistent with what is reported in the literature, as coordination increase, the absorption shifts to higher wavelengths.[121]

Catalytic Activity

The impetus for synthesizing a family of catalysts with geometries other than the primary tetrahedral geometry is to determine if it will be a more active catalyst than its tetrahedral analogue. In order to compare these new second generation catalysts to first generation their catalytic properties are investigated for the oxidation of 2, 3, 5-trimethylphenol (TMP) to 2, 4, 6-trimethylbenzoquinone (TMBQ) and 2, 6-dimethyoxyphenol (syringol) to 2, 6-dimethyoxybenzoquinone (DMOBQ). The catalytic test reactions followed the same protocol described for first generation catalysts.

Table 29 and Table 30 compare the catalytic activity of second generation titanosilicates with pyridine for the oxidation of TMP to TMBQ and DMOP to DMOBQ, respectively. The TOF for the 3C-2nd gen with py and 4C-2nd gen with py for the oxidation of phenols to benzoquinones are very similar. At first glance, this may seem surprising because both 4C-1st gen and 3C-1st gen exhibit distinct catalytic activities that result from the different connectivities at titanium site in these samples. However, in the case of second generation catalysts, the active sites of both 3C-2nd gen with py and 4C-2nd gen with py are virtually identical. The precursors for both catalysts are believed to be six coordinate titanium complexes, both containing two pyridine blocking ligands. After the catalysts are cross-linked with the tin-cube building block, both catalysts remain in a six-coordinate geometry each containing four Ti-O bonds and two pyridine ligands. Similarly, after the second cross-linking reaction with Me_2SiCl_2, both lose approximately 10 – 15% of the initial starting amount of pyridine blocking ligand. In contrast to both 4C-2nd gen with py and 3C-2nd gen with py, the 2C-2nd gen with py exhibits a significantly higher TOF. Unfortunately, there is clear evidence that the titanium centers in 2C-2nd gen catalysts leach during the reaction, which is discussed in more detail below. For this reason, 2C-2nd gen catalysts cannot be considered true heterogeneous catalysts.

The remaining blocking ligand on both 3C-2nd gen RT and 4C-2nd gen RT must be removed before these catalysts have open active sites. Table 31 and Table 32 compare the catalytic activity of second generation catalysts with blocking ligand removed (2nd gen py-removed) for the oxidation of TMP and DMOP, respectively. From the TOFs, the most active catalyst with blocking ligand removed for the oxidation of phenols to benzoquinones is the 3-connected catalyst. The

Table 29 Summary of catalytic properties for 2nd generation Ti catalysts with pyridine blocking ligands for the oxidation of TMP to TMBQ.

Catalyst	TOF 2 min	Conversion % 60 min (± 5)	Selectivity % 60 min (±4)	Yield % 60 min (±4)
TMP + H_2O_2	n/a	0	0	0
Si-Platform Me_2SiCl_2	n/a	0	0	0
4C-Ti-2nd Gen with py	0.6 (± 0.1)	58	68	39
3C-Ti-2nd Gen with py	0.5 (± 0.1)	52	70	36.4
2C-Ti-2nd Gen with py *	1.28 (±0.07)	100	40	40

* Titanium leaches from support.

Table 30 Summary of catalytic properties for 2nd generation Ti catalysts with pyridine blocking ligands for the oxidation of DMOP to DMOBQ.

Catalyst	TOF 2 min	Conversion 60 min (±5)	Selectivity % 60 min (±5)	Yield % 60 min (±5)
DMOP + H_2O_2	n/a	3	5	.15
Si-Platform Me_2SiCl_2	n/a	10	6.4	6.4
4C-Ti-2nd Gen with py	0.9 (±0.3)	94	69	65
3C-Ti-2nd Gen with py	0.83 (±0.05)	100	74	74
2C-Ti-2nd Gen with py *	1.1 (± 0.1)	100	83	84

* Titanium leaches from support.

Table 31 Summary of catalytic properties for 2nd generation Ti catalysts pyridine removed for the oxidation of TMP to TMBQ.

Catalyst	TOF 2 min	Conversion 60 min (± 5)	Selectivity % 3 min (±4)	Yield % 30 min (±4)
TMP + H_2O_2	n/a	0	0	0
Si-Platform Me_2SiCl_2	n/a	0	0	0
4C-Ti-2nd Gen py-removed	0.91 (± 0.1)	60	65	39
3C-Ti-2nd Gen py-removed	3.1 (± 0.1)	100	66	66
2C-Ti-2nd Gen py-removed *	1.3 (± 0.1)	100	71	71

* Titanium leaches from support.

Table 32 Summary of catalytic properties for 2nd generation Ti catalysts pyridine removed for the oxidation of DMOP to DMOBQ.

Catalyst	TOF 2 min	Time of 100% Conversion (min)	Selectivity % At 100% Conversion (±4)	Yield % (±5)
DMOP + H_2O_2	n/a	3	5	.15
Si-Platform Me_2SiCl_2	n/a	10	6.4	6.4
4C-Ti-2nd Gen py-removed	1.2 (±0.5)	96	74	71
3C-Ti-2nd Gen py-removed	2.58 (± 0.5)	100	76	76
2C-Ti-2nd Gen py-removed *	1.8 (± 0.2)	100	71	71

* Titanium leaches from support.

TOF for 3C-2nd gen py removed is approximately 3 times faster than its first-generation analogue for the conversion of TMP and 1.5 times faster for the conversion of DMOP.

One explanation for why the 3C-2nd gen py removed catalyst exhibits the highest activity is the stabilization of the three linkages and the mobility of one alkoxy ligand. With both 2C-2nd gen py-removed and 4C-2nd gen py-removed, the geometries about the active site are predicted to be distorted tetrahedral and square planar, respectively. In contrast, the 3C-2nd gen py-removed geometry is less obvious. The three siloxy linkage are fixed in the plane while the free alkoxy ligand can move about the active site, Figure 117. This abnormal geometry may explain the increased activity observed of the 3C-2nd py-removed catalysts.

While clear distinctions between individual Ti connectivities and catalytic activities have been established, 2C is unstable as a heterogeneous catalyst, and 3C is more active than 4C, the major goal of this research is to investigate the influence of the active site geometry on catalytic activity. XAS studies showed by altering the metal precursor, the geometry of the resulting catalyst could be altered as well. Therefore, the catalytic activity of catalysts with the same connectivity to the matrix, but altered geometries are compared. Table 33 and Table 34 show the internal comparison of connectivities with altered geometries.

In the case of both 3-connected and 4-connected catalysts, altering of the geometry of the active sites leads to changes seen in catalytic activity. By initially imprinting the catalyst with a six coordinate active site and then removing the imprinting ligands, in this case pyridine, the

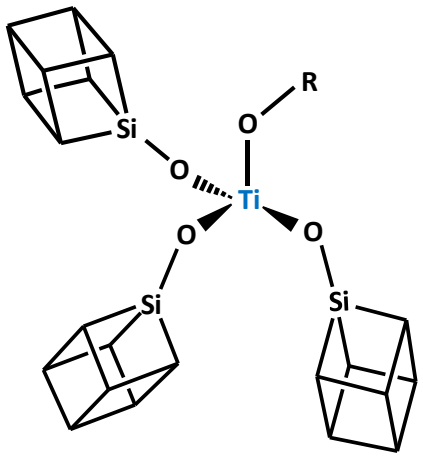

Figure 117 Illustration of a suspected geometry of 3C-2^{2n} gen py-removed catalyst.

Table 33 Comparison of catalytic activities between catalyst with the same connectivities but different geometries for the oxidation of TMP to TMBQ.

Catalyst	TOF 2 min	Conversion % 60 min (± 5)	Selectivity % 60 min (±4)	Yield % 60 min (±4)
4C-Ti-1st Gen Me_2SiCl_2	0.75 (±0.03)	63	62	39
4C-Ti-2nd Gen with py	0.6 (± 0.1)	58	68	39
4C-Ti-2nd Gen py-removed	0.91 (± 0.1)	60	65	39
3C-Ti-1st Gen Me_2SiCl_2	0.90 (±0.1)	87	66	57
3C-Ti-2nd Gen with py	0.5 (± 0.1)	52	70	36.4
3C-Ti-2nd Gen py-removed	3.1 (± 0.1)	100	66	66
2C-Ti-1st Gen Me_2SiCl_2 *	1.27 (± 0.06)	100	40	40
2C-Ti-2nd Gen with py *	1.28 (±0.07)	100	40	40
2C-Ti-2nd Gen py-removed*	1.3 (± 0.1)	100	71	71

* Titanium leaches from support.

Table 34 Comparison of catalytic activities between catalyst with the same connectivities but different geometries for the oxidation of DMOP to DMOBQ.

Catalyst	TOF 2 min	Conversion % 60 min (± 5)	Selectivity % 60 min (±4)	Yield % 60 min (±4)
4C-Ti-1st Gen Me_2SiCl_2	0.23 (± 0.03)	50	77	38.5
4C-Ti-2nd Gen with py	0.9 (±0.3)	94	69	65
4C-Ti-2nd Gen py-removed	1.2 (±0.5)	96	74	71
3C-Ti-1st Gen Me_2SiCl_2	1.04 (± 0.06)	100	59	59
3C-Ti-2nd Gen with py	0.83 (±0.05)	100	74	74
3C-Ti-2nd Gen py-removed	2.58 (± 0.5)	100	76	76
2C-Ti-1st Gen Me_2SiCl_2 *	1.6 (± 0.2)	100	64	64
2C-Ti-2nd Gen with py *	1.1 (± 0.1)	100	83	84
2C-Ti-2nd Gen py-removed *	1.8 (± 0.2)	100	71	71

* Titanium leaches from support.

catalytic active of the 3C-Ti and 4C-Ti sites are enhanced. Noteworthy is the fact that the selectivity of the catalysts remained the same even when their activities increased. Often as activity of a catalyst increases, the selectivity of the catalyst decreases.

While the family of 2-connected catalysts cannot be presented as true heterogeneous catalysts because of leaching, their activities may still be compared. Table 33 and Table 34 compare the three 2-connected catalysts (2C-Ti-1st gen, 2C-Ti-2nd gen with py_2, and 2C-Ti-2^{n} gen py removed) for the oxidation of TMP to TMBQ and syringol to DMOBQ. In both cases, the TOFs at two minutes are virtually the same. This is an indication that the catalysts are probably the same. There are two explanations for the observed TOFs. The first is all catalysts leach to same active species (which will be discussed below). Second, the blocking ligands are weakly bound and the catalyst reverts back to a more tetrahedral like geometry in the cases of 2-connected second generation catalyst. The two free alkoxy ligands are able to stabilize the geometry after the loss of blocking ligands to revert back to a psuedotetrahedral geometry as exhibited by first generation catalysts and the catalysts are virtually the same.

General Conclusion

In conclusion, two families of heterogeneous catalysts were successfully synthesized and their catalytic properties investigated for the oxidation of phenols to benzoquinones. The catalytic activities of the 2C-Ti, 3C-Ti, and 4C-Ti matrices were clearly different indicating connectivity plays a critical role in activity. In addition to connectivity, by altering the geometry of the active site, it is possible to increase the activity of a catalyst without decreasing the catalyst's selectivity. A major concern that is often overlooked in the literature, is the notion of leaching. The next section provides more information on the issue of leaching and confirms that the catalysts presented here, except for the 2-connected family, are truly heterogeneous.

Stability and Recyclability

An issue that must be addressed in heterogeneous catalysis is leaching. If any component of the active site becomes dethatched from the solid surfaces, several different scenarios result. The soluble components (usually a metal cation) may or may not exhibit catalytic activity after leaching. Furthermore, normally the original surface site, will no longer be active and therefore whatever activity is observed for the catalyst will not be due to the original site. In most instances the heterogenous catalyst will not be recyclable and therefore loses one of the important advantages of constraining catalyst sites to remain bound to a support surface.[70,71] In order to describe both first and second generation catalysts as being truly heterogeneous, the stability

of these catalysts had to be assessed. Three experiments are conducted to determine if these catalysts are truly heterogeneous and are described below.

First, each catalyst is filtered from the solution and activity of the remaining filtrate is investigated. Secondly, the weight percent of titanium in the filtrate is determined. Lastly, the weight percent of titanium in the remaining solid is measured.

Stability (Leaching) Protocol

To address the issue of leaching under standard reaction conditions, the catalysts of interest are prepared as described in Chapter 2. However, the catalysis reactions are scaled up to 100 μmol of Ti. Thirty minutes after the addition of oxidant the catalyst is filtered, as quickly as possible using Fisher Brand 0.45 μm PTFE membrane syringe filters, and the mother liquor is added to a clean reaction vial containing a 10 mm magnetic stir. A 50 μL aliquot of is taken and added to a NMR tube containing 500 μL of $CDCl_3$ and $MgSO_4$. The NMR tube is then capped, shaken, and placed into a dry ice-isopropanol bath. The reaction vial is then capped with clean septum screw top lid and returned to the oil bath. The reaction is then allowed to proceed for an additional 60 minutes. Two aliquots were taken to evaluate the activity of any species in solution, 25 minutes and 60 minutes after the reaction is returned to the oil bath. The aliquots are analyzed using the described outline workup protocol, Chapter 2.

Once the last aliquot is taken, the solution is added to a platinum crucible and heated to evaporate the remaining solvent. Platinum crucibles are used because standard ceramic crucibles contain titanium and contribute to the overall titanium content of the sample. The vial is washed with both acetone and ultrapure water to ensure both organic and aqueous ions are washed into the platinum crucible. After carefully removing wash solvents and other volatiles, the crucible is then placed in a box furnace and calcined at 550 ^{0} C for four hours to remove any organics. Once the crucible is cooled to room temperature, it is weighed. Approximately 1 mL of both concentrated HF and concentrated HNO_3 are added to the crucible to dissolve any solid remaining after calcination. After 30 minutes, the solution is added to a tared polypropylene bottle, the crucible rinsed three times with ultrapure H_2O and diluted to roughly 25 g. The actual amount of water does not matter if the total mass of solution is known. The now empty crucible is allowed to air dry overnight and the final mass recorded the next day. The difference in crucible mass is assumed to be the mass of solid remaining after calcination. This solution is then analyzed via ICP-OES and the amount of Ti in solution (if any) calculated.

To conclude the leaching study, the mass of Ti remaining in solid catalyst after filtration is determined. The catalyst is dried overnight at room temperature. The solid is transferred to a polypropylene bottle whose mass is known. Approximately 1 mL of both concentrated HF and concentrated HNO_3 are added to the bottle. The acids are allowed to completely digest the catalyst overnight. After digestion, the solution is diluted with ultrapure water to an approximate total weight of 50 g; the actual amount does not matter provided the total mass is known. The solution is then analyzed via ICP-OES and a new wt% Ti calculated. From this weight percent, the amount of titanium in the recovered catalyst is determined and compared to the initial mass of titanium in the reaction, Table 35.

The masses of titanium present in each component of the reaction (solution vs. solid) are compared instead of wt.% Ti because of the loss of imprinting ligands and trimethyltin chloride during the reaction. Second generation with pyridine catalysts are not heated to remove the volatile trimethyltin chloride that is a byproduct of the cross-linking reactions with cube to prevent loss of the pyridine blocking groups. Therefore, trimethyltin chloride is still present when the initial wt. % Ti is determined. During the catalysis reaction, trimethyltin chloride is present in the reaction solution, therefore when the wt.% Ti is determined after the reaction, the wt.% Ti appears to increase. If titanium does not leach into the solution, the mass of titanium before and after catalysis should be same i.e., 5 mg before catalysis, 5 mg after catalysis. However, it is important to note that there is some loss of catalyst in both NMR aliquots and during filtration.

In a similar procedure, tin leaching is also quantified. After the second dose, trimethyltin groups remain on unreacted corners of the tin-cube. The ratio of titanium to tin ranges between 0.5 – 2 tin per titanium. These remaining tin groups have the potential to leach into the matrix as well as titanium. Previous studies have shown that tin does not play an active role in catalysis, therefore, tin leaching is only characterized by ICP-OES (no catalysis characterization). The same procedures are used as described above for titanium to detect tin in the mother liquor and in the recovered catalysts.

Results and Discussion Leaching

The results of stability and recovery experiments of both first and second generation catalysts along with grafted Ti-MCM-41 are summarized in Table 35. In contrast to the 3C-Ti and 4C-Ti, all 2C-Ti catalysts leach regardless of the active site geometry. Additionally, the leached species are active catalysts. Therefore, the observed catalytic activity is either a combination of both the leached homogenous species and the remaining heterogeneous species, or it may only

be a result of the leached homogenous species. As predicted, titanium grafted on MCM-41 also leaches. 3C-Ti-1st gen, 3C-Ti-2nd gen with py, 3C-Ti-2nd gen py removed, and 4C-Ti-1st gen exhibit small amounts of active <1%. The measured activities remained constant within the error of NMR integration (1.5%) and therefore we describe them as stable heterogeneous catalysts.

Furthermore, titanium is not observed by ICP in the mother liquor. While there is always a chance for titanium to be present in solution below the limit of detection, we do not believe this is the case for these catalysts. The limit of detection for titanium by ICP-OES is 0.5 ppb. In the work presented here, at least 100 μmol (4.78 mg) of titanium were added to the catalytic reaction. If only one percent of that titanium leached, 47.8 μg, and the total mass of solution was 25 g, the concentration of titanium in solution would be 1.9 ppm which is well above the detection limit for titanium.

The result of the Sn leaching study can be found in Table 36. In contrast to Ti, Sn leaching is observed in both families of 3C-Ti and 4C-Ti regardless of generation (2C-Ti catalysts are predicted to leach as well, but are not considered in the study). The quantity of Sn in solution ranges from ~2.5 – 8.5% of the initial amount of residual Sn in the catalyst. However, it is difficult to say the exact source of Sn. There are three scenarios that could potential lead to Sn in solution: 1) trimethyltin chloride is trapped inside the pores of the silicate matrix and during catalysis is released into solution; 2) unreacted corners of the tin-cube undergo a new chemical process releasing Sn from the matrix and into the reaction solution; 3) a combination of both scenarios. Unfortunately, at this time the source of Sn in solution has not been determined.

In addition to tin in solution, only ~50% of the initial amount of tin is recovered in the remaining solid leaving roughly 40% of Sn unaccounted for. One possible explanation is trimethyltin chloride is trapped in the pores of the silicon matrix, but is released during catalysis. The trimethyltin chloride is then lost as a result of its high volatility.

Recyclability Protocol

One of the main advantages of heterogeneous catalysts over homogeneous catalysis is their easy of recovery and recyclability. In order to be considered a viable heterogeneous catalyst, it must be resilient to reaction conditions and remain active when recycled repeatedly. First and second generation single-site catalysts were evaluated by two different methods. Both methods are initiated in the same manner as the above described “phenol oxidation protocol”, but differ in the method of recyclability.

Table 35 Summary of leaching studies for first and second generation titanium catalysts for oxidation of phenols to benzoquinones with aqueous hydrogen peroxide.

Catalyst	% Conversion 60 min after filtration (±1.5%)	% of Quinone formed 60 min after filtration (± 1.5%)	% Ti in Solution (± 5%)	% Ti recovered (± 2.0%)
2C-1st Gen*	100	47	83	0.0
2C-2nd Gen with py*	14	10	15	30
2C-2nd Gen py-Removed*	72.5	12.4	15	85
3C-1st Gen	0.75	0.32	0.0	95
3C-2nd Gen with py	0.0	0.55	0.0	60
3C-2nd Gen py-Removed	0.42	0.85	0.0	94
4C-1st Gen	0.73	0.73	0.0	89
4C-2nd Gen with py	0.0	0.0	0.0	93
4C-2nd Gen py-Removed	0.0	0.0	0.0	89
G-Ti-MCM-41*	6.30	10.5	8.7	56

* Titanium leaches from support.

Table 36 Results of Sn leaching detected by ICP-OES.

Catalyst	% mass recovered	Initial Mass Sn (mg)	Mass Sn Recovered (mg)	Mass Sn in Mother liquor	% Sn Leached
4C-Ti-1st Gen Me_2SiCl_2	83	9.052	3.99	0.76	8.4
4C-Ti-2nd Gen py-removed	89	5.502	2.901	0.16	2.9
3C-Ti-2nd Gen py-removed	82	5.73	2.79	0.36	6.3

In the first method, after the majority of phenol is oxidized (time varies depending on catalyst of interest) an additional 20 equivalence of substrate and 250 equivalence of oxidant are added to the existing solution and monitored as a single dose. This cycle is repeated four times.

The second method used for recovery and reusability required extraction of the catalysts from the original reactions. Again, after the majority of substrate was oxidized, stirring was halted and the catalyst allowed to settle to the bottom of the reaction vial. The solution was decanted off and the catalyst washed three times with hot acetonitrile to remove any remaining substrate, oxidant, product, and internal standard. Assuming no loss of catalyst, the reaction vial was removed from the oil bath and dried. Clean acetonitrile was added to the reaction vial to obtain a titanium concentration close to the initial catalyst solution (3.9 mM Ti). A 50 µL aliquot was added to a NMR tube containing 500 µL $CDCl_3$, $MgSO_4$, and 1.5 µL of mesitylene, capped, shaken, and submerged into a dry ice-isopropanol bath. The mesitylene was added as a secondary internal standard to determine the number of mmol (if any) of 4, 4'dimethoxybenzoquinone (internal standard) remained in the new reaction solution. To the reaction vial, ~ 25 mg of internal standard and 20 equivalence of substrate were added. The solution is allowed to equilibrate at 65 ^{0} C for 30 minutes with constant stirring, 500 rpm. After the solution reached equilibrium temperature, 250 equivalence of aqueous hydrogen peroxide was added to initiate the reaction. Aliquots were taken over a period of 2-4 hours to monitor the reaction and NMR spectra obtained as previously described. This cycle is repeated four times.

Results and Discussion of Recyclability

Unfortunately, the first method recyclability testing resulted in deactivation of the catalysts. As substrate and additional oxidant are repeatedly added in the presence of product and unreacted oxidant, over time the catalyst stops working. On the contrary, catalysts recycled via filtration remain active.

Figure 118 illustrates the recovery and recyclability of 3C-Ti-1st gen (green) and 3C-2nd gen py removed (blue). Each reaction is characterized one hour after the addition of oxidant. Both catalysts show reasonable recyclability with respect to catalytic activity. However, there is a slight decrease in the amount of substrate converted with each cycle. When aliquots are taken, stirring is not stopped and therefore, some of the catalyst is removed from the reaction flask every time an aliquot is taken. Hence, the actual number of active sites is potentially decreasing with each aliquot. However, it is noteworthy that each catalytic cycle reaches 100% if allowed to react

for a longer period of time illustrated in red for 3C-2nd gen py removed and orange for 3C-1st gen in Figure 118.

Reproducibility

A subtle but major concern with developing a synthetic protocol is the ability for others to reproduce the exact catalysts. To investigate the reproducibility of these catalysts, Dr. Austin Albert synthesized a family of first generation catalysts using the same synthetic approach as described in this work. The catalysts synthesized by Dr. Albert are then used to catalyze the oxidation of TMP to TMBQ under the same reaction conditions.

It was found that the catalysts synthesized by Dr. Albert were identical to the catalysts synthesized in the work. The turn over frequencies, percent conversions, and percent selectivites were consistent with those reported here. Therefore, it can be concluded that the synthetic strategy described in this work is reproducible.

Investigation of Intermediates and Byproducts of TMP Oxidation

During the oxidation of 2,3,5-trimethylphenol to 2,3,6-trimethylbennoquinone, the color of the reaction solution evolves. Initially, it is colorless with a suspension of catalyst particles. As the reaction progresses, the color of the solution changes from clear to red to yellow within fifteen minutes of peroxide addition. The initially clear solution and the final yellow solution are expected, phenols are colorless while their corresponding quinones are deep yellow. The appearance of the red color led to a brief study into possible side products/intermediates that are responsible for this color change. Three different characterization techniques were used to investigate the color change 1) NMR, 2) EPR, 3) GC-MS.

The red solution color appears within approximately five minutes of the addition of hydrogen peroxide. Therefore, several aliquots are taken between two and fifteen minutes to observe proton signals via NMR spectroscopy that may identify the molecules responsible for this color change. Figure 119 shows a typically NMR spectrum during the first fifteen minutes of the reaction. Unfortunately, there is little evidence for proton signals corresponding to reaction intermediates in these NMR spectra.

The literature suggests the oxidation of phenols to benzoquinones proceeds via a radical mechanism.[59,109,] Consequently, the intermediates responsible for the deep red color may be paramagnetic and undetectable by NMR. In order to identify possible intermediates, EPR is also used to analyze each aliquot. EPR samples are prepared according to the following protocol:

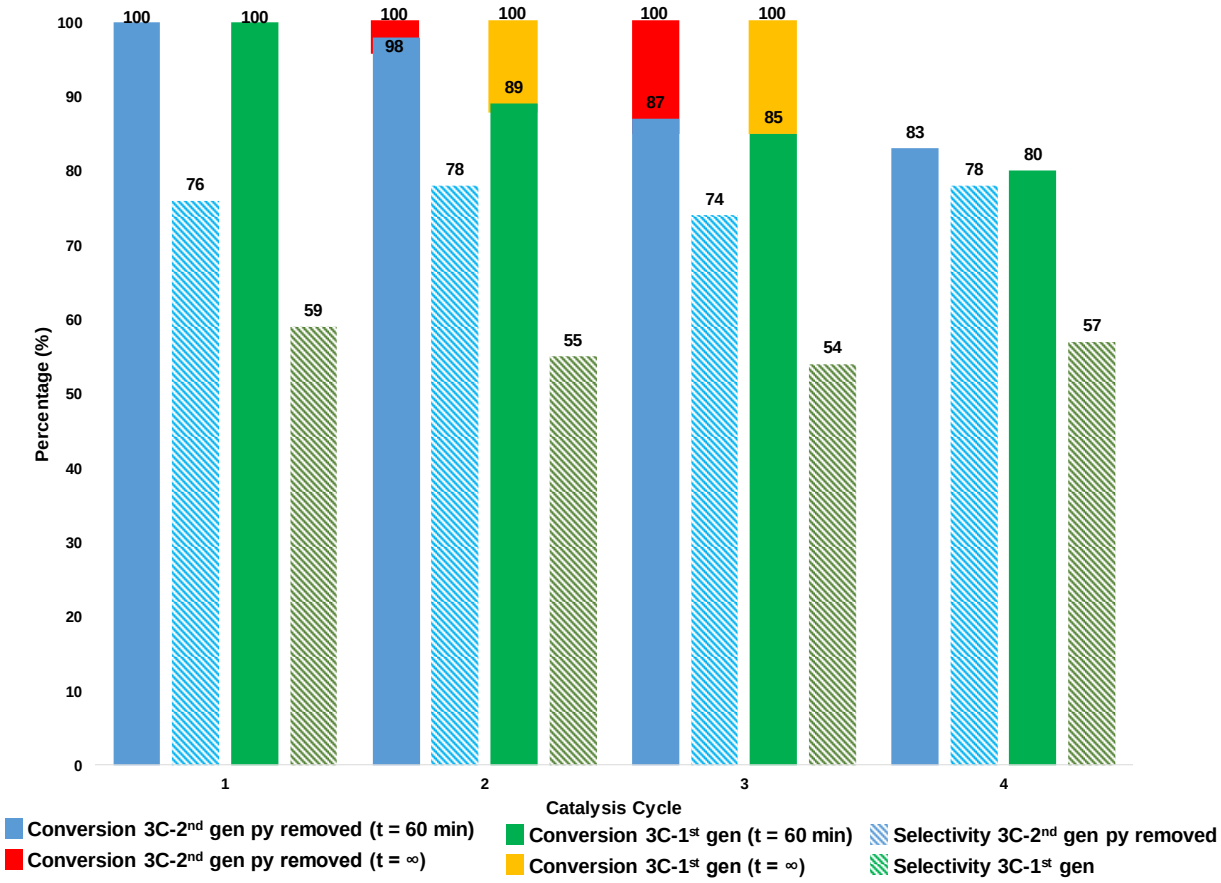

Figure 118 Recyclability of 3C-2nd gen py-removed (blue) and 3C-1st gen (green) in terms of conversion (solids) and selectivity (hashed). The additional bars (red and orange) on cycles 2 and 3 illustrate the percent conversion at infinity.

1. Reaction solutions are prepared according to the same catalysis procedure outlined in Chapter 2.
2. Three 50 µL aliquots are taken at t = 0, 5, 10 minutes via a calibrated Wheation™ Socorex Acura™ Single Channel Variable Volume Micropipetter.
3. Each aliquot is added directly to a quartz EPR tube and diluted with chloroform to approximately 5 mM of TMP. The aliquots are diluted with chloroform because the reaction solvent, acetonitrile, has a high dielectric constant which may decrease the signal to noise ratio.
4. The EPR tubes are then submerged in a dry ice/isopropanol bath to quench the reaction.
5. Each sample is then analyzed at room temperature using a Bruker EMX (X-band) Spectrometer.

After several attempts, the EPR spectra did not show any evidence for radical intermediates.

While it was not possible to identify the reaction intermediates responsible for the deep red color, three different side products have been isolated and identified via NMR.

Approximately fifteen minutes after the addition of peroxide, two sets of doubles appear in the NMR Spectra between 5.9 – 6.8 ppm, Figure 120. A brief investigation into these side products is conducted through collaboration with Dr. Carlos Steren. o reduce the complexity of the reaction mixture, internal standard is not used during the analysis of these side products.

Isolation of Alkylphenol Side Products

A 9 dram (~33 mL) vial containing a 10 mm stir bar and septa cap is weighed, tarred, and taken into a nitrogen atmosphere glovebox. Approximately 200 mg of catalyst, 4C-Ti-1st gen, is added to the vial, brought out of the glovebox, and reweighed to obtain an accurate measure of the amount of catalyst present. Calculations are carried out to determine the appropriate amount of acetonitrile, substrate, and aqueous hydrogen peroxide necessary to achieve the following mole ratios: 3.6 mM Ti (approximately 19 mL acetonitrile), 1 Ti : 30 TMP, and 1 Ti : 250 H_2O_2. Acetonitrile is added to the reaction vial via syringe followed by the addition of TMP. The reaction vial is then placed in a 65 ^{o}C oil bath and allowed to equilibrate to temperature for 30 minutes with constant stirring at 500 RPM. To initiate the reaction, 250 equivalents (~1.3 mL) of aqueous hydrogen peroxide is added to the reaction vial. The reaction is allowed to proceed for 60 minutes after which a 50 µL aliquot is taken and analyzed via NMR to ensure the side products are present,

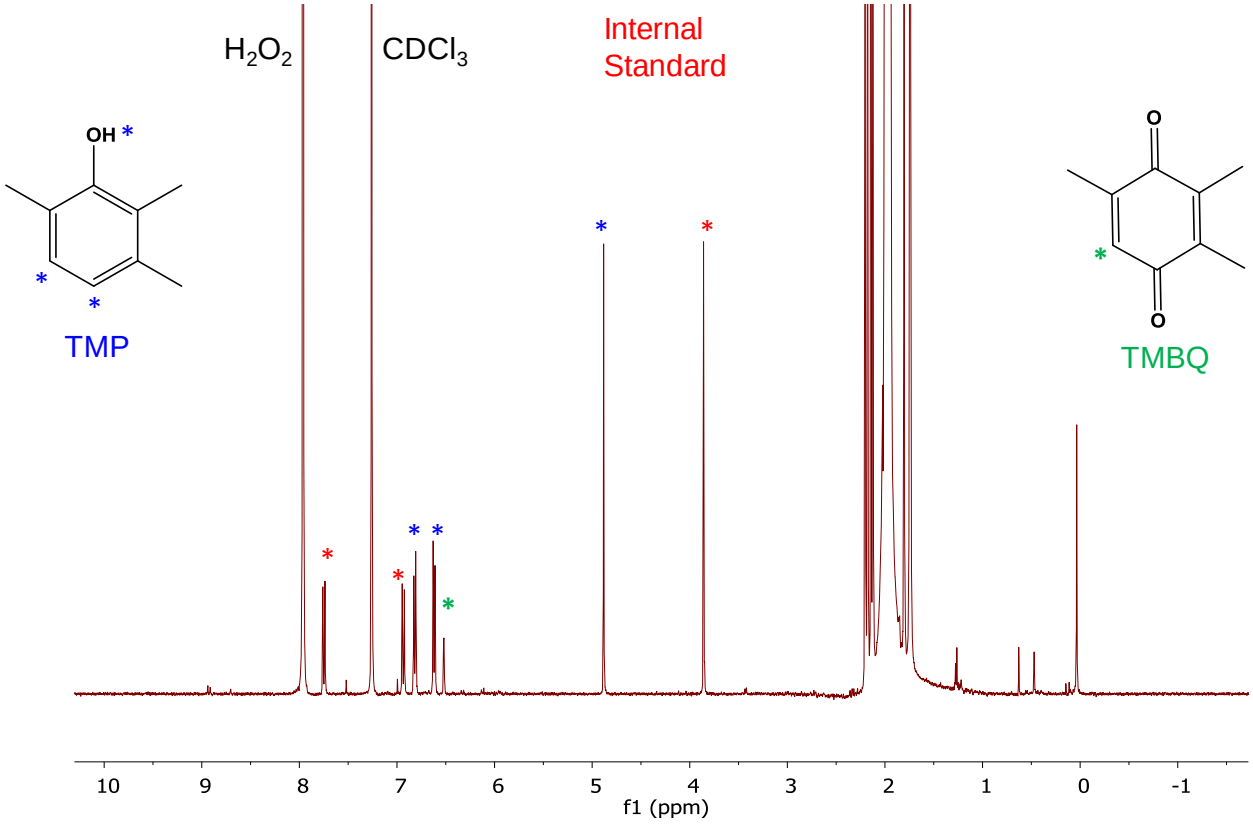

Figure 119 NMR spectrum of a typical aliquot take ten minutes after the addition of hydrogen peroxide.

Figure 120. For this study, 4C-Ti-1st gen catalysts were investigated, but all catalysts, regardless of connectivity or generation, exhibit the same byproducts.

After the side products are confirmed by NMR, the reaction is filtered to remove any solid material from the reaction solution. The solution is then concentrated by evaporating approximately 75% of the acetonitrile under vacuum. The remaining solution is added to a silica gel column prepared with hexane. The products are eluted with mixtures of hexane and ethyl acetate. There are three primary fractions that contain the unidentified molecules in the original reaction mixture. In the first fraction, both TMP and TMBQ are eluted along with a small amount of each side product followed by two additional fractions containing primarily isolated side products.

To better understand the side products, Dr. Steren analyzed the initial reaction aliquot and the three column fractions using several 1D and 2D NMR experiments: ^{1}H, ^{13}C, DOSY, NOESY, COSY, HMBC, and HSQC. By combining these techniques and using the ChemDraw Professional NMR predictor, the two major side products identified are most consistent with ortho-hydroxylation products. In addition to the two ortho-hydroxylated ketones, a third side product is identified as the dimerization of side product B through a Diels-Alder reaction. Figure 121 illustrates the proposed structure for the three side products identified in this NMR study. The following paragraphs aim to briefly describe the methodology used to identify these side products in the oxidation of trimethylphenol to trimethylbenzoquinone. The process will be described for only side product A, but this same process is followed to identify both product B and the dimerization product.

The aromatic and ring proton region of the H^{1} NMR spectrum for side product A is shown in Figure 122. The methyl region has been omitted due to large solvent peaks. From this spectrum, a clear set of doublets can be seen centered around ~6.72 ppm and 5.96 ppm along with a single feature at ~9.12 ppm. In addition to proton NMR, several other NMR experiments are investigated to identify the remainder of the molecule.

Heteronuclear Multiple Bond Correlation (HMBC) NMR experiments give correlations between carbons and protons separated by two or three bonds. The correlations between carbon and proton atoms over one bond are suppressed. The HMBC spectrum of the initial reaction

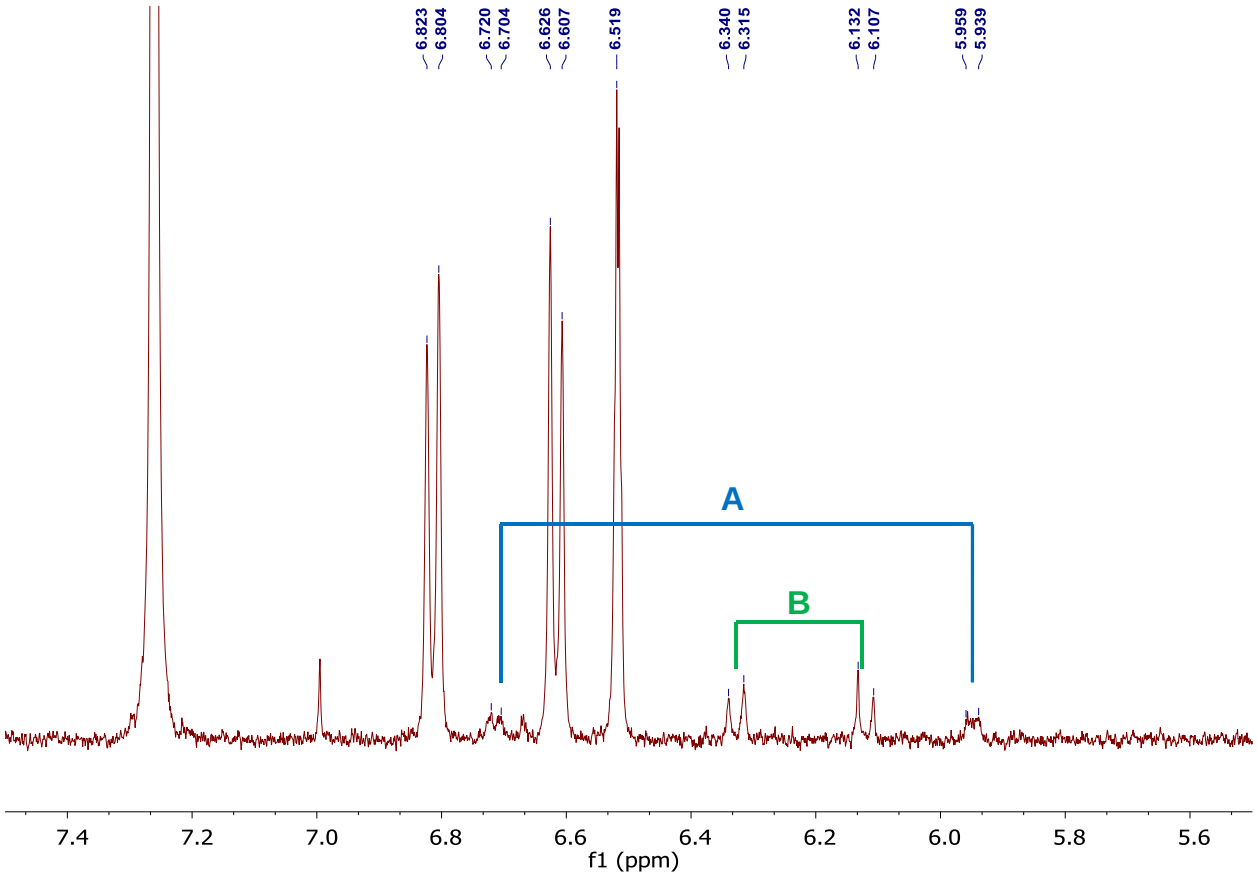

Figure 120 Typical NMR spectrum taken at 60 minutes after the addition of hydrogen peroxide illustration the two sets of doublets corresponding to the two major side products.

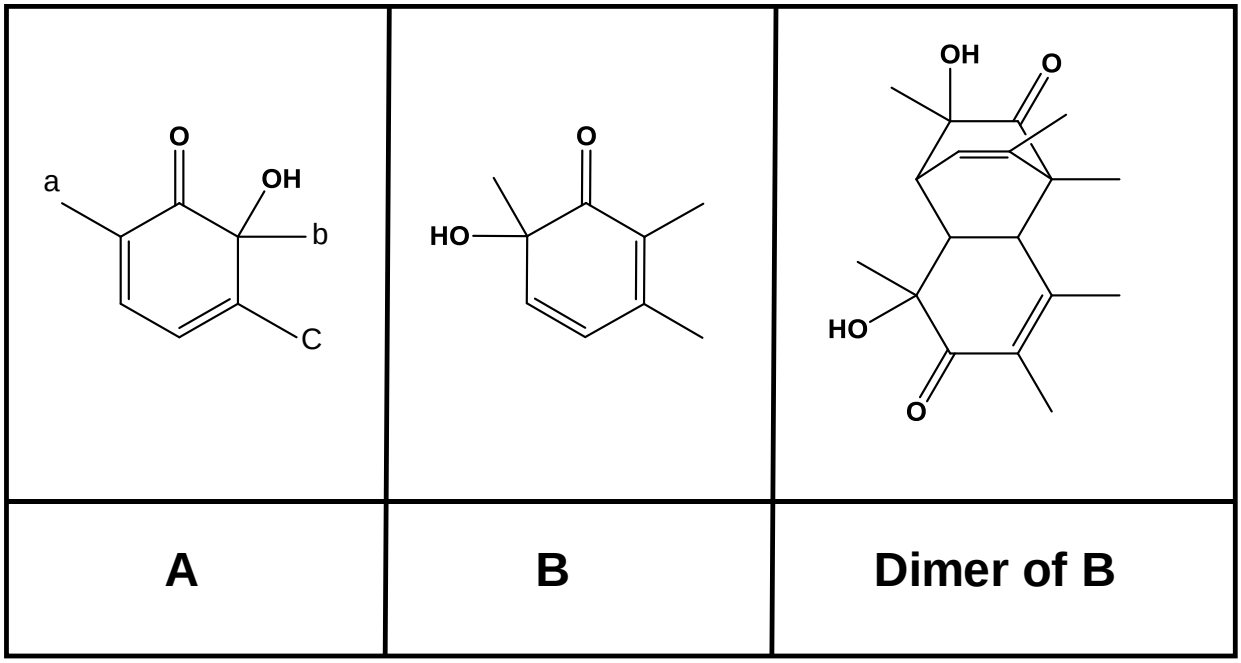

Figure 121 Proposed structures of three side products formed during the oxidation of TMP.

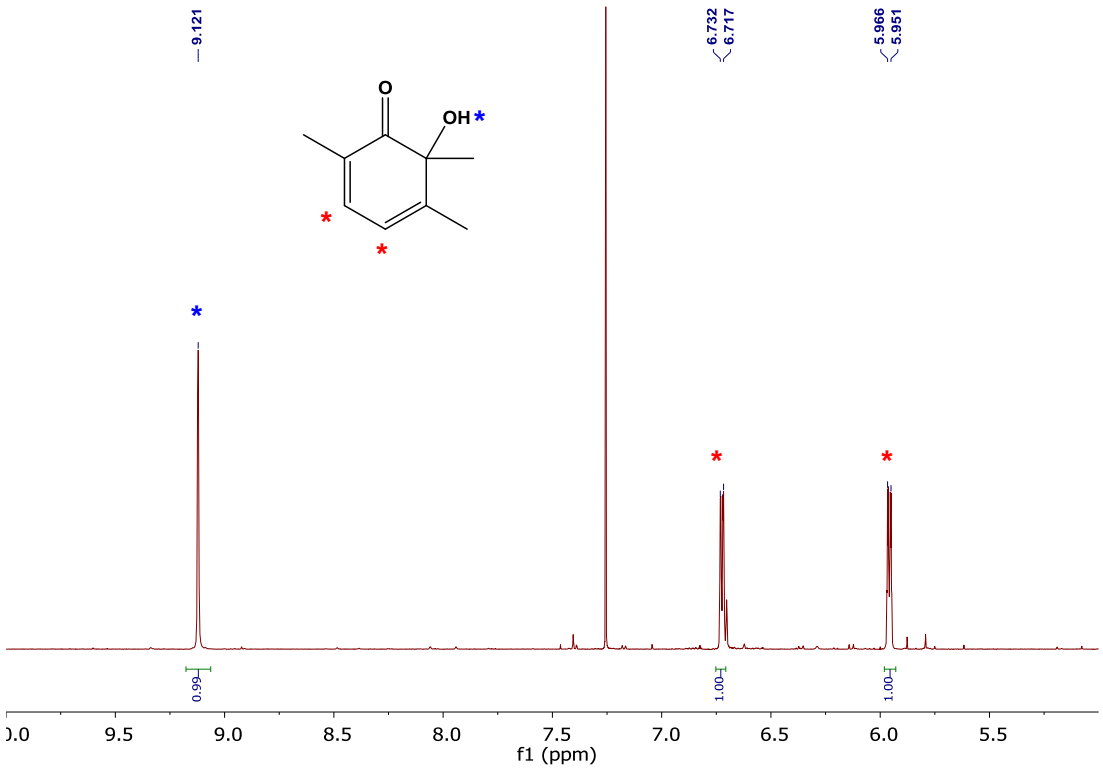

Figure 122 ^{1}H NMR spectrum of the isolated side product A.

mixture before separation, Figure 123, identifies four non-protonated carbons between 200 – 205 ppm connected to two methyl groups, a and b, on nearby carbons. Non-protonated carbon shifts at ~ 200 ppm are consistent with carbonyl groups. The methyl groups are predicted to be three carbons away and not four because there is a third methyl group, c, that shows an HMBC correlation to methyl b, but not to the carbon with a chemical shift of ~200 ppm.

A specific pattern is observed using HMBC, 88.1 ppm correlates to 203.5 ppm which correlates to 130.0 ppm, Figure 124. The chemical shift at 203.5 ppm is consistent with a carbonyl group and the chemical shift of 88.1 ppm corresponds to a carbon without double bonds but it is not consistent with a CH group with a connection to a methyl group. This carbon is determined to be connected to a methyl group and a hydroxyl group. In contrast, a chemical shift of 130.0 ppm indicates the carbon contains one double bond. Figure 125 illustrates the structural pattern consistent with these chemical shifts. The rest of the molecule is determined by combining the spectral interpretations from all other NMR experiments. The large coupling ($^4J_{HH}$) observed in side product A is due to significant electron density consistent with the alternating double bonds of structure A.

One concern with these side products is the possibility of the hydroxy groups being peroxy groups. However, ChemDraw Professional predicted a significant difference in the carbon shifts between a hydroxy group and a peroxy group. If a peroxy group is present on the ring, the carbon signal occurs at ~ 104 ppm while the hydroxy carbon signal is at 80 ppm. The HMBC experiment shows the carbon signal at ~84 ppm, most consistent with the substituent being a hydroxy group. In addition to HMBC, HSQC, COSY, and NOESY were used to identify the correlation of the byproducts, Figures 125-127 respectively.

By combining all the data collected from individual NMR experiments the structure of the ortho-hydroxylated ketone has been confirmed. Figure 129 and Table 37 illustrate the ^{13}C and ^1H assignments for product A. Product B was determined using the same procedure described above and its assignments and confirmed structure can be seen in Figure 130 and Table 38.

In addition to the monomeric byproducts, a third byproduct is identified. In the same column fraction as side product B, an additional ring proton is identified and assigned to the dimer of side product B, Figure 131. However, when Dr. Steren obtained additional NMR data for this fraction several days later, the major product was the dimer, Figure 132. We believe byproduct B undergoes a Diels-Alder reaction producing the corresponding dimer after the catalyst has been

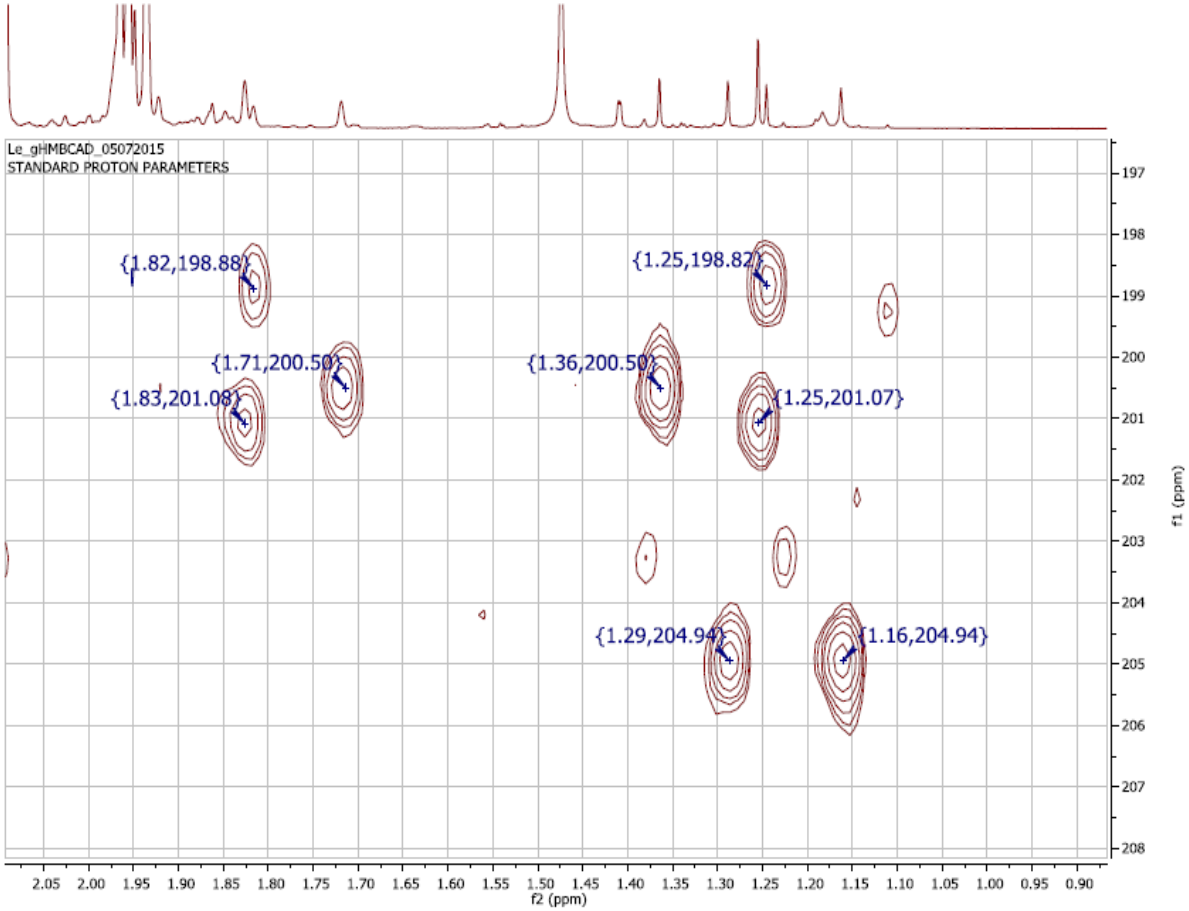

Figure 123 HMBC spectrum of reaction mixture before separation identifying four different non-protonated carbons.

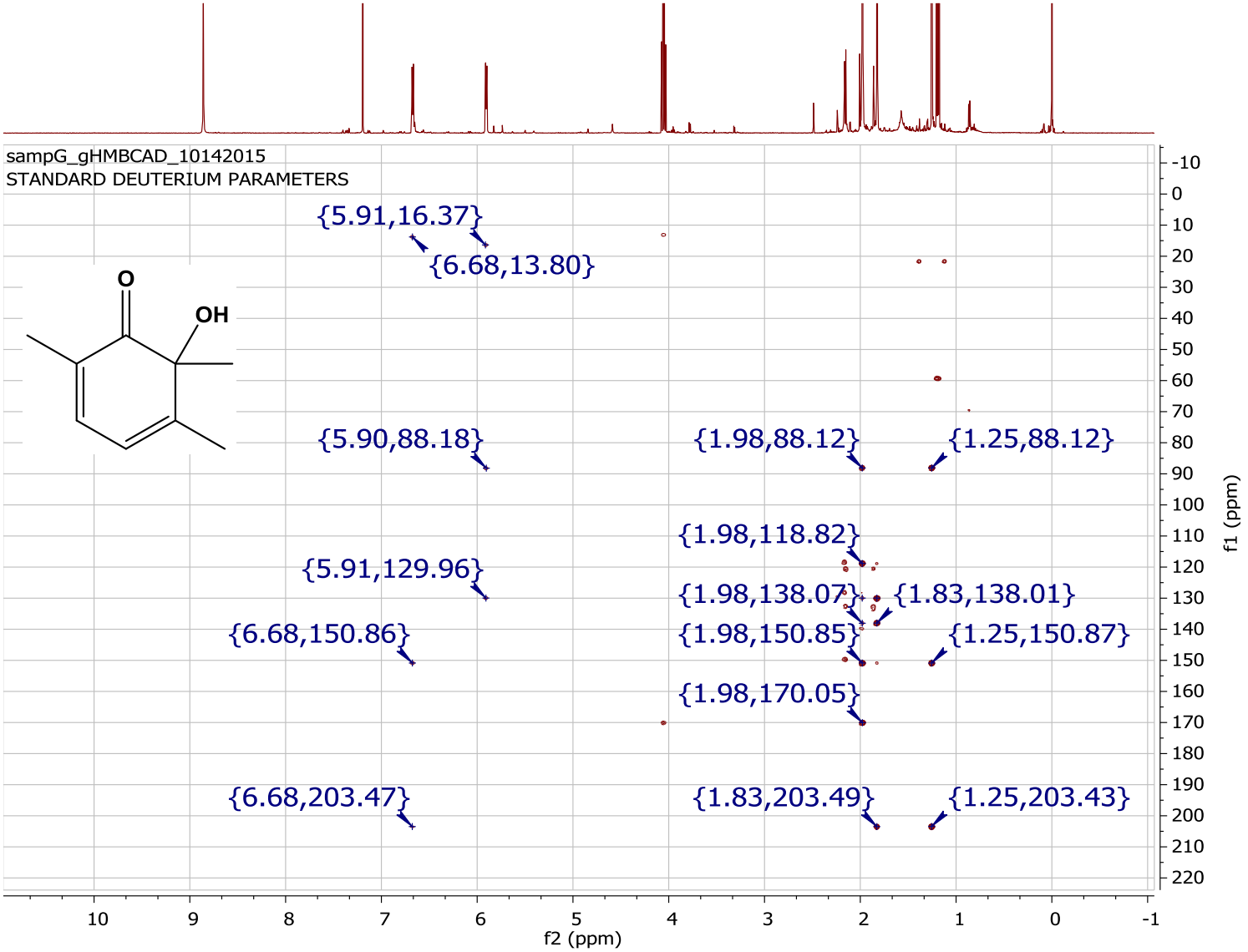

Figure 124 HMBC spectrum of side product A.

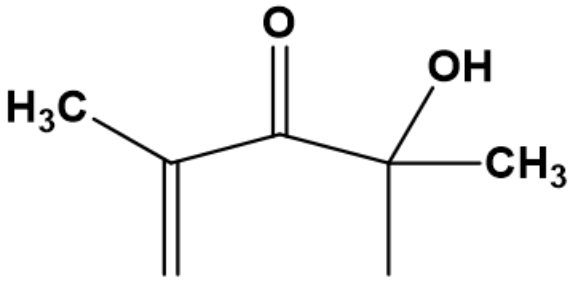

Figure 125 Structural pattern confirmed through HMBC experiments.

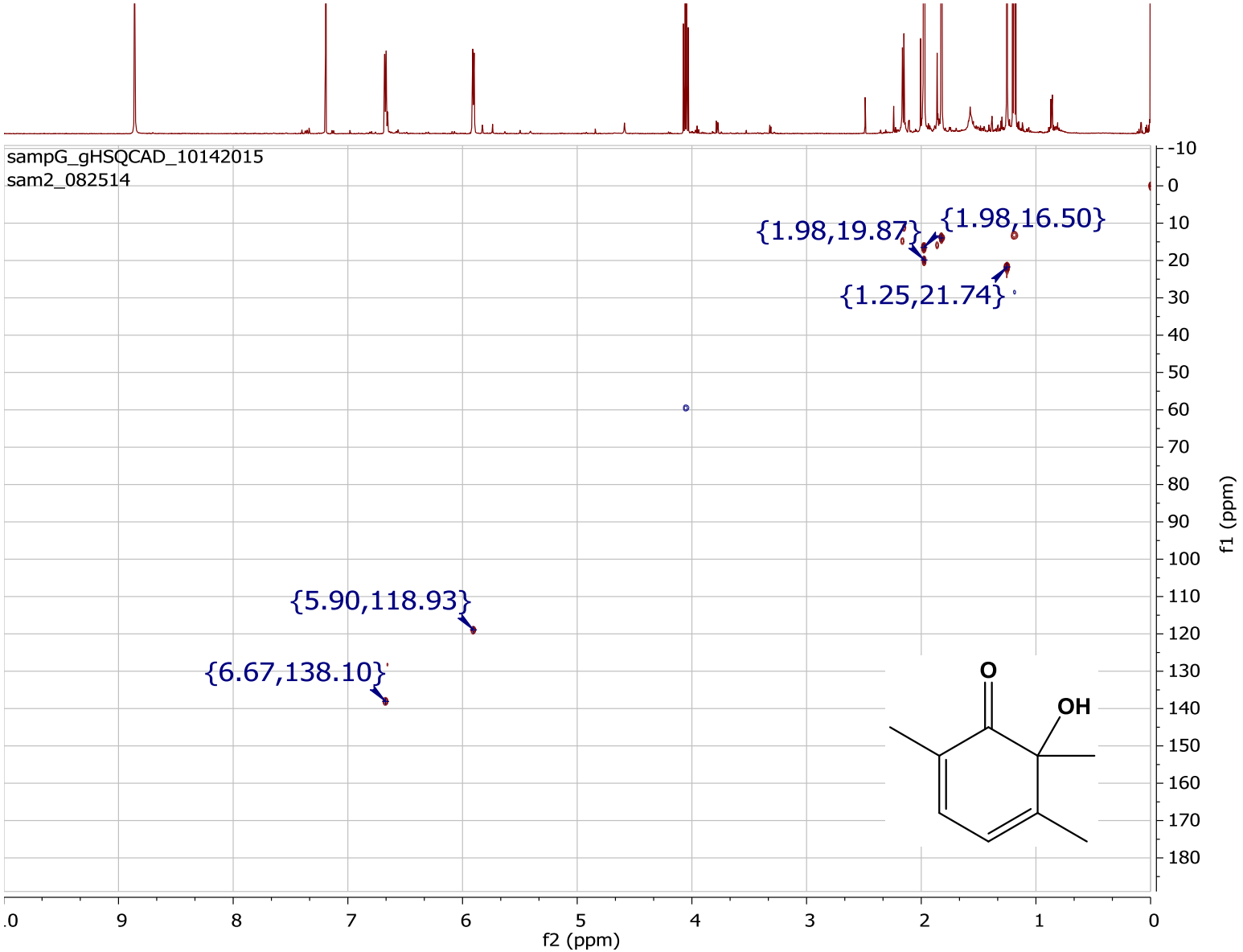

Figure 126 HSQC of side product A.

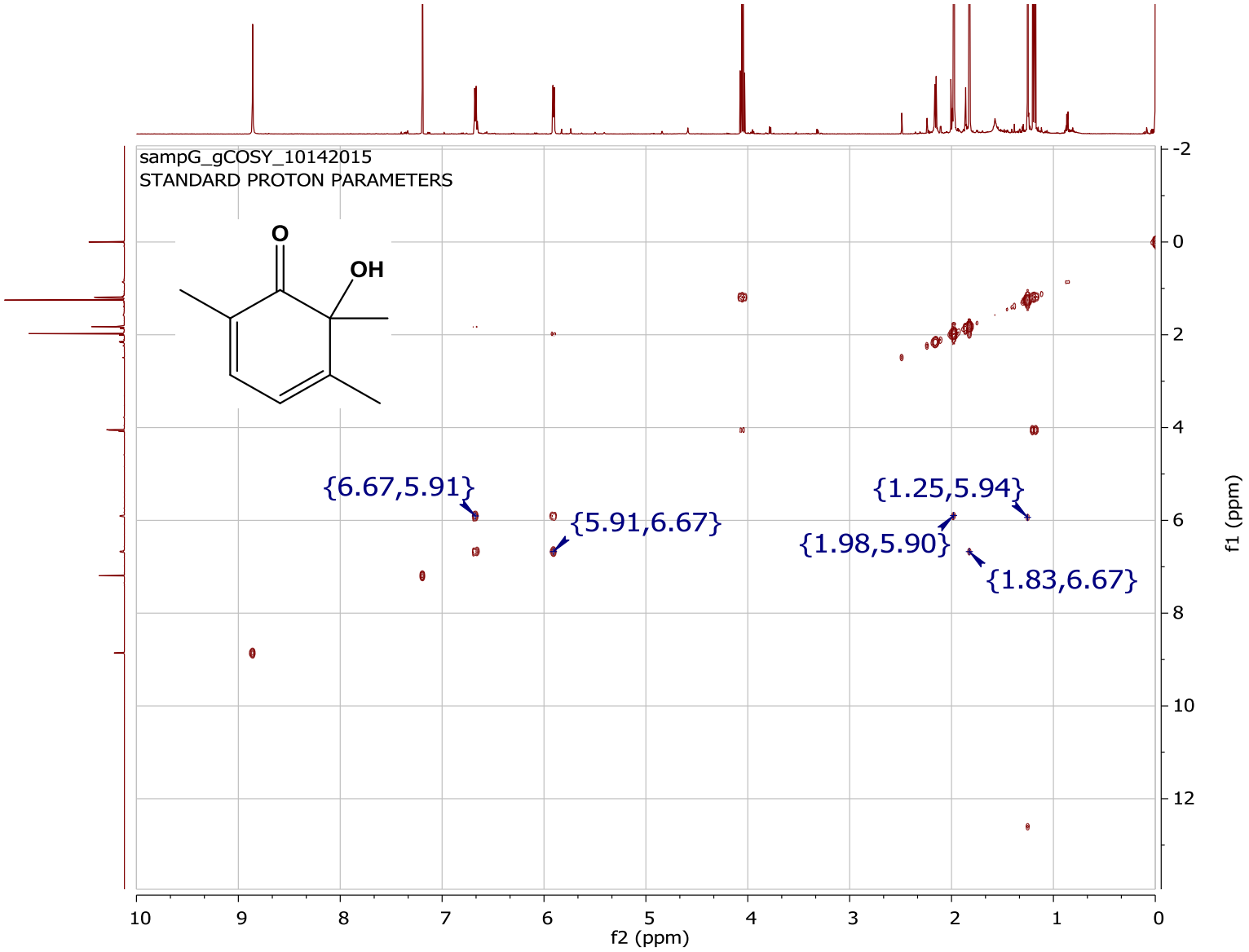

Figure 127 COSY spectrum of side product A.

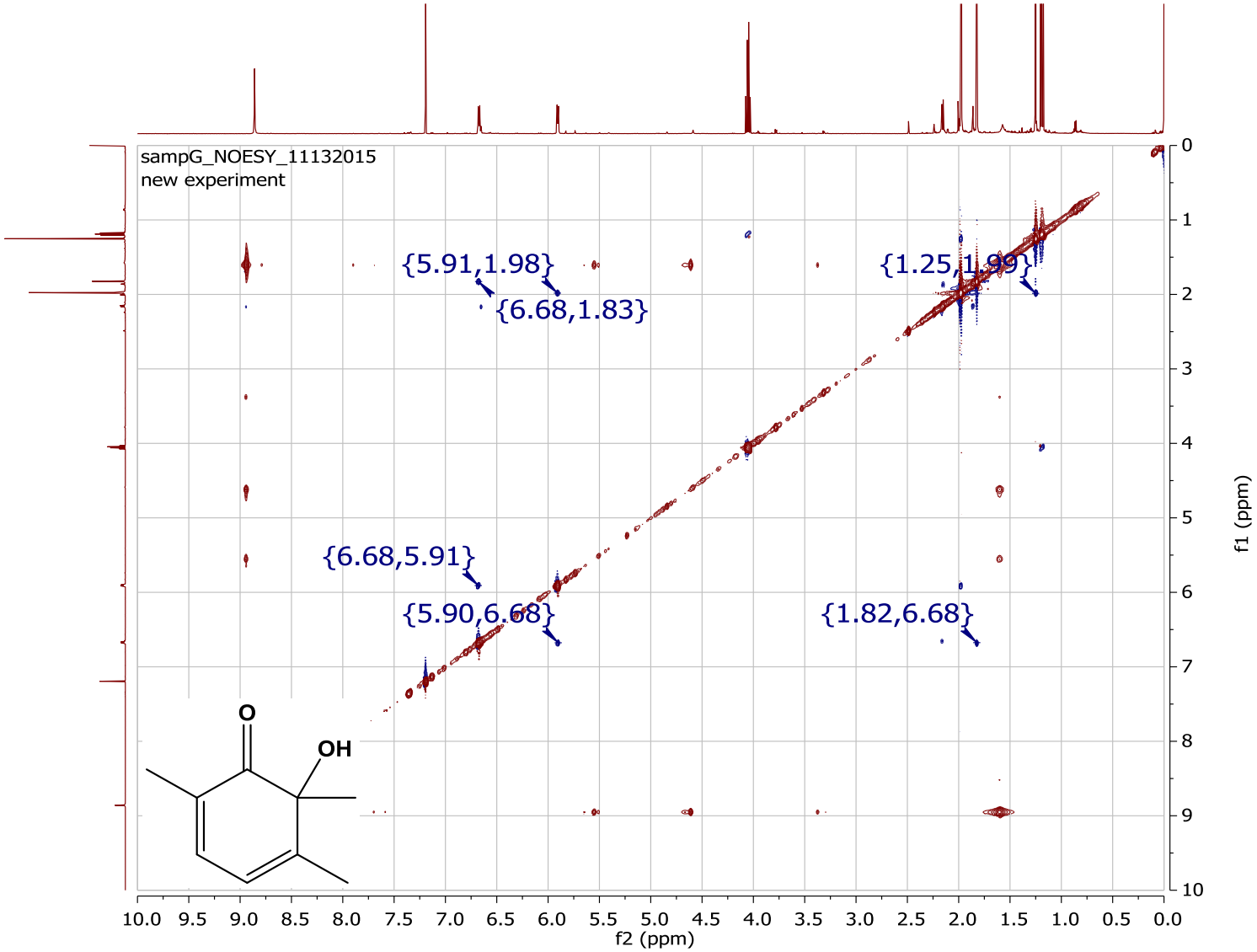

Figure 128 NOESY spectrum of side product A.

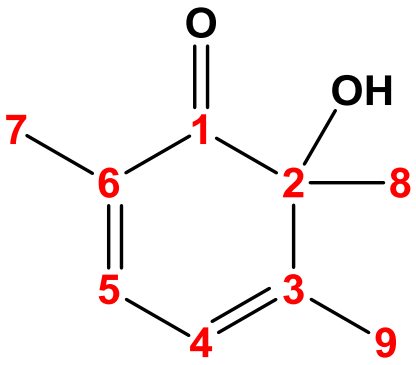

Figure 129 Side product A with number carbon atoms.

Table 37 Carbon and proton assignments for side product A.

C and H #	^{13}C shift (ppm)	^{1}H shift (ppm)
1	203.5	-
2	88.1	-
3	150.9	-
4	118.9	5.90
5	138.1	6.67
6	130.0	-
7	13.95	1.83
8	21.74	1.25
9	16.50	1.98
OH	-	9.12

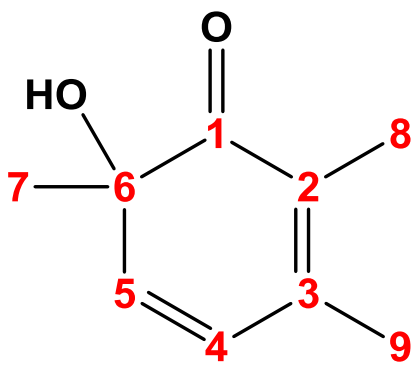

Figure 130 Structure of side product B with numbered carbon atoms.

Table 38 Carbon and proton assignments for side product B.

C and H #	^{13}C shift (ppm)	^{1}H shift (ppm)
1	198.8	-
2	128.4	-
3	145.6	-
4	127.3	6.06
5	138.4	6.24
6	81.31	-
7	21.8	1.17
8	13.7	1.82
9	14.8	1.97
OH	-	10.46

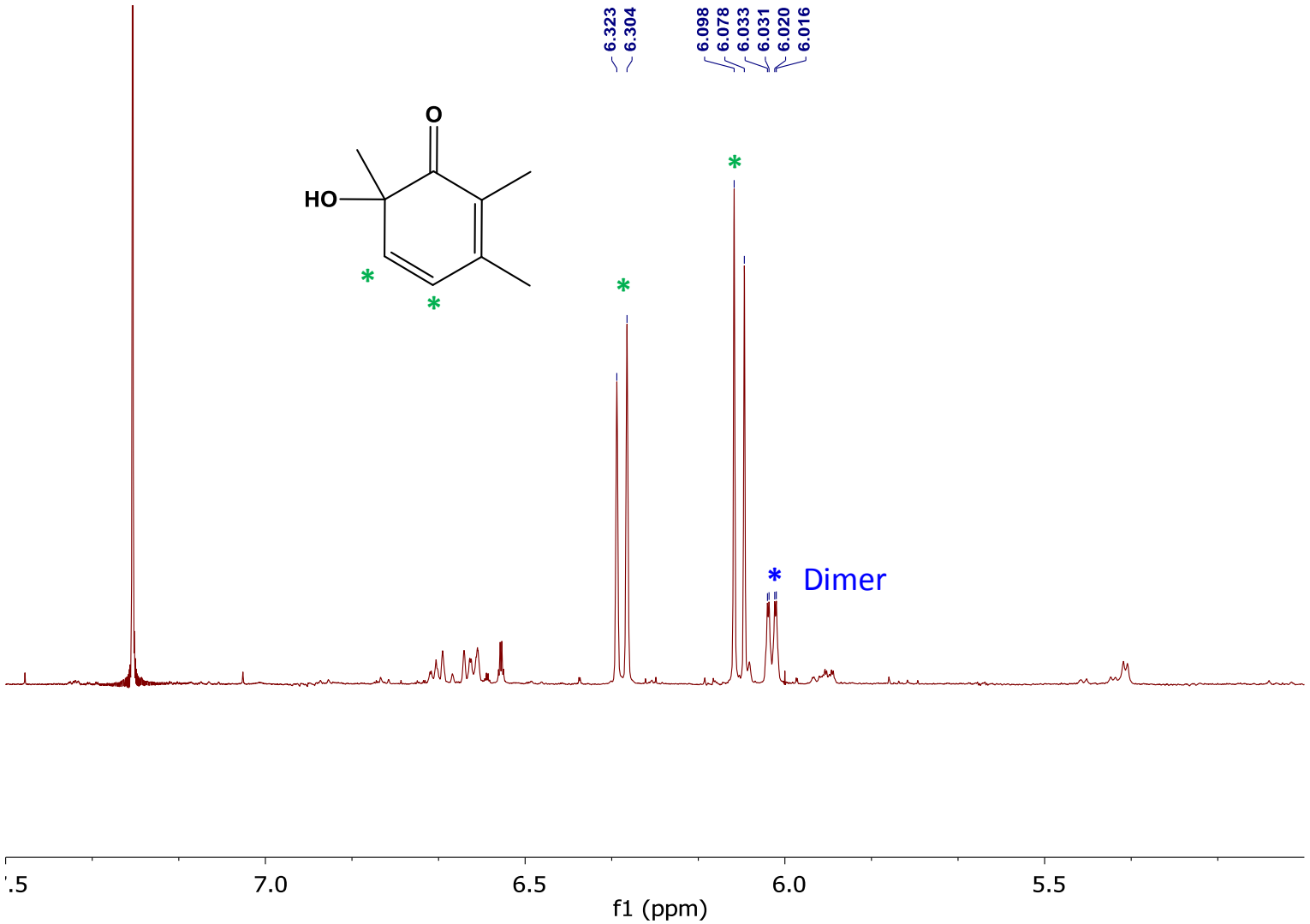

Figure 131 NMR spectrum of column fraction containing both side product B and its corresponding dimer.

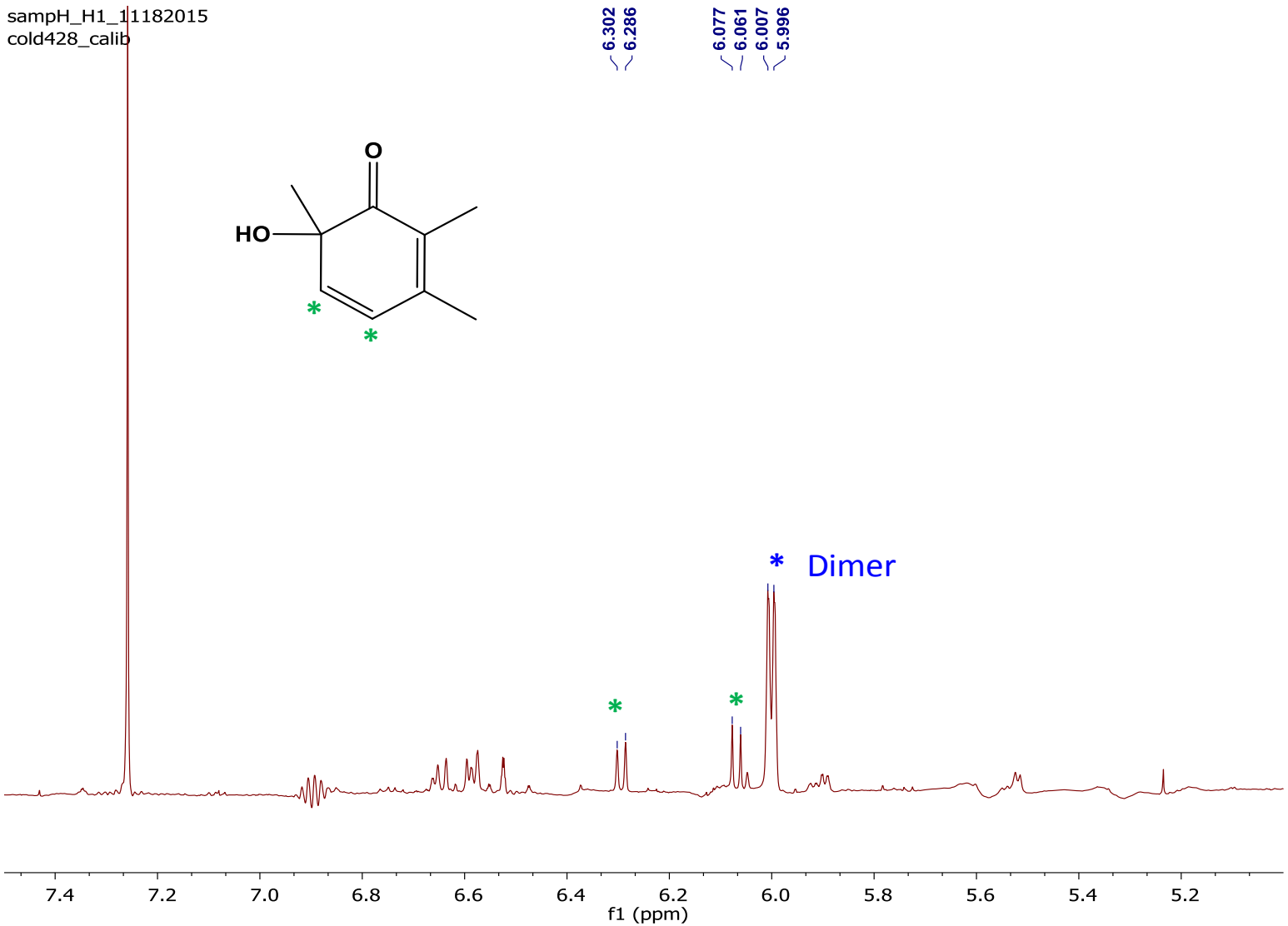

Figure 132 Proton spectrum illustration increase in dimer concentration and decrease in the concentration of side product B.

removed from the reaction mixture. Figure 133 and Table 39 illustrate the assigned carbon and proton shifts from all NMR experiments for the dimer.

To conclude the investigation of byproducts, GC-MS data is obtained on both column fractions containing side products A and B. GC-MS analyses suggest hydroxy groups and not peroxy groups. The molecular ion peaks for both aliquots containing the ortho-substituted quinones have a mass to charge ratio of 152. If the groups were peroxy groups and not hydroxy groups, the molecular ion peaks would be 168 m/z. Therefore, the primary side products are most consistent with ortho-hydroxylated rings.

It is important to note that after TMP has been consumed, these side products begin to decompose into side products not detectable via NMR spectroscopy. At the end of the reaction, the mass balance ranges between 55-70% depending on the catalyst used. However, during the reaction, if all three side products are added to the mass balance, the maximum reaches approximately 90% for all reactions.

General Conclusion

The intermediates responsible for the color change in reaction solution during the oxidation of TMP to TMBQ remain undetermined. However, three side products have been identified through the use of NMR spectroscopy and GC-MS. These side product are most consistent with orhto-hydroxylated ketones and the a dimerization product from one of the ortho-hydroxylated ketones. While they contribute a significant amount to the mass balance during the reaction, they are consumed by peroxide after the substrate, TMP, has been completely reacted. At this time, it is unclear as to what compounds these byproducts are converted.

Chapter V Conclusion

Isolated mononuclear titanium catalysts with targeted connectivities and both equilibrium and non-equilibrium geometries in silicate matrices are employed as catalysts in the oxidation of phenols to benzoquinone. High conversions and fair selectivities are exhibited by all catalysts, but the connectivities of the active site to the matrix play a critical role in both the activity and stability of these catalysts. Two connected titanium centers in these matrices are not stable to catalysis conditions and exhibit significant leaching of titanium into the solution where it is also an active catalyst.

In addition to connectivity, the geometry of the active site influences catalytic activity as well. While the energy needed to remove blocking ligands from the 4C-Ti sites may have allowed

the imprinted geometry to relax back to a distorted tetrahedral, the 3C-Ti-2nd gen py removed catalysts exhibited much higher catalytic activity than its tetrahedral analog. This notion of imprinting the active site opens new synthetic approaches to tailoring heterogeneous catalysts.

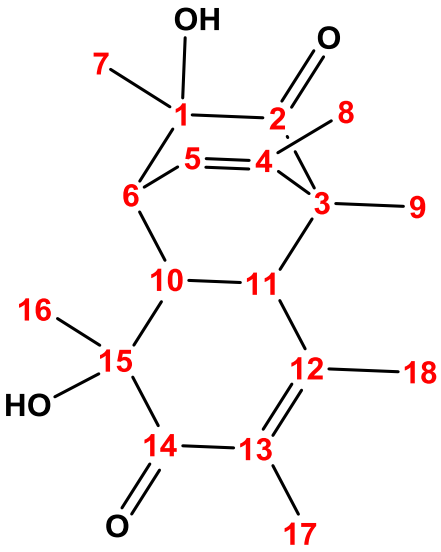

Figure 133 Proposed structure of the dimer with numbered carbon atoms.

Table 39 Carbon and proton assignments for the dimer byproduct.

C and H # (Ring 1)	^{13}C Shift (ppm)	^{1}H shift (ppm)	C and H # (Ring 2)	^{13}C Shift (ppm)	^{1}H shift (ppm)
1	**82.3**	**-**	**10**	**40.7**	**2.93**
2	**206.8**	**-**	**11**	**48.0**	**2.87**
3	**56.3**	**-**	**12**	**148.4**	**-**
4	**137.4**	**-**	**13**	**132.2**	**-**
5	**132.2**	**6.0**	**14**	**203.7**	**-**
6	**40.5**	**3.39**	**15**	**83.5**	**-**
7	**20.7**	**1.25**	**16**	**26.6**	**1.36**
8	**18.3**	**1.39**	**17**	**13.2**	**1.71**
9	**14.1**	**1.14**	**18**	**23.4**	**1.91**
OH	**-**	**-**	**OH**	**-**	**-**

Chapter VI: First and Second Generation as Epoxidation Catalysts

Introduction

Catalysis plays an important role in our everyday lives from the production of fuels to fine chemicals. One of the most important catalytic reactions is selective oxidation.[122] One selective oxidation reaction that has gained a tremendous amount of attention in heterogeneous catalysis is epoxidation. Epoxides are advantageous in organic synthesis because they can readily be converted to diols, amino alcohols, etc. which are necessary for a variety of consumer products.[123] Over the last few decades, numerous catalysts have been investigates as selective oxidation catalysts but titanosilicates are the most promising as epoxidation catalysts.[122] Titanosilicates have shown to be highly active and selective as epoxidation catalysts with a variety of oxidants.[122,124,125] Literature suggest that the active species responsible for the observed high activity and selectivity are isolated tetrahedral Ti(IV) sites.[122]

One of the most studied epoxidation reactions is the conversion of cyclohexene to cyclohexene oxide. Figure 134 illustrates the epoxidation of cyclohexene with cumene hydroperoxide. Unfortunately, it is also one of the most difficult reactions to investigate because it frequently undergoes allylic oxidation and/or epoxide ring opening.[126] Studies have shown that solvent plays a critical role in reducing these unwanted side reactions and ultimately increase selectivity of the desired epoxide.[124,127]

The titanosilicate catalysts synthesized in this work were investigated as potential catalysts for the oxidation of phenols to benzoquinones. However, in contrast to hydroxylation, isolated tetrahedral Ti(IV) site have been reported as the active sites responsible for the high activity and selectivity presented by titanosilicates in epoxidation reactions.[122] Therefore, the catalysts synthesized in Chapter 5 have the potential to provide a structure function relationship between catalytic activity and the geometry of the active site along with its connectivity to the silicate matrix.

Catalytic Protocol

A 9 dram (~33 mL) vial with a septa cap is tared and taken into a nitrogen atmosphere glovebox. Approximately 50 mg of catalysts is then added, capped and reweighed outside of the glovebox to determine the exact amount of catalyst. The approximate volume of decane (typically around 1.5 mL) needed to create a 6mM titanium solution is added to the reaction vial via syringe. Calculations are performed to determine the exact amount of oxidant (cumene hydroperoxide)

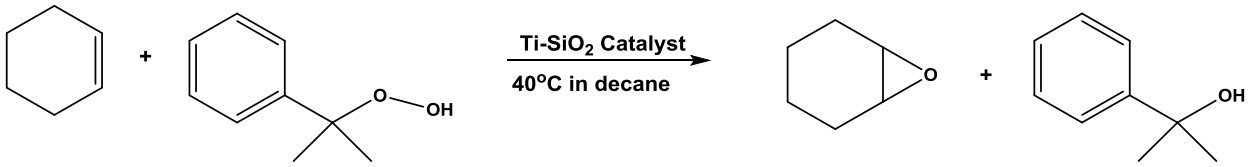

Figure 134 Illustration of the epoxidation of cyclohexene to cyclohexene oxide with cumene hydroperoxide in the presence of a titanosilicate catalyst.

and substrate (cyclohexene) need for the following molar ratio 1 : 25 : 250; Ti : cyclohexene : cumene hydroperoxide. The amounts of decane, cyclohexene, and cumene hydroperoxide are always dependent on the amount of catalyst and its weight percent titanium. The titanium weight percent is always determined by ICP-OES. Following the addition of solvent, 261 µL of mesitylene (internal standard) is added to the reaction via a calibrated Wheaton™ Socorex Acura™ 835 Pipet along with a 10 mm stir bar. The calculated volume of cyclohexene is subsequently added in the same manor. The vial is then capped and placed in a 40°C oil bath. The calculated amount of cumene hydroperoxide is added to a separate vial, capped and placed in the same oil bath. Both vials are allowed to equilibrate to the reaction temperature for 20 minutes. After the solutions reach equilibrium temperature, the cumene hydroperoxide is removed from the oil bath, wiped clean (to avoid contamination with silicon oil), and poured into the reaction vial to initiate the conversion of cyclohexene to cyclohexene oxide. The reaction is allowed to stir for 2 minutes before the first aliquot is taken. This initial mixing allows for the solution to become homogenous. At this point, a 50 µL aliquot is taken and added to a clean NMR tube followed by 600 µL of deuterated chloroform. The NMR tube is then capped and quenched in a dry ice/isopropanol bath. Six additional aliquots are taken over a two hour time period following the same protocol.

Characterization of Epoxidation Aliquots

Proton NMR spectroscopy is used to characterize each aliquot of the reaction. The NMR spectra are collected using a Varian VNMRS 500 MHz under the following conditions: 25°C, 16 scans, 10 second relaxation delay, and 45° pulse. It is important to note that the relaxation delay has been investigate and no significant changes in integrations are observed between a 10 second and 20 second delay. Figure 135 is an example of a typical NMR spectrum of a reaction aliquot. Each spectrum is analyzed using MestraNova V1.2 NMR. The workup protocol is performed as follows:

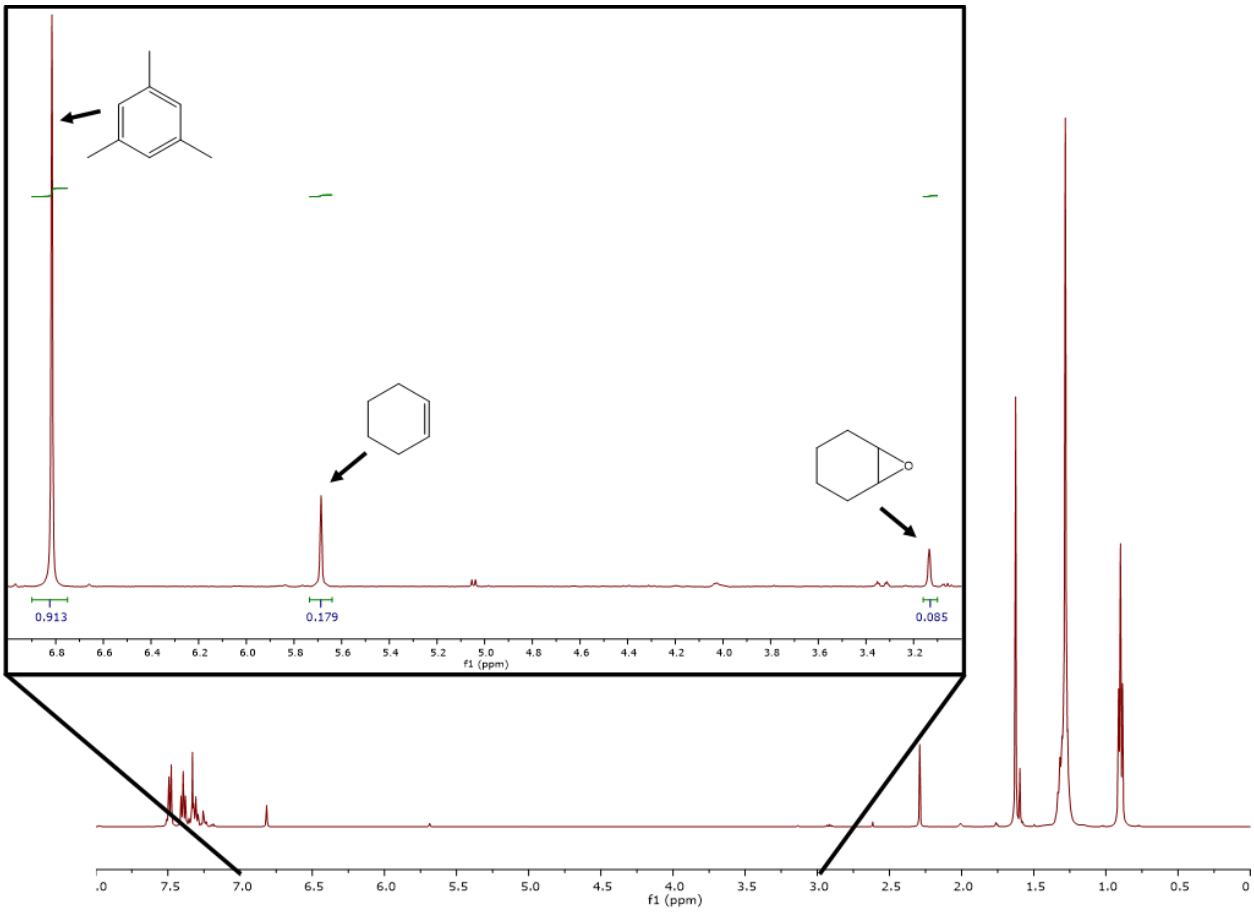

Figure 135 An example of a typical NMR spectrum form an aliquot of the epoxidation reaction. Figure obtained from ref [128].

- Window set to 10 – ppm
- Auto phased
    - Followed by manual phase corrections
- Baseline Corrected (Whittaker smoothing)
- Line broadening 0.5 Hz
- Integrated per Table 40
- Mesitylene peak at 6.812 ppm set to an integration of three
- Kinetic plots generated.

Results and Discussion of First Generation Titanosilicate Catalysts

The results of the epoxidation of cyclohexene with cumene hydroperoxide characterized by first generation titanosilicates along with two literature catalysts and a titanium free catalyst are summarized in Table 41.

The results of the titanium free platform demonstrate that neither the mesoporous silicate matrix nor the remaining tin sites catalyze the epoxidation of cyclohexene. In contrast, the two literature catalysts, TS-1 and grafted-Ti-MCM-41, along with first generation Ti catalysts synthesized in this work exhibit catalytic activity indicating titanium is the active species responsible for the conversion of cyclohexene to cyclohexene oxide.

The catalytic activities and selectivities of the first generation catalysts synthesized in this work are better than both TS-1 and grafted-Ti-MCM-41. TS-1 proves to be the least active and least selectivity catalyst investigated. The lack of significant conversion is a result of

Table 40 Proton integrations of the epoxidation of cyclohexene to cyclohexene oxide.

Compound	Integration Region	Number of Proton
Mesitylene	6.900 – 6.750	3
Cyclohexene	5.735 – 5.640	2
Cyclohexene Oxide	3.160 – 3.100	2
Cumene Hydroperoxide	1.660 – 1.609	6
Cumyl Alcohol	1.608 – 1.585	6

the microporous structure preventing diffusion of substrate through the pores and reaching the active site. In contrast, grafted-Ti-MCM-41 is a mesoporous heterogeneous catalyst with multiple types of active sites. The activity and selectivity of this material is better than TS-1 illustrating the need for a mesoporous structure. However, it shows to be less active in comparison to the activities of the 3C-Ti and 2C-Ti catalysts and is less selective than all three first generation catalysts. In comparison to grafted-Ti-MCM-41, the first generation catalysts synthesized in this work are single-single site catalysts and may explain the increase in selectivity. Because these catalysts are single-site, turn over frequencies can be used to directly characterize the active site.

Each first generation catalyst presents its own catalytic properties. It can be seen that the 2C-Ti catalyst is more active than the 3C-Ti catalyst which is more active than the 4C-Ti catalyst. Similar to phenol oxidation, one explanation for the observed differences is the accessibility of the active sites. In a 2C- first generation catalyst, the titanium active site is bound to the silicate matrix by only two linkages. The two additional ligands are terminating alkoxy ligands that are free to move around the active site or exchange in order for substrate to bind. The 3C-Ti site has three Ti-O-Si linkages to the silicate matrix and one free alkoxy ligand while the 4C-Ti center is

Table 41 Summary of catalytic properties for cyclohexene epoxidation of first generation titanosilicates, TS-1, grafted Ti-MCM-41, and a Ti free platform.

Catalysts	TOF (5 min) (± 0.02)	%Conversion (60 min) (± 5)	%Selectivity (60 min) (± 5)	%Yield (60 min) (± 5)
TS-1	0.02	4	39	1.6
G-Ti-MCM-41 ±	-	26	75	20
Ti-Free Platform	0	0	0	0
2C-1st Gen	0.18	52	100	52
3C-1st Gen	0.08	42	100	42
4C-1st Gen	0.05	15	94	14

± TOF is not an accurate representation because the catalyst is not single-site and the number of catalytically active sites cannot be determined.

completely embedded in the matrix by for Ti-O-Si linkages and thus limits substrate binding. The differences in catalytic activity may be attributed to the accessibility of the active site.

It has been proposed in the literature that the first step in this reaction mechanism is the coordination of peroxide with subsequent breaking of a Ti-O-Si linkage, Figure 136.[124] This step is potentially a high-energy step based on both electronic and steric effects. The free alkoxy ligands of both the 2C- and 3C- titanium catalysts potentially reduce the energy needed for this initial step in comparison to the 4C-Ti catalyst. In addition, the matrix around the active site may also influence the binding of oxidant and substrate. With the 4C-Ti centers being completely embedded in the matrix, the robust building block cage around the active center may increase the energy barrier needed for oxidant binding and ultimately lead to the observed reduction in activity.

Results and Discussion of Second Generation Titanosilicate Catalysts

The literature suggests that tetrahedral Ti(IV) sites are responsible for the high activity and selectivity demonstrated by titanosilicates in epoxidation reactions. The synthetic strategy presented in this work has allowed us to alter the geometry around the titanium active sites to geometries other than tetrahedral. First generation catalysts have targeted connectivities from the active site to the matrix while second generation catalysts have the same tailored connectivities but the active sites have geometries other than tetrahedral. Therefore, comparing the catalytic activities of first and second generation catalysts in the epoxidation of cyclohexene may illustrate how geometry of the active site effects catalytic activity and selectivity.

Table 42 summarizes the catalytic activity of first and second generation titanosilicate catalysts with and without blocking ligand present for the targeted connectivities, 2C-Ti (green), 3C-Ti (blue), and 4C-Ti (purple). Several different comparisons can be made from this table and will be described below.

A relationship between the connectivity of first generation catalysts and catalytic activity has been described above, 2C-1st gen >3C-1st gen > 4C-1st gen. This same trend is seen when comparing the TOFs of catalysts with the same altered geometry and different connectivities, i.e., 2C-2nd gen with py_2 > 3C-2nd gen with py_2 > 4C-2nd gen with py_2 and 2C-2nd gen py removed > 2C-2nd gen py removed > 4C-2nd gen py removed. This is additional evidence that the number of linkages to the matrix plays a crucial role in the catalytic activity of titanosilicates.

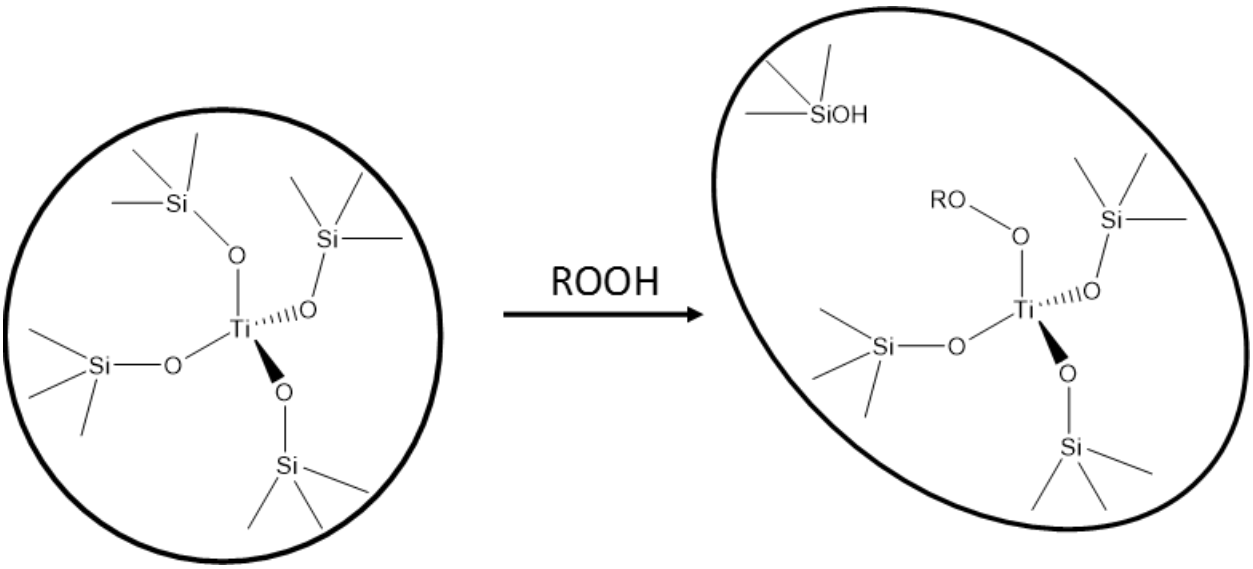

Figure 136 Illustration of a 4C-Ti fully embedded site reacting with peroxide and ultimately breaking a Ti-O-Si linkage.

Table 42 Summary of catalytic activity for all catalysts synthesized in this work for the epoxidation of cyclohexene.

Catalysts	TOF (5 min) (± 0.02)	%Conversion (60 min) (± 5)	%Selectivity (60 min) (± 5)	%Yield (60 min) (± 5)
2C-1st Gen	0.18	52	100	52
2C-2nd Gen with py_2	0.12	38	100	38
2C-2nd Gen py removed	.13	45	100	45
3C-1st Gen	0.08	42	100	42
3C-2nd Gen with py_2	0.09	18	94	17
3C-2nd Gen py removed	0.09	12	100	12
4C-1st Gen	0.05	15	94	14
4C-2nd Gen with py_2	0.01	35	42	15
4C-2nd Gen py removed	0.07	30	100	30

However, a major goal of this research is to investigate the effect of active site geometry on the activity and selectivity of oxidation reactions. Therefore, catalysts with the same connectivity but altered geometries are also compared, i.e. 2C-1st gen compared to 2C-2nd gen with py_2 and 2C-2nd gen py removed. The same comparisons are made for the families of 3C-Ti and 4C-Ti catalyst. Based on turn over frequencies, percent conversions, and selectivities, catalysts with 2-connections to the matrix are not affected by changes in active site geometries. One explanation for this observation is that the 2C-Ti-2nd gen catalysts have tetrahedral active sites similar to 2C-1st gen. In the case of 2C-2nd gen pyridine removed, during the heating process to remove pyridine, it is plausible the two free alkoxy ligands re-arrange to stabilize the loss of blocking ligand. While the active site is still bound to the silicate matrix, there are only two linkages locked in place and the resulting geometry is most likely a distorted tetrahedral. Similarly, during the reaction with 2C-2nd gen with py_2, pyridine blocking ligands are lost and detected in the NMR spectra of the aliquots. Therefore, it is possible that as pyridine is lost during the reaction, the alkoxy ligands are re-arranging to form a pseudo-tetrahedral geometry around the active site.

A second explanation for the observed catalytic activity is that the geometry of the active site does not affect the catalytic properties in cyclohexene epoxidation.

Similar to 2C- catalysts, the TOFs for 3C- catalysts regardless of active site geometry are identical. In Chapter 5, the catalytic activities observed for 3C- catalyst were significant different between 3C-1st gen and 3C-2nd gen py removed. The 3C-2nd gen py removed catalyst was approximately three times more active than 3C-1st gen catalyst suggesting the geometry of the active site was indeed altered to a more open accessible site. Therefore, it can be concluded that the geometry of the active site does not play a critical role in the epoxidation of cyclohexene.

In the case of 4-connected catalysts, two catalysts present similar activities and selectivities, 4C-1st gen and 4C-2nd gen removed, while the activity and selectivity of 4C-2nd gen with py_2 is significantly reduced. The decrease in catalytic activity and selectivity of the 4C-2nd gen with py_2 catalyst is most likely a result of catalyst poisoning. Catalyst poisoning occurs when a molecule is present in the catalytic reaction and it absorbs to the active site reducing the catalytic activity and sometimes the selectivity of the desired product.[65] In Chapter 5, the loss of blocking ligands after the second cross-linking was extensively studied. It was concluded that the amount of pyridine lost at room temperature was a function of connectivity, i.e., 2C lost more pyridine than 3C- which lost more blocking ligand than 4C-. Less than 10% of the pyridine was removed from the 4C-titanium active sites. Therefore, it is likely that the remaining pyridine blocking ligands of

4C-2nd gen with py_2 catalysts are acting as a catalyst poison and thus decreasing its activity and selectivity.

Similar to the 3C- catalysts, the 4C-1st gen and 4C-2nd gen py removed catalysts exhibited similar activities and selectivities in the epoxidation of cyclohexene to cyclohexene oxide. Again, in the oxidation of phenols to benzoquinones, the 4C-2nd gen py removed catalyst was more active than the 4C-1st gen catalysts suggesting the geometries around the active site were different. Therefore, it can be concluded that geometry does not play an active role in the epoxidation of cyclohexene.

Stability of 2-Connected Catalysts

As previously described, a major concern with heterogeneous catalysts is leaching of the active site from the matrix yielding a homogenous catalyst in solution. Information about the longevity and recyclability of a catalyst can ultimately be studied by investigating the notion of leaching.

In Chapter 5, leaching of both first and second generation catalysts was investigated by catalytic activity and ICP analyses. In contrast to epoxidation reactions presented here, alkylphenols were converted to their corresponding benzoquinones using aqueous hydrogen peroxide. It was concluded that both first and second generation catalysts with three and four connections to the matrix were stable and did not leach under these reaction conditions. However, the 2C-Ti catalysts, regardless of their coordination geometry leached from the matrix and were shown to be active species in solution. In contrast, to aqueous hydrogen peroxide, organic peroxides have been shown to be less likely to cause leaching of the metal active site. However, it is still of vital importance to investigate the stability of atomically dispersed titanosilicates under these epoxidation reaction conditions.

Leaching studies followed the same procedure outlined in Chapter 5. However, recovery of the remaining solid catalysts after filtration has not been investigated. The family of 2C-Ti catalysts have been studied as model catalysts. Table 43 summarizes the results of leaching study for 2C-Ti catalysts. It can be seen that all three 2C-Ti catalysts are stable heterogenous catalysts with cumeme hydroperoxide as the oxidant. Because the 2C catalysts exhibited excellent stability under these reaction conditions, it was assumed that both 4C- Ti and 3C-Ti catalysts are stable as well. In addition, the 3C-Ti and 4C-Ti catalysts were shown to be stable under typically more harsh reactions conditions, i.e., H_2O_2. Furthermore, leaching studies for first

Table 43 Summary of the leaching studies for the family of 2C-Ti.

Catalysts	mmol Cyclohexene After filtration	mmol Cylcohexne after 1 hour	mmol Cyclohexene oxide after filtration	mmol Cyclohexene oxide after1 hour	% Ti in solution (ICP) (± 2%)
2C-1st Gen	1.13	1.11	0.66	0.65	0
2C-2nd Gen with py_2	0.200	0.198	0.519	.521	0.5
2C-2nd Gen py removed	0.141	0.144	0.148	0.147	0

generation 4C-Ti and 3C-Ti with cumene hydroperoxide were previously investigated by Dr. Austin Albert and were found to be stable.[128]

Summary

Two families of single-site titanium catalysts with target connectivities and tailored geometries have been synthesized and investigated for their uses as olefin epoxidation catalysts, specifically epoxidation of cyclohexene, with cumene hydroperoxide. All catalysts, except for the 4C-2nd generation catalysts with py_2 (6-coordinate, saturated active site), were activity and highly selective for the conversion of cyclohexene to cyclohexene oxide. A relationship between connectivity and activity has been established, 2C-Ti > 3C-Ti > 4C-Ti. The reactions were investigated at 40 ^{0} C because the 2C-Ti catalyzed reactions occur very quickly. However, the 3C-Ti and 4C-Ti are much slower. In future studies, it would be beneficial to increase the reaction temperature to investigate the catalytic properties of both 3C-Ti and 4C-Ti.

In comparison to phenol oxidation, the geometry of the active site does not enhance or inhibit the catalytic activity or selectivity in this epoxidation reaction. The difference between phenol oxidation and epoxidation can be explained by the difference in their proposed mechanisms. The literature suggests that the oxidation of phenols to benzoquinones follow a radical mechanism while epoxidation reactions are a result of an atom transfer mechanism.[129-131] Because these reactions follow different mechanisms, it is not surprising that active site geometries play different roles depending on the reaction being investigated.

Furthermore, under epoxidation reaction conditions, the catalysts synthesized in this work were proven to be stable, i.e., the active site did not leach from the matrix. After filtering the catalyst from the reaction mixture, catalytic activity ceased. In addition, trace amounts of titanium metal were not detected in the mother liquor by elemental analysis.

Chapter VII: Research Conclusions and Future Work

General Conclusion

This dissertation describes the synthesis and characterization of novel single-site heterogeneous catalysts. This work was a continuation from an ongoing research project to develop new synthetic strategies for targeting the local environment of metal active sites in heterogeneous catalysis. The local environment in this works includes coordination geometry and connectivity of both the active metal center and the surrounding support matrix.

First Generation Catalysts with Targeted Connectivities

The synthesis of targeted single-site titanosilicates relies heavily on a molecular building block and a synthetic strategy. Octatrimethyltin sphererosilicate was employed as the molecular building block along with the method of sequential additions to incorporate isolated single-site titanium centers into the silicate matrices. By reacting mononuclear tetrahedral titanium precursors in a limiting amount, all titanium active sites have the same number of linkages to the matrix. These oligomers are then further crosslinked with dichlorodimethylsilane to build a robust rigid matrix around the active site. The resulting catalysts possess high surface areas and contain only one type of active site therefore meeting the single-site criterion.

Through several independent characterization techniques, the titanium active sites of these matrices are best described as tetrahedral therefore maintaining the geometry of the initial titanium precursor.

The catalytic properties of these first generation catalysts were studied for the oxidation of phenols to benzoquinones and the epoxidation of cyclohexene to cyclohexene oxide Distinct catalytic activities were observed for each unique titanium connectivity under identical reaction conditions for both phenol oxidation and epoxidation. It was concluded that as the number of linkages to the matrix increases the energy barrier for substrate and or oxidant binding increases and ultimately the catalytic activity decreases, i.e., 4C- < 3C- < 2C-.

The proposed initial step in mechanism for both phenol oxidation and cyclohexene epoxidation is a high energy step that involves the binding of oxidant to the titanium active site while simultaneously breaking a Ti-O-Si linkage. One possible way to overcome this high energy step would be to synthesize catalytic active sites coordination geometries that are more open and therefore more accessible than the preferred tetrahedral geometry, e.g., square planar.

Second Generation Catalysts with Targeted Connectivities and Altered Geometries

This same synthetic strategy was applied to target titanosilicate catalysts with geometries other than tetrahedral while maintaining unique connectivities. By adding blocking ligand to the mononuclear precursors before the second dose crosslinking, catalyst with targeted connectivities and non-tetrahedral geometries were synthesized. While difficult to determine the exact geometries of these new second generation catalysts, there catalytic activities suggest the active sites are indeed more open.

The catalytic properties of second generation catalysts were studied for both the oxidation of phenols and the epoxidation of cyclohexene. A relationship between active site geometry and activity was established for both the 4C-Ti and 3C-Ti catalysts in the oxidation of phenols to benzoquinones. As the geometry of the active site became more open, the activity increased while maintaining decent selectivity, Figure 137. Unfortunately, the 2C-Ti catalyst leached form the matrices in the presence of aqueous hydrogen peroxide. On the contrary, both families of 3C-Ti and 4C-Ti catalysts were determined to be stable in the presence of aqueous hydrogen peroxide. This is of utmost importance because the list of titanosilicates stable under aqueous hydrogen peroxide is very limited and while not all connectivities exhibited stability, two have and they can be applied as catalysts in the field of green chemistry.

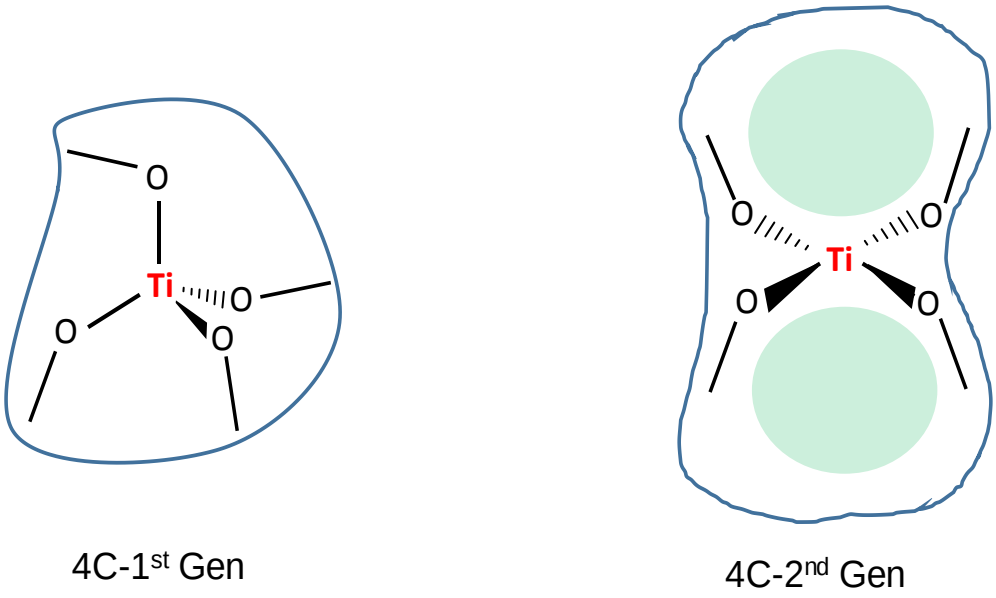

Figure 137 Illustration of imprinting the catalytic center of a 4C-Ti to a more open site.

In contrast to phenol oxidation, the geometry of the active site did not play role in cyclohexene epoxidation. This observed difference is thought to occur because phenol oxidation and epoxidation occur via different reaction mechanisms. These results demonstrate that with carefully designed synthetic strategies, heterogeneous catalysts can be tailored at the atomic level similar to homogeneous catalysts.

Future Work

Removal of Tin

In Chapter 4, several different passivation techniques were investigated, but each attempt had a major flaw. Because the tin centers did not play an active role in catalysis, the efforts to remove Sn from the matrix were put on hold. However, it was concluded that Sn has been leached from the matrix becoming a homogeneous species in solution. While it is uncertain the source of tin (trapped trimethyltin chloride or unreacted tin-cube corners), it still poses problems in industrial application. Therefore, the need for a passivation step to remove Sn from the matrix still exists.

One passivation technique that exhibited some success was the use of methyl-*tert*-butyl ether. This step was ultimately abandoned due to the production of HCl, but Sn was removed from the matrix. The reaction was dried at 80 ^{0} C overnight under vacuum to remove volatile trimethyltin chloride. These reaction conditions are more harsh than the conditions described by Wakabayashi *et.al.[103]* By optimizing the reaction conditions, MTBE may prove to be a viable passivation technique. In addition, passivation with chlorosilanes may provide a solution to removing unreacted tin groups from the matrix.

Addition of Blocking Ligand

In Chapter 5, the idea of third generation catalysts was briefly investigated. A third generation catalyst is one in which a tetrahedral precursor is initially employed during the first dose to establish the connectivity. Once the connectivity has been established blocking ligand is added to imprint the geometry around the active site. Unlike after the second cross-linking, the oligomers synthesized in the first dose are flexible allowing the geometry to be altered. It may be advantageous to pursue this synthetic approach because there is excess blocking ligand present during synthesis. Much effort has been spent on ensuring the blocking ligand remained bound to the titanium active site throughout synthesis without adding excess ligand. However, by first establishing connectivity and then adding excess blocking ligand, if trace amounts of acid are

present, the excess blocking ligand will act as an acid scavenger and there should be minimal loss of blocking ligand during synthesis.

Toluene was used as the reaction solvent throughout the synthesis of both first and second generation catalysts. One approach to minimize the lack of blocking ligand is to use the blocking ligand as the reaction solvent (in this case pyridine). It is predicted that catalysts synthesized in this manor will have the same properties as second generation catalysts with blocking ligand.

In addition to a third generation with blocking ligand, by heating the catalysts, the blocking ligands can be removed. Investigation into the catalytic and spectroscopic properties of these catalysts may provide more information about the active site of second generation catalysts without blocking ligand. If the properties are the same, it suggests the time at which the geometry is altered (precursor or after establishing connectivity) produces the same catalysts. On the other hand, if the catalytic properties are different than the analogous second generation catalysts, it may suggest premature loss of blocking ligand in the case of the second generation catalyst.

Furthermore, the catalytic properties of second generation catalysts with blocking ligand removed after the first dose should also be investigated. These catalysts are predicted to have similar properties to first generation catalysts. Before the second cross-linking reaction, the oligomers are flexible. If the blocking ligands are removed before the robust matrix is built around the active site, the catalytic center is projected to stabilize to the lowest energy geometry, tetrahedral.

Cis Precursors

Catalysts are an important part of our day to day lives from the production of fuels to high value chemicals. Because of their significance, the need for designing new and better catalysts is constantly on the rise. The general methodology developed by the Barnes group for synthesizing catalysts with not only targeted connectivities, but also specific non-equilibrium geometries offers a new and simple way to synthesize single-site heterogeneous catalysts. Therefore, research into geometries other than tetrahedral, octahedral, and square planar may be beneficial. The precursors in this work are best described six coordinate pseudo-octahedral complexes. The bispyridine and bistetrahydrofuran precursors were best described as *trans* complexes. One may consider investigating the properties of *cis* complexes. If the blocking ligands are in the cis position, after their removal, even larger substrates may gain access to the active site. Additionally, the geometry of the active site would be best described as see-saw if

the surround matrix remained fixed in their right angle relationships, Figure 138. This unique geometry is potentially unstable and theoretically highly reactive.

Polynuclear- Active sites

Kholdeeva and coworkers have investigated the use of grafted titanosilicates for the oxidation of alkylphenols to their corresponding benzoquinones. They have shown that polynuclear titanium clusters are more active and selective than their corresponding mononuclear catalysts, Figure 139 assuming the titanium species remain isolated at low enough titanium concentrations. Figure 140 shows the proposed mechanism for the oxidation of phenols with polynuclear titanium active sites.

The building block approach in combination with the method of sequential additions have proven to be capable to in cooperate different titanium precursors with different geometries and connectivities into the matrix. Similarly, this strategy can be applied to targeting nuclearity, mononuclear versus polynuclear, figure #. By utilizing titanium precursor with different nuclearity, Figure 141 (dinuclear Ti_2, trinuclear Ti_3, and tetranuclear Ti_4,) an entire new family of catalyst may be synthesized. By investigating the catalytic properties of these potential single-site polynuclear titanium catalysts in comparison to mononuclear titanium, a clearer understanding of the actual mechanism of alkylphenol oxidation may be obtained.

Epoxidation with Aqueous H_2O_2

The high activity and selectivity observed for titanosilicates in epoxidation is a result of isolated tetrahedral Ti(IV) sites.[122] TS-1 is one of the only known titanosilicates to be stable in the presence of aqueous hydrogen peroxide, but it is severely limited by its microporosity.[132] In contrast to TS-1, grafted mesoporous titanosilicates have shown high activity and selectivity for a wide range of substrates, but are limited to the use of alkyl hydroperoxides as an oxidant.[122] In the presence of aqueous H_2O_2, they have shown to rapidly undergo hydrolysis deactivating the catalyst.

The catalysts synthesized in this work, are isolated atomically dispersed amorphous titanosilicates with mesoporoisty and tailored connectivities to the matrix. These catalysts have shown to be highly active and selective with larger molecule in comparison to TS-1, e.g. trimethylphenol and cyclohexene. The catalysts with three and four connections to the matrix have shown to be stable with aqueous hydrogen peroxide in the oxidation of phenols to benzoquinones. Therefore, these catalysts are excellent candidates as epoxidation catalysts with

aqueous hydrogen peroxide. Aqueous hydrogen peroxide is favored in industry because it is considered a “green” oxidant because its only byproduct is water.[133]

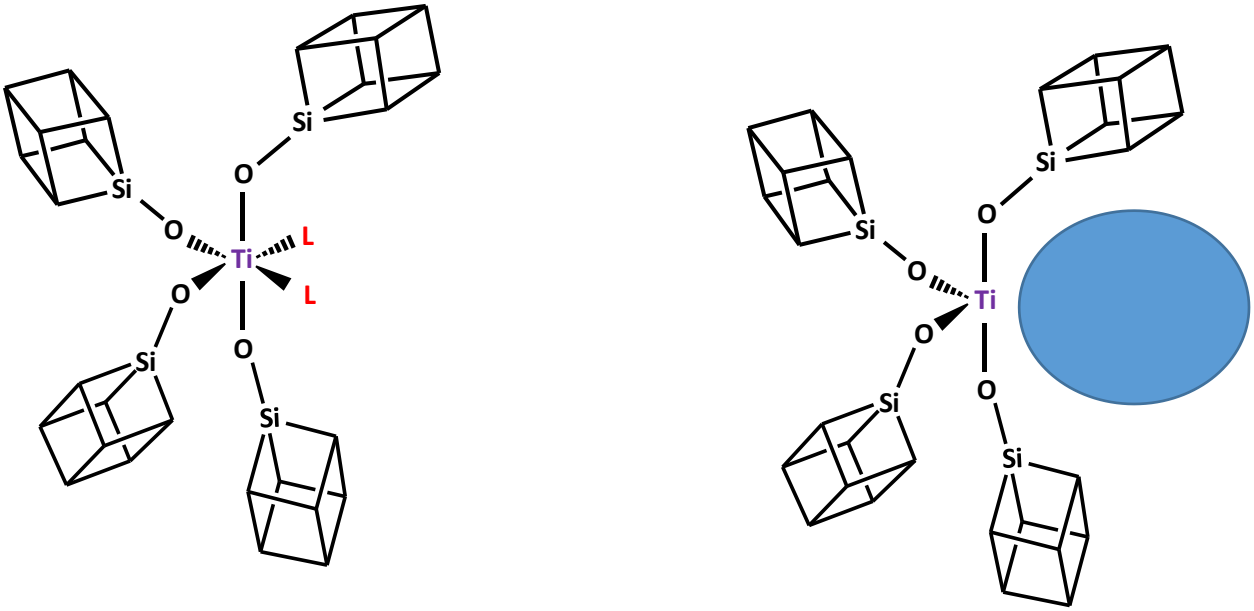

Figure 138 Proposed structures of a 4C-2nd gen catalysts imprinted with a cis molecular precursor (left) and the proposed resulting active site after the active site is locked into the matrix and blocking ligand are removed (right).

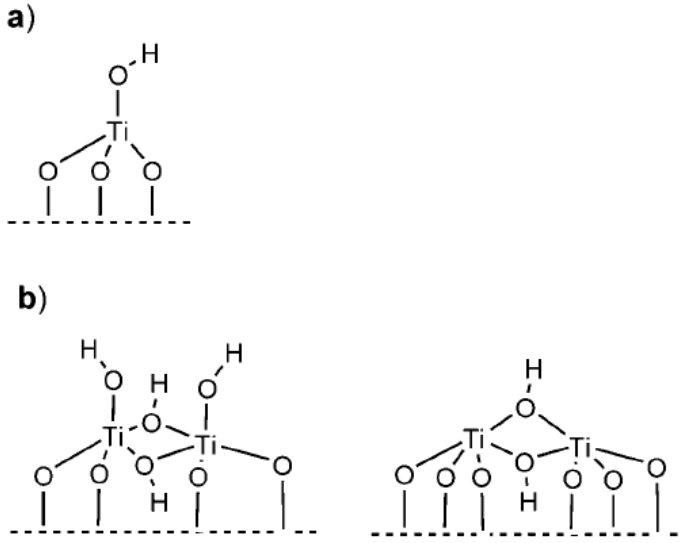

Figure 139 Illustration of mononuclear titanosilicates (a) and dinuclear titanosilicates (b).

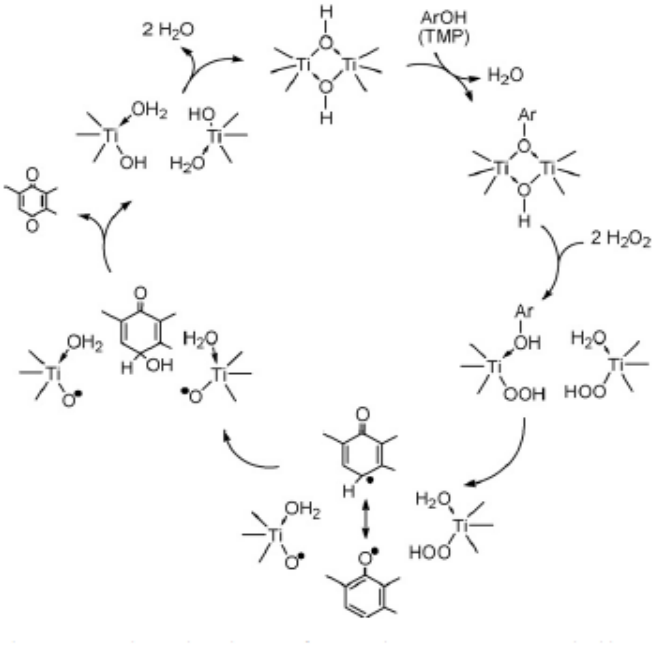

Figure 140 Proposed mechanism for the oxidation of phenols with dinuclear titanium catalysts. Figure obtained from ref [59].

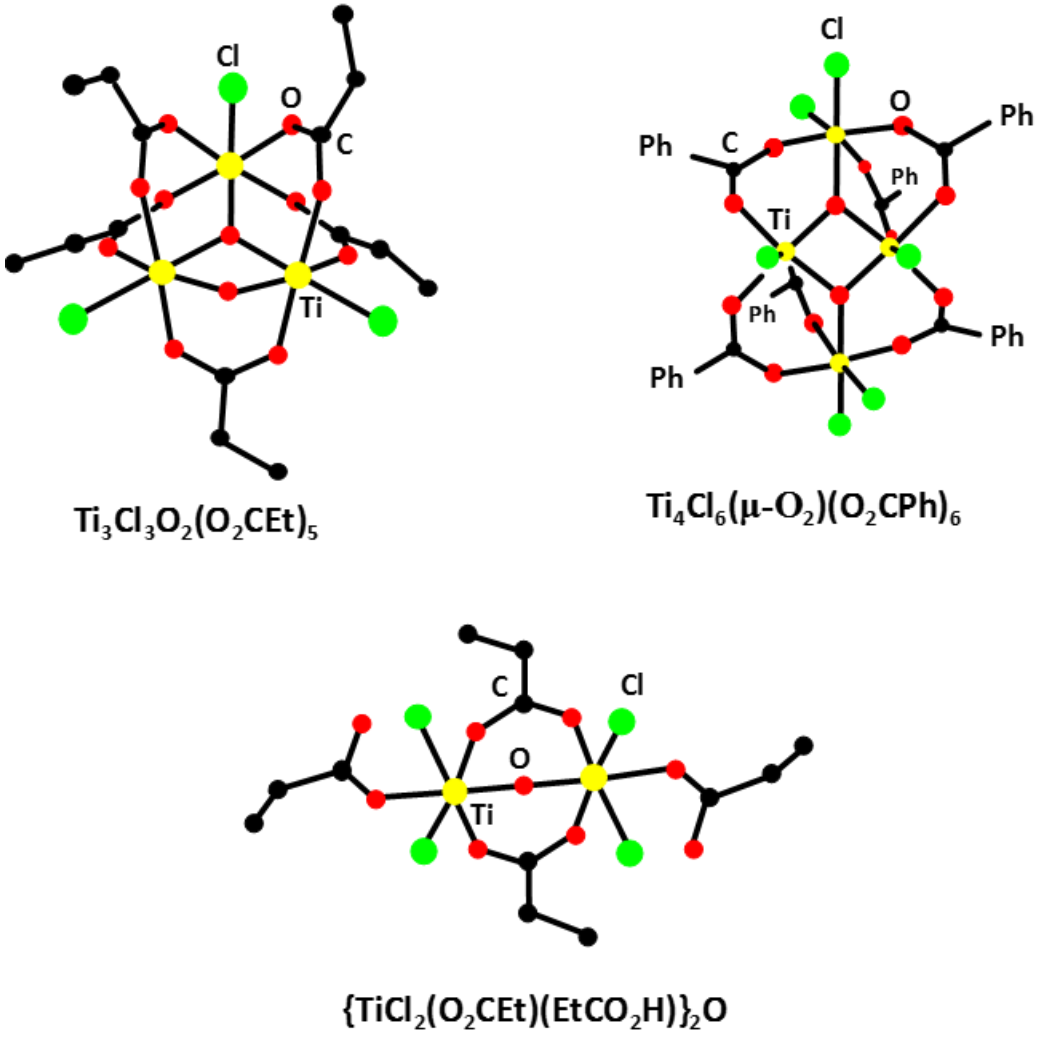

Figure 141 Polynuclear titanium precursors, Trinuclear (top left), tetranuclear (top right), and dinuclear (bottom). The titanium atoms are illustrated in yellow, bridging oxygens in red, and reactive chloride ligands in green.

References

(1) Lindstroem, B.; Pettersson, L. J., A brief history of catalysis. *CATTECH* **2003**, *7*, 130.

(2) Jon Jacob Berzelius-The Man Who Invented Catalysis? https://www.kth.se/en/che/archive/arkiv/berzelius August 24

(3) Robertson, A. J. B., Early history of catalysis. *Platinum Met. Rev.* **1975**, *19*, 64.

(4) Cronk Reaction Coordinate Catalyst http://guweb2.gonzaga.edu/faculty/cronk/CHEM240/images/reaction_coordinate_catalyst_lg.gif 09-28-2016

(5) Armor, J. N., A history of industrial catalysis. *Catal. Today* **2011**, *163*, 3.

(6) Fechete, I.; Wang, Y.; Vedrine, J. C., The past, present and future of heterogeneous catalysis. *Catal. Today* **2012**, *189*, 2.

(7) Gates, B. C. *Catalytic Chemistry*; John Wiley & Sons, Inc.: United States of America, 1991.

(8) Grunes, J.; Zhu, J.; Somorjai, G. A., Catalysis and nanoscience. *Chem. Commun. (Cambridge, U. K.)* **2003**, 2257.

(9) Gates, B. C.; Huber, G. W.; Marshall, C. L.; Ross, P. N.; Siirola, J.; Wang, Y., Catalysts for emerging energy applications. *MRS Bull.* **2008**, *33*, 429.

(10) Crotti, C.; Farnetti, E., Selective oxidation of glycerol catalyzed by iron complexes. *Journal of Molecular Catalysis A: Chemical* **2015**, *396*, 353.

(11) Lichtenegger, G. J.; Gruber-Woelfler, H., Strategies to develop leaching-free heterogeneous catalysts. *Chim. Oggi* **2015**, *33*, 12.

(12) Baiker, A., Supercritical fluids in heterogeneous catalysis. *Chemical Reviews* **1999**, *99*, 453.

(13) Kozhevnikov, I. V., Catalysis by heteropoly acids and multicomponent polyoxometalates in liquid-phase reactions. *Chemical Reviews* **1998**, *98*, 171.

(14) Medlin, J. W.; Marshall, S.; Schwartz, D. K.; University of Colorado, USA . 2012, p 60pp.

(15) Zhang, J.; Biradar, A. V.; Pramanik, S.; Emge, T. J.; Asefa, T.; Li, J., A new layered metal-organic framework as a promising heterogeneous catalyst for olefin epoxidation reactions. *Chem. Commun. (Cambridge, U. K.)* **2012**, *48*, 6541.

(16) Pelletier, J. D. A.; Basset, J.-M., Catalysis by Design: Well-Defined Single-Site Heterogeneous Catalysts. *Acc. Chem. Res.* **2016**, *49*, 664.

(17) Satterfield, C. N. *Heterogenous Catalysts in Industrial Practices*; Second ed.; McGraw-Hill, Inc. , 1991.

(18) Ross, J. *Heterogeneous Catalysis Fundamentals and Applications*; First ed.; John Wiley and Sons, 2011.

(19) Bell, A. T., The Impact of Nanoscience on Heterogeneous Catalysis. *Science (Washington, DC, U. S.)* **2003**, *299*, 1688.

(20) Pierre, A. C. *Introduction to Sol-Gel Processing*; Springer Link 1998.

(21) Hench, L. L.; West, J. K., The sol-gel process. *Chem. Rev.* **1990**, *90*, 33.

(22) Livage, J., Sol-gel synthesis of heterogeneous catalysts from aqueous solutions. *Catal. Today* **1998**, *41*, 3.

(23) Livage, J.; Sanchez, C., Sol-gel chemistry. *J. Non-Cryst. Solids* **1992**, *145*, 11.

(24) Melde, B. J.; Johnson, B. J.; Charles, P. T., Mesoporous silicate materials in sensing. *Sensors* **2008**, *8*, 5202.

(25) Debecker, D. P.; Mutin, P. H., Non-hydrolytic sol–gel routes to heterogeneous catalysts. *Chemical Society Reviews* **2012**, *41*, 3624.

(26) Debecker, D. P.; Hulea, V.; Mutin, P. H., Mesoporous mixed oxide catalysts via non-hydrolytic sol-gel: A review. *Appl. Catal., A* **2013**, *451*, 192.

(27) Cheng, F.; Tao, Z.; Liang, J.; Chen, J., Template-Directed Materials for Rechargeable Lithium-Ion Batteries†. *Chemistry of Materials* **2007**, *20*, 667.

(28) ALOthman, Z. A., A review: fundamental aspects of silicate mesoporous materials. *Materials* **2012**, *5*, 2874.

(29) Selvam, P.; Bhatia, S. K.; Sonwane, C. G., Recent advances in processing and characterization of periodic mesoporous MCM-41 silicate molecular sieves. *Industrial & Engineering Chemistry Research* **2001**, *40*, 3237.

(30) Texter, J. *Reactions and synthesis in surfactant systems*; CRC Press, 2001.

(31) Corma, A.; Navarro, M. T.; Perez Pariente, J., Synthesis of an ultralarge pore titanium silicate isomorphous to MCM-41 and its application as a catalyst for selective oxidation of hydrocarbons. *J. Chem. Soc., Chem. Commun.* **1994**, 147.

(32) Pham, A. L.-T.; Sedlak, D. L.; Doyle, F. M., Dissolution of mesoporous silica supports in aqueous solutions: Implications for mesoporous silica-based water treatment processes. *Appl. Catal., B* **2012**, *126*, 258.

(33) Lind, C.; Gates, S. D.; Pedoussaut, N. M.; Baiz, T. I., Novel materials through non-hydrolytic sol-gel processing: Negative thermal expansion oxides and beyond. *Materials* **2010**, *3*, 2567.

(34) Andrianainarivelo, M.; Corriu, R. J.; Leclercq, D.; Mutin, P. H.; Vioux, A., Nonhydrolytic Sol-Gel process: Aluminium and zirconium titanate gels. *Journal of Sol-Gel Science and Technology* **1997**, *8*, 89.

(35) Alves, A. K.; Bergmann, C. P.; Berutti, F. A. *Novel Sythesis and Characterization of Nanostructured Materials*; Springer-Verlag Berlin Heidelberg, 2013.

(36) Yang, B.; Jiang, J.-G.; Zhang, K.; Wu, P., Synthesis of Novel Titanosilicate Catalysts by Simultaneous Isomorphous Substitution and Interlayer Expansion of Zeolitic Layered Silicates. *Chem. Mater.* **2016**, *28*, 5295.

(37) Peskov, M. Zeolites http://asdn.net/asdn/chemistry/zeolites.php 08/20/2016

(38) Rimoldi, M.; Mezzetti, A., Site isolated complexes of late transition metals grafted on silica: challenges and chances for synthesis and catalysis. *Catal. Sci. Technol.* **2014**, *4*, 2724.

(39) Thomas, J. M., The societal significance of catalysis and the growing practical importance of single-site heterogeneous catalysts. *Proc. R. Soc. A* **2012**, *468*, 1884.

(40) Thomas, J. M.; Raja, R.; Lewis, D. W., Single-site heterogeneous catalysts. *Angew. Chem., Int. Ed.* **2005**, *44*, 6456.

(41) Thomas, J. M., The tortuous tale of the catalytically active site. *Top. Catal.* **2006**, *38*, 3.

(42) Chen, N., University of Tennessee, 2012.

(43) Kresge, C. T.; Leonowicz, M. E.; Roth, W. J.; Vartuli, J. C.; Beck, J. S., Ordered mesoporous molecular sieves synthesized by a liquid-crystal template mechanism. *Nature (London)* **1992**, *359*, 710.

(44) Maschmeyer, T.; Rey, F.; Sankar, G.; Thomas, J. M., Heterogeneous catalysts obtained by grafting metallocene complexes onto mesoporous silica. *Nature (London)* **1995**, *378*, 159.

(45) Shannon, I. J.; Maschmeyer, T.; Oldroyd, R. D.; Sankar, G.; Thomas, J. M.; Pernot, H.; Balikdjian, J.-P.; Che, M., Metallocene-derived, isolated MoVI active centers on mesoporous silica for the catalytic dehydrogenation of methanol. *J. Chem. Soc., Faraday Trans.* **1998**, *94*, 1495.

(46) Sakthivel, A.; Zhao, J.; Kuehn, F. E., Cyclopentadienyl molybdenum complexes grafted on zeolites - synthesis and catalytic application. *Catal. Lett.* **2005**, *102*, 115.

(47) Jin, T.; Liu, C.; Li, G., Heterogenization of a macrocyclic cobalt complex for photocatalytic CO2 reduction. *J. Coord. Chem.* **2016**, *69*, 1748.

(48) Drenchev, N.; Svadlak, D.; Setnicka, M.; Cicimanec, P.; Bulanek, R., Characterization of vanadium sites on vanadium-containing mesoporous silica catalysts and their catalytic behaviour in propane ODH. *Sci. Pap. Univ. Pardubice, Ser. A* **2014**, *20*, 273.

(49) Abbet, S.; Sanchez, A.; Heiz, U.; Schneider, W. D.; Ferrari, A. M.; Pacchioni, G.; Roesch, N., Acetylene Cyclotrimerization on Supported Size-Selected Pdn Clusters (1 ≤ n ≤ 30): One Atom Is Enough! *J. Am. Chem. Soc.* **2000**, *122*, 3453.

(50) McKittrick, M. W.; Jones, C. W., Toward Single-Site, Immobilized Molecular Catalysts: Site-Isolated Ti Ethylene Polymerization Catalysts Supported on Porous Silica. *J. Am. Chem. Soc.* **2004**, *126*, 3052.

(51) Nicholas, C. P.; Ahn, H.; Marks, T. J., Synthesis, Spectroscopy, and Catalytic Properties of Cationic Organozirconium Adsorbates on "Super Acidic" Sulfated Alumina. "Single-Site" Heterogeneous Catalysts with Virtually 100% Active Sites. *J. Am. Chem. Soc.* **2003**, *125*, 4325.

(52) Coperet, C.; Chabanas, M.; Saint-Arroman, R. P.; Basset, J.-M., Homogeneous and heterogeneous catalysis: bridging the gap through surface organometallic chemistry. *Angew. Chem., Int. Ed.* **2003**, *42*, 156.

(53) Bianchini, C.; Burnaby, D. G.; Evans, J.; Frediani, P.; Meli, A.; Oberhauser, W.; Psaro, R.; Sordelli, L.; Vizza, F., Preparation, Characterization, and Performance of Tripodal Polyphosphine Rhodium Catalysts Immobilized on Silica via Hydrogen Bonding. *J. Am. Chem. Soc.* **1999**, *121*, 5961.

(54) Jones, M. D.; Raja, R.; Thomas, J. M.; Johnson, B. F. G.; Lewis, D. W.; Rouzaud, J.; Harris, K. D. M., Enhancing the enantioselectivity of novel homogeneous organometallic hydrogenation catalysts. *Angew. Chem., Int. Ed.* **2003**, *42*, 4326.

(55) Corma, A.; Garcia, H., Supramolecular host-guest systems in zeolites prepared by ship-in-a-bottle synthesis. *Eur. J. Inorg. Chem.* **2004**, 1143.

(56) Bordiga, S.; Damin, A.; Bonino, F.; Lamberti, C. In *Surface and Interfacial Organometallic Chemistry and Catalysis*; Springer: 2005, p 37.

(57) Henry, P. F.; Weller, M. T.; Wilson, C. C., Structural investigation of TS-1: Determination of the true nonrandom titanium framework substitution and silicon vacancy distribution from powder neutron diffraction studies using isotopes. *The Journal of Physical Chemistry B* **2001**, *105*, 7452.

(58) De Vos, D. E.; Dams, M.; Sels, B. F.; Jacobs, P. A., Ordered mesoporous and microporous molecular sieves functionalized with transition metal complexes as catalysts for selective organic transformations. *Chemical Reviews* **2002**, *102*, 3615.

(59) Kholdeeva, O. A.; Ivanchikova, I. D.; Guidotti, M.; Ravasio, N.; Sgobba, M.; Barmatova, M. V., How to reach 100% selectivity in H 2 O 2-based oxidation of 2, 3, 6-trimethylphenol to trimethyl-p-benzoquinone over Ti, Si-catalysts. *Catalysis Today* **2009**, *141*, 330.

(60) Kholdeeva, O. A.; Mel'gunov, M. S.; Shmakov, A. N.; Trukhan, N. N.; Kriventsov, V. V.; Zaikovskii, V. I.; Malyshev, M. E.; Romannikov, V. N., A new mesoporous titanium-silicate Ti-MMM-2: a highly active and hydrothermally stable catalyst for H2O2-based selective oxidations. *Catal. Today* **2004**, *91-92*, 205.

(61) Kholdeeva, O. A.; Trukhan, N. N., Mesoporous titanium silicates as catalysts for the liquid-phase selective oxidation of organic compounds. *Russ. Chem. Rev.* **2006**, *75*, 411.

(62) Kholdeeva, O. A.; Ivanchikova, I. D.; Maksimchuk, N. V.; Mel'gunov, M. S.; Chang, J.-S.; Guidotti, M.; Shutilov, A. A.; Zaikovskii, V. I., Environmentally Benign Oxidation of Alkylphenols to p-Benzoquinones: A Comparative Study of Various Ti-Containing Catalysts. *Topics in Catalysis* **2014**, *57*, 1377.

(63) Bligaard, T.; Bullock, R. M.; Campbell, C. T.; Chen, J. G.; Gates, B. C.; Gorte, R. J.; Jones, C. W.; Jones, W. D.; Kitchin, J. R.; Scott, S. L., Toward Benchmarking in Catalysis Science: Best Practices, Challenges, and Opportunities. *ACS Catal.* **2016**, *6*, 2590.

(64) Boudart, M., Turnover rates in heterogeneous catalysis. *Chemical reviews* **1995**, *95*, 661.

(65) Satterfield, C. N. *Heterogeneous Catalsysis in Industrial Practice*; 2nd ed.; McGraw-Hill, INC: United States of America, 1991.

(66) Somorjai, G. A.; Park, J. Y., Molecular factors of catalytic selectivity. *Angewandte Chemie International Edition* **2008**, *47*, 9212.

(67) Zaera, F., Regio-, Stereo-, and Enantioselectivity in Hydrocarbon Conversion on Metal Surfaces. *Acc. Chem. Res.* **2009**, *42*, 1152.

(68) Zaera, F., New Challenges in Heterogeneous Catalysis for the 21st Century. *Catal. Lett.* **2012**, *142*, 501.

(69) Ziolek, M., Catalytic liquid-phase oxidation in heterogeneous system as green chemistry goal—advantages and disadvantages of MCM-41 used as catalyst. *Catalysis Today* **2004**, *90*, 145.

(70) Davies, L. J.; McMorn, P.; Bethell, D.; Page, P. C. B.; King, F.; Hancock, F. E.; Hutchings, G. J., Epoxidation of Crotyl Alcohol Using Ti-Containing Heterogeneous Catalysts: Comments on the Loss of Ti by Leaching. *J. Catal.* **2001**, *198*, 319.

(71) Arends, I.; Sheldon, R., Activities and stabilities of heterogeneous catalysts in selective liquid phase oxidations: recent developments. *Applied Catalysis A: General* **2001**, *212*, 175.

(72) Barnes, C. E.; Wiley-VCH Verlag GmbH & Co. KGaA: 2009, p 137.

(73) Mayes, R. T., University of Tennessee, 2009.

(74) Feher, F. J.; Weller, K. J., Synthesis and characterization of labile spherosilicates: [(Me3SnO)8Si8O12] and [(Me4SbO)8Si8O12]. *Inorg. Chem.* **1991**, *30*, 880.

(75) Barnes, C. E.; Sharp, K.; Albert, A. A.; Peretich, M. E.; Fulvio, P.; Ciesielski, P. N.; Donohoe, B. S., Metal-silicate catalysts: single site, mesoporous systems without templates. *ScienceJet* **2015**, *4*, 107/1.

(76) Clark, J. C.; Barnes, C. E., Reaction of the Si8O20(SnMe3)8 Building Block with Silyl Chlorides: A New Synthetic Methodology for Preparing Nanostructured Building Block Solids. *Chem. Mater.* **2007**, *19*, 3212.

(77) Kamigaito, M.; Sawamoto, M.; Higashimura, T., Alkoxy-Substituted Titanium(IV) Chlorides as Lewis Acid Activators for Living Cationic Polymerization of Isobutyl Vinyl Ether: Control of Lewis Acidity in the Design of Initiating Systems. *Macromolecules* **1995**, *28*, 5671.

(78) Rizzo, V.; Pinciroli, V., Quantitative NMR in synthetic and combinatorial chemistry. *Journal of pharmaceutical and biomedical analysis* **2005**, *38*, 851.

(79) Malz, F.; Jancke, H., Validation of quantitative NMR. *Journal of pharmaceutical and biomedical analysis* **2005**, *38*, 813.

(80) Van Every, K. W.; Griffiths, P. R., Characterization of diffuse reflectance FT-IR spectrometry for heterogeneous catalyst studies. *Applied spectroscopy* **1991**, *45*, 347.

(81) Boccuti, M.; Rao, K.; Zecchina, A.; Leofanti, G.; Petrini, G., Spectroscopic characterization of silicalite and titanium-silicalite. *Studies in Surface Science and Catalysis* **1989**, *48*, 133.

(82) Gao, X.; Wachs, I. E., Titania–silica as catalysts: molecular structural characteristics and physico-chemical properties. *Catalysis Today* **1999**, *51*, 233.

(83) Gao, X.; Bare, S. R.; Fierro, J.; Banares, M. A.; Wachs, I. E., Preparation and in-situ spectroscopic characterization of molecularly dispersed titanium oxide on silica. *The Journal of Physical Chemistry B* **1998**, *102*, 5653.

(84) Hernandez, C.; Pierre, A. C., Influence of the Sol-Gel Acidic Synthesis Conditions on the Porous Texture and Acidity of SiO2-Al2O3 Catalysts with a Low Al Proportion. *Langmuir* **2000**, *16*, 530.

(85) *Modern Techniques in Applied Molecular Spectroscopy*; John Wiley & Sons, Inc., 1998.

(86) Svehla, G. *Comprehensive Analytical Chemistry*; Elsevier Scientific Publishing Company 1975; Vol. IV.

(87) Weckhuysen, B. M.; Schoonheydt, R. A., Recent progress in diffuse reflectance spectroscopy of supported metal oxide catalysts. *Catalysis Today* **1999**, *49*, 441.

(88) Do, T. O.; Loic, L. N.; Bonneviot, L., Electron transfer bands of titanium sites in dehydrated silicalites and in TiO2-SiO2 gel. *Chem. Commun. (Cambridge)* **1996**, 299.

(89) http://www.mcmaster.com/

(90) Newville, M.; University of Chicago: 2004.

(91) Westre, T. E.; Kennepohl, P.; DeWitt, J. G.; Hedman, B.; Hodgson, K. O.; Solomon, E. I., A Multiplet Analysis of Fe K-Edge 1s → 3d Pre-Edge Features of Iron Complexes. *J. Am. Chem. Soc.* **1997**, *119*, 6297.

(92) George, S. D.; Brant, P.; Solomon, E. I., Metal and ligand K-edge XAS of organotitanium complexes: metal 4p and 3d contributions to pre-edge intensity and their contributions to bonding. *J Am Chem Soc* **2005**, *127*, 667.

(93) Farges, F.; Brown, G. E., Jr.; Rehr, J. J., Ti K-edge XANES studies of Ti coordination and disorder in oxide compounds: Comparison between theory and experiment. *Phys. Rev. B: Condens. Matter* **1997**, *56*, 1809.

(94) Ravel, B. The Artemis User Guide https://bruceravel.github.io/demeter/artug/extended/ss.html 09/24/2016

(95) Calvin, S. *XAFS for Everyone*; CRC Press, 2013.

(96) Teo, B. K.; Joy, D. C. *EXAFS Spectroscopy Techniques and Applications*; Plenum Press, 1981.

(97) Newville, M., IFEFFIT: interactive XAFS analysis and FEFF fitting. *J. Synchrotron Radiat.* **2001**, *8*, 322.

(98) Newville, M., EXAFS analysis using FEFF and FEFFIT. *J. Synchrotron Radiat.* **2001**, *8*, 96.

(99) Lee, M.-Y.; Jiao, J.; Mayes, R.; Hagaman, E.; Barnes, C. E., The targeted synthesis of single site vanadyl species on the surface and in the framework of silicate building block materials. *Catal. Today* **2011**, *160*, 153.

(100) Alhamami, M.; Doan, H.; Cheng, C.-H., A review on breathing behaviors of metal-organic-frameworks (MOFs) for gas adsorption. *Materials* **2014**, *7*, 3198.

(101) Balbuena, P. B.; Gubbins, K. E., Theoretical interpretation of adsorption behavior of simple fluids in slit pores. *Langmuir* **1993**, *9*, 1801.

(102) Farges, F., Coordination of Ti in crystalline and glassy fresnoites: a high-resolution XANES spectroscopy study at the Ti K-edge. *J. Non-Cryst. Solids* **1996**, *204*, 53.

(103) Wakabayashi, R.; Sugiura, Y.; Shibue, T.; Kuroda, K., Practical Conversion of Chlorosilanes into Alkoxysilanes without Generating HCl. *Angew. Chem., Int. Ed.* **2011**, *50*, 10708.

(104) Abbot, J. G., Univeristy of Tennessee, Knoxville, 2010.

(105) Aravind, P. R.; Mukundan, P.; Pillai, P. K.; Warrier, K. G. K., Mesoporous silica-alumina aerogels with high thermal pore stability through hybrid sol-gel route followed by subcritical drying. *Microporous Mesoporous Mater.* **2006**, *96*, 14.

(106) Trombetta, M.; Armaroli, T.; Alejandre, A. d. G.; Solis, J. R.; Busca, G., An FT-IR study of the internal and external surfaces of HZSM5 zeolite. *Applied Catalysis A: General* **2000**, *192*, 125.

(107) Lamberti, C.; Bordiga, S.; Arduino, D.; Zecchina, A.; Geobaldo, F.; Spano, G.; Genoni, F.; Petrini, G.; Carati, A.; Villain, F.; Vlaic, G., Evidence of the Presence of Two Different Framework Ti(IV) Species in Ti-Silicalite-1 in Vacuo Conditions: an EXAFS and a Photoluminescence Study. *J. Phys. Chem. B* **1998**, *102*, 6382.

(108) Deng, X.; Wang, Y.; Shen, L.; Wu, H.; Liu, Y.; He, M., Low-Cost Synthesis of Titanium Silicalite-1 (TS-1) with Highly Catalytic Oxidation Performance through a Controlled Hydrolysis Process. *Ind. Eng. Chem. Res.* **2013**, *52*, 1190.

(109) Trukhan, N.; Kholdeeva, O., Kinetics and Mechanism of 2, 3, 6-Trimethylphenol Oxidation by Hydrogen Peroxide in the Presence of TiO2–SiO2 Aerogel. *Kinetics and catalysis* **2003**, *44*, 347.

(110) Zalomaeva, O. V.; Trukhan, N. N.; Ivanchikova, I. D.; Panchenko, A. A.; Roduner, E.; Talsi, E. P.; Sorokin, A. B.; Rogov, V. A.; Kholdeeva, O. A., EPR study on the mechanism of H2O2-based oxidation of alkylphenols over titanium single-site catalysts. *J. Mol. Catal. A: Chem.* **2007**, *277*, 185.

(111) Oberti, R.; Ungaretti, L.; Cannillo, E.; Hawthorne, F. C., The behaviour of Ti in amphiboles: I. Four-and six-coordinate Ti in richterite. *European Journal of Mineralogy* **1992**, *4*, 425.

(112) Sevast'yanova, T.; Suvorov, A., Thermochemical Parameters of Formation of Titanium Tetrachloride Adducts as a Measure of Donor-Acceptor Bond Strength. *RUSSIAN JOURNAL OF COORDINATION CHEMISTRY C/C OF KOORDINATSIONNAIA KHIMIIA* **1997**, *23*, 761.

(113) Kawano, Y.; Hase, Y.; Sala, O., Vibrational spectra of adducts of acetonitrile with titanium and tin tetb achloride. *Journal of Molecular Structure* **1976**, *30*, 45.

(114) Lis, T.; Ejfler, J.; Utko, J.; Sobota, P., The crystal structure of cis and trans isomers of [TiCl4 (thf) 2]. *Polish. J. Chem. 1992, 66, 93* **1992**, *99*.

(115) Manzer, L. E., Tetrahydrofuran complexes of selected early transition metals. *Inorg. Synth.* **1982**, *21*, 135.

(116) Mobilio, S.; Boscherini, F.; Meneghini, C. *Synchrotron Radiation: Basics, Methods and Applications*; Springer, 2014.

(117) Ravel, B. EXAFS Modeling (Feffit / Artemis / SixPack) http://cars9.uchicago.edu/ifeffit/FAQ/FeffitModeling 06/24/2016

(118) Hulme, R.; Leigh, G. J.; Beattie, I. R., Crystal structure of trans-dipyridinetetrachlorogermanium (IV) and of its Si and Ti analogs. *J. Chem. Soc.* **1960**, 366.

(119) Rao, G., Infra-red spectra of the complexes of titanium and zirconium tetrahalides with organic ligands. I Pyridine Complexes. *Zeitschrift für anorganische und allgemeine Chemie* **1960**, *304*, 176.

(120) Rao, G., Unsymmetrical nature of the pyridine complexes of titanium tetrafluoride and tetraiodide. *Naturwissenschaften* **1959**, *46*, 556.

(121) Lopez, T.; Sanchez, E.; Bosch, P.; Meas, Y.; Gomez, R., FTIR and UV-Vis (diffuse reflectance) spectroscopic characterization of TiO 2 sol-gel. *Materials chemistry and physics* **1992**, *32*, 141.

(122) Yang, Q.; Wang, S.; Lu, J.; Xiong, G.; Feng, Z.; Xin, Q.; Li, C., Epoxidation of styrene on Si/Ti/SiO 2 catalysts prepared by chemical grafting. *Applied Catalysis A: General* **2000**, *194*, 507.

(123) Sensarma, S.; Bouh, A. O.; Scott, S. L.; Alper, H., Olefin epoxidation catalyzed by an air-stable supported titanium catalyst. *J. Mol. Catal. A: Chem.* **2003**, *203*, 145.

(124) Guidotti, M.; Pirovano, C.; Ravasio, N.; Lázaro, B.; Fraile, J. M.; Mayoral, J. A.; Coq, B.; Galarneau, A., The use of H 2 O 2 over titanium-grafted mesoporous silica catalysts: a step further towards sustainable epoxidation. *Green Chemistry* **2009**, *11*, 1421.

(125) Klunduk, M. C.; Maschmeyer, T.; Thomas, J. M.; Johnson, B. F., The influence of steric congestion on the catalytic performance of TiIV active centers in the epoxidation of alkenes. *Chemistry–A European Journal* **1999**, *5*, 1481.

(126) El-Korso, S.; Khaldi, I.; Bedrane, S.; Choukchou-Braham, A.; Thibault-Starzyk, F.; Bachir, R., Liquid phase cyclohexene oxidation over vanadia based catalysts with tert-butyl hydroperoxide: Epoxidation versus allylic oxidation. *Journal of Molecular Catalysis A: Chemical* **2014**, *394*, 89.

(127) Jarupatrakorn, J.; Tilley, T. D., Silica-supported, single-site titanium catalysts for olefin epoxidation. A molecular precursor strategy for control of catalyst structure. *Journal of the American Chemical Society* **2002**, *124*, 8380.

(128) Albert, A., University of Tennessee, 2016.

(129) Deubel, D. V.; Frenking, G.; Gisdakis, P.; Herrmann, W. A.; Rösch, N.; Sundermeyer, J., Olefin Epoxidation with Inorganic Peroxides. Solutions to four long-standing controversies on the mechanism of oxygen transfer. *Accounts of chemical research* **2004**, *37*, 645.

(130) Danov, S.; Krasnov, V.; Sulimov, A.; Ovcharova, A., Mechanism of olefin epoxidation in the presence of a titanium-containing zeolite. *Russian Journal of Physical Chemistry A* **2013**, *87*, 1809.

(131) Danov, S. M.; Orekhov, S. V.; Fedosov, A. E.; Fedosova, M. E.; Shishkin, A. I., Patterns of phenol oxidation process with an aqueous solution of hydrogen peroxide. *Theor. Found. Chem. Eng.* **2016**, *50*, 525.

(132) Guidotti, M.; Ravasio, N.; Psaro, R.; Ferraris, G.; Moretti, G., Epoxidation on titanium-containing silicates: do structural features really affect the catalytic performance? *J. Catal.* **2003**, *214*, 242.

(133) Lueangchaichaweng, W.; Li, L.; Wang, Q.-Y.; Su, B.-L.; Aprile, C.; Pescarmona, P. P., Novel mesoporous composites of gallia nanoparticles and silica as catalysts for the epoxidation of alkenes with hydrogen peroxide. *Catalysis today* **2013**, *203*, 66.

Vita

Lena Elenchin was born in Pine Grove, PA, on February 13, 1989 where she grew up and graduated from Pine Grove Area High School in June of 2007. She then enrolled at Kutztown University of Pennsylvania and obtained two Bachelor's of Sciences; Chemistry (ACS Certification) and Biochemistry in May of 2011. While at Kutztown University, she conducted undergraduate research with Dr. Julie Palkendo on the detection of pesticides on fruit using solid phase microextraction. She also investigated catalytic reduction of CO_2 with chelating N-heterocyclic carbenes under the supervision of Dr. Douglas Swartz.

In August 2011, she moved to Knoxville, TN, and enrolled in the Chemistry Graduate School at the University of Tennessee-Knoxville, where she began work on a doctoral degree in inorganic chemistry under the guidance of Dr. Craig E. Barnes. Her research was part of an ongoing project which involved the synthesis and characterization of single-site heterogeneous titanosilicates for selective oxidation reactions. She completed the requirements for the Doctor of Philosophy in chemistry in December 2016.